Fracture Characterization and Analysis of Debonded Sandwich Composites

Saseendran, Vishnu

Publication date:
2017

Document Version
Publisher's PDF, also known as Version of record

Fracture Characterization and Analysis of Debonded Sandwich Composites

PhD Thesis

$$(EIv'')''=q-\rho A\ddot{v}$$

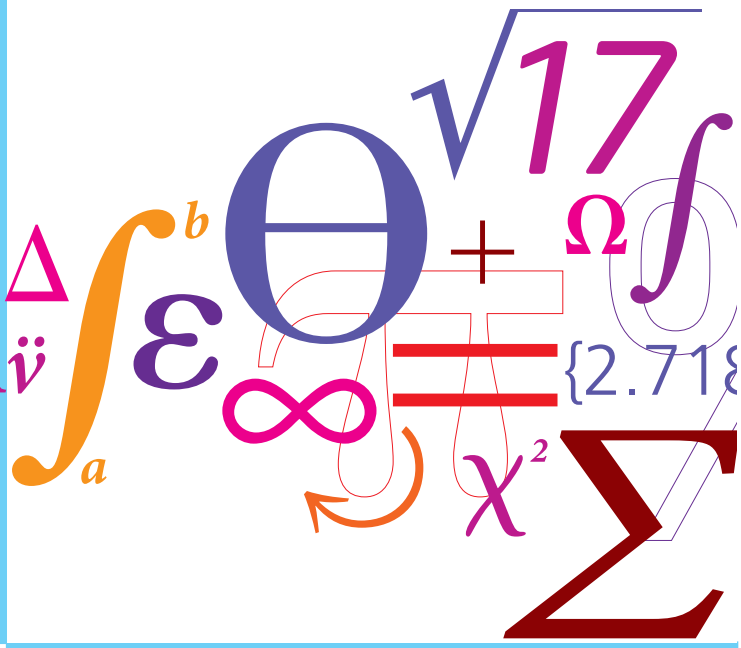

Vishnu Saseendran
DCAMM Special Report No. S241
December 2017

DTU Mechanical Engineering
Department of Mechanical Engineering

Fracture Characterization and Analysis of Debonded Sandwich Composites

Vishnu Saseendran

TECHNICAL UNIVERSITY OF DENMARK
DEPARTMENT OF MECHANICAL ENGINEERING
LIGHTWEIGHT STRUCTURES GROUP

DECEMBER 2017

Published in Denmark by:
Technical University of Denmark

Technical University of Denmark
Lightweight Structures Group
Section of Solid Mechanics, Department of Mechanical Engineering
Nils Koppels Allé, Building 404
DK-2800 Kgs. Lyngby
Denmark

Tel: (+45) 45 25 19 60
Fax: (+45) 45 25 19 61
www.mek.dtu.dk

Publicaion Reference Data:
V. Saseendran,
Fracture Characterization and Analysis of Debonded Sandwich Composites
Ph.D. Thesis
Technical University of Denmark, Section of Solid Mechanics
Depatment of Mechanical Engineering
December 2017
ISBN 978-87-7475-524-1
DCAMM Special Report No. S241
Keywords: Sandwich Composite; Debond; Face/core interface; LEFM; Mode-mixity; Phase angle; CSDE; Honeycomb; PVC foam; DCB-UBM; SCB; Elastic foundation

We all have to live together,
so we might as well live together happily.

- H. H. The 14^{th} Dalai Lama

Preface

This Thesis is submitted to the Technical University of Denmark in partial fulfillment of the requirements for the degree of Doctor of Philosophy, Ph.D. The work has been carried out in the Lightweight Structures Group under the Section of Solid Mechanics, Department of Mechanical Engineering, Technical University of Denmark, during the period from October 2014 to December 2017, including three months leave of absence. The project was supervised by Associate Professor Christian Berggreen and Professor Leif A. Carlsson (Florida Atlantic University).

Damage in sandwich composite structures, in particular face/core interface debond (or disbond) phenomenon was investigated under the ambit of linear elastic fracture mechanics. In this work, emphasis was laid out in the development of analytical, numerical and experimental methodologies to better understand the interface fracture mechanics of sandwich composites.

The study was financially supported by the Danish Centre for Composite Structures and Materials (DCCSM), funded by the Danish Council for Strategic Research within Sustainable Energy and Environment (Grant: 09-067212). During a four months period from October 2016 to January 2017, the work was carried out at the Florida Atlantic University, Boca Raton and at the NASA Langley Research Center, Hampton, USA.

A three months leave of absence (April - June, 2017) was taken to work on the project - Disbond of Sandwich Structures (DoSS), funded by the European Aviation Safety Agency (EASA). The numerical and experimental methodologies developed during the Ph.D. phase were utilized during this tenure and mixed-mode fracture testing of aerospace grade honeycomb core sandwich composites was carried out.

Kgs. Lyngby, Denmark
December 2017

Vishnu Saseendran

Acknowledgements

As the adage *"A journey of a thousand miles begins with a single step"* goes, I took my initial step towards this Ph.D., shortly after I defended my Master's thesis in the summer of 2014. First and foremost, I would like to thank my supervisor Associate Prof. Chrisitian Berggreen for offering me this position in his group. I am extremely grateful for his relentless support and facilitating progressive discussions. Special thanks to my co-supervisor, Prof. Leif Carlsson, Florida Atlantic University for letting me pick his brain on many occasions. I am also grateful for his continued guidance and encouragement throughout this project.

This study was supported by the Danish Centre for Composite Structures and Materials (DCCSM), funded by the Danish Council for Strategic Research within Sustainable Energy and Environment. The financial support is gratefully acknowledged. Travel grant supports from the Otto Mønsteds Foundation and Kaj & Hermilla Ostenfelds Foundation for the research stay abroad are highly appreciated. Furthermore, the financial support from the European Aviation Safety Agency (EASA) to work on aerospace grade sandwich composites is also gratefully acknowledged.

A part of the work was carried out at the Florida Atlantic University and at the NASA Langley Research Center, USA from October 2016 - January 2017. I would like to thank Prof. Carlsson for hosting me in his group at FAU and for the many outings. Special thanks to Seija Carlsson for the very warm welcome at Boca Raton.

I would like to thank Dr. Ronald Krueger, Associate Research Fellow, National Institute of Aerospace and resident at the NASA Langley Research Center, Hampton, USA for inviting and hosting me at NASA. I am grateful for his support especially in bouncing off ideas on numerical fracture models. I would also like to thank the group members of DDTRB, NASA Langley Research Center for making me feel welcome in the group during my visit. I would like to specially thank Dr. Mark McElroy and Dr. James Ratcliffe for helping me meander through a myriad of administrative conundrums at Hampton!

This research has helped me connect with a lot of experts in the sandwich composite realm. On that note, I would like to thank Ralf Hilgers, AIRBUS Operations GmbH, Hamburg for his encouragement and keen interest in this work. Furthermore, the support from AIRBUS

in the form of specimens supplied in kind is gratefully acknowledged. Yannick Albertone, DuPont, Geneva, Ralf Schäuble, Fraunhofer Institute for Microstructure of Materials and Systems, and other members of the sandwich disbond task group also deserve special mention. Their valuable inputs and encouragement through numerous discussions are greatly acknowledged here. I would also like to thank Falk Hähnel and Alexander Bugiel, TU Dresden for exchanging ideas regarding honeycomb core homogenization techniques.

A significant part of this Thesis was carried out at the DTU Structural Lab in Building 119, part of the Villum Center for Advanced Structural and Material Testing (CASMaT). Thanks to Johan, Tim and Troels who helped maintain the controllers and pumps. Special thanks to Christopher Augustsson, MTS Systems Norden, Sweden for his support and floating simulation tactics about implementation of cascade control. In addition, I am very grateful to my new and old office mates for creating a very friendly environ, and for the many vivifying discussions ranging from bi-material interfaces to South India! Thanks to Vasileios and Troels for pitching many of their numerical modeling approaches which have always been enriching. Thanks also go to my colleagues turned good friends for their support over the years and lending an ear when I face snags.

Boundless gratitude to my guru for bolstering my morale during inclement times. Special thanks to my mom, *Shiji Saseendran* for bracing me wholeheartedly throughout my sojourn here in the Europe. Last but not the least, I would like to thank *Amrita* for her endless support.

Vishnu Saseendran
December 2017

Abstract

Sandwich composites marked by their characteristic high stiffness to weight ratio have received wide attention from various industrial sectors for weight critical applications. Sandwich constructions invariably comprise of different materials with distinct material properties, and are prone to peculiar failure modes. A critical and most common damage mode is face/core debonding (or disbonding). Debonds can occur due to several reasons - insufficient wetting of face sheet and core during the production process, blunt body impacts, tool drop or by prolonged exposure to in-service loads. The presence of a debond compromises the safety of the structure, as lack of adhesion between face sheet and core in a sandwich undermines the integrity of the entire structure.

Nowadays, structures are pushed close to their performance limits leading to significant reduction of built-in reserve margins. Therefore, from the design and analysis perspective of sandwich structures, adequate tools are necessary for damage assessment. In order to assess the critical strain energy release rate of the face/core interface or fracture toughness, accurate methodologies need to be developed. The aim of this Thesis is to develop robust fracture mechanical based tools to characterize face/core debonds. Primarily, the focus was laid on fracture based test methods to assess the strength of the sandwich interface such as the Single Cantilever Beam (SCB) and the Double Cantilever Beam loaded with Uneven Bending Moments (DCB-UBM).

A parametric study is conducted to analyze the SCB sandwich specimen from a mode mixity perspective based on the numerical mode-mixity method - Crack Surface Displacement Extrapolation (CSDE) method. For a wide array of sandwich systems it was shown that despite conforming to the existing sizing study, mode-mixity deviate away from mode I conditions during a SCB test. Recommendations are laid out based on the modelled results to ensure that the debonding occurs under mode I conditions corresponding to a peel loading on the face sheet. The conclusions from this finite element based parametric study can serve as input to the ASTM International draft standard currently being developed.

Analysis of a force loaded SCB sandwich specimen using the Winkler model is presented. This analysis is further extended to a moment loaded SCB sandwich specimen. A new

foundation modulus expression is introduced and good agreement between analytical expressions and finite element simulations are obtained for both moment and force loading configurations. The effect of shear contribution on the mode-mixity phase angle, ψ, for both force and moment loaded SCB sandwich specimens is investigated. The phase angle is higher at short crack lengths and reaches a plateau as the crack length increases, which is in accordance with the decrease in shear component for a force loaded SCB sandwich specimen. The current foundation analysis for a moment loaded SCB specimen paves way for further development in the analysis of a moment loaded DCB sandwich specimen.

The Double Cantilever Beam specimen loaded with Unequal or Uneven Bending Moments (DCB-UBM) applied to sandwich composites is capable of achieving a constant mode-mixity condition throughout the test. Moreover, the DCB-UBM specimen is capable of performing fracture tests in mode I, mode II and mixed mode I/II conditions. Closed-form expressions for energy-release rate and mode-mixity phase angle for a symmetric DCB-UBM sandwich specimen reinforced with stiff layers are derived. The mode-mixity phase angle is expressed in terms of a single scalar parameter, ω which depends only on geometry of the sandwich system and is independent of the applied loading. The algebraic expressions are derived by analyzing the reinforced sandwich beam using the laminate beam theory and the J-integral. These derived expressions are an addition to the literature.

A novel DCB-UBM test rig capable of applying pure moments independently, is implemented in this Thesis. The presented rig is high-load and fatigue rated as well as overcomes many shortcomings of the traditional concept presented in the literature. A control algorithm based on Cascade control system is developed using a dedicated controller to perform static and fatigue testing. A data reduction procedure, based on the measured moments is deduced to obtain interface fracture toughness. Fracture testing of PVC foam and aerospace grade honeycomb core sandwich specimens are carried out using the newly developed test rig in mode I, mode II and mixed-mode conditions.

The theoretical, numerical and experimental fracture methodologies developed in this Thesis pave way to establish a framework in performing interface fracture toughness characterization of typical sandwich composites. The tools developed here have contributed to the international fracture standard development and have kindled interest of the community in creation of a mixed-mode fracture testing standard based on the DCB-UBM test methodology.

Keywords: Sandwich Composite; Debond; Face/core interface; LEFM; Mode-mixity; Phase angle; CSDE; Honeycomb; PVC foam; DCB-UBM; SCB; Elastic foundation

Synopsis

Sandwichkompositter mærket af deres karakteristiske højstivhed til vægtforhold har fået stor opmærksomhed fra forskellige industrisektorer til vægtkritiske applikationer. Sandwichkonstruktioner består af forskellige materialer med forskellige materialegenskaber og er tilbøjelige til særlige svigtningsmetoder. En kritisk og mest almindelig skadefunktion er ansigts- / kerneforbindende (eller disbonding). Debanter kan forekomme på grund af flere årsager - utilstrækkelig befugtning af forsideark og kerne under produktionsprocessen, stumme kropsbelastninger, værktøjsfald eller ved længerevarende eksponering for servicebelastninger. Tilstedeværelsen af debond kompromitterer strukturens sikkerhed, da manglende adhæsion mellem ansigtsarket og kernen i en sandwich underminerer integriteten af hele strukturen.

I dag skubbes strukturer tæt på deres præstationsgrænser, der fører til en betydelig reduktion af indbyggede reservemargener. Derfor er det nødvendigt med passende værktøjer til skadesvurdering ud fra konstruktion og analyse af sandwichstrukturer. For at vurdere den kritiske belastningsenergiudsliphastighed for ansigt / kerneinterface eller brudsejhed skal nøjagtige metoder udvikles. Formålet med denne afhandling er at udvikle robuste brudstyrkebaserede mekanismer til at karakterisere ansigts- / kerneforbindelser. Primært blev fokus lagt på brudbaserede testmetoder til vurdering af styrken af sandwich-grænsefladen, såsom Single Cantilever Beam (SCB) og Double Cantilever Beam, der var lastet med ujævne bøjningsmomenter (DCB-UBM).

En parametrisk undersøgelse udføres for at analysere SCB sandwich-prøven ud fra et mode mixitetsperspektiv baseret på den numeriske modus-mixity metode - Crack Surface Displacement Extrapolation (CSDE) metode. For et bredt udvalg af sandwichsystemer blev det vist, at modemixiteten afviger fra tilstand I-forholdene under en SCB-test, selv om den overholder det eksisterende dimensioneringsstudie. Anbefalinger udformes ud fra de modellerede resultater for at sikre, at debonding forekommer under tilstand I-tilstand, der svarer til en skrælning på ansigtsarket. Konklusionerne fra denne finite elementbaserede parametriske undersøgelse kan tjene som input til ASTM International udkastet standard, der for øjeblikket er ved at blive udviklet.

Analyse af et kraftbelastet SCB sandwich-prøve ved brug af Winkler-modellen er præsenteret. Denne analyse forlænges yderligere til et øjebliksbelastet SCB sandwichprøve. Et

nyt fundament moduludtryk introduceres, og der opnås god overensstemmelse mellem analytiske udtryk og finite element simuleringer til både moment og force load konfigurationer. Effekten af forskydningsbidrag på mode-mixitetsfasevinklen, Mode-mixity Phase Angle, for både kraft- og momentbelastede SCB sandwich-prøver undersøges. Fasevinklen er højere ved korte knæklængder og når et plateau, da sprænglængden stiger, hvilket er i overensstemmelse med faldet i forskydningskomponenten til et kraftbelastet SCB sandwichprøve. Den nuværende fundamentanalyse for et øjebliksbelastet SCB-prøve baner vejen for yderligere udvikling i analysen af et øjebliksbelastet DCB sandwichprøve.

Et testprincip for en dobbelt konsol bjælke belastet med uens bøjningsmomenter (DCB-UBM) anvendt til sandwich komposit er i stand til at opnå et konstant mode-mixity betingelser i en eksperimentel test. Desuden er DCB-UBM testprincippet i stand til at udføre brudmekanisktest for mode I, mode II og mixed-mode I/II dominerede forhold. "Closed form expressions for energy release rate og mode-mixity fasevinkel for en symmetrisk DCB-UBM sandwich testemne som er forstærket med stive lag er udledt analytisk. Mode-mixity fasevinklen kan udtrykkes i form af en enkelt skalarparameter, ω som kun afhænger af geometrien af sandwich systemet som desuden er uafhængig af den påførte belastning. Det algebraiske udtryk er udledt ved at analysr den forstærkede sandwich bjælke ved hjælp af laminat bjælketeori og J-integralet. Disse udtryk er tilføjelser til eksisterende litteratur.

En ny DCB-UBM test rig, der er i stand til at påføre to uafhængig momenter, er implementeret i denne afhandling. Test riggen er designet til høj belastning samt udmattelse såvel som det forbedre mange af de problemer der er tilstede i den eksisterende litteratur. En kontrol algoritme der er baseret på Cascade kontrol system er udviklet ved brug af en dedikeret controller til at udføre både statisk- og udmattelsestest. En data reduktionsprocedure som er baseret på de målte momenter er udledt for at bestemme brudsejheden af et interface/grænseflade. Brudmekanisk test af sandwich testemner med PVC skum og luftfartsklasse honeycomb kernemateriale er udsat for hovedsaligt mode I, mode II og mixed-mode belastning.

De teoretiske, numeriske og eksperimentelle brudmetoder udviklet i denne afhandling baner vejen for at etabler en teoretisk ramme til at udføre brudmekanisk karakterisering af brudsejheden for typiske sandwich kompositter. De værktøjer, der er udviklet her, har bidraget til den internationale brudmekanisk standestandardudvikling og har givet anledning til interesse for at oprette en mixed-mode brudmekaniskstandard baseret på DCB-UBM testmetoden.

Publications

Publications appended to this Thesis.

[P1] **V. Saseendran**, C. Berggreen, and R. Krueger, "Mode mixity analysis of face/core debonds in a single cantilever beam sandwich specimen", *Journal of Sandwich Structures & Materials*, 2018. DOI: 10.1177/1099636218788223.

[P2] **V. Saseendran**, L. A. Carlsson, and C. Berggreen, "Shear and foundation effects on crack root rotation and mode-mixity in moment- and force-loaded single cantilever beam sandwich specimen", *Journal of Composite Materials*, vol. 52, no. 18, pp. 2537-2547, 2018. DOI: 10.1177/21998317749714.

[P3] C. Berggreen,**V. Saseendran**, and L. A. Carlsson, "A modified DCB-UBM test method for interfacial fracture toughness characterization of sandwich composites", *Engineering Fracture Mechanics*, 2018. DOI: 10.1016/j.engfracmech.2018.06.036.

[P4] **V. Saseendran**, L. A. Carlsson, and C. Berggreen, "Fracture mechanics analysis of reinforced DCB sandwich debond specimen loaded by moments", *AIAA Journal*, vol. 56, no. 1, pp. 413-422, 2018. DOI: 10.2514/1.J056039.

[P5] **V. Saseendran**, and C. Berggreen, "Mixed-mode fracture evaluation of aerospace grade honeycomb core sandwich specimens using the Double Cantilever Beam- Uneven Bending Moment test method", *Journal of Sandwich Structures & Materials*, 2018. DOI: 10.1177/1099636218777964.

Conference Proceedings/Other Publications

The following articles/conference proceedings were published during the Ph.D. study, but do not constitute to this manuscript.

- R. Krueger et al., "Characterizing face sheet/core disbonding using the single cantilever beam test: Results from an international round robin", *NASA Technical Report*, (***co-author***, *document due for public release*).
- V. Karatzas, **V. Saseendran**, C. Berggreen, and N. Tsouvalis, "A parametric investigation for the design of composite patch repairs employing linear elastic fracture mechanics", (*in manuscript*).
- **V. Saseendran** et al. "Disbond of sandwich structures - DoSS", *Technical Report - EASA.2016.C20*, 2017.
- **V. Saseendran**, and C. Berggreen, "On fracture testing of sandwich face/core interface using the DCB-UBM methodology in fatigue", *2nd International Symposium on Multiscale Experimental Mechanics: Multiscale Fatigue*, Kgs. Lyngby, Denmark, 2017.
- **V. Saseendran**, and C. Berggreen. "Honeycomb sandwich face/core fracture toughness measurements using the DCB-UBM test method − DoSS project", *Technical Report - Technical University of Denmark*, 2017
- **V. Saseendran**, C. Berggreen, and L. A. Carlsson, "Mixed mode fracture testing of foam core sandwich using the DCB-UBM test method", *8th International Conference on Fracture of Polymers, Composites and Adhesives*, Les Diablerets, Switzerland, 2017.
- **V. Saseendran**, C. Berggreen, and L. A. Carlsson, "Fracture characterization of PVC foam core sandwich specimen using the DCB-UBM test method", *21st International Conference on Composite Materials*, Xi'an, China, 2017.

- F. Attanasio, and **V. Saseendran**, "Determination of face/core fracture toughness in aircraft honeycomb sandwich composites using the SCB test method", *1st International Symposium on Multiscale Experimental Mechanics: Multiscale Fatigue*, Røskilde, Denmark, 2016.
- **V. Saseendran**, C. Berggreen, and L. A. Carlsson, "Fracture toughness characterization of honeycomb core sandwich composites in mode I: A comparative study", *11th International Conference on Sandwich Structures*, Dania Beach, USA, 2016.
- **V. Saseendran**, C. Berggreen, and L. A. Carlsson, "Fracture testing of honeycomb core sandwich composites using the DCB-UBM test", *20th International Conference on Composite Materials*, Copenhagen, Denmark, 2015.

Contents

Nomenclature

Latin Symbols

h	Characteristic length of the crack problem	[-]
h_d	Doubler layer thickness	[mm]
k	Elastic foundation modulus	$[N/mm^2]$
L_b	Length of intact portion in SCB specimen	[mm]
L_{hinge}	Length of hinge	[mm]
P	Applied load	$[N]$
$\overline{E}$	Young's modulus	$[\mathrm{N}/m^2]$
b	Width of sandwich specimen	$[mm]$
d	Distance between centroid of upper and lower face sheets	$[mm]$
dA	Incremental area	$[mm^2]$
da	Incremental crack length	$[mm]$
E	Young's modulus	$[\mathrm{N}/m^2]$
E_c	Core modulus	$[mm]$
E_f	Facesheet modulus	$[mm]$
G	Energy-release rate	[N/m]
G_I	Mode I energy-release rate	[N/m]
G_{1c}	Mode I interface fracture toughness	[N/m]
G_{III}	Mode III energy-release rate	[N/m]
G_{II}	Mode II energy-release rate	[N/m]
h_r	Reinforcement layer thickness	[mm]
h_c	Core thickness	$[mm]$

h_f	Facesheet thickness	$[mm]$
I_c	Area moment of inertia of core	$[mm^4]$
I_f	Area moment of inertia of face sheet	$[mm^4]$
K_{II}	Mode II Stress intensity factor	$[N/m^{3/2}]$
K_I	Mode I Stress intensity factor	$[N/m^{3/2}]$
L_{rod}	Loading rod length	$[mm]$
M_d	Moment on debonded arm	[Nm]
M_1	Moment applied on arm-1	$[Nm]$
M_2	Moment applied on arm-2	$[Nm]$
S_{ij}	Components of compliance matrix	[mm/N]
U	Stored elastic strain energy	[J]
W	Work performed by external forces	[J]
a	Pre-crack length	$[mm]$
a_{max}	Maximum crack length	[mm]

Greek Symbols

α	Dundur's parameter	[-]
β	Dundur's bi-material parameter	[-]
δ	Displacement	$[mm]$
λ	Ratio of stiffness of foundation to the upper beam	[-]
ν_c	Poisson's ratio of core	[-]
ν_f	Poisson's ratio of face sheet	[-]
ω	Load independent scalar quantity (Omega Parameter)	[deg]
ϕ	Crack root rotation angle	[deg]
ψ	Mode-mixity Phase Angle	[deg]
θ_1	Rotation of arm-1	$[deg]$
δ_x	Sliding displacement	[mm]
δ_y	Opening displacement	[mm]
Γ	Interface fracture toughness	[N/m]
κ_m	Muskhelishwili's constant	[-]
Λ	Dimensionless constant	[-]
Π	Stored potential energy	[J]
σ_{xx}	Normal stress	$[N/mm^2]$
σ_{yy}	Shear stress	$[N/mm^2]$
ε	Oscillatory index	[-]

Abbreviations

ADT	Angular Displacement Transducer
ASTM	American Society for Testing and Materials
CFRP	Carbon Fiber Reinforced Plastic
CNFS	Center Notch Flexure Sandwich
COV	Coefficient of Variation
CSB	Cracked Sandwich Beam
CSDE	Crack Surface Displacement Extrapolation
CSD	Crack Surface Displacement
DCB-UBM	Double Cantilever Beam loaded with Uneven Bending Moments
DCB	Double Cantilever Beam
DIC	Digital Image Correlation
ELSS	End-Loaded Sandwich Specimen
FEA	Finite Element Analysis
FE	Finite Element
GAG	Ground Air Ground
HPU	Hydraulic Power Unit
HSM	Hydraulic Service Manifold
LEFM	Linear Elastic Fracture Mechanics
MBT	Modified Beam Theory
MMB	Mixed-Mode Bending
MR	Moment Ratio
SCB	Single Cantilever Beam
SCB	Single Cantilever Beam
TLC	Torsion Load Cell
UD	Unidirectional
VARTM	Vacuum Assisted Resin Transfer Molding
VCCT	Virtual Crack Closure Technique
VCE	Virtual Crack Extension

Chapter 1

Introduction

A brief introduction to sandwich composites and the critical damage mode - face/core interface failure due to debonding is provided in this chapter. The major research objectives and accomplishments of the presented Ph.D. work are also presented.

1.1 Background: Introduction to Sandwich Structures

Sandwich composite structures are widely chosen in many applications due to their superior performance over metals and monolithic composite materials. A typical sandwich can be treated as a "tri-material", comprising of two face sheets and a core. In general, the face sheets are identical and are made up of laminate composite materials. The employability of sandwich structures vary depending on the type of industry. Based on the intended sector, the lightweight core material varies from cellular foams, honeycomb or balsa. The application sectors of sandwich include, but are not limited to, aerospace, automotive, sports, wind, naval and many high performance applications. Composite materials, especially sandwiches have been utilized by various industry clientele for the past several decades. For instance, in the automotive industry sandwich composites are widely used in truck trailers to improve weight capacity as well as to preserve the pay load at desired temperatures. In addition, use of sandwich components as energy absorbers in automobiles has been widely investigated. In naval applications they are employed in bulk head and deck panels. Primary aerostructures that employ sandwich include wing leading edge, aileron balance panels, engine nacelle components, thrust reversers, rudder and radomes. Secondary aircraft structures include, over head bins, floor panels, cabin interior etc. Figure 1.1 illustrates major applications of sandwich composites across different industries. A more detailed illustration of the various parts made of sandwich in an ATR aircraft is provided in Figure 1.2.

In a sandwich composite, the face sheets support bending loads and the core transfers the shear force. The overall bending stiffness can be obtained using the parallel axis theorem,

(a) Visby Class corvette (*picture courtesy*, Saab Kockums AB).

(b) 88.5m wind turbine blade (*picture courtesy*, LM Wind Power).

(c) Airbus A350-1000 approaching Hamburg Finkenwerder (XFW) after a test flight(*picture courtesy*, airliners.net).

Figure 1.1. Typical examples of primary users of sandwich composites.

and can be expressed for a typical cross-section (see Figure 1.2) as [1]:

$$E_x I = 2E_x^f I_f + E_x^c I_c \tag{1.1}$$

where I_c and I_f are the moments of inertia with respect to the neutral axis of the core and face sheet, respectively, given by: $I_c = bh_c^3/12$ and $I_f = bh_f^3\Big/12 + bh_f d^2/4$, h_f is the face sheet thickness, h_c is the core thickness and d is the distance between centroids of upper and lower face sheets. The moduli of face sheet and core are E_f and E_c respectively.

The bending stiffness of a sandwich beam element (per width, b) can be expressed as: $D_x = E_x I/b$ (see Equation 1.1). The outstanding overall bending and shear stiffness to weight ratios are what make the sandwich composites stand apart from the regular metals or laminates. Core material is chosen by taking into account the operating load conditions; e.g. susceptibility to resist shear or buckling failure, low density with adequate compressive and shear strength and stiffness. In general, the core is the weak constituent in a sandwich structure.

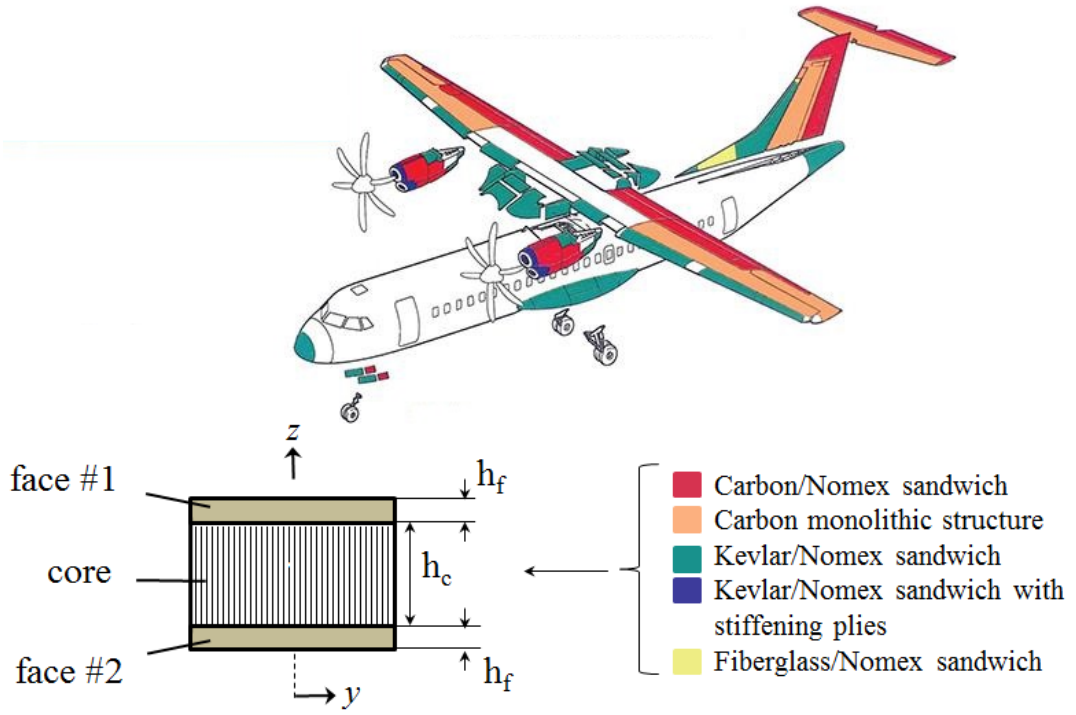

Figure 1.2. Cross-sectional view of a typical sandwich beam element and various face/core systems used in ATR - 72 series type aircraft (*picture courtesy*, ATR Aircraft).

1.2 Failure Modes in Sandwich Structures

With the advent of new processing techniques and production capabilities, utilization of sandwich composites across various sectors is slated to increase tremendously. To ensure safe and reliable service of structures, the failure phenomenon associated with sandwich components must be addressed carefully. The most prominent modes of failure associated with sandwich, described by Zenkert et al. [2] are: face/core interface debonding or "disbonding", core shear failure, face wrinkling, shear crimping, core indentation, core or face sheet failure and buckling of the entire structure. Due to the afore-mentioned unusual damage modes, the safety factors during design stage of sandwich structures are invariably kept at high values.

The most notorious damage mode is the face/core interface failure, as lack of adhesion between face sheet and core leads to degradation of integrity of the entire structure. The debonds may occur as production defects due to insufficient wetting of face sheet and core, due to trapped air bubbles, by in-service loading over a period of time, due to over-loading or impact instigated debonds. Several in-service damages have been attributed to debonding such as rudder structural failure and other control surface malfunctions in the aerospace sector [3, 4]. Studies have shown that debonds can grow when subjected to cyclic loads in wind turbine blades [5]. The debond damage incurred on typical sandwich structures are shown in Figure 1.3. Therefore, the face/core debond characteristics must be assessed with a high degree of confidence to ensure reliable operation of a sandwich structure throughout the entire load envelope. The strength of a face/core interface can

be determined by measuring the energy required to separate face sheet from the core, usually referred to as the interface fracture toughness. For a sandwich face/core interface, the measured fracture toughness must be mapped for a range of mode-mixity values. This is one of the primary focus areas of this Thesis and further details are provided in subsequent chapters.

(a) Keel damage due to grounding (*picture courtesy*, Sailor's Wharf, FL).

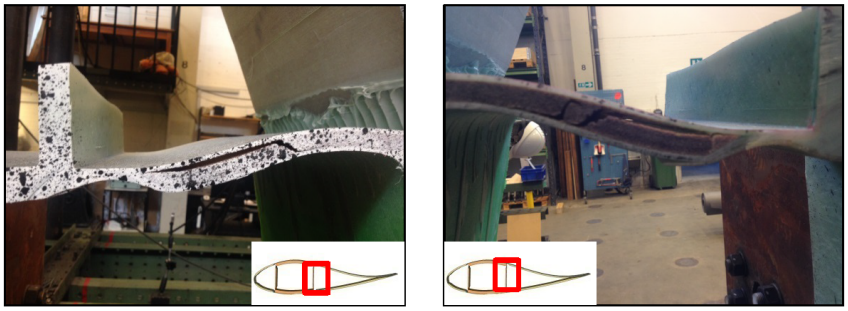

(b) Debond damage in wind turbine blade [5].

(c) Rudder residuals of Air Transat A310 [3].

Figure 1.3. Face/core interface damage incurred on typical sandwich structures.

1.3 Research Objectives and Achievements

Guidelines to prevent failure caused by prominent sandwich damage modes (except damage due to debonds) already exist in the literature [2, 6]. However, specialized fracture mechanics based tools are required to address the debond problem. To ensure continued employability of sandwich and for future structural applications, the debond associated damage growth must be addressed. The debond phenomenon is also of particular interest to certification authorities. Moreover, a framework based on analytical, numerical and experimental methods will better equip the industry in understanding the crack growth phenomenon. A bottom-up approach can be undertaken to understand the debonding phenomenon in sandwich structures. An illustration of such an approach is shown in Figure 1.4.

Damage incurred on large sandwich structures, for instance, a wind turbine rotor blade or an aircraft fuselage can be analyzed with the aid of numerical tools. In order to perform such simulations, the critical strain energy-release rate or fracture toughness of the interface must be provided as input. The fracture toughness data is one of the critical parameters which is unique for a sandwich interface and can be ascertained using fracture mechanical tests. In the pyramid scheme shown in Figure 1.4, the interface fracture toughness is obtained at the bottom most block using fracture mechanics based test methods. The generated interface toughness data can then be used on a sub-element level where verifications are performed using both experiments and simulations. In the next level of hierarchy, the fracture parameters are used to investigate debond growth under more complex loading scenarios, e.g., cyclic in-plane compression or Ground Air Ground (GAG) loading. In the element level, limited series of testing can be done to validate the simulations. With the increased level of confidence, the fracture data can then be used for more complex structural analysis. The complexity in geometry and loads as well as the cost of tests increase with hierarchy in the pyramid scheme, as illustrated in Figure 1.4. The primary objective of this Thesis is to develop efficient tools to perform fracture mechanical characterization of debonded sandwich composites at the coupon level.

The work presented in this Ph.D. project focuses on the bottom-most building block in the pyramid scheme (see Figure 1.4). The success of a structural analysis situated at the apex of the pyramid depends on reliable fracture parameters provided as input. Therefore, it is of paramount importance that the interface fracture toughness must be measured accurately. Standard fracture mechanical tests already exist for composite laminates [7, 8, 9, 10, 11]. However, no such standard test method exist for fracture characterization in sandwich composites. In order to overcome this shortcoming, a task group under ASTM Committee D30 (WK56166) was formed with an aim to introduce a new test method for measuring peel-dominated interface fracture toughness of sandwich constructions. As is the case with monolithic laminates, mode I debonding, where the face sheet is peeled from the core is the most critical mode in sandwich composites. The task group is spear headed by both industry and research institutions with participation from academia, and identified the Single Cantilever Beam (SCB) sandwich specimen as the suitable candidate for peel-dominant fracture characterization in sandwich composites. An international round robin exercise was carried out using the SCB sandwich specimen [12] to estimate mode I fracture toughness of honeycomb core sandwich specimens.

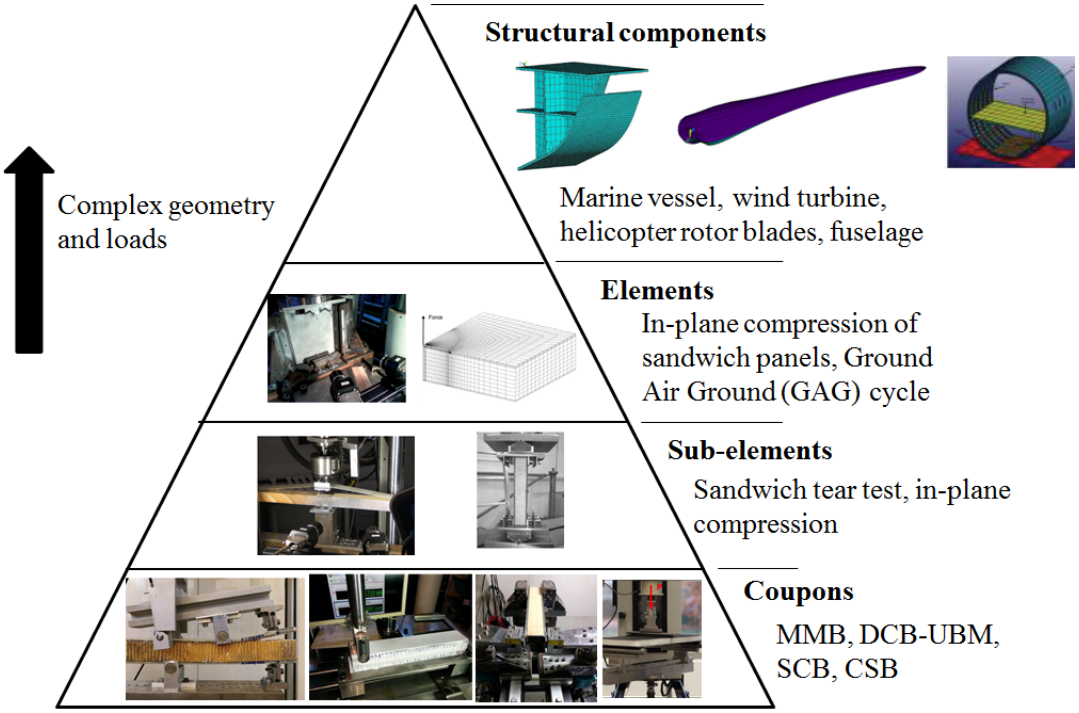

Figure 1.4. Building block approach with increasing complexity in geometry and loading. Impetus was given to the bottom block in this Ph.D.

The fracture mechanical based numerical model developed in this project was utilized to evaluate the general applicability of the SCB sandwich specimen when introduced as an international standard. The parametric study explored a wide array of sandwich interfaces to ascertain whether the fracture measurement will lie in the mode I regime or not. Conclusions and recommendations from this study will serve as an appendage to the existing study from the literature which is currently adopted in the draft standard [13]. In addition, focus was laid on development of a mixed mode fracture test methodology for characterization of sandwich interfaces. In that line, significant work was carried out on the fracture specimen - Double Cantilever Beam loaded with Uneven or unequal Bending Moments or in short DCB-UBM.

Algebraic expressions for the energy-release rate and the mode-mixity were derived for a debonded DCB-UBM specimen reinforced with stiff layers. The energy-release rate was obtained using the J-integral expression coupled with the laminate beam theory. The expression was derived for the pure moment loading - DCB-UBM fracture specimen case. For a reinforced sandwich tri-material, just as in the bi-material case, the mode-mixity was obtained in terms of a single scalar quantity, ω, which is independent of the applied loading. The derivation of the single scalar parameter that is insensitive to changes in the mode-mixity is extremely useful to the engineering community and is a strong addition to the literature. Moreover, it was demonstrated in this project using a novel test rig that by independently controlling the application of moments, it is possible to achieve a wide range of mode-mixity conditions. Mixed mode fracture testing was performed on foam and honeycomb core specimens using this newly developed test rig.

The majority of the work carried out in this project was financially supported by the Danish Centre for Composite Structures and Materials (DCCSM), funded by the Danish Council for Strategic Research within Sustainable Energy and Environment. Four journal articles (P1 - P4) and five conference proceedings are the result of this support. Mixed-mode fracture evaluation of aircraft grade honeycomb core specimens was carried out as part of the project - Disbond of Sandwich Structures (DoSS) funded by the European Aviation Safety Agency (EASA), which resulted in two technical reports and one journal article (P5).

1.4 Thesis Outline

This is a summary style Thesis where the chapters are presented based on the results from journal articles. A brief introduction to the specific subject matter is discussed prior to summarizing the main results from the papers. Therefore, the reader is encouraged to look into the appended papers for more detailed discussions. Note that the chapters and papers are arranged in a manner such that a common line interconnects the various studies performed in this Thesis. A brief summary of the chapters is given below:

Chapter 2: The bi-material fracture mechanics approach applied at the sandwich face/core interface is presented. An introduction to the numerical mode-mixity method, Crack Surface Displacement Extrapolation Method (CSDE) is also provided followed by a brief overview of various fracture mechanical test methods utilized in sandwich constructions.

Chapter 3: Summary of the parametric study using the numerical SCB sandwich model is presented based on Paper P1. In addition, results from the foundation analysis of a moment- and force- loaded SCB sandwich specimen from Paper P2 are presented .

Chapter 4[1]: This chapter is based on Papers P3 - P5. The analytical model for a typical Double Cantilever Beam loaded with Uneven Bending Moments (DCB-UBM) bonded with stiffer reinforcement layers is provided. A brief discussion of the test rig and control algorithm implementation followed by results from fracture mechanical testing of foam and honeycomb core sandwich specimens are provided.

Chapter 5: The major outcomes of this Thesis along with future aspects that can be pursued are presented in this chapter. The efforts to initiate standardization of mixed mode fracture characterization of sandwich composites using the DCB-UBM specimen is also discussed.

[1]This also includes knowledge and insight from the author's previous work within the domain of debond phenomenon and in particular, Double Cantilever Beam (DCB) specimen loaded with moments [14, 15].

Chapter 2

Fracture Mechanics at the Face/Core Interface

The fracture mechanics approach utilized in the face/core interface is provided in this chapter. The debond in a sandwich is considered akin to a crack in a bi-material interface, and is treated under the ambit of Linear Elastic Fracture Mechanics (LEFM). The mode-mixity method, Crack Surface Displacement Extrapolation Method (CSDE) is also presented. A short review of prominent fracture mechanical test methods that exist in the literature are also presented.

2.1 Linear Elastic Fracture Mechanics

The foundation of the present day fracture mechanics was laid down by Griffith almost a century ago when he applied the first law of thermodynamics to study cracks in brittle materials [16]. Griffith propounded that the crack is caused by sudden annihilation of the tractions acting on the surface and that the crack can grow only if the total energy decreases or remains constant. Now, employing an elastic potential for a cracked body:

$$\Pi = W - U \tag{2.1}$$

where Π is the potential energy, W is the work performed by the external forces and U is the stored strain energy in the body. Therefore, in order for the crack to propagate a greater amount of energy is required to overcome the surface energy of the material. Irwin and Kies [17] extended Griffith's concept by considering plastic deformations around the crack tip and proposed that the energy-release rate can be expressed as a measure of the available energy for crack growth as:

$$G = -\frac{d\Pi}{dA} \tag{2.2}$$

where dA denotes the area over which incremental crack growth takes place. Thus, the crack grows under equilibrium conditions and the external work performed equals the energy needed to create new surfaces. The critical energy required to create an incremental crack area is referred to as the fracture toughness, G_c or Γ.

$$G = -\frac{dW_s}{dA} \tag{2.3}$$

where W_s is the energy required for the creation of new surfaces. Thus, crack propagation occurs when the externally supplied energy is greater than the fracture toughness or the critical energy-release rate, $G > G_c$.

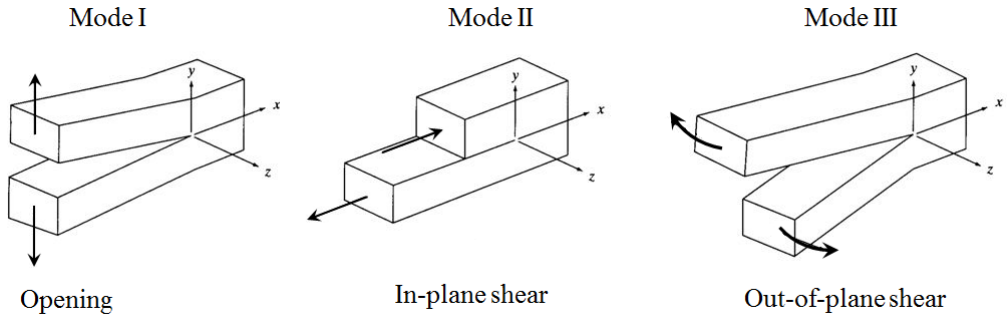

Figure 2.1. Fracture modes: mode I (opening), mode II (in-plane shear) and mode III (out-of-plane shear).

The external load causes the crack to be opened in any of the three basic fracture modes (see Figure 2.1): opening mode (mode I), in-plane shear (mode II) and out-of-plane shear (mode III). Based on the applied loading, the crack might be loaded predominantly in either one of the three modes or often in combination of different modes. In general, the total energy-release, G, associated is decomposed and expressed as a summation of the basic fracture modes:

$$G = G_I + G_{II} + G_{III} \tag{2.4}$$

where G_I, G_{II} and G_{III} are the energy-release rate associated with mode I, II and III, receptively. For the simplicity of analysis in a 2-D scenario, only mode I and mode II are considered. The stress singularity which exists very close to the crack tip in a typical 2-D crack case (see Figure 2.2) was described by Suo and Hutchinson [18] in a polar coordinate system as:

$$G_{ij} = \frac{K_I}{\sqrt{2\pi r}}\sigma_{ij}^I(\theta) + \frac{K_{II}}{\sqrt{2\pi r}}\sigma_{ij}^{II}(\theta) + T(r,\theta)\delta_{i1}\delta_{1j} \tag{2.5}$$

where δ_{ij} is the Kronecker's delta, T is the non-singular stress field parallel to the crack-surfaces, r and θ are the radius and angle respectively, with the origin located at the crack tip. The shape of the stress field is given by the two terms $\sigma_{ij}^I(\theta)$ and $\sigma_{ij}^{II}(\theta)$ which are functions of θ.

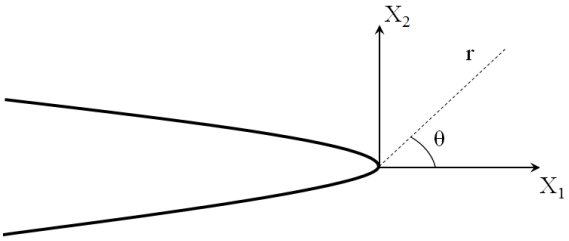

Figure 2.2. Homogeneous crack-tip field definitions.

In the 2-D crack tip definition illustrated in the Figure 2.2, only two cases of modes exist. In such a 2-D scenario, it can be noted that under mode I condition the stress field is symmetric with respect to the crack line such that:

$$\sigma_{22}^{I} = 1 \quad \text{and} \quad \sigma_{12}^{I} = 0 \quad \text{for} \quad \theta = 0 \tag{2.6}$$

Similarly, for a pure mode II loading case, the stress field is anti-symmetric with respect to the crack line resulting in:

$$\sigma_{22}^{I} = 0 \quad \text{and} \quad \sigma_{12}^{II} = 1 \quad \text{for} \quad \theta = 0 \tag{2.7}$$

Therefore, the stress intensity factors K_I and K_{II} can be defined in terms of the stress amplitudes as:

$$\sigma_{22} = \frac{K_I}{\sqrt{2\pi r}};\ \sigma_{12} = \frac{K_{II}}{\sqrt{2\pi r}}; \quad \text{for} \quad \theta = 0 \tag{2.8}$$

Now, the mode-mixity may be expressed as the ratio of the two stress intensity factors as:

$$\psi = arctan\left(\frac{K_{II}}{K_I}\right) \tag{2.9}$$

Irwin derived the relation between the stress intensity factors K_I and K_{II} and the energy-release rate, G as:

$$G = \frac{K_I^2 + K_{II}^2}{\overline{E}} \tag{2.10}$$

where $\overline{E}$ is the Young's modulus for plane stress and plane strain conditions defined as:

$$\overline{E} = E \quad \text{for plane stress} \tag{2.11a}$$

$$\overline{E} = \frac{E}{1-\nu^2} \quad \text{for plane strain} \tag{2.11b}$$

The displacement field near the crack tip zone can be expressed in terms of stress intensity factors, with δ_2 representing the relative crack flank opening, and δ_1, the relative crack flank sliding or shearing (see Figure 2.3).

$$\delta_2 = \frac{8K_I}{\overline{E}}\sqrt{\frac{r}{2\pi}};\ \delta_1 = \frac{8K_{II}}{\overline{E}}\sqrt{\frac{r}{2\pi}} \tag{2.12}$$

The near tip stress field can be described using both the stress intensity factors K as well as the energy-release rate, G. In the case of metals, stress intensity factors are extensively employed. However, in composite materials energy-release rate, G, is used to quantify the near tip stress fields. The definition of local crack tip stress field to obtain K is not so straightforward in the case of laminate composites. The calculation of stress intensity factors for composites comprising of orthotropic materials will result in oscillatory singularities and complex terms involving both real and imaginary parts complicating the use of linear elastic fracture mechanics [18].

2.2 Bi-material Fracture Mechanics

Many modern day materials are layered; meaning they are comprised of multiple material systems having varying properties. The fracture mechanics to deal with interfaces on layered materials is different from that of homogeneous materials. A simple explanation supporting this claim is the fact that cracks in isotropic, homogeneous materials propagate such that pure mode I conditions exist at the crack tip. Despite the possibility that the initial loading may differ from mode I, the crack will kink and propagate in a direction where pure mode I condition exists. On the other hand, crack growth in an interface between two different material systems will not demonstrate such a behavior [19]. The crack propagation in an interface between dissimilar materials is invariably mixed-mode in nature. This is the result of difference in properties of the two materials across the interface which generates both shear and normal stress fields at the crack tip. In case of face/core interface debonds in sandwich composites, the crack lies inherently between two materials where a huge elastic mismatch exists. The critical energy-release rate or fracture toughness of the interface is highly influenced by the mode-mixity [20]. Therefore, in case of bi-material fracture mechanics it is vital to ascertain the mode-mixity in order to fully describe the energy-release rate.

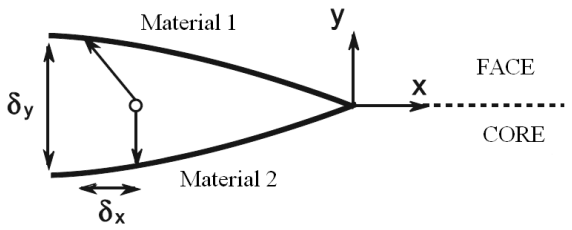

Figure 2.3. Interface crack tip geometry in sandwich composite

The displacements and stresses in the case of an interface crack between two dissimilar materials were derived by Suo and Hutchinson [21] under the premise that the materials

were isotropic elastic layers. The face/core interface crack tip is described in a similar way, where the debond is present between two different materials; face and core (see Figure 2.3). Therefore, the displacement and stress field at the face/core interface are described by [21]:

$$\sqrt{\frac{H_{11}}{H_{22}}}\delta_y + i\delta_x = \frac{2H_{11}K|x|^{\frac{1}{2}+i\varepsilon}}{\sqrt{2\pi}(1+2i\varepsilon)\cosh(\pi\varepsilon)} \tag{2.13}$$

$$\sqrt{\frac{H_{22}}{H_{11}}}\sigma_{yy} + i\sigma_{xy} = \frac{K|x|^{i\varepsilon}}{\sqrt{2\pi x}} \tag{2.14}$$

where K is the complex stress intensity factor defined as:

$$K = K_1 + iK_2 \tag{2.15}$$

and δ_y and δ_x are the relative opening and sliding displacements of the crack flanks, σ_{xx} and σ_{yy} are the normal and shear stresses, respectively. The closed form expressions in case of homogeneous material system in section 2.1 is described in 1-2 coordinate system. In order to distinguish the face/core debond interface, a x-y coordinate system is used here where the longitudinal tensor can be identified with x and the transverse tensor with y (see Figure 2.3). The bi-material constants H_{11} and H_{22} in Equations 2.13 and 2.14 are given by:

$$H_{11} = \left[2n\lambda^{1/4}\sqrt{S_{11}S_{22}}\right]_1 + \left[2n\lambda^{1/4}\sqrt{S_{11}S_{22}}\right]_2 \tag{2.16}$$

$$H_{22} = \left[2n\lambda^{-1/4}\sqrt{S_{11}S_{22}}\right]_1 + \left[2n\lambda^{-1/4}\sqrt{S_{11}S_{22}}\right]_2 \tag{2.17}$$

The oscillatory index, ε, is given by :

$$\varepsilon = \frac{1}{2\pi}\ln\left(\frac{1-\beta}{1+\beta}\right) \tag{2.18}$$

where β is a bi-material interface constant (Dundur's bi-material parameter) defined as [22]:

$$\beta = \frac{\left[S_{12} + \sqrt{S_{11}S_{22}}\right]_2 - \left[S_{12} + \sqrt{S_{11}S_{22}}\right]_1}{\sqrt{H_{11}H_{22}}} \tag{2.19}$$

Parameters λ and n are non-dimensional orthotropic constants expressed in terms of the components of the compliance matrix S_{ij}.

$$\lambda = \frac{S_{11}}{S_{22}} \tag{2.20a}$$

$$n = \sqrt{0.5\,(1+\rho)} \quad \text{where} \quad \rho = \frac{2S_{12} + S_{66}}{2\sqrt{S_{11}S_{22}}} \tag{2.20b}$$

$$S_{11} = \frac{1}{E_1} \ , \ S_{12} = S_{21} = -\frac{\nu_{12}}{E_1} = -\frac{\nu_{21}}{E_2} \tag{2.20c}$$

$$S_{22} = \frac{1}{E_2} \quad \text{and} \quad S_{66} = -\frac{1}{G_{12}} \tag{2.20d}$$

The above set of equations are defined for plane stress conditions,where $\overline{E} = E$ (see Equation 2.11a). For plane strain conditions, the components of the compliance should be slightly modified as:

$$S^*_{ij} = S_{ij} - \frac{S_{i3}S_{j3}}{S_{33}} \tag{2.21}$$

where i and j correspond to the x and y direction according to the coordinate system shown in Figure 2.3. The displacement and stress field expressions for a bi-material interface are similar to the ones defined for homogeneous materials (refer to section 2.1). However, it should be noted that in the case of a face/core bi-material interface, the stress intensity factors K_1 and K_2 no longer serve as the stress amplitudes for mode I and mode II. This is due to the mix-up of traditional stress intensity factor definition and can be attributed to the term $|x|^{i\varepsilon}$.

$$K|x|^{i\varepsilon} = [K_1 \cos(\varepsilon \ln x) - K_2 \cos(\varepsilon \ln x)] + i\,[K_2 \cos(\varepsilon \ln x) + K_1 \cos(\varepsilon \ln x)] \tag{2.22}$$

Therefore, in order to distinguish between traditional homogeneous and non-homogeneous stress intensity factors, Arabic numerals are used in the case of bi-material stress intensity factors. The interface stress intensity factors (Arabic) have the same role as the ones used in the case of homogeneous, isotropic materials (roman). The mode component, K_1, is the amplitude of the singularity of the normal stresses ahead of the crack tip and the associated normal separation of crack flanks, whilst K_2 governs the shear stress on the interface and the relative shearing displacement. The term $|x|^{i\varepsilon}$ is also responsible for introducing oscillatory behavior in the stress solution towards the crack tip as $x \to 0$. This oscillation can be filtered out using a mode-mixity method as such oscillations are restricted only to a very small zone near the crack tip.

The mode-mixity can be expressed using the definition provided by Hutchinson and Suo [18] as:

$$\psi = \tan^{-1}\left[\frac{\Im\left(Kh^{i\varepsilon}\right)}{\Re\left(Kh^{i\varepsilon}\right)}\right] \tag{2.23}$$

where h is the characteristic length of the crack problem chosen arbitrarily.

Now, the complex stress intensity factor (Equation 2.15) can be related to strain energy release rate as [23]:

$$G = \frac{H_{11}|K|^2}{4\cosh^2(\pi\varepsilon)} \tag{2.24}$$

The displacement field formulated in Equation 2.13 can be used to express the energy release rate and the mode-mixity phase-angle in terms of the relative opening and sliding displacements of the crack flanks as [18]:

$$G = \frac{\pi\left(1+4\varepsilon^2\right)}{8H_{11}|x|}\left(\frac{H_{11}}{H_{22}}\delta_y^2+\delta_x^2\right) \tag{2.25}$$

$$\psi = \tan^{-1}\left(\sqrt{\frac{H_{22}}{H_{11}}}\frac{\delta_x}{\delta_y}\right) - \varepsilon\ln\left(\frac{|x|}{h}\right) + \tan^{-1}\left(2\varepsilon\right) \tag{2.26}$$

This characteristic length, h is chosen in a way such that the phase angle, ψ can be related to a parameter of the specimen although it does not have a physical meaning. The parameter h is often considered to be the thickness of the face sheet, h_f so that the critical minimum value of the critical energy-release rate is located at $\psi = 0$.

2.3 CSDE Mode-mixity Method

In the previous section, the expressions to obtain energy-release rate (G) and mode-mixity phase angle (ψ), in terms of relative opening and sliding displacements of the crack flanks for a bi-material interface were provided (see Equations 2.25 and 2.26). Therefore, G and ψ can be formulated in a user-written subroutine in any commercial finite element software package to predict whether the crack propagation may occur or not. There are several finite element based mode-mixity methods available in the literature to extract energy-release rate and mode-mixity phase angle of a typical bi-material interface. The prominent methods include: Virtual Crack Extension method (VCE), introduced by Matos et al. [24], the Virtual Crack Closure Technique (VCCT) first presented by Rybicki and Kanninen [25] in classical form, which was later modified for orthotropic materials by Beuth [26] and the Crack Surface Displacement (CSD) method [24, 27, 28].

It was reported by Williams [29] that, both energy-release rate and phase angle exhibit oscillatory behavior close to the crack tip. He examined crack in two separate isotropic homogeneous regions and this sharp oscillatory behavior is proportional to $r^{-1/2}$. However, such oscillations are physically impossible as it implies interpenetration of crack flanks. Erdogan [30] observed that this region of oscillation was in the order of 10^{-6} of the crack length. It was also found that the first event of crack flank interpenetration occurs at 10^{-4} of the crack length [31]. Therefore, this oscillatory behavior should be mathematically avoided for an accurate estimation of both energy-release rate and mode-mixity especially in the case of a sandwich face/core interface where the oscillations are pronounced.

A new mode-mixity method which circumvents the problem of crack tip oscillation called the Crack Surface Displacement Extrapolation (CSDE) method was introduced by Berggreen et al. [32]. The CSDE method uses the relative crack flank displacements, δx, and δy, to calculate both energy-release rate, G and phase angle, ψ (see Equations 2.25 and 2.26). In addition, this method exploits the fact that both G and ψ is linear in the K-dominant zone (before the oscillatory field) close to the crack tip. The linear variation is utilized

to extrapolate both energy-release rate and mode-mixity phase angle to the crack tip by calculating the slope, thereby completely avoiding the oscillatory region. A schematic illustration of the CSDE method is provided in Figure 2.4.

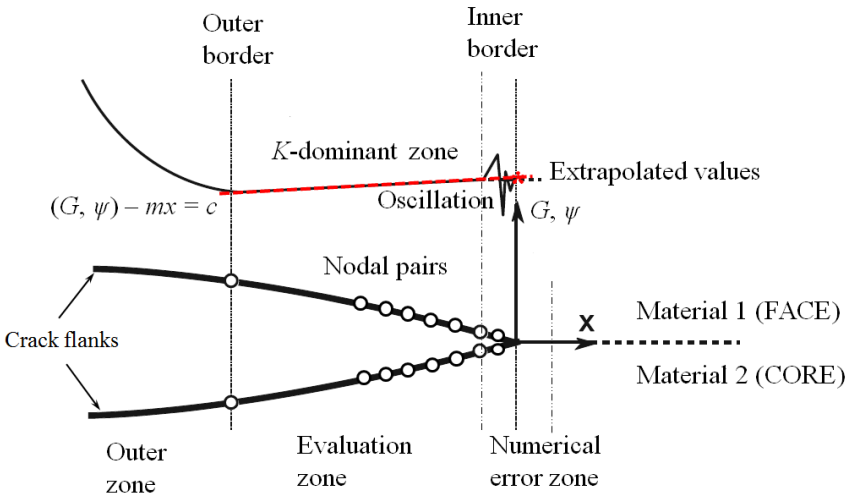

Figure 2.4. A schematic illustration of the CSDE method.

The CSDE method can be easily implemented as a user-written subroutine along with any standard Finite-Element (FE) code. In this Thesis, the CSDE method was implemented along with the FE-code, ANSYS® [33]. The user-written subroutine identifies the linear transition zone. This routine determines the inner and outer zone by stepping forward and backward after computing the energy-release rate. As the K-dominant zone has to be linear, the subroutine identifies the nodal pair coordinates at which the linearity ceases to exist. In sandwich constructions where there is predominant face/core interface stiffness difference and large crack-tip distortions (which in-turn lead to oscillations), the CSDE method has been proved to be very robust against the other listed mode-decomposition methods [32, 34].

The phase angle expression in Equation 2.26 includes parameters such as oscillatory index, ε, and Dundur's parameter, β to calculate mode-mixity phase angle which is referred to as the full formulation, ψ_F. The CSDE method calculates ψ_F using actual values of ε and β. The linear elastic solution shows that the crack faces interpenetrate and stresses oscillate near the crack-tip region. This oscillation is however, confined to a very limited zone around the crack-tip. To circumvent the problems of oscillation and interpenetration, it is convenient to assume $\beta = 0$ in Equation 2.26. The stress-field becomes square-root singular for $\varepsilon = 0$ and K_1 and K_2 for homogeneous bi-materials recover their physical meaning, $K = K_I + K_{II}$. This approach is denoted as "reduced" formulation. The phase angle for this approach becomes:

$$\psi_R = tan^{-1}\left(\frac{\delta_x}{\delta_y}\right) \tag{2.27}$$

In terms of the reduced phase angle (in degrees), a pure mode I corresponds to 0°, and 90° corresponds to a pure mode II loading at the crack tip. For brevity, the reduced

formulation is used without the subscript and is denoted as ψ. Similarly, the energy-release rate can be expressed as:

$$G = \frac{\pi(\delta_x^2 + \delta_y^2)}{2x(c_1 + c_2)} \tag{2.28}$$

where x is the distance from the crack tip and c_1 and c_2 are stiffness parameters of the face sheet and core given by:

$$c_m = \frac{\kappa_m + 1}{S_m} \tag{2.29}$$

The parameter, κ_m, is Muskhelishwili's constant given by [35]: $\kappa_m = (3 - 4\nu_m)$ for plane strain and $\kappa_m = (3 - \nu_m)/(1 + \nu_m)$ for plane stress, where ν_m is Poisson's ratio with m = 1 and 2 for the face and core, respectively and S_m is the shear modulus.

2.3.1 LEFM Applied to Bi-material Interfacial Cracks

A note is provided with regard to the assumptions made under the ambit of LEFM used in the analyses throughout this Thesis. The assumptions presented here are similar to the ones made in the literature by several other researchers [34, 36]. The numerical tools presented in this Thesis do not focus on the debond damage causing event, rather impetus was laid out to understand the subsequent influence caused due to the debond. Therefore, the debonding phenomenon was treated with a set of assumptions which are laid out as follows:

1. The facesheet and core in the debonded and intact regions of a specimen were assumed to exhibit identical, orthotropic material properties. Thermal residual stresses resulting from the sandwich fabrication process, which may affect the crack tip loading conditions were not considered.
2. The face/core interface was treated akin to a plane interface between two solids and the debond represented an area where there is lack of an adhesion between the two solids. In addition, to prevent interpenetration or overlapping of the cracked surfaces, the debonded region was also modeled using frictionless contact surfaces. In the commercial code ANSYS®, the contact surfaces were modeled using the element types - TARGET169 and CONTACT172. The contact modeling is computationally expensive and was kept as an add-on feature to check the presence of interpenetration of crack flanks.
3. The core was modeled as homogeneous in the numerical models. For instance, the cellular micro-structure in case of a PVC foam and the hexagonal cells in a honeycomb core were neglected. The homogenization of honeycomb cores posed certain challenges which were solved using both analytical and numerical approaches.
4. The failure process zone is assumed to be much smaller when compared with the K-dominant zone, which is of the order $h/50$ with $h = h_f$.

2.4 Fracture Mechanical Testing of Sandwich Composites

A short review of various sandwich fracture specimens available in the literature are provided in this section. Figure 2.5 illustrates some of the prominent sandwich fracture specimens. Several fracture mechanical methods have been developed over the past two decades for characterizing face/core interface of a typical sandwich system. Most of the specimens designed for fracture characterization of sandwich interfaces are generally based on interfacial fracture tests of monolithic laminate specimens. It is worth noting that a standard test method to assess interface toughness in sandwich composites does not exist. On the other hand, several ASTM International standards are available for assessing delamination toughness in laminate composites [7, 8, 9, 10, 11].

Prasad and Carlsson used a modified Double Cantilever Beam (DCB) (Figure 2.5a) sandwich specimen [37, 38] to investigate debonding in foam core sandwich specimens. A kinematic model of the DCB sandwich specimen, based on foundation model, also exists [39]. Carlsson et al. [40, 41] developed a Cracked Sandwich Beam (CSB) (Figure 2.5b) to characterize shear failure in sandwich specimens. Tilted Sandwich Debond (TSD) specimen was introduced by Li and Carlsson [42] and a kinematic analysis based on foundation model was also developed by the same authors [43, 44]. The TSD test set-up was modified by Berggreen et al. to test compliant foam cores [45, 46]. By tilting the specimen by a specific angle, θ, interface crack propagation is ensured for certain class of sandwich specimens in the TSD test method.

Cantwell and Davies [47] used a Single Cantilever Beam (SCB) (Figure 2.5e) sandwich specimen to study debonding in honeycomb core sandwich specimens by modifying a peel test. The SCB test setup was modified by the same authors to test GFRP/balsa sandwich specimen by applying the peel load on the bottom face sheet [48]. The SCB sandwich specimen has gained wide attention recently owing to its simplicity and is currently under the process of becoming an international standard. A sizing study of the SCB sandwich specimen was performed by Ratcliffe and Reeder [49].

The Mixed-Mode Bending (MMB) (Figure 2.5d) specimen first introduced by Reeder and Crews [50] is extensively used in estimation of delamination fracture toughness of monolithic composites and is an ASTM International standard [9]. The MMB specimen was extended to sandwich composites by Quispitupa et al. [51, 52, 53, 54]. In recent years, fatigue testing of MMB sandwich composites using a G-control method was also developed by Manca et al. [55, 56]. The DCB specimen loaded with unequal or uneven moments was first introduced by Sørensen et al.[57] and was later extended to sandwich composites by Lundsgaard-Larsen et al. [58]. In this Thesis, focus was laid on SCB and DCB-UBM (Figure 2.5f) sandwich specimens. Other sandwich specimens that are worth noting are the End-Loaded Sandwich Specimen (ELSS) and Center Notch Flexure Sandwich (CNFS) [59].

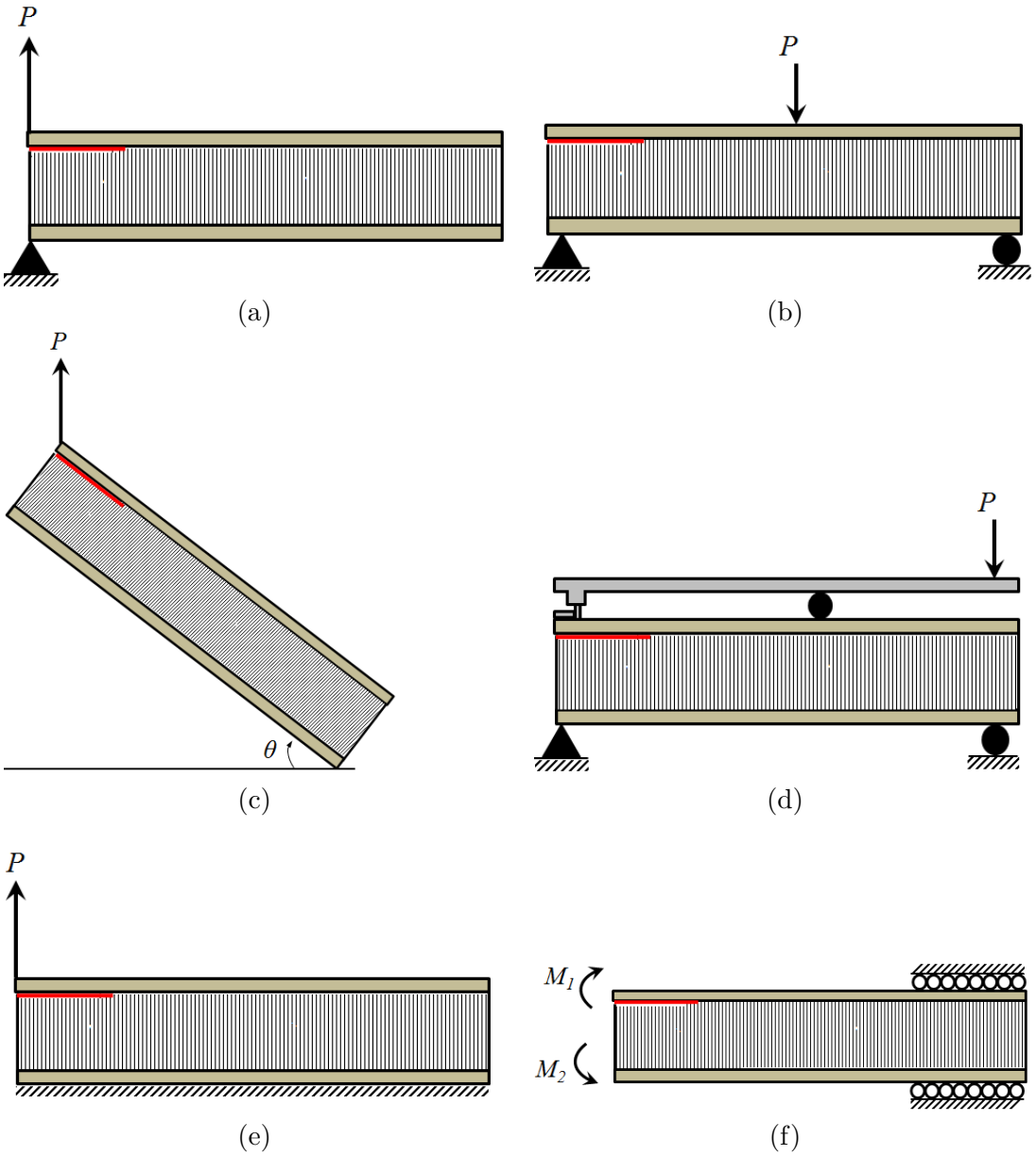

Figure 2.5. Sandwich fracture specimens: (a) DCB, (b) CSB, (c) TSD, (d) MMB, (e) SCB and (f) DCB - UBM

Chapter 3

Fracture Mechanics Analysis of SCB Sandwich Specimen

This chapter summarizes the results from Papers P1 and P2, in which the Single Cantilever Beam (SCB) sandwich specimen was the subject of focus. A parametric study using the numerical mode-mixity method, CSDE was performed on the SCB sandwich specimen and recommendations with regard to modification of the test methodology was provided. Furthermore, foundation analysis of a moment- and force- loaded SCB sandwich fracture specimens were carried out. Detailed discussions and results can be found in the papers provided in Appendix A.

3.1 Introduction

Similar to laminates, the most critical debonding phenomenon in sandwich composites is likely to be mode I dominated in which the face sheet is peeled off from the core. The SCB test configuration was found to be the most suitable for measuring debond toughness associated with the peel loading scenario. The SCB sandwich specimen, first discussed in [48, 60] comprises of a pre-crack, a, between the upper face sheet and the core. A loading rod is used to apply a peel dominant force to separate face sheet from the core. The specimen is rigidly held to the base by firmly fixing the lower face sheet to prevent any displacement or rotation. Figure 3.1a provides a schematic illustration of the SCB sandwich specimen. The pre-crack (a), is a discontinuity in the face/core interface usually introduced in the production phase in the form of a Teflon® film. The pre-crack can also be introduced by saw-cut and further sharpening of the crack front. A loading rod through which a pulling force is applied, is attached to the upper debonded face sheet using a piano hinge. The loading rod and hinge collectively ensure that the load application point remains vertical.

SCB testing is conducted in displacement control by pulling the loading rod at a constant rate. The specimen is unloaded when the crack length increases to a_1, see Figure 3.1b. A

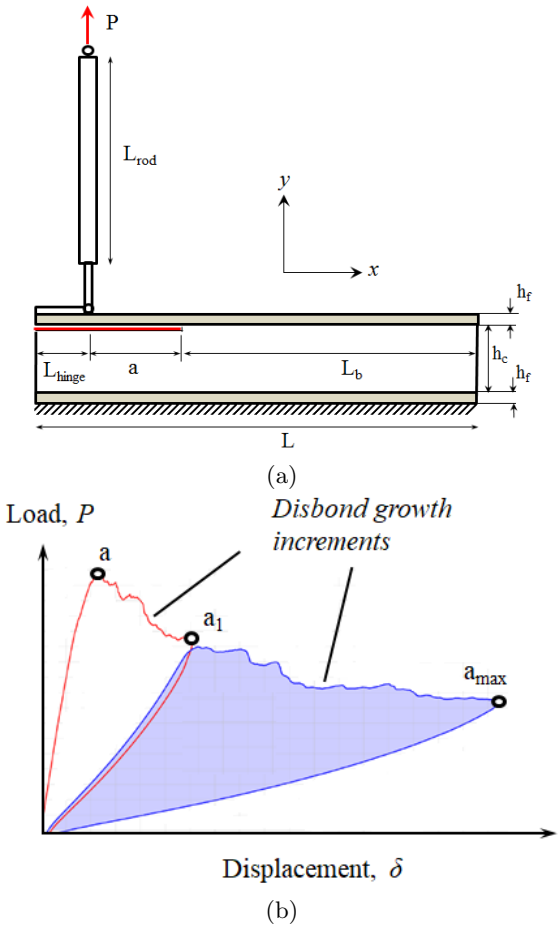

Figure 3.1. (a) Schematic illustration of SCB sandwich specimen, and (b) typical force-displacement response of a SCB sandwich specimen.

suitable image recording device is used for accurate estimation of the crack lengths. Various methods to reduce the energy-release rate have been proposed for the SCB sandwich test [61]: area method, modified beam theory and compliance calibration method. The latter two methods require a linear force-displacement response, which specimens with thin face sheets may not yield. The area method is widely used to encompass fracture testing of a wide array of sandwich configurations. The strain energy-release rate is calculated from the load-displacement response (P vs. δ) curve obtained during a test. For an incremental increase in debond length by da, the energy-release rate is given by:

$$G = \frac{1}{b}\frac{dU}{da} \tag{3.1}$$

where U is the elastic strain energy in the specimen, which can be calculated from area beneath the P vs. δ curve in Figure 3.1b, and b is the width of specimen.

Efforts are underway to create a mode I dominant ASTM International standard and SCB sandwich specimen was identified as the most promising candidate due to the following reasons [62]:

1. The test involves a simple loading fixture
2. Debond front conditions were found to be uniform over debond lengths
3. Debonding was found to take place along or near the face/core interface, rather than kinking into the core
4. The data reduction method used for computing debond toughness involves a straightforward compliance calibration procedure.

Recently, a round robin exercise [12] spear-headed by the aerospace industry was carried out to test the efficacy of the SCB sandwich specimen. When developed as an industrial standard, the SCB fracture test is poised to be used by different industry clientele and in configurations in which the stiffness mismatch across the sandwich interface varies with each user. Therefore, in order to establish a reliable test protocol, the critical strain energy-release rate measured using the SCB test method must be under mode I conditions at all crack lengths. The existing SCB specimen design is based on kinematic solution detailed by Ratcliffe and Reeder [49]. The compliance based solution in [49] is based on a beam on elastic foundation approach originally introduced by Kanninen [63]. Several limitations were imposed on the SCB sandwich specimen by restricting the specimen geometry, pre-crack length (a), loading rod length (L_{rod}), face and core thicknesses (h_f, h_c), such that the shear component at the crack tip is kept to a minimum.

The sizing study detailed in [49] ensures that the SCB specimen response remains linear; however this approach overlooks the mode-mixity condition at the crack tip. Crack propagation along a sandwich face sheet/core interface is invariably mixed mode in nature due to the inherent elastic mismatch across the interface. A major consequence is that the energy-release rate becomes a function of mode-mixity [18]. The mode-mixity can be expressed in terms of a phase angle, ψ, which can be defined as the arc tangent of the ratio of sliding to opening displacement of the crack tip [18] (refer to section 2.2). An exhaustive experimental campaign to determine the mode-mixity influence in the SCB test spanning numerous specimens will be very expensive. At the time of compiling of this Thesis, a closed form expression to accurately ascertain mode-mixity phase angle at various crack lengths for a typical SCB sandwich fracture specimen did not exist. A parametric analysis was conducted to study what influence of various material and geometrical parameters of the SCB sandwich specimen have on the mode-mixity. This analysis was based on the numerical fracture mechanical tool, the Crack Surface Displacement Extrapolation (CSDE) method [32] (refer to section 2.3) and was the subject of [P1].

3.2 Parametric Fracture Analysis of SCB Sandwich Specimen - Paper P1

This section outlines the results presented in Paper P1. Hypothetical sandwich systems were studied to identify the critical governing parameters that influence crack tip mode-mixity in a SCB sandwich specimen. The SCB specimen was investigated from a local crack tip mode-mixity perspective using the CSDE method. The influence of critical parameters which may affect the mode-mixity condition were studied. In addition, rep-

resentative sandwich configurations from aerospace, marine and wind sectors were also investigated. Major inferences from [P1] are given below [1].

In terms of phase angle (in degrees), a pure mode I corresponds to 0°, and 90° corresponds to a pure mode II loading at the crack tip. For the parametric analysis, a mode I dominance is assumed to exist within the bounds: -10° $\leq \psi \leq$ 10°. Detailed description of the SCB finite element model is provided in section 3.2.1. The list of parameters which may influence whether the fracture testing remains in mode I regime is provided in Table 3.1.

Table 3.1. Parameters altered in the SCB parametric numerical study.

SCB Parameters	
Core modulus, E_c [MPa]	100, 500, 1000
Facesheet Modulus, E_f [GPa]	5, 10, 50, 100, 200, 250
Core thickness, h_c [mm]	10, 40
Facesheet thickness, h_f [mm]	0.5, 3, 7
Loading rod length, L_{rod} [mm]	120, 250, 500

The Poisson's ratio of both face sheet and core were held constant at $\nu_f = 0.30$ and $\nu_c = 0.35$, respectively for the initial study. Throughout the analysis, length of the hinge was kept constant at, $L_{hinge} = 12.7$ mm, and the total length of the SCB specimen is given by: $L = L_{hinge} + a_{max} + L_b$.

For all analysis cases, the maximum debond length was held constant at, $a_{max} = 150$ mm. For the preliminary analysis, a specimen length, $L = 300$ mm was found to satisfy the minimum required length criterion defined in Equation 3.2 for all combinations of face/core materials enlisted in Table 3.1. Using the values provided in Table 3.1, the Dundur's parameter [64], $\alpha = \left(\bar{E}_1 - \bar{E}_2\right)/\left(\bar{E}_1 + \bar{E}_2\right)$ varied from 0.65 to 0.99 which are typical values found in a face/core interface.

3.2.1 Finite Element Model of SCB Sandwich Specimen

The Finite Element (FE) model of the SCB sandwich specimen employed for the parametric study is presented in Figure 3.2. The 2-D plane strain FE model was built using the commercial code, ANSYS® [33] and consisted of iso-parametric plane elements with a smallest element edge length of 2.5 μm. A 4-node linear PLANE 42 element type was used at the crack tip region in a small zone within a radius of four elements, to capture large near tip distortions and 8-node parabolic element type PLANE 82 were used in rest of the model[2]. The loading rod was modeled using a Beam (BEAM 3 element type) element which carries only tension and was hinged above the top face sheet. The hinge leaf was avoided in the analysis. Fixed boundary conditions were applied on the lower face sheet. A unit load per width ($P/b = 1$ N/mm) was applied on the loading rod. The CSDE mixed-mode partitioning method was implemented as a separate subroutine and

[1] The reader is advised to refer to Paper P1 for detailed discussions and results.

[2] The PLANE 42 and 82 element types have been archived in the ANSYS® element library and have been replaced with PLANE 182 and 183 element types, respectively.

utilizes only the relative crack flanks displacements. A highly dense mesh is required close to the crack tip, in-order to capture the K-dominant zone (see Figure 3.2). It should be noted that the results from the linear elements were not employed in the determination of mode-mixity phase angle using the CSDE method.

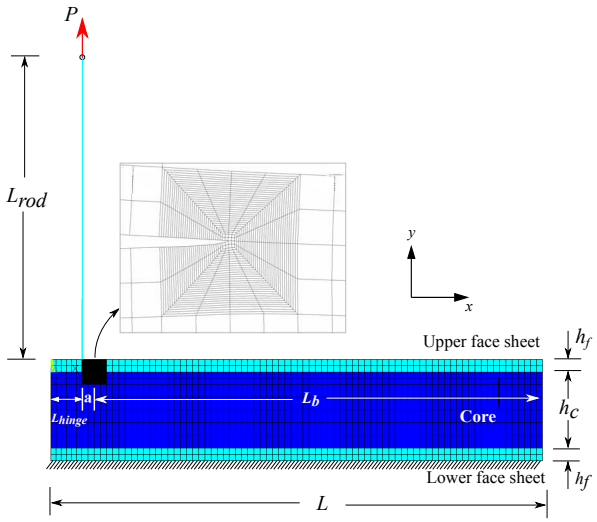

Figure 3.2. Finite Element Model of the SCB sandwich specimen with highly densified mesh in the crack tip region.

In addition, to prevent interpenetration or overlapping of the cracked surfaces, the debonded region was modeled using frictionless contact surfaces. In the commercial code ANSYS®, these contact surfaces were modeled using the element types - TARGET169 and CONTACT172. The contact modeling was computationally expensive and was used only to check for instances of interpenetration. When a case of crack flank interference was observed, the analysis was stopped. The FE analysis was carried out using the geometrical non-linear solver.

3.2.2 Influence of Core and Face sheet Moduli (E_f, E_c)

The effect of both face sheet and core moduli on the mode-mixity phase angle was investigated by choosing three core moduli, E_c = 100, 500 and 1000 MPa, with the face sheet moduli chosen in the range, E_f = 5 to 250 GPa. It was found that depending on the face sheet modulus, the face sheet thickness (h_f) along with the ratio of face sheet and core modulus, $\Sigma = E_f/E_c$ influence the mode-mixity phase angle, ψ. At small values of Σ, the phase angle (ψ) shifted toward the negative region, and for all the core moduli analyzed, ψ increased with Σ. Figure 3.3 shows the change in phase angle, ψ, with crack length and Σ for E_c = 1000 MPa. The mode I dominant regime (-10° $\leq \psi \leq$ 10°) can be identified from the plots using the scale bar. It is noted that, with increasing core stiffness and at small crack lengths, the phase angle deviated away from mode I regime. Thus, there is a significant influence by both face sheet and core moduli on the mode-mixity. In addition, core Poisson's ratio (ν_c) was also seen to influence the mode-mixity. For constant face sheet and core moduli, the mode-mixity phase angle increases and deviate away from mode I conditions with a decrease in ν_c.

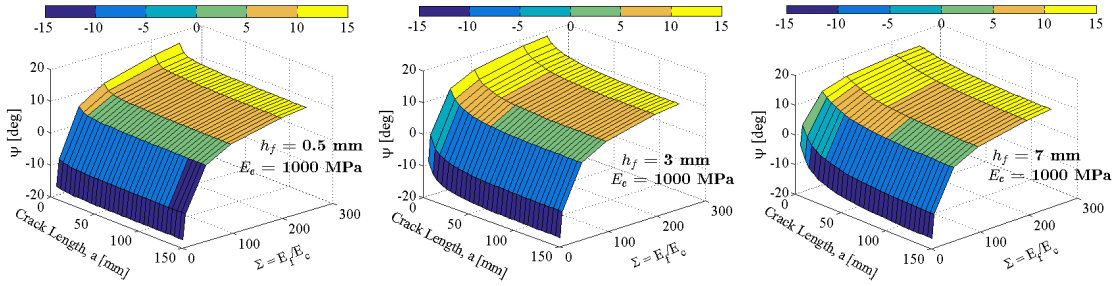

(a) (b) (c)

Figure 3.3. Mode-mixity phase angle (ψ) vs. crack length for E_c = 1000 MPa: (a) h_f = 0.5 mm (b) h_f = 3 mm (c) h_f = 7 mm. (h_c = 40 mm, L = 300 mm, L_{rod} = 500 mm)

3.2.3 Effect of Facesheet and Core Thickness (h_c, h_f)

It was observed that for constant face sheet thickness (h_f) stiffer fcesheets led to increasingly positive values of ψ, thereby deviating away from the mode I bounds. For a thicker core, the difference in phase angle for a thin and thick face sheet when crack length, a $\rightarrow$ a$_{max}$ is about 2°. In addition, for a thin core, a thicker face sheet yielded lower phase angle, ψ.

3.2.4 Effect of Intact Portion Length (L_b)

The intact length portion, L_b, is the remaining portion left in the length of the specimen when crack length, a, reaches a$_{max}$ (see Figure 3.1a). A minimum L_b, proposed in the literature is given by [43, 49]:

$$L_{b,\min} = \frac{2.7}{\lambda} \tag{3.2}$$

The parameter, λ, can be roughly described as the ratio of stiffness of the foundation to that of the debonded upper beam, expressed as:

$$\lambda = \sqrt[4]{\frac{k}{4E_f I}} = \left[\frac{3k}{E_f h_f^3 b}\right]^{1/4} \tag{3.3}$$

where k is the elastic foundation modulus. Equation 3.2 depends on the choice of k. The foundation modulus, k has been obtained empirically and several expressions exist in the literature [39, 43, 52, 63]. Based on the analysis using an Al/H100 specimen, the foundation modulus proposed by Li and Carlsson [43] was found to capture the shift in the phase angle well.

3.2.5 Influence of Loading Rod Length (L_{rod})

For the considered sandwich construction, modeled results showed significant deviation from mode I regime with loading rods shorter than 500 mm. Hence, a minimum rod length based on specimen length was proposed as: $L_{rod} \geq 1.70\ L$.

3.2.6 SCB Sandwich Specimen Reinforced with Doubler Layer

Fracture testing of sandwich specimens with thin face sheets, invariably causes excessive deformation [65]. A non-linear behavior will render it impossible to employ data reduction methods such as the modified beam theory (MBT) and the compliance calibration method. One way to circumvent this issue is by reinforcing the face sheets with a stiff layer usually referred to as "doublers" [66]. Furthermore, addition of a doubler layer may prevent the undesirable face sheet damage. The numerical study was extended to SCB sandwich specimens with doubler layers to ascertain whether the mode-mixity condition will remain within the mode I regime. Several materials with varying thickness were investigated and was found that addition of doublers will increase the mode-mixity phase angle, ψ, in the positive regime. This observation qualitatively agreed with a similar analysis performed on TSD sandwich specimen [45].

During the course of the analysis with doublers, the specimens were sized such that a minimum intact portion length, L_b was selected based on Equation 3.2. It was found that addition of doubler layer atop the debonded face sheet will cause the mode-mixity to spike at increased crack lengths, see Figure 3.4 for $h_d \geq 2$ mm. Therefore, the expression provided in Equation 3.2 was modified to include the flexural stiffness of the entire debonded beam reinforced with a doubler layer.

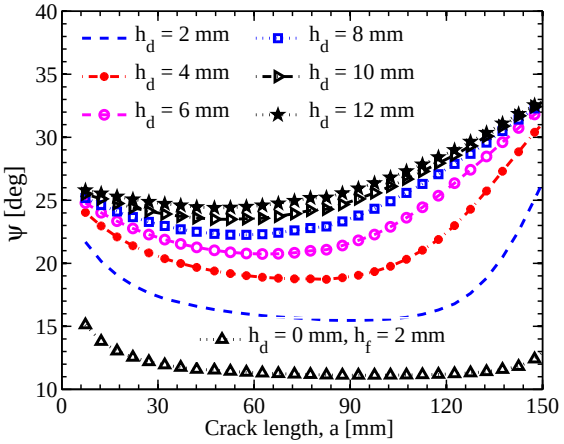

Figure 3.4. Phase angle (ψ) vs. crack length for a GFRP/H100 SCB sandwich specimen reinforced with doubler ($h_f = 2$ mm, $h_c = 25$ mm).

3.2.7 Case Studies

The numerical study was also extended to representative specimens found in typical industrial sectors such as marine, aerospace and wind. It was found that despite concurring to the sizing method detailed in [49], certain class of specimens violated mode I conditions. Figure 3.5 shows phase angle, ψ, vs. crack length for sandwich specimens found across several industrial sectors. The mode I bound is demarcated using a dotted line in Figure 3.5. For detailed description of material properties and test parameters, refer to [P1]. During the parametric study involving hypothetical and real sandwich configura-

tions, specimens that do not bound to the sizing requirements were also found to accord to the mode I conditions.

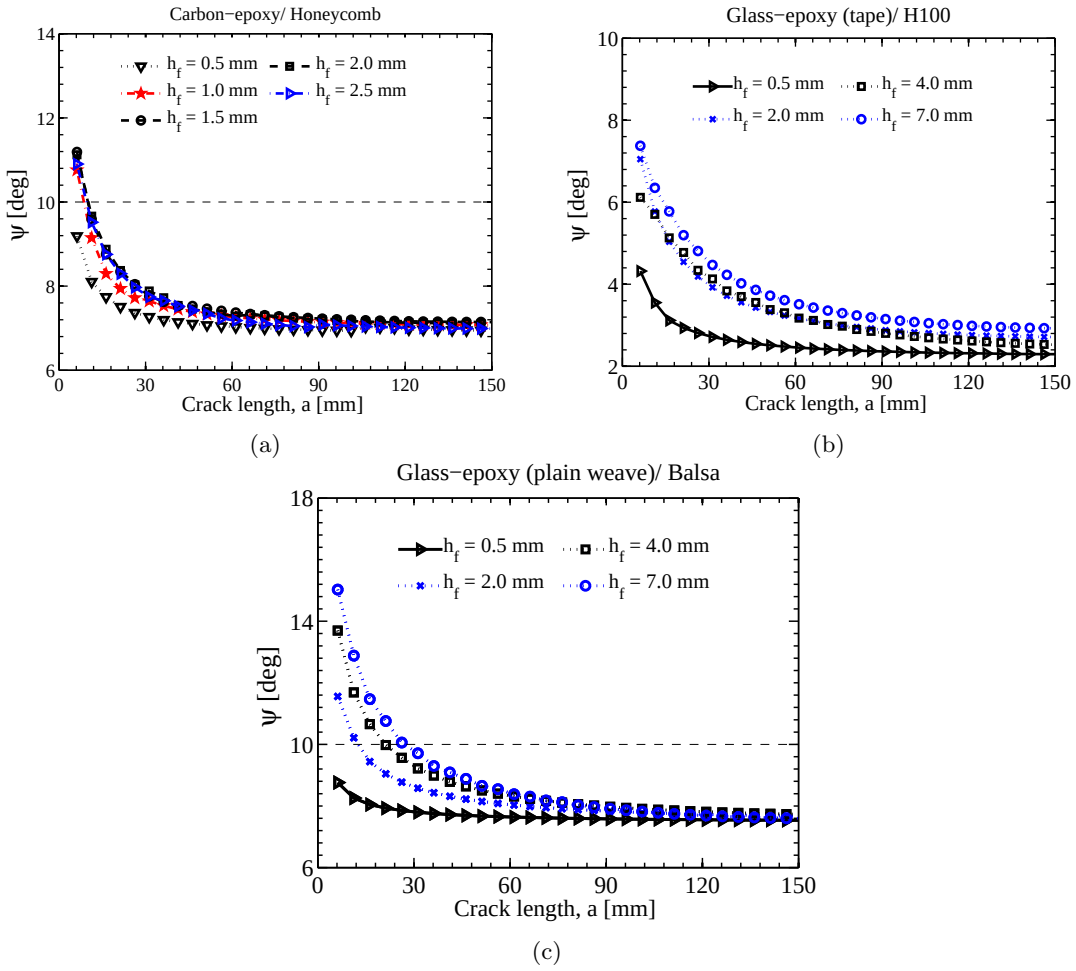

Figure 3.5. Mode-mixity phase angle (ψ) vs. crack length for (a) aerospace ($\Sigma = 1350$, $\alpha = 0.99$) (b) marine ($\Sigma = 138$, $\alpha = 0.99$), and (c) wind energy ($\Sigma = 7.2$, $\alpha = 0.75$). (L = 300 mm, $L_{rod} = 500$ mm).

3.3 Foundation Effects and Root Rotation in SCB Sandwich Specimen - Paper P2

The Paper P2 examined foundation effects on crack root rotation, energy-release rate and mode-mixity phase angle (ψ) on two loading cases of SCB sandwich specimen: moment and force loadings. The moment-loaded SCB sandwich specimen was treated using the Winkler mechanical model initially utilized by Kanninen for a DCB specimen [63]. A robust analytical framework was developed to capture the influence of transverse shear effects. The closed form expression proposed by Li et al. [67] was calibrated using Finite Element Analysis (FEA) for both types of loadings and consistent results were obtained. The following sections outline a brief summary of the findings presented in [P2].

Analysis of fracture specimens in the literature consider a sandwich element under axial force and moment loading, devoid of transverse shear forces [68, 69]. However, transverse shear component is inevitable in most fracture specimens such as SCB, DCB, ENF, TSD and MMB [39, 42, 48, 53, 70]. A significant influence of the foundation effect is that it causes the vertical section of the debonded upper face sheet layer to rotate [67]. The root rotation affects the fracture parameters and therefore, must be incorporated in the analysis. The crack root rotation[3] as shown in Figure 3.6, is not uniform across the section [71, 72]. Earlier attempts to incorporate the shear effects were done by Lu et al. [73], who considered a homogeneous cantilever beam with an embedded delamination and utilized FEA to compute the energy-release rate. Li et al. [67] found large influence of transverse shear on the energy-release rate and the mode-mixity phase angle (ψ) at short crack lengths. Andrews and Massabò [74] proposed a crack element approach where transverse shear forces act and developed a superposition scheme. In their approach, the root rotation depends linearly on crack tip stress resultants and obtained compliance coefficients numerically.

The foundation effects on crack root rotation, energy-release rate and mode-mixity phase angle was investigated for two cases of loading of SCB specimen in [P2], ie., moment and force loadings. The analytical framework and the analysis of moment-loaded SCB specimen case are provided in the subsequent sections.

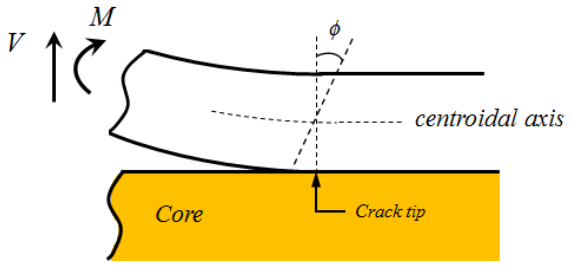

Figure 3.6. Illustration of crack tip root rotation.

3.3.1 Moment Loaded Semi-infinite Beam on Elastic Foundation

The sandwich DCB-UBM specimen (see Figure 2.5f) can be perceived as an upper face sheet resting on the core loaded with an end moment. Figure 3.7 shows a simplified foundation model approach of the DCB-UBM specimen wherein the lower face sheet is rigidly fixed. This configuration yields a SCB sandwich specimen loaded with an edge couple. The deformation kinematics of such a moment loaded specimen can be solved using the beam on elastic foundation approach. In the literature, the core has been modeled using higher-order sandwich theories [75, 76] as well as using the Winkler mechanical model [39, 43, 49, 67, 77, 78], which have been proven to be adequate. The Winkler model was followed in [P2] and the governing equation for deflection, *w(x)*, presented by Barber [72] is of the form:

[3]For the uninformed reader, this should not be confused with the angle between the section and centroidal axis, which is the shear strain at the crack tip.

$$EI\frac{d^4w}{dx^4} + kH(x)w = 0 \tag{3.4a}$$

$$H(x) = \begin{cases} 1, x > 0 \\ 0, x < 0 \end{cases} \tag{3.4b}$$

where the Heaviside step function, *H(x)*, determines which part of beam is the solution of the Equation 3.4a sought for.

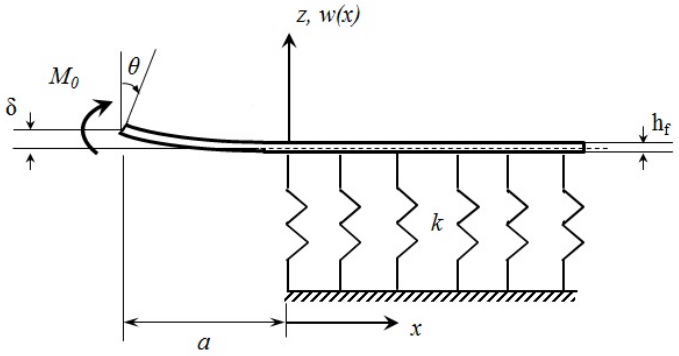

Figure 3.7. Foundation model of moment loaded SCB sandwich specimen.

The general solution of Equation 3.4 is of the form:

$$w(x) = \begin{cases} B_3e^{-\lambda x}\cos(\lambda x) + B_4e^{-\lambda x}sin(\lambda x), x > 0 \\ C_1\frac{x^3}{6} + C_2\frac{x^2}{2} + C_3x + C_4, x < 0 \end{cases} \tag{3.5}$$

where the parameter λ is given in Equation 3.3. The displacement solution was solved for the two intervals $(-a \leq x \leq 0)$ and $(0 \leq x \leq \infty)$. The beam was considered to be semi-infinite by ignoring the end effects and Equation 3.5 was solved by ensuring the deflection, slope and shear force to be continuous in both intervals and at $x = 0$. The constants in Equation 3.5 were obtained by utilizing appropriate boundary conditions and progressive derivative yielded rotation.

$$w(x) = M_o\begin{cases} \frac{x^2}{2EI} - \frac{4\lambda^3x}{k} + \frac{2\lambda^2}{k} & (-a \leq x \leq 0) \\ \frac{2\lambda^2}{k}\left[f_1(\lambda x) - f_2(\lambda x)\right] & (0 \leq x \leq \infty) \end{cases} \tag{3.6}$$

$$\theta(x) = \frac{dw}{dx} = M_o\begin{cases} \frac{x^2}{2EI} - \frac{4\lambda^3x}{k} + \frac{2\lambda^2}{k} & (-a \leq x \leq 0) \\ \frac{2\lambda^2}{k}\left[f_1(\lambda x) - f_2(\lambda x)\right] & (0 \leq x \leq \infty) \end{cases} \tag{3.7}$$

The functions f_1 and f_2 are provided in Equation 3.8.

$$f_1(\lambda x) = e^{-\lambda x}\cos(\lambda x) \tag{3.8a}$$

$$f_2(\lambda x) = e^{-\lambda x}\sin(\lambda x) \tag{3.8b}$$

The energy-release rate for a moment loaded beam is of the form:

$$G = \frac{M_o^2}{2b}\frac{dC}{da} = \frac{M_o^2}{2bEI} \tag{3.9}$$

where the compliance, $C = (a/EI) + \left(4\lambda^3/k\right)$ (see Equation 3.6). It should be noted that the energy-release rate of a moment loaded beam is independent of crack length and depends only on the applied moment and flexural rigidity (EI) of the beam. Moreover, both deflection and rotation of a beam with built-in end can be recovered from Equations 3.6 and 3.7 as $k \to \infty$.

3.3.2 FEA of Moment and Force Loaded SCB Sandwich Specimen

A detailed FEA of both moment and force loaded SCB sandwich specimen was performed using a typical Al/H100 sandwich configuration. The 2-D FE-model was similar to the one discussed in section 3.2.1. For the moment loaded case, a master node was inserted at the neutral axis of the debonded upper beam to apply the pure moment, M_o. The elastic foundation modulus, k, has been proposed by several researchers empirically and has the capability to influence the deformation characteristics of beams treated with Winkler model. A new elastic foundation modulus was proposed in [P2] corresponding to $(1/4)^{th}$ of the core thickness:

$$k = \frac{E_c b}{h_c/4} \tag{3.10}$$

Figure 3.8 shows deflection and rotation of a moment-loaded Al/H100 SCB sandwich specimen. The new foundation modulus (Equation 3.10) provided a close match with the FEA results when compared with other foundation modulus expressions proposed in the literature. The deformation characteristics for a force loaded SCB sandwich specimen has been examined by several researchers [43, 49] and a brief overview is also provided in the Appendix of [P2]. Energy-release rate for both loading cases also agreed with FEA results. It should be noted that the foundation modulus, k, does not contribute to moment loaded energy-release rate expression (see Equation 3.9). On the other hand, k, affects the energy-release rate for the force loading case (see Figure 3.9) and the newly proposed k (Equation 3.10) provided close correlation to FEA results [4].

3.3.3 Crack Tip Root Rotation

The approach by Li et al. [67], who proposed a dimensionless expression for crack tip root rotation was employed in [P2]. This expression is a function of axial force, shear force and bending moments as well as elastic constant and geometry of the debonded face sheet. The root rotation at the crack tip was assumed to follow Euler-Bernoulli theory and was obtained directly from the rotation of debonded face sheet derived using the foundation

[4] The energy-release rate was obtained numerically using the CSDE method, see section 2.3.

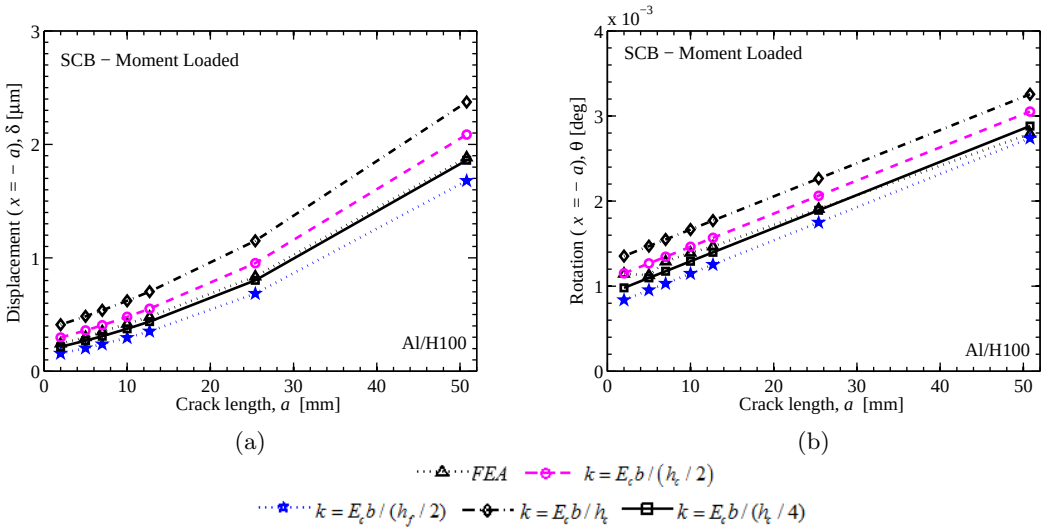

Figure 3.8. (a) Deflection and (b) rotation of a moment-loaded Al/H100 SCB sandwich specimen.

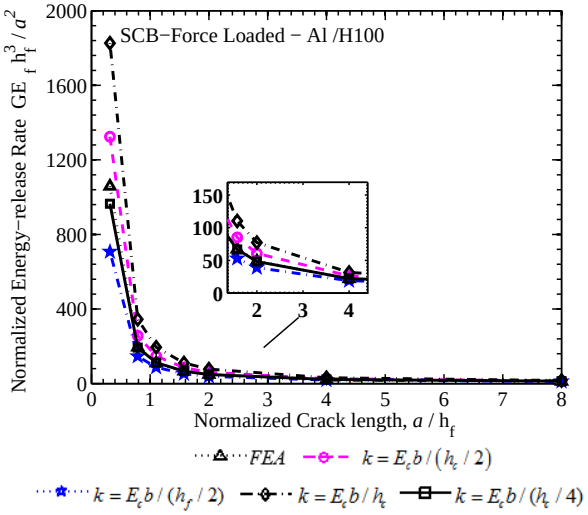

Figure 3.9. Normalized energy-release rate vs. crack length for a force-loaded Al/H100 SCB specimen calculated using FEA and foundation model.

model approach (see Equation 3.7). The root rotation angle, ϕ, proposed by Li et al. [67] is given by:

$$\phi_A = c_M \frac{M}{\bar{E}_f h_f^2} + c_N \frac{N}{\bar{E}_f h_f} + c_V \frac{V}{\bar{E}_f h_f} \tag{3.11}$$

where the coefficients c_M, c_P and c_V depend on the face sheet and core stiffnesses. Figure 3.10 shows the comparison of crack root rotation angle (ϕ) calculated using the foundation model approach and the one obtained from FEA, for a moment-loaded SCB specimen at a short crack length. It was observed that the rotation angle is quite sensitive to the

foundation modulus, k, and the newly proposed k (Equation 3.10) gives close agreement to FEA results. The coefficients in Equation 3.11 were also calibrated using FEA for a force loaded specimen and was found to agree closely with FEA results for a range of crack lengths. The analysis performed in [P2] rendered confidence to the formulation proposed by Li et al. [67].

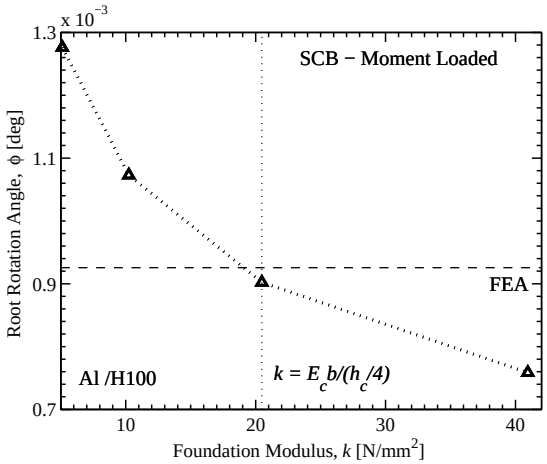

Figure 3.10. Crack root rotation angle (ϕ) vs. foundation modulus, k, for a moment loaded SCB specimen, at $a = 2$ mm.

3.3.4 Influence of Shear on Phase Angle (ψ)

The force loaded SCB sandwich specimen contains a shear component and bending moment at the crack tip. For reliable fracture toughness assessment, the transverse shear force must be accounted in the calculation of energy-release rate. The original expressions for mode-mixity and energy-release rate derived by Suo and Hutchinson [21] ignores the shear component. The crack tip mode-mixity phase angle (ψ) calculated for a range of crack lengths showed that ψ increases at shorter crack lengths. This observation qualitatively agrees with results from similar analysis [67, P1]. Furthermore, for the moment-loaded SCB specimen, the phase angle seems consistent with the trend of ψ as $V/M \to 0$.

The deformation characteristics estimated using beam on elastic foundation approach was shown to be robust in estimating crack tip root rotation. The foundation effects play a vital role in the magnitude of root rotation angle. The approach outlined in [P2] will aid in establishing compliance coefficients for a wide array of sandwich configurations (both force- and moment-loaded), which may be used to estimate the root rotation angle. In addition, the presented analysis in [P2] helped in understanding compliance, energy-release rate and mode-mixity of moment loaded sandwich specimen, such as the DCB-UBM specimen.

Chapter 4

Fracture Characterization using DCB-UBM Sandwich Specimen

This chapter summarizes the work presented in Papers [P3 - P5]. The Double Cantilever Beam loaded with Uneven Bending Moments (DCB-UBM) sandwich specimen is the subject of focus. A basic introduction to the test principle and novel test rig concept are provided. Closed-form expressions for both energy-release rate and mode-mixity phase angle, derived for the case of a reinforced DCB-UBM are summarized. The reader is encouraged to refer to the appended papers in Appendix A for detailed discussions and test results.

4.1 Introduction

The Double Cantilever Beam loaded with Uneven Bending Moments (DCB-UBM) specimen was first introduced by Sørensen et al. [57], for determination of delamination toughness in monolithic composites and was later extended to sandwich constructions by Lundsgaard-Larsen et al. [58]. The principle of the fracture specimen is shown in Figure 4.1, in which the crack flanks are subjected to pure moments. The mode-mixity phase angle (ψ), can be altered by varying the ratio of moments between the arms, $MR = M_1/M_2$. Therefore, by holding the moment ratio (MR) constant throughout the test, crack propagates under a fixed mode-mixity condition. There are several methods in which the MR can be held constant, and each method is unique to the test rig construction. A brief summary on the traditional way of applying moments and the unique novel concept utilized in this Thesis are provided in sections 4.1.1 and 4.2, respectively.

The DCB-UBM fracture specimens have been widely used in estimation of cohesive laws in both monolithic laminates as well as sandwiches [58, 79, 80, 81]. In a DCB-UBM specimen, the energy-release rate is independent of the crack length [57, 58, 82], which makes it attractive from the view-point of fracture testing as no crack monitoring device is required. Moreover, large process zones with a stable crack growth can be achieved.

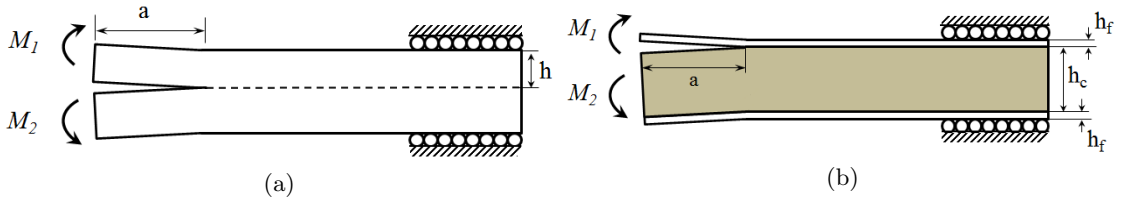

Figure 4.1. Schematic illustration of DCB-UBM (a) laminate specimen (b) sandwich composite specimen.

4.1.1 Review on DCB-UBM Test Set-ups

In a DCB-UBM fracture specimen, pure moments are applied on the crack flanks. In the past, many designs have been proposed each characterized by a unique jig and fixture design. A schematic illustration of different test set-up designs available in the literature are provided in Figure 4.2. It is observed that all these designs employ a pair of forces to translate an equivalent moment. Freiman et al. [83] applied a pair of pure moments on a ceramic DCB specimen to study the fracture response in mode I conditions. The set-up is simple in construction (see Figure 4.2a) and was found to be robust for the tested ceramic material. However, the fixture induces local stress concentrations leading to a local failure. Sørensen et al. [84] modified this test configuration by applying moments without inducing any wedging forces or frictions. Their design was based on a fixture using wire and roller, and initially employed this set-up to measure fracture resistance in ceramics. Later, the design was altered in [57] to account for a wide variety of specimens such as laminates and sandwich composites [58, 79, 81, 85]. Nonetheless, the test principle of translating pure moments from a conventional axial testing machine with the aid of wires and rollers remain the same. A schematic illustration of the latest version of the test rig by Sørensen et al. [57] is shown in Figure 4.2b.

A stand alone test rig was also proposed by Sørensen et al. [80] for fracture testing of brittle materials inside an environmental scanning electron microscope. This fixture loads a DCB specimen with pure bending moments by using steel band and roller. The design however, can only be utilized for in *situ* fracture measurements. Berglund and Lindhagen [86] designed a test-rig which can be mounted on a conventional axial testing machine and avoided the use of rollers and wires, see Figure 4.2c. Recently, Pappas [87] modified this concept to one which is much more advanced in the machine design level, see Figure 4.2d. The proposed test rig is complex in design and inevitably requires a CAD model to establish the kinematic relations of the specimen. Special mention is made here on the rig developed by Plausinis and Spelt [88] for testing creep in adhesive joints, which was based on short wire system and was also used for cyclic tests [89].

4.2 DCB-UBM Test Rig - Principle and Construction - Paper P3

The test principle along with the configuration and assembly of the DCB-UBM test rig developed in-house is described in this section. It must be noted that the key idea in DCB-UBM test methodology, is to apply pure moments on specimen edges to achieve a

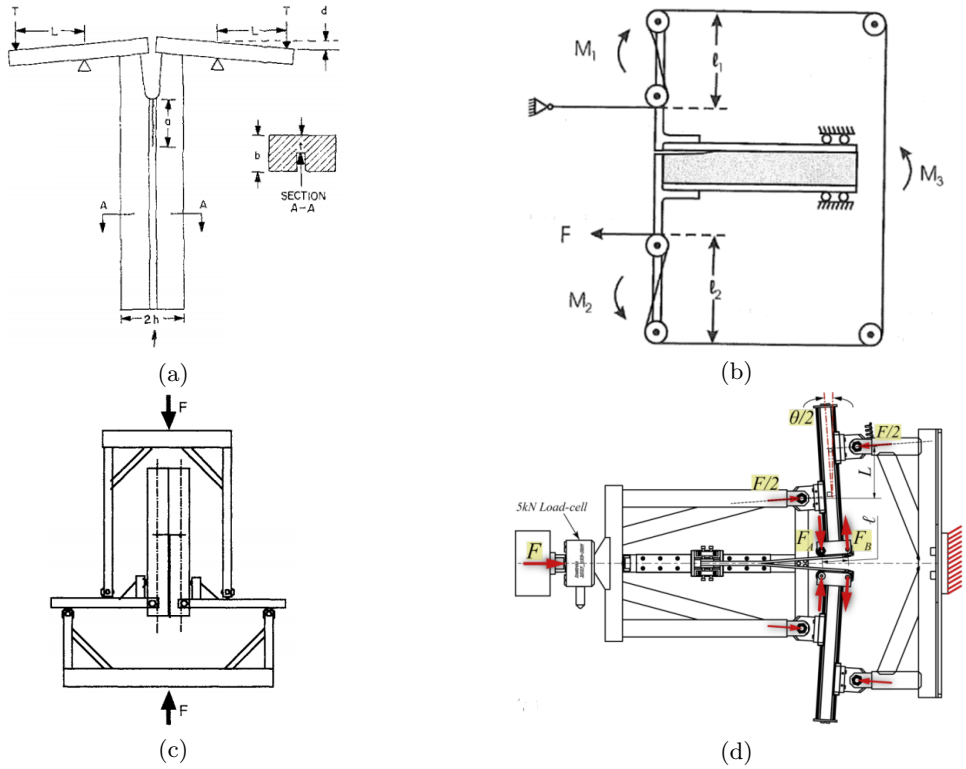

Figure 4.2. Pure moment configurations applied on DCB specimen available in the literature (a) Freiman et al.[83] (b) Sørensen et al.[57], (c) Berglund and Lindhagen [86] and (d) Pappas [87].

steady state crack propagation. The presented rig was the subject of focus in Paper P3, and was assembled in the DTU Structural Lab.

4.2.1 High Fidelity Fatigue Rated Novel DCB-UBM Test Rig

In all test rigs in the literature, efforts were made to apply pure moments to the crack flanks with the help of specialized jig and fixture design, which can be mounted to a conventional axial testing machine. Such an arrangement severely limits the magnitude of applied moments and the achievable range of moment ratio (MR). A novel and unique way of introducing the moments through independent torsional actuators is introduced here, which is capable of applying moments up to 565 Nm and can achieve a wide range of MR. The proposed design is a compact and stand-alone rig which can be utilized for fracture testing of laminates, sandwiches or sub-components. Most of the test designs in the literature [57, 84, 86, 87] contain long wires, rollers or complicated fixture designs (see Figure 4.2), which make them difficult to operate under fatigue due to problems such as resonance or misalignment. The proposed test rig circumvents all these challenges, paving way to extending the test methodology to fatigue[1].

[1]The proposed rig was configured in fatigue mode and pilot testing on honeycomb core specimens were conducted [90].

The test principle of this novel rig is presented in Figure 4.3. As shown, two independent servo-hydraulic torsional actuators apply moments to the specimen edges which are mounted atop carriage plates. To maintain a pure moment loading scenario, all in-plane and out-of-plane forces must remain negligible. Hence, the actuators atop the carriage plates are mounted on raceway shafts using track rollers. Carriages run clearance-free on the guide-ways and track rollers are greased with gap seals on both sides to prevent dust accumulation. The inner and outer rings of the track rollers and guide-way raceway shafts are made from corrosion-resistant steel. The carriage system can support a static moment of 800 Nm around the z-axis (considered in the out-of-plane direction of the paper). The pre-crack and post crack propagation scenarios are also illustrated in Figure 4.3. As the crack grows, the actuators slide along the x and y axes accounting for any set of moment ratios (MR) as well as large rotations. Furthermore, to accommodate a range of specimen lengths, the two actuators must be able to slide along the y-axis.

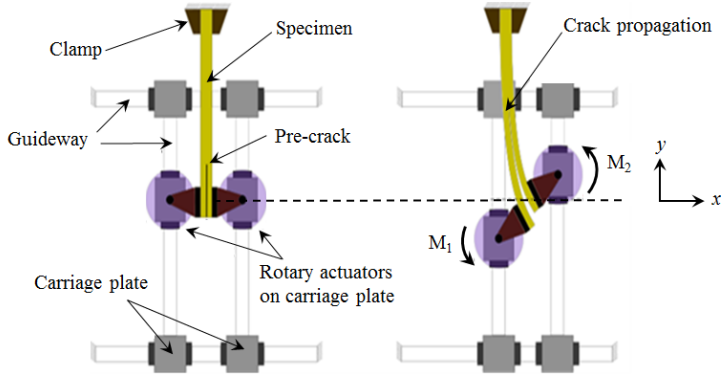

Figure 4.3. Principle of the modified DCB-UBM test rig with torsional actuators mounted on carriage plates (left) prior to start of the test and (right) crack propagation caused due to application of moments, M_1 and M_2.

4.2.2 Design of Test Rig and Control Algorithm

The schematic view of the assembled DCB-UBM test rig is shown in Figure 4.4 and specifications are provided in Table 4.1. The rig was supplied with a constant supply of 207 Bar pressure from a Hydraulic Power Unit (HPU) and have dedicated Hydraulic Service Manifold (HSM) to each actuator providing independent pressure regulation for precise control and uniform distribution of hydraulic fluid. The torsional actuator, Torsion Load Cell (TLC) and Angular Displacement Transducer (ADT) were mounted in a sequential arrangement on the carriage plate, see Figure 4.6. A MTS FlexTest® SE [91] controller was modified by adding a second channel so that independent channels were available for the two actuators. A control algorithm was developed for quasi-static fracture testing in MTS MP Elite® [92] control software. The flowchart of the algorithm is provided in Figure 4.5[2].

The tests were conducted in angular control, by applying a rotation command to the master arm, Arm-1 (debonded arm) in Figure 4.7. Arm-2 was configured to follow Arm-1, such that the ratio of moments between the two arms (MR) remains constant through

[2]For fatigue tests, the same algorithm can be utilized with a cyclic command.

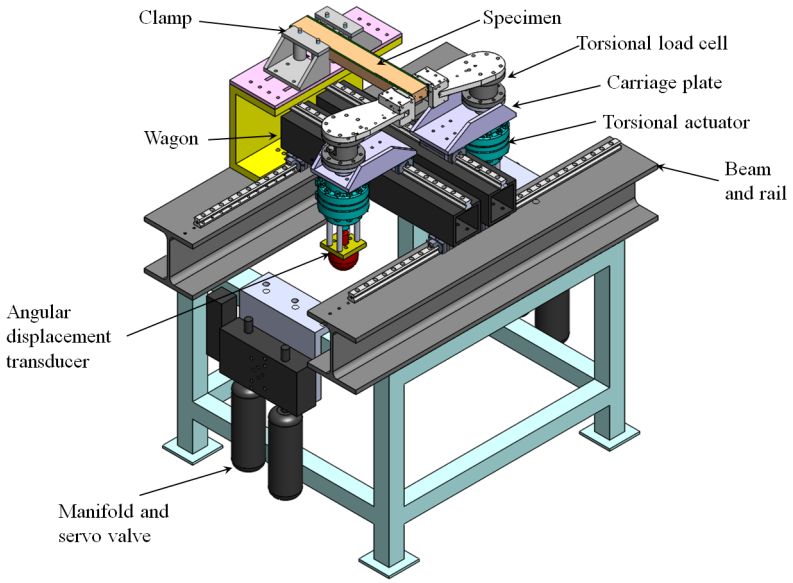

Figure 4.4. Schematic illustration of DCB-UBM test rig developed at DTU, consisting of two independent servo-hydraulic torsional actuators.

out the test. The moment ratio, *MR* was provided as input prior to start of the test along with the test speed. For quasi-static tests, usually a speed of 5 - 10 °/min is recommended. In addition, a static and null pacing type compensator was added in order to compensate for the unexpected perturbations encountered by the specimen during crack propagation. Moment and angle readings from both actuators were acquired constantly at a rate of 5 Hz using the MTS MP Elite®[92] software.

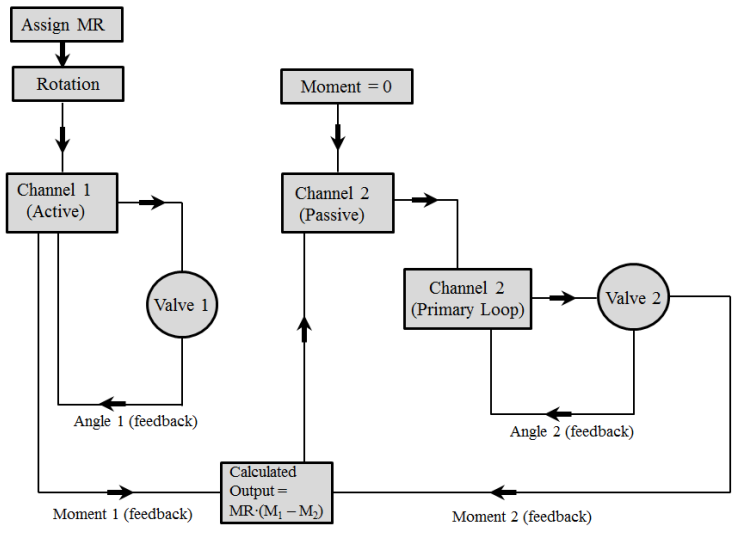

Figure 4.5. DCB-UBM control algorithm (cascade).

Table 4.1. DCB-UBM test rig specifications.

Test Machine Specifications	
Machine Identification	DCB-UBM
Test Machine Manufacturer	In-house assembled
Type of Test Machine	Mixed mode fracture test rig
Maximum load	750 kN
Torsion Load Cell (TLC) [93]	
Manufacturer	Sensor Data T150 series
Maximum Load	565 Nm
Serial No.	T150-410
Construction	SAE 4340 Alloy Steel
Angular Displacement Transducer (ADT) [94]	
Manufacturer	Trans Tek Inc.
Model No.	Series 0603-0000
Displ. Range	$\pm 60°$
Max. Angular Velocity	$1.44°/s$
Data Acquisition and Software	
Data Acquisition	MTS MP Elite® [92]
Control System	MTS FlexTest® SE [91]
Data Reduction	MATLAB
Rotary Actuators	
Manufacturer	Fluitronics GmbH
Model No.	SS-001-2V
Serial No.	12-1004-70
Max. Capacity	773 Nm at 207 Bar

Figure 4.6. Sequential arrangement of TLC, actuator and ADT on the carriage plate.

4.2.3 Sizing of the DCB-UBM Specimen: Addition of Doubler Layers

Sandwich specimens with thin compliant face sheets are often reinforced with stiff layers to prevent premature failure [66]. The reinforcements are known as "doublers", and are bonded to the face sheets to prevent excessive crack tip rotation during fracture testing thereby keeping the analysis within ambit of LEFM. From a load application point of view, the doubler layers enable easy end tab attachment with screws, see Figure 4.7. It should be noted that the thickness of doubler layers were chosen such that they do not undergo yielding prior to crack propagation. In this Thesis, the steel doubler layers of IMPAX® SUPREME [95] type with a thickness, $h_r = 6mm$ was chosen. Steel reinforcement layers were used previously by Lundsgaard-Larsen et al. [58] to measure cohesive laws in E-glass/PVC foam specimens that exhibited large scale fiber bridging. As pointed out in [58, 96] addition of doubler layers have only minor influence on the energy-release rate values and it is expected that more accurate interface toughness measurements can be obtained, especially when the face sheets are compliant.

The distance from the clamp to the extended position of the load arm in the y-direction is 670 mm, see Figure 4.7. A standard DCB-UBM specimen length of 500 mm was chosen, enabling testing of each specimen at several mode mixity phase angles. Moreover, the proposed rig is able to test specimens up to a length of 720 mm enabling testing of sub-components. An appropriate width of the DCB-UBM specimen was drawn from previous interface studies as well as from a limited number of pilot tests. A specimen width in the order of 25-40 mm was found to be apt for foam core specimens [46, 49, 97], whereas for honeycomb core specimens, at least six cells across width were recommended (30-60 mm) [49, 98].

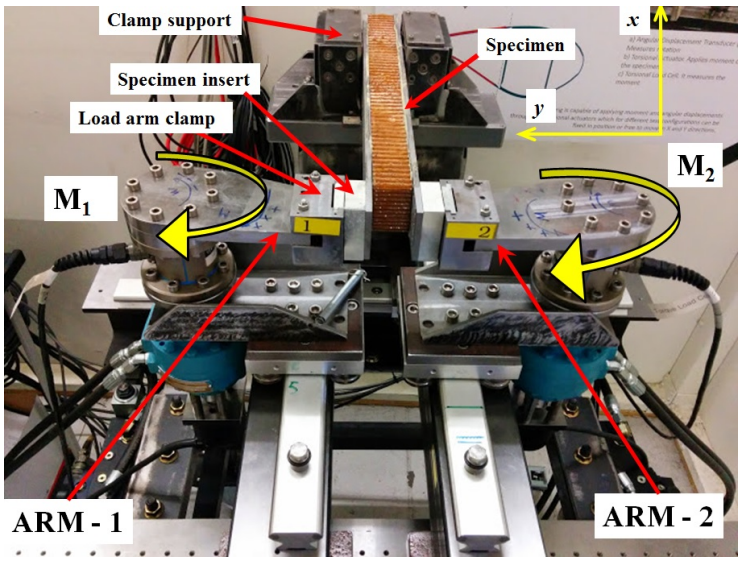

Figure 4.7. A honeycomb core sandwich specimen held between the two actuator arms in the DCB-UBM test rig.

4.2.4 Data Reduction Scheme

The recorded moments from each arms were used to compute the energy-release rate. A typical moment vs. rotation plot of a honeycomb core sandwich specimen is shown in Figure 4.8a. The crack initiation can be noted from the stark departure from the loading curve (M_1 vs. θ_1) of the debonded beam. The slope becomes close to zero as the disbond increases by Δa in Figure 4.8. Lundsgaard-Larsen et al. [58] provided the J-integral expression for a reinforced DCB specimen subjected to moments as:

$$J = \sum_{p=1}^{10} \frac{\bar{E}_p M_b^2}{6\left(A_b D_b - D_1^2\right)^2} \left[A_b^2\left(y_{p-1}^3 - y_p^3\right) - 3A_b B_b\left(y_{p-1}^2 - y_p^2\right) + 3B_b^2\left(y_{p-1} - y_p\right)\right] \quad (4.1)$$

where A, B and D are extensional, bending and coupling terms, y_p is the distance between neutral axis between ply p and p -1. The subscript b refers to each beam, whilst p refers to the path evaluated using the J-integral (Equation 4.1), as shown in Figure 4.9. In addition to the J-integral approach, the energy-release rate for a moment loaded beam can also be expressed in terms of the compliance as [P2]:

$$C = \frac{\theta}{M} = \frac{\mathrm{a}}{(EI)} \quad (4.2)$$

Now, the energy-release rate for a single beam is:

$$G = \frac{M^2}{2b}\left(\frac{dC}{da}\right) = \frac{M^2}{2b\,(EI)} \quad (4.3)$$

where b is the width of the beam. The flexural rigidity term (EI) of each beam can be obtained using laminate beam theory[3]: $\left(D - B^2/A\right)$[99]. Now, the total energy-release rate of the entire DCB-UBM specimen is of the form:

$$G = \frac{M_1^2}{2b(EI)_{\#1}} + \frac{M_2^2}{2b(EI)_{\#2}} + \frac{M_3^2}{2b(EI)_{\#3}} \quad (4.4)$$

Note that Equations 4.1 and 4.3 are independent of crack length, a. Upon substitution of measured moments into either of these equations, the initiation crack propagation can be identified from the departure of slope in G vs. θ curve as shown in Figure 4.8b. A MATLAB script was implemented to estimate the energy-release rate with the help of laminate beam theory. The rotation of master arm (arm-1 in Figure 4.7), θ_1, is considered for the plots, as the primary rotation command was supplied to the master arm. The profile of both G vs. θ_1 and M vs. θ_1 remain similar enabling easy identification of crack initiation and advancement.

[3]For symmetric case, $B = 0$, yielding $EI = D$.

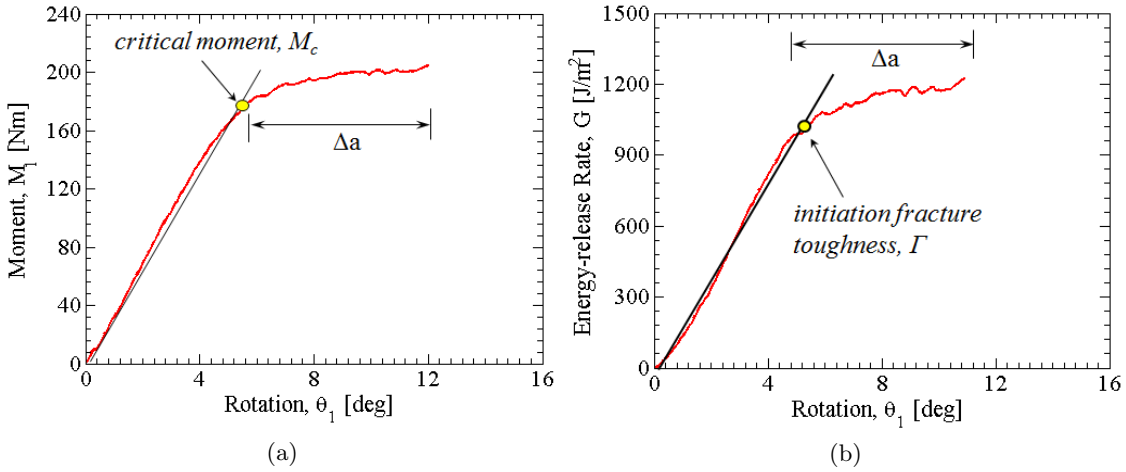

Figure 4.8. Typical moment and energy-release rate plots for a CFRP/C1-4.8-32 honeycomb core specimen with $h_f = 1.4$ mm, $h_c = 40$ mm (a) Moment, M_1 vs. Rotation, θ_1 and (b) Energy-release rate, G vs. Rotation, θ_1 of the debonded beam.

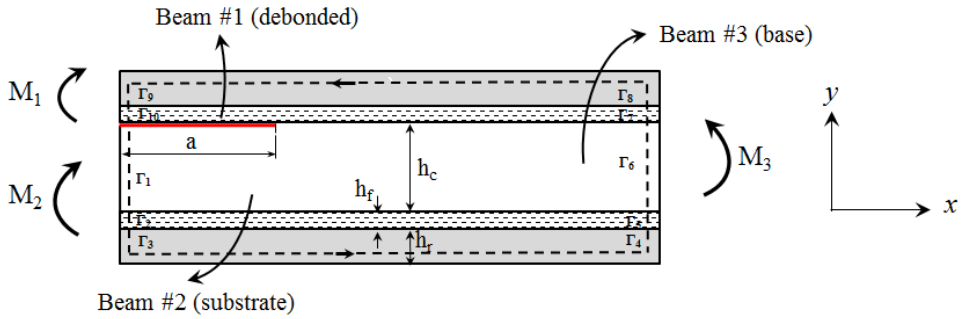

Figure 4.9. J-integral path in DCB-UBM sandwich specimen reinforced with steel reinforcement layers.

4.2.5 Determination of Phase Angle (ψ) using the CSDE Mode-mixity Method

In the DCB-UBM sandwich specimen, the mode-mixity is held constant throughout the crack propagation by maintaining a fixed ratio of moments, see Figure 4.3. For a face/core interface, the moment ratio, MR, pertaining to a specific mode-mixity that need to be input to the controller prior to each test can be obtained numerically. The numerical method - CSDE, was utilized to create a map of MR vs. phase angle (ψ) for the interface under consideration. As discussed in section 3.2.1, the CSDE method was implemented in conjunction with the commercial FE-code, ANSYS®. The FE-model of a DCB-UBM sandwich specimen is shown in Figure 4.10 and comprised of 4-node linear (PLANE182 type) and 8-node parabolic (PLANE183 type) elements. The linear elements were used near the crack tip to capture large strains, with a smallest element edge length of 2.5 μm. The mode-mixity phase angle (ψ) was obtained in terms of the relative crack flank displacements, see Equation 2.27.

Prior to testing, FE-analysis was performed to create a map of moment ratio, MR vs.

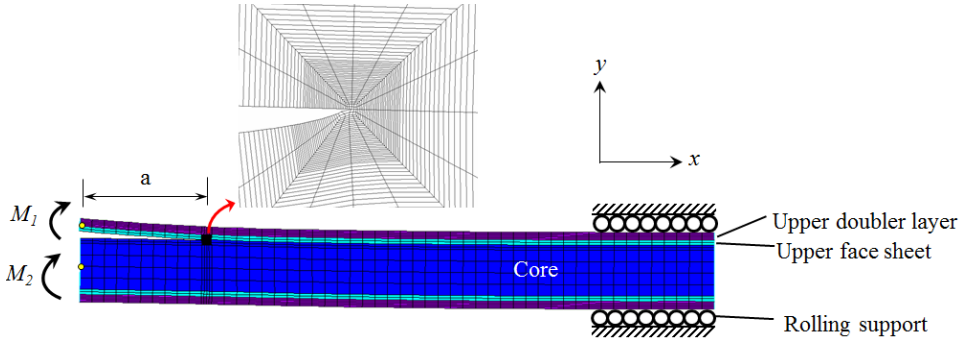

Figure 4.10. Finite Element Model of the DCB-UBM sandwich specimen reinforced with stiff layers and with highly densified mesh in the crack tip region.

phase angle, ψ, for the various sandwich configurations tested in this Thesis [90, P3, P5]. The mode-mixity phase angle (ψ) can also be obtained using the analytic method which was the subject of Paper P4 and is presented in section 4.3. The total length of the specimen was chosen to be 500 mm with a pre-crack length of 200 mm for all analyses. The phase angle was obtained by selecting magnitude of moments, M_1 and M_2 such that an energy-release rate $G \simeq 100$ J/m^2 was achieved. The sign of MR is dependent on the sign of the applied moments, M_1 and M_2. There are three possible ways of rotating the crack flanks (see Figure 4.11): a) M_1 and M_2 rotate clock-wise (CW), b) M_1 and M_2 rotate counter-clock wise direction (CCW) or c) M_1 and M_2 open relative to each other (open) with respect to the plane of the paper. The rotation of the beam in counter clock-wise direction was taken as positive which yielded $MR > 0$ for the two cases when both beams rotate in CW and CCW directions. Contact elements (TARGET169 and CONTACT172) were used to check for crack flank interpenetration.

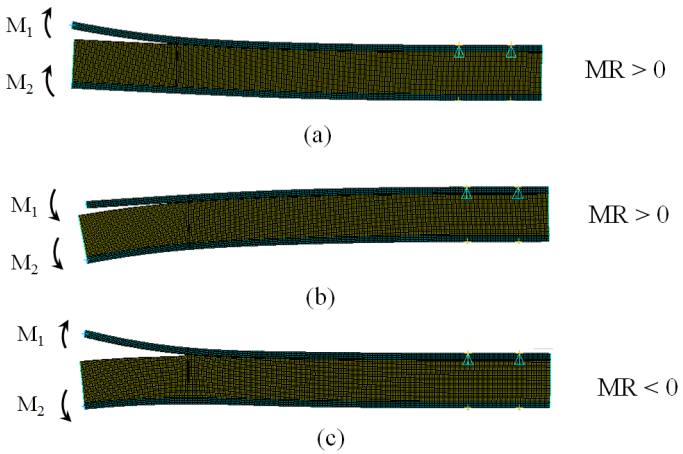

Figure 4.11. Moment Ratio (MR) sign convention for a sandwich DCB-UBM specimen, where (a) $MR > 0$, corresponds to both moments rotating clock-wise (b) $MR > 0$ when the two moments rotate counter clock-wise, and (c) $MR < 0$, for both moments acting opposite to each other.

Figure 4.12 shows a map of MR vs. ψ for a typical marine grade E-glass/H45 specimen and an aerospace grade CFRP/honeycomb core DCB-UBM sandwich specimen. The

influence of core thickness (h_c) on the phase angle is clearly evident from the plots. For a constant MR, a thinner core results in higher values of ψ in the negative scale for $MR \leq\sim$ -1 and for $MR \geq\sim 1$. However, the difference in phase angle is small in the range -1 $< MR <$ 1 for the two core types shown in Figure 4.12. For fracture testing, it is preferred to select those MR values corresponding to a negative phase angle, as a negative value of ψ indicates the propensity of the crack to propagate into the face sheet. In general, face sheets are tougher and therefore, the crack will propagate hugging the interface.

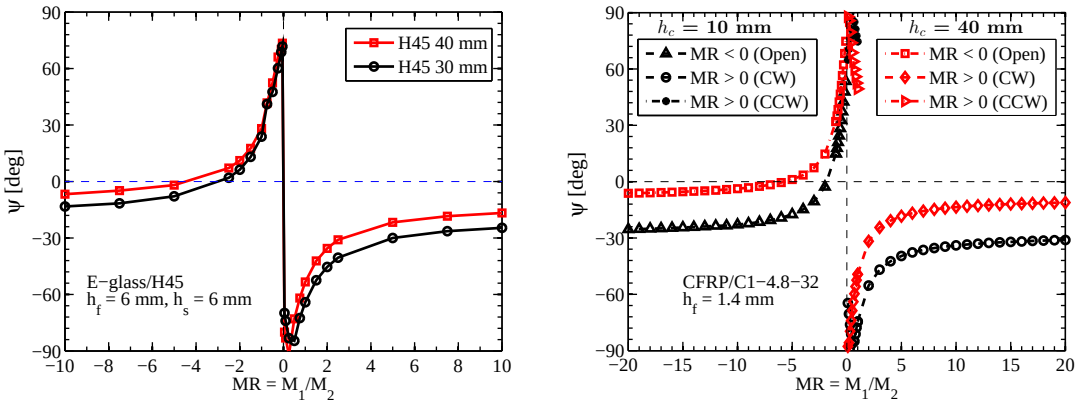

(a) (b)

Figure 4.12. MR vs. ψ for typical DCB-UBM sandwich specimens (a) E-glass/H45 specimen, with $h_f = 6$ mm, and (b) CFRP/honeycomb core specimen with $h_f = 1.4$ mm.

4.2.6 Mixed mode Fracture Testing of PVC Foam Core Specimens

Mixed mode interface fracture characterization of a typical marine grade sandwich configuration comprising of E-glass/epoxy face sheet and H45 PVC foam core was conducted in [P3]. DCB-UBM specimens (450 x 30 mm) were cut from sandwich panel which was prepared using Vacuum Assisted Resin Transfer Molding (VARTM) processing. The face sheets composed of eight unidirectional (UD) E-glass plies with a stacking sequence -$[0/90/0/90]_s$ and Araldite® LY 1568 / Aradur® 3489 epoxy system [100] was used with a curing time of 24 hours. The face sheet thickness was, $h_f = 6$ mm after curing of the resin. The mechanical properties of face sheet were obtained using standard ASTM tests [101, 102] and the core and steel mechanical properties from the respective supplier data sheets [95, 103]. The steel doubler layers were attached using Araldite®2015 [104] and load tabs were attached to the specimen using six steel screws.

Fracture testing was carried out in mode I, mode II and mixed mode conditions, where the moment ratio (MR) values corresponding to the desired mode-mixity phase angle is obtained using the CSDE method as outlined in section 4.2.5. In total, ten specimens were tested and testing were carried out at MR = -5, -10, 7.5, 5, 3, 1.3, 2 and 1 corresponding to a phase angle, ψ = -8°, -13.3°, -26.4°, -30°, -40°, -50°, -45.4° and -64.1°, respectively. Figure 4.13a shows the plot of measured moment vs. rotation of the debonded arm. The robustness of the controller in maintaining the moment ratio constant throughout the

crack propagation can be noted from Figure 4.13b. Face/core interface crack propagation was observed for all the phase angles, see Figure 4.14a for DCB-UBM fracture testing at ψ = -26.4°. Fracture surface obtained for the case ψ = -64° is shown in Figure 4.14b. For the predominant mode II case ($\psi = 64.1°$), a crack jump of $\sim$ 20 - 50 mm was observed along the interface exhibited as stick slip behavior. The measured interface fracture toughness values ranged from about 180 - 600 J/m^2 and are comparable (at mode I and mixed mode conditions) to the values obtained using the MMB and TSD test methods for a similar sandwich configuration [36, 97].

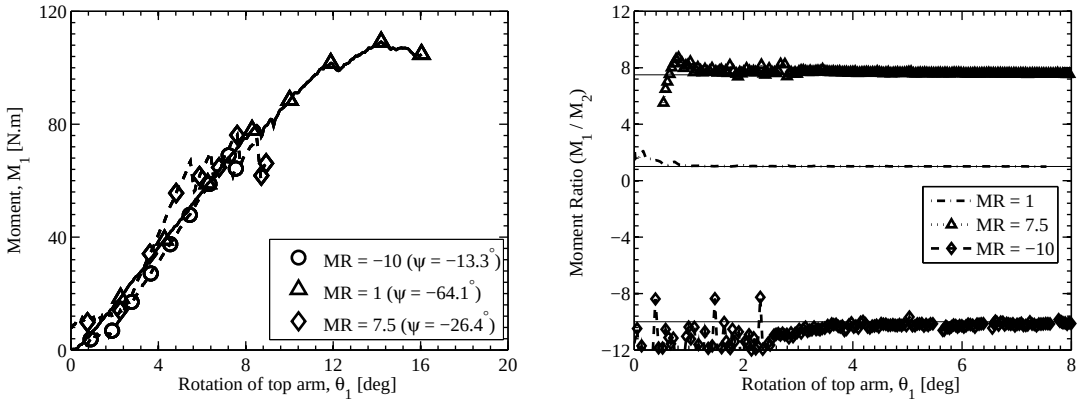

(a) (b)

Figure 4.13. Moment vs. rotation of the debonded arm (θ_1) and (b) moment ratio (MR) vs. rotation of the debonded arm (θ_1).

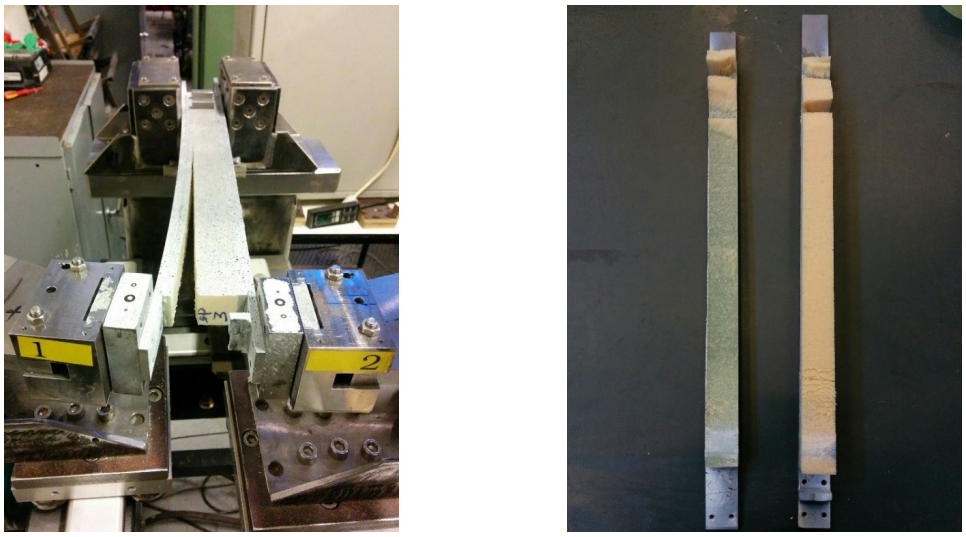

(a) (b)

Figure 4.14. DCB-UBM fracture testing of E-glass/H45 sandwich specimen (a) face/core interface crack propagation at MR = 7.5 (ψ = -26.4°) (b) Fracture surfaces for MR = 1 (ψ = -64.1°).

4.3 Energy-release Rate and Mode-mixity in Reinforced DCB-UBM Sandwich Specimens - Paper P4

Closed-form algebraic expressions for the energy-release rate and the mode mixity phase angle were derived for a typical debonded asymmetric sandwich element by Kardomateas et al. [69]. These expressions cannot be utilized for the moment loaded DCB specimens reinforced with doubler layers (refer to 4.2.3). The doubler layers play a pivotal role in fracture testing of specimens with thin face sheets, especially the ones used in the aerospace sector. Moreover, as mentioned in [P3], the doublers aid in direct application of moments though attachment of load carrying tabs. Therefore, the existing closed-form expressions must be expanded to specimens with reinforcement layers, and was carried out in Paper P4. Both energy-release rate and mode-mixity phase angle (ψ) for a reinforced DCB-UBM specimen was derived in [P4].

A superposition scheme was employed for the analysis of reinforced DCB-UBM sandwich specimen, see Figure 4.15. This approach is similar to the principle implemented by Suo and Hutchinson in [21]. The primary premise behind this scheme is that both energy-release rate and stress intensify factors of the cracked and un-cracked configuration remain the same (Figure 4.15). The three original loading parameters were reduced to two independent terms, P and M_d. Laminate beam theory [105] was used to find the stress distribution in each sub-beam, thereby obtaining the constants in the relationship between the loading parameters and independent terms.

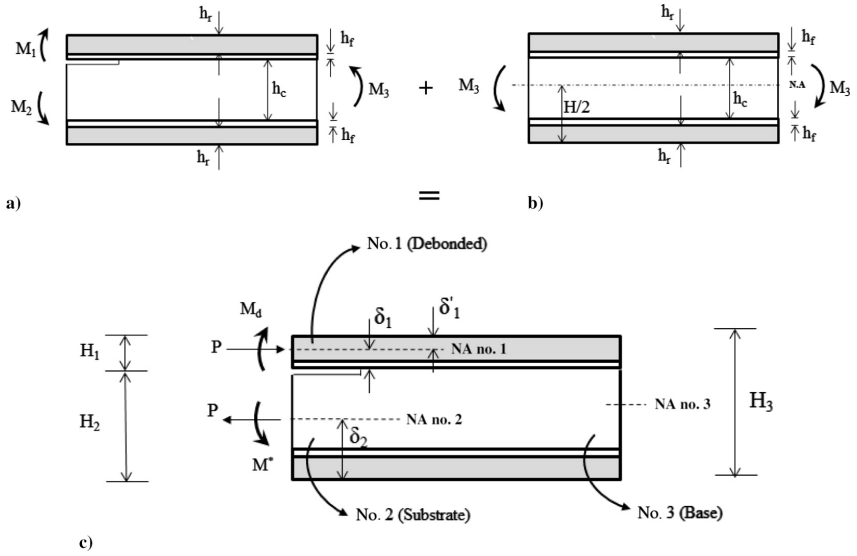

Figure 4.15. Superposition scheme of sandwich geometry reinforced with stiff layers.

J-integral approach [106] was used to calculate the energy-release rate of the sandwich beam element obtained from the result of the super-position scheme, see Figure 4.16. The J-integral is non-zero only along the vertical paths near the left edge marked Γ_1 – Γ_3 and $\Gamma_9 - \Gamma_{10}$. For the horizontal paths $dy = 0$ and, the normal vector is directed along the y-axis: $\sigma_{ij} n_j = 0$, making no contribution to J. Furthermore, the vertical paths ($\Gamma_4 - \Gamma_8$) along right edge do not contribute to J as no load acts on that edge (see Figure 4.16). A

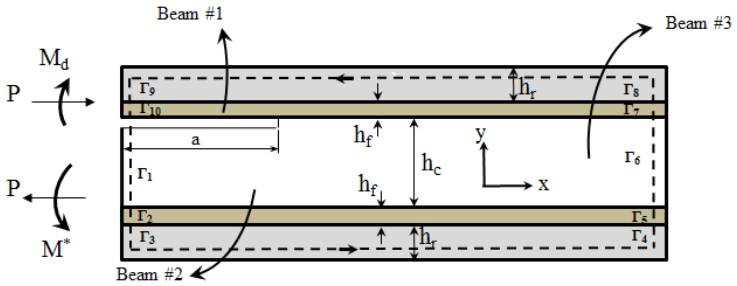

Figure 4.16. J-integral of sandwich element.

detailed derivation of the J-integral is provided in [P4] and is given by:

$$G = P^2\left(\frac{L_1}{(\bar{E}h)_d^2} + \frac{V_1}{(\bar{E}h)_s^2} + \frac{V_2{\Delta_1}^2}{H_s^2} + \frac{V_3\Delta_1}{(\bar{E}h)_s H_s}\right) + {M_d}^2\left(\frac{L_2}{H_d^2} + \frac{V_2}{H_s^2}\right) + M_d P\left(\frac{2V_2\Delta_1}{H_s^2} + \frac{L_3}{(\bar{E}h)_d H_d} + \frac{V_3}{(\bar{E}h)_s H_s}\right) \tag{4.5}$$

In order to find the mode-mixity phase angle (ψ), the relationship between energy-release rate and stress intensity factor, K was utilized: $G = B|K|^2$. Equation 4.5 was re-arranged in a quadratic form to find the roots for K containing both real and imaginary parts. Following the approach in Kardomateas et al. [69], Thouless et al. [107] and Hutchinson et al. [21], the stress intensity factor, K can be written as:

$$K = \frac{1}{\sqrt{B}}\left(-aP\sqrt{a_1} + bM_d\sqrt{a_2}\right) h_f^{-i\varepsilon} \tag{4.6}$$

Utilizing the phase angle definition given in [21] and from [107], ψ for a reinforced DCB-UBM sandwich specimen is given by:

$$\tan\psi = \frac{\lambda\sin\omega - \cos(\omega+\gamma)}{\lambda\cos\omega + \sin(\omega+\gamma)} \tag{4.7}$$

where the effect of reinforced face sheets are introduced through parameters a_1 and a_2. Now, the parameter ω, is expressed in terms of the phase angle, ψ, as:

$$\omega = \tan^{-1}\left[\frac{\cos\gamma + (\lambda + \sin\gamma)\tan\psi}{\lambda + \sin\gamma - \cos\gamma\tan\psi}\right] \tag{4.8}$$

The scalar quantity, ω, (Equation 4.8) is derived in terms of the mode-mixity phase angle which is independent of any loading just as in the bi-material or tri-material case. The ω value for a particular sandwich configuration and geometry can be extracted for only a single loading combination using a numerical mode-mixity method. Therefore, the analysis presented in [P4] extends the formulas in the literature which exist for interface cracks in tri-material and bi-material. The provided algebraic expressions can also be utilized for a laminate comprising of n-layers. For a balanced and symmetric laminate, a homogenized modulus can be obtained using laminate plate theory. Hence, the derived

expressions are a practical tool for assessing both mode-mixity phase angle and energy-release rate for a wide array of sandwich types used in the industry. An investigation was also carried out to study the influence of reinforcement layer thickness, h_r, on the scalar quantity, ω. It should be noted that Equations 4.5 and 4.1 yield similar results to the expressions provided in [58, 69]. Such a direct comparison was made by making the reinforcement layer modulus equal to that of the face sheets and making the sum of each face sheet thickness and reinforcement thickness equal to the face thickness analyzed in [69].

4.3.1 Influence of Reinforcement Layer Thickness on ω Parameter

To understand the effect of reinforcement layer thickness (h_r) on the scalar quantity, an exhaustive parametric study was conducted. A difference of 10.1 % in ω was obtained between thin and thick reinforcement layer thicknesses for an Al/H100 sandwich configuration. In general, the reinforced fracture specimen - DCB-UBM is most often used with a constant doubler layer thickness. Therefore, the observed difference may be considered insignificant when only a single doubler layer thickness will be used for the whole test campaign. To further extend the analysis, the effect of h_r on ω was investigated by changing core and face sheet material systems. Curve fitting parameters were derived for typical specimens to capture the change in h_r. Such a trend in h_r vs. ω quantified using a polynomial curve fit for Al/PVC core and E-glass/PVC core systems are provided in Table 4.2.

Table 4.2. Curve fitting parameters for ω vs. h_r plot for E-glass/PVC core and aluminum/PVC core sandwich systems.

Aluminum/PVC Core, $\omega = \zeta_1 \cdot h_r + \zeta_2$	
Al/H45	ζ_1 = -1.649, ζ_2 = 61.33
Al/H100	ζ_1 = -1.252, ζ_2 = 65.4
Al/H250	ζ_1 = -1.158, ζ_2 = 65.22
E-glass/PVC Core, $\omega = \eta_1 \cdot h_r^2 + \eta_2 \cdot h_r + \eta_3$	
E-glass/H45	η_1 = -0.111, η_2 = 1.34, η_3 76.1
E-glass/H100	η_1 = -0.401, η_2 = 1.71, η_3 = 70.5
E-glass/H250	η_1 = -0.389, η_2 = 2.90, η_3 = 65.4

4.4 Mixed Mode Fracture Characterization of Honeycomb Core Sandwich Specimens - Paper P5

Honeycomb core sandwich composites are widely used in the aerospace sector and find applications in flight control surfaces as well as in the interior of the aircraft. In order to have a robust design framework, the critical strain energy-release rate associated with the face/core interface must be ascertained with utmost confidence. Fracture characterization of aerospace grade honeycomb core sandwich specimens were carried out using the

DCB-UBM test methodology and is presented in Paper P5. The novel rig designed in-house [P3] was utilized (see section 4.2). Primarily, aerospace grade sandwich specimens manufactured by Shütz GmbH were utilized. Two core types of Shütz make - Cormaster C1 [108] and Cormaster N636 [109] were investigated. The Cormaster C1 type comprised of Nomex® T412 paper, whilst the Cormaster CN636 type was made from para-aramid (Kevlar) N636 paper material. A plain weave Carbon Fiber Reinforced Plastic (CFRP) prepreg (Hexcel fabric with HexPly® 913 epoxy resin)) [110] was chosen as face sheet with two stacking sequences: [0/90] and [45/0/0/45] with a nominal thickness of 0.35 and 1.40 mm, respectively.

Mixed mode fracture screening was conducted by selecting moment ratio (MR) values from a MR vs. phase angle (ψ) map obtained using the CSDE method. A brief overview of the FE-model of the DCB-UBM specimen is provided in section 4.2.5 and a detailed discussion can be found in Appendix A of [P5]. The sandwich panels were manufactured and supplied by AIRBUS GmbH. The DCB-UBM specimens were later cut in-house using a diamond cutter and the doubler layers were glued. More information on panel and specimen preparation can be found in [111, P5]. Core and face sheet material properties were invariably required for FEA. The face sheet properties were obtained using standard ASTM tests [101, 102, 112]. The technical data sheet of most core supplier's/manufacturer provide only out of plane modulus, shear modulus in LT and WT directions [108, 109, 113]. A schematic illustration of honeycomb cell with coordinate system is shown in Figure 4.17. For honeycomb cores, L- is referred to as the ribbon direction, W- as transverse and T- as through thickness direction. The analytic approach used to obtain the homogenized core properties is discussed in the next section.

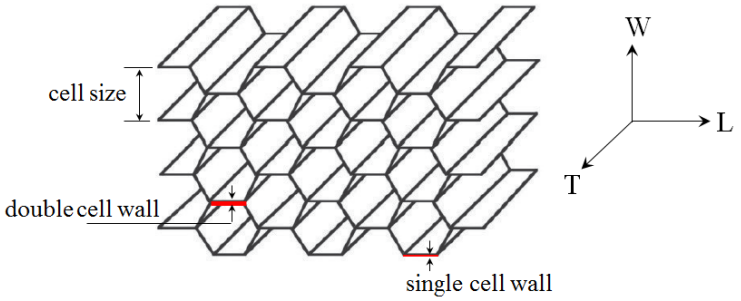

Figure 4.17. Schematic illustration of a typical hexagonal honeycomb core cell with single and double cell walls.

4.4.1 Honeycomb core: Homogenization Approach

FEA in conjunction with the CSDE method was employed to select MR that corresponds to a particular phase angle, ψ. In the FE-model, the honeycomb core was modeled as a homogenized continuous system. Discrete modeling of cell walls along with densified mesh required at the crack tip by CSDE (see section 4.2.5), will render a computationally expensive model. On the contrary, homogenized properties of core are readily not available and need to deduced. Several works exist in the literature to determine effective elastic and inelastic properties of regular honeycombs with a hexagonal structure using numerical and analytical approaches [114, 115, 116, 117, 118, 119, 120].

In the analytical approach proposed by Gibson and Ashby [119], linear elastic mechanical properties of regular cellular structures are obtained using beam theory. This approach can also be applied to regular hexagonal honeycomb cores and require elastic properties of the paper material as input. Foo et al. [121] measured the mechanical properties of the paper material and compared with experimental and analytical results of the entire core. Similar tests of the core structure was also carried out in [122, 123] and good agreement between test results and analytical approach in [119] was obtained. The original expressions for homogenized core properties proposed by Gibson and Ashby [119] was extended to a wide range of honeycomb cores with double walls by Malek and Gibson in [124]. In [P5], the core properties were obtained using the analytical expressions proposed by Malek and Gibson [124], by substituting the measured paper mechanical properties [125]. Exhaustive tests on the entire core structure were also carried out in [125]. The obtained core elastic properties for Cormaster C1 and N636 types are provided in Table 4.3 [4] [111, 125].

Table 4.3. Material properties for honeycomb cores.

	C1-4.8-32	**C1-4.8-64**	**C1-4.8-96**	**CN1-4.8-32**
E_L [MPa]	0.075	0.226	0.492	0.104
E_W [MPa]	0.075	0.226	0.492	0.104
E_T [MPa]	121.9	176.3	228.5	298.1
G_{LW} [MPa]	0.033	0.01	0.022	0.092
G_{TL} [MPa]	20.7	29.9	38.7	59.6
G_{TW} [MPa]	13.1	18.9	24.5	35.9
ν_{LW}	1	1	1	1
ν_{TL}	0.354	0.36	0.354	0.354
ν_{TW}	0.35	0.35	0.35	0.354
Density [kg/m^3]	32	64	96	32
Paper thickness [μm]	56	81	105	62

Comment on core Poisson's ratio:
In the analytical formulation by Gibson and Ashby [119], the Poisson's ratio is a function of the geometry of the honeycomb unit cell which can be ascertained accurately. During the initial phase of this Ph.D. project, modeling was performed by considering ν_{LW} to be equal to that of the honeycomb paper material. Such an assumption had profound impact on the near tip behavior, which in-turn affected the mode-mixity calculated using the CSDE method. This phenomenon is illustrated in Figure 4.18, where crack tip mesh distortions have been stabilized when $\nu_{LW} \simeq 1$ [5]. It should be noted that the CSDE method utilizes only the relative crack flank displacements hence, excessive near tip element distortions will yield inaccurate results. This was further corroborated from experimental results in [125], where Digital Image Correlation (DIC) technique was used to accurately estimate Poisson's ratio.

[4] For brevity, the honeycomb core is designated as core type - cell size - density, e.g., C1-4.8-32 refers to Cormaster C1 type core with a 4.8 mm cell size and a density of 32 kg/m^3.

[5] Similar observation was also made by researchers who used VCCT method [111, 112].

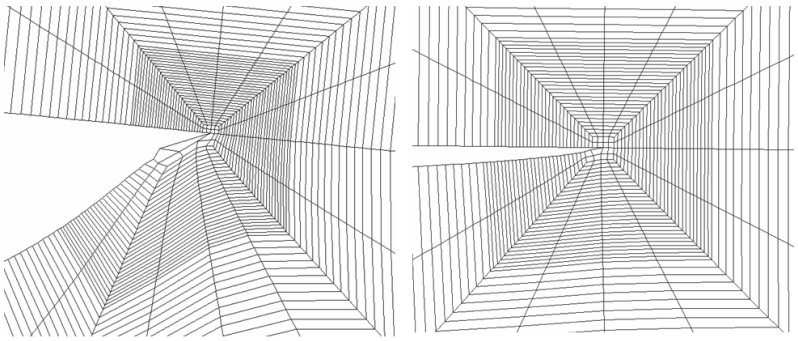

Figure 4.18. Crack tip element distortion before (left) and after (right) core homogenization approach with $\nu_{LW} \simeq 1$.

4.4.2 Test Procedure

A total of twenty specimens were tested to study the effect that honeycomb core density, paper material, crack propagation direction and face sheet thickness have on interface fracture toughness. As mentioned previously, a single DCB-UBM specimen can be utilized to test at several mode-mixity phase angle values. Therefore, to accumulate more data points, fracture testing was performed at a specific phase-angle multiple times. This was achieved by un-loading the specimen when the debond propagated ≈ 10 mm (corresponding to two cells). The recorded moments from both arms were used to deduce the energy released (see section 4.2.4). Testing was carried out in both L- and W- crack directions of the core. The chosen moment ratio (MR) values and the corresponding mode-mixity phase angle for the various core types tested in [P5] are provided in Table 4.4. It should be noted that in Table 4.4, $MR < 0$ corresponds to arms opening relative to each other, whereas, $MR > 0$ refers to arms rotating in clock-wise direction with respect to the plane of paper. As mentioned previously in [P1], a pure mode I scenario in terms of phase angle (in degrees) corresponds to 0°, whereas a pure mode II loading exist at 90°.

To realize mixed mode screening of honeycomb core specimens, the interface fracture toughness need to be characterized over a range of mode-mixity phase angle values, $\Gamma(\psi)$. The initiation fracture toughness, Γ, obtained during the tests were fitted using a phenomenological expression proposed by Hutchinson and Suo [18]:

$$\Gamma(\psi) = G_{1c}\left(1 + \tan^2\left[(1-\Lambda)\,\psi\right]\right) \tag{4.9}$$

where G_{1c} is the mode I fracture toughness ($\Gamma(\psi = 0°)$) and Λ is a dimensionless constant. The fracture toughness values were fitted by eye using Equation 4.9 for all the tested specimens.

4.4.3 Test Results and Discussions

Figure 4.19 shows the interface fracture toughness as a function of mode-mixity phase angle (ψ) for specimens with Cormaster C1 and N636 type cores. Note that, the presented results are for constant face sheet properties. It was observed that specimens

Table 4.4. Moment ratio (MR) chosen for testing DCB-UBM honeycomb core specimens with various core types. Phase angle (ψ) is provided in parenthesis.

Core Type	Moment Ratio (ψ [deg])
W - direction	
C1-4.8-32 (h_f = 0.35 mm)	1 (-49°), 1.5(-40°), 2 (-32°), 3 (-24°), 5 (-19°), -20 (-6°), -10 (-4°)
C1-4.8-32 (h_f = 1.40 mm)	1 (-52°), 2 (-35°), 3 (-29°), 10 (-20°), -20 (-14°), -10 (-12°), -3 (-2°)
C1-4.8-64 (h_f = 1.40 mm)	1 (-52°), 2 (-35°), 3 (-29°), 10 (-20°), -20 (-14°), -3 (-2°)
C1-4.8-96 (h_f = 1.40 mm)	2 (-36°), 3 (-29°), -3 (-8°), -3 (-2°)
CN1-4.8-32 (h_f = 1.40 mm)	1 (-54°), 2 (-36°), 7.5 (-21°), 10 (-18°), -6 (-6°)
L - direction	
C1-4.8-32 (h_f = 0.35 mm)	1 (-49°), 2 (-32°), 5 (-19°), 15 (-12°), -20 (-6°), -10 (-4°)
C1-4.8-32 (h_f = 1.40 mm)	1 (-49°), 2 (-32°), 3 (-24°), 5 (-19°), -20 (-6°), -10 (-4°), -7.5 (-2°)
C1-4.8-64 (h_f = 1.40 mm)	1 (-52°), 2 (-35°), 3 (-29°), 10 (-20°), -20 (-14°), -3 (-2°)
C1-4.8-96 (h_f = 1.40 mm)	2 (-36°), 5 (-25°), -20 (-17°), -5 (-12°), -3 (-2°)
CN1-4.8-32 (h_f = 1.40 mm)	1 (-54°), 2 (-36°), 7.5 (-21°), 10 (-18°), -20 (-12°), -6 (-6°)

with Cormaster C1 core comprising of Nomex® T412 paper were tougher compared to specimens with Cormaster N636 type. The mode I fracture toughness in W-direction for the C1 type specimens were approximately double as that of CN1 type specimens. Furthermore, the interface fracture toughness increases with rise in core density and was observed to be always higher in W-direction for all the core types considered in [P5]. A bar-chart depicting mode I fracture toughness for various core densities along with coefficient of variation (COV) is shown in Figure 4.20a. Fracture testing was also performed on specimens with thin face sheets (h_f = 0.35 mm). It was found that, for constant core properties, specimens with thin face sheets exhibited higher fracture toughness compared to specimens with thick face sheets.

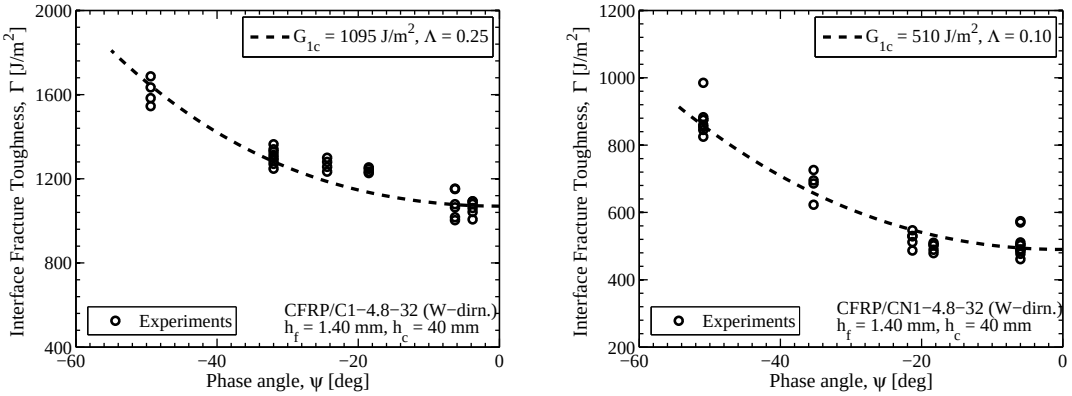

(a) (b)

Figure 4.19. Interface fracture toughness (Γ) vs. phase angle (ψ) for a honeycomb core sandwich specimen with CFRP face sheet; h_f = 1.40 mm and h_c = 40 mm (a) C1 core type (W-direction), and (b) CN1 core type (W-direction).

For most of the specimens, crack propagation was observed to occur just beneath the

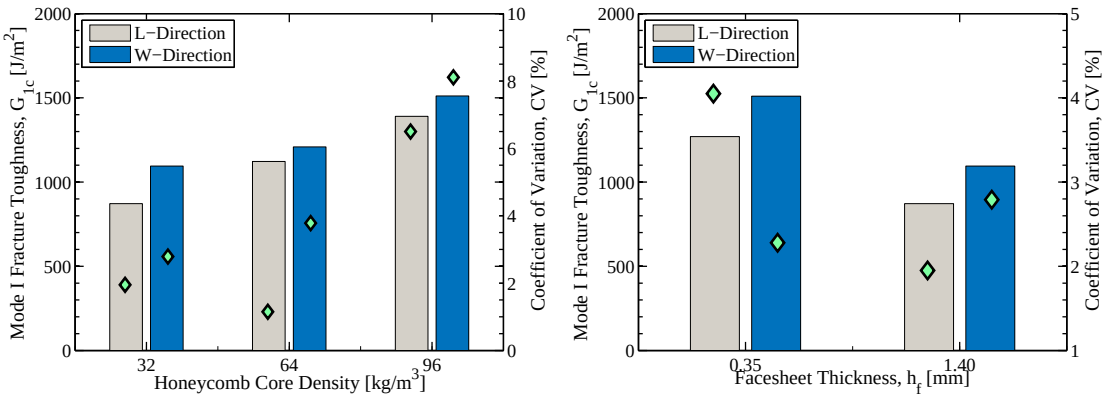

Figure 4.20. Mode I fracture toughness (G_{1c}) and COV for CFRP/C1-type honeycomb core sandwich specimens with $h_c = 40$ mm (a) G_{1c} variation across core densities (b) G_{1c} comparison with face sheet thickness.

meniscus layer. There appears to be scatter in the experimental data (see Figure 4.19). This may be attributed to the highly non-uniform crack path in honeycomb core specimens. During the manufacturing phase of sandwich specimens, the adhesive layer which bonds the face sheet with the core, may percolate at certain locations in the specimen during curing, which leads to creation of resin rich cells. The crack kinks into the core and climbs back again to the interface when encountered with such resin rich pocket during advancement. In general, the crack advances through the path of least resistance which may explain the kinking of crack to circumvent the local resin rich cells. Figure 4.21a shows this behavior on C1-4.8-32 specimen with $h_f = 1.4$ mm and a detailed view can be noted in Figure 4.21c for a similar specimen with $h_f = 0.35$ mm. The crack surface for the 32 kg/m^3 dense core with thin face sheet is shown in Figure 4.21b, depicting interface crack propagation throughout the tested length of the specimen .

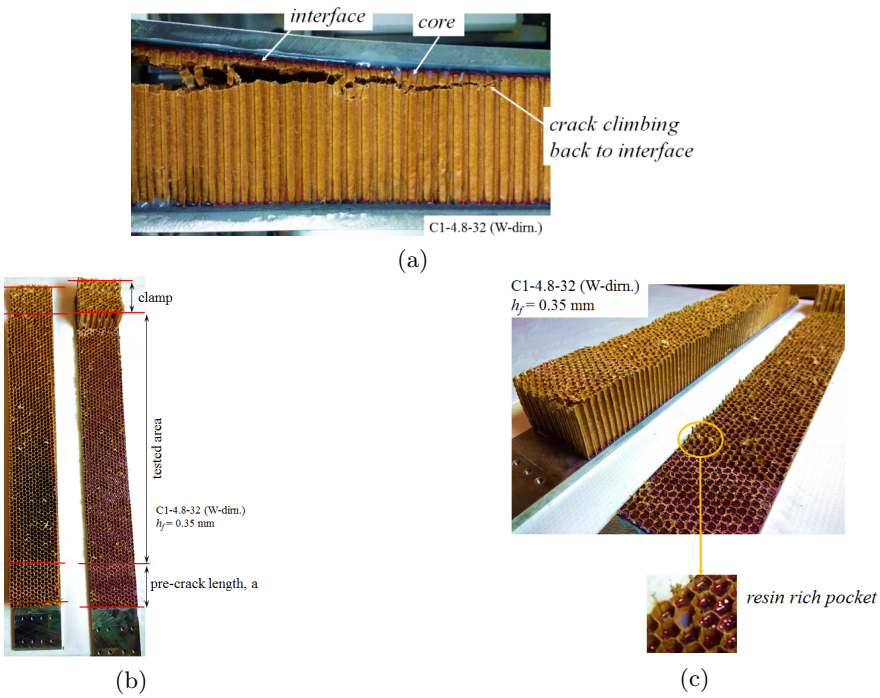

Figure 4.21. Interface crack propagation and fracture surfaces for CFRP/C1-type honeycomb core specimens with $h_c = 40$ mm; (a) crack climbing back to interface in C1-32 core type specimen (W-direction) with $h_f = 1.4$ mm, and (b) C1-type specimen showing interface crack propagation throughout the tested length of the specimen, and (c) resin rich cell in C1-4.8-32 specimen with $h_f = 0.35$ mm.

Chapter 5

Conclusions and Outlook

The current Ph.D. work treated the interface fracture problem in typical sandwich composites. The presented work encompassed experimental, theoretical and numerical aspects. The outcome of this project has been presented in the five papers [P1 - P5] appended to this Thesis. The experimental results and numerical analyses enhanced the knowledge on face/core interface fracture problem. The analytic expressions derived in the current work are an addition to the literature and will help in the development of DCB-UBM as a standard fracture specimen.

Mode-mixity variation in sandwich composites

It is a well known fact that the crack propagation in an interface between two dissimilar materials will occur in mixed mode conditions. The major consequence of this behavior is that a full map of interface fracture toughness variation as a function of mode-mixity is required. The debond growth in SCB sandwich specimen, which is designed to be used as a "peel" or mode I dominant test invariably occur under mixed mode conditions. The parametric study conducted in [P1] showed that the existing sizing method for SCB specimens [49] yielded configurations which remain in mode I regime. Moreover, the study also revealed that, despite conforming to the sizing requirements, a certain class of specimens was also found to deviate away from the mode I bounds. In general, for a constant face sheet thickness (h_f), stiffer face sheets led to increasingly positive values of mode-mixity phase angle (ψ) which deviate away from the mode I conditions.

For the modeled results in [P1], significant deviation from the mode I regime with loading rods shorter than 500 mm was observed. A rod length in terms of the length of the SCB specimen was recommended as: $L_{rod} \geq 1.70L$. Addition of reinforcement layers on a SCB sandwich specimen was shown to deteriorate the mode-mixity condition and shifted the debonding away from mode I conditions. The mode-mixity phase angle at short crack lengths was found to be higher, hence the initial loading cycle corresponding to a crack increment of ∼30 mm was recommended to be disregarded. Furthermore, the recommendations laid out in [P1] is an addition to the existing sizing study [49], and will help potential experimentalists to obtain reliable mode I fracture toughness data

corresponding to a peel dominant loading on the debonded face sheet. The conclusions and recommendations from the parametric study in [P1] can also serve as inputs in the formulation of the peel dominant ASTM International draft standard [13].

Foundation effects in debonded sandwich specimens

The original expressions for energy-release rate and mode-mixity phase angle, derived for a bi-material interface [18] assume that shear forces are absent at the crack tip. However, there exist many sandwich fracture tests which contain shear component at the crack tip, e.g., SCB, MMB etc. For reliable fracture toughness measurements, the transverse shear must be taken into consideration by incorporating crack tip root rotation. The approach in [67] was utilized in [P2] and the crack tip root expressions were calibrated using FEA results for a typical moment- and force- loaded SCB sandwich specimen. Good agreement between FEA and analytical expressions were obtained in [P2] lending confidence to the approach in [67].

Compliance and energy-release rate results for a moment-loaded SCB specimen was derived in [P2] using the Winkler mechanical model, and were compared with detailed finite element results. In addition, good agreement between compliance and energy-release rate expressions for force-loaded SCB sandwich specimen and FEA was obtained. A foundation modulus where $(1/4)^{th}$ of the core acts as a foundation was introduced in [P2], and was seen to agree well with numerically obtained results for both force and moment loading configurations. The increased dominance of shear component at short crack lengths was reflected on the mode-mixity phase angle (ψ) for a force-loaded SCB sandwich specimen, further corroborating the findings and recommendations in [P1]. The deformation characteristics was accurately estimated for both force- and moment- loaded SCB configurations using beam on elastic foundation approach in [P2].

Mixed mode fracture testing of sandwich composites

It is highly desirable that the mode-mixity conditions remain constant throughout the crack propagation in a specimen, which lays foundation to the need for a steady-state fracture specimen. The DCB-UBM sandwich specimen is such and significant progress in development of this specimen was made in this Thesis. To overcome the challenges in the traditional DCB-UBM test rigs, a novel test rig capable of applying pure moments through independent torsional actuators was realized in [P3]. The rig presented in [P3] is stand-alone, compact and is able to achieve large moment values. A dedicated controller was programmed to perform fracture tests under quasi-static and fatigue conditions.

In the DCB-UBM sandwich specimen, a constant mode-mixity condition can be achieved by controlling the ratio of moments between the two arms (see section 4.2). Therefore, addition of reinforcement layers or "doublers" will not have any additional impact on the mode-mixity as long as the moment ratio (MR) corresponding to the desired mode-mixity phase angle (ψ) is held constant throughout the crack propagation. This works in favor of the sandwich specimens with thin face sheets enabling to perform fracture analysis under the ambit of LEFM by preventing excessive face sheet rotation. Application of doublers also work in advantage of the newly developed rig, and aids in direct application of moments through dedicated actuators as described in [P3]. The closed form algebraic

expressions for the energy-release rate and the mode-mixity phase angle (ψ) were determined for a typical reinforced sandwich specimen loaded with unequal moments in [P4]. The provided expressions in [P4] are analytic except for a load-independent scalar parameter, ω. The phase angle, ψ, was expressed in terms of ω, and specific determination of ω requires that the interface problem be solved for a single loading case. The value of ω varied weakly with the doubler thickness, and the dependence was expressed by a curve fitting polynomial for typical sandwich configurations in [P4]. This variation is not that substantial, as a constant doubler thickness is typically employed during fracture tests (see [P3] and [P5]).

Mixed mode fracture testing of foam and honeycomb core sandwich specimens comprising of thin and thick face sheets were carried out in this Thesis using the novel DCB-UBM test rig in [P3] and [P5]. The interface fracture toughness increased with mode-mixity phase angle (ψ) and a phenomenological expression was utilized to express fracture toughness as a function of mode-mixity, $\Gamma(\psi)$. For the foam core specimens with E-glass face sheets, the fracture toughness was found to be in the range 180 - 600 J/m^2 and the toughness values in predominant mode I and mixed mode conditions are comparable to the results obtained using the MMB and TSD test methods for a similar specimen [P3]. Mixed mode fracture characterization of aerospace grade honeycomb core specimens with thin and thick face sheets were also carried out using the DCB-UBM test methodology, and was presented in [P5]. These tests enabled a parametric analysis of toughness variation based on honeycomb core density, paper material, crack propagation direction and face sheet thickness. The experimental campaign in [P5] yielded toughness values in the range 400 - 1800 J/m^2. Similar to [P3], a full map of fracture toughness variation with mode-mixity ($\Gamma(\psi)$) was obtained for various honeycomb core specimen configurations.

5.1 Outlook and Recommendations

From the results and discussions presented in Papers [P1 - P5], the following proposals for future work as well as recommendations can be made.

1. *Mode I fracture toughness characterization using the SCB test method*

   The parametric analysis presented in [P1] is an extension in efforts to fence the SCB sandwich specimen such that debonding occurs in mode I conditions emulating a peel dominant loading on the face sheet. In order to employ the measured fracture toughness values with high degree of confidence in numerical models, it is desired to have a closed form expression to determine the mode-mixity phase angle (ψ) akin to a DCB-UBM specimen [69, P4]. In the absence of such an expression, it is advised to proceed with caution. It is also highly recommended to perform a limited series of mode-mixity analyses prior to testing.

2. *Reinforced DCB-UBM sandwich specimen and test methodology*

   Reinforcement of DCB-UBM sandwich specimens with doubler layers were shown to prevent excessive rotation, thereby restricting the fracture analysis in LEFM regime. Direct application of moments on crack flanks through dedicated actuators

were shown to be effective in characterization of specimens especially in predominant mode II conditions. The current test rig and the outlined test methodology are industry ready for quasi-static testing. The closed form expressions derived in [P4] may be used to extract ω parameter for a particular sandwich configuration of interest, enabling to realize a map of moment ratio (MR) vs. phase angle (ψ). However, stiffness degradation of doublers are not accounted in the derived expressions. Therefore, experimentalists are advised to characterize the doublers carefully, especially in fatigue tests.

3. *Compliance solution for DCB-UBM specimen*

   Fatigue testing in the current DCB-UBM test rig may pose many challenges such as inertia effect, friction etc. Hence, it is highly desirable to negate such effects at the specimen level through an appropriate data reduction scheme, such as compliance calibration method. Initial step in this direction was taken in [P2] in which the analysis aids in understanding compliance, energy-release rate and mode-mixity of a debonded specimen loaded with moment, such as the DCB-UBM. The natural next step is to expand the approach in [P2] to a DCB specimen loaded with unequal bending moments using a beam on elastic foundation approach. Such an analysis also paves way in incorporating a more robust data reduction scheme in which the energy-release rate can be deduced in terms of the specimen compliance.

4. *Towards development of a mixed mode fracture standard*

   The DCB-UBM test methodology currently represents the most effective way to perform interface fracture toughness characterization under a wide range of mixed mode conditions. Moreover, the test methodology is robust enough for assessment of delamination fracture toughness in laminates and can also be utilized for other cohesive interfaces. Therefore, development of DCB-UBM specimen as a fracture test standard will further strengthen the building-block approach and help in creation of coupon data in mixed mode conditions.

5. *Damage tolerance of debond damaged sandwich structures*

   Damage tolerance of debond damaged sandwich structures is pertinent and in recent years considerable research has been pursued in this line. Berggreen [34] conducted both numerical and experimental studies to investigate damage tolerance in foam core sandwich structures used in naval applications. Moslemain [36] conducted quasi-static as well as fatigue studies on debond damaged sandwich structures under mixed mode conditions. Manca et al. [97] extended fracture toughness characterization to fatigue loading using the MMB sandwich specimen. The methodologies developed in this Thesis further bolsters the efforts toward damage tolerance analysis. The current industrial design strategies avoid entering in a damage tolerant domain or selecting an immediate repair strategy leading to a highly over designed component. For high risk applications such as in the aerospace sector, a less conservative approach is adopted wherein proactive methodologies based on Non-Destructive Inspection (NDI) are highly used. It is the author's conviction that the propensity of the industry is to design components which either prevent the crack growth or stymie the instigated disbond through arresting mechanisms.

References

[1] L. A. Carlsson and G. A. Kardomateas, *Structural and Failure Mechanics of Sandwich Composites*. Springer Science & Business Media, 2011.

[2] D. Zenkert, *An Investigation to Sandwich Construction*. Chameleon Press, London, 1995.

[3] T. S. B. of Canada (TSB), "Loss of rudder, Airbus 310-308, Air Transat Flight 961," 2005.

[4] E. H. Glaessgen, J. R. Reeder, D. W. Sleight, J. T. Wang, I. S. Raju, and C. E. Harris, "Debonding failure of sandwich-composite cryogenic fuel tank with internal core pressure," *Journal of spacecraft and rockets*, vol. 42, no. 4, pp. 613–627, 2005.

[5] U. Vantini, "Investigating Effects of Pure Shear Deformation in Wind Turbine Blade Sub-Structures," Master's thesis, Politechnico Di Milano, 2014.

[6] CMH-17, *Composite Materials Handbook Volume 6. Structural Sandwich Composites*. SAE International, 2013.

[7] ASTM International, "ASTM D5528-13 Standard Test Method for Mode I Interlaminar Fracture Toughness of Unidirectional Fiber-Reinforced Polymer Matrix Composites," 2013.

[8] ASTM International, "ASTM D6115-97 Standard Test Method for Mode I Fatigue Delamination Growth Onset of Unidirectional Fiber-Reinforced Polymer Matrix Composites,," 2011.

[9] ASTM International, "ASTM D6671/D6671M-13e1 Standard Test Method for Mixed Mode I-Mode II Interlaminar Fracture Toughness of Unidirectional Fiber Reinforced Polymer Matrix Composites,," 2013.

[10] ASTM International, "ASTM D7905/D7905M-14 Standard Test Method for Determination of the Mode II Interlaminar Fracture Toughness of Unidirectional Fiber-Reinforced Polymer Matrix Composites," 2014.

[11] ASTM International, "ASTM E1922-04 Standard Test Method for Translaminar Fracture Toughness of Laminated and Pultruded Polymer Matrix Composite Materials," 2015.

[12] R. Krueger, Z.-M. Chen, J. Ratcliffe, D. Adams, W. Seneviratne, C. Oline, C. Berggreen, F. Attanasio, V. Saseendran, Y. Albertone, R. Schauble, and S.-C. Fimmen, "Characterizing Face Sheet/Core Disbonding Using the Single Cantilever Beam Test: Results from an International Round Robin," *NASA Technical Report (Manuscript in preperation)*, 2017.

[13] J. Ratcliffe and D. Adams, "Preliminary Round Robin SCB Test Procedure (ASTM WK56166)," *ASTM Draft standard in preperation*, 2015.

[14] C. Berggreen, K. Anyfantis, V. Saseendran, and M. Manoucher, "Fracture characterization of interfaces with a new DCB-UBM test rig," 16^{th} *International Conference on Experimental Mechanics (ICEM16), Cambridge, UK*, 7- 11 July, 2014.

[15] V. Saseendran, "Fracture Mechanical Testing of Sandwich Composites," Master's thesis, Technical University of Denmark, 2014.

[16] A. A. Griffith, "The phenomena of rupture and flow in solids," *Philosophical transactions of the royal society of london. Series A, containing papers of a mathematical or physical character*, vol. 221, pp. 163–198, 1921.

[17] G. Irwin and J. Kies, "Fracturing and fracture dynamics," *Welding Journal*, vol. 31, no. 2, pp. 95–100, 1952.

[18] J. W. Hutchinson and Z. Suo, "Mixed mode cracking in layered materials," *Advances in applied mechanics*, vol. 29, pp. 63–191, 1991.

[19] H. Ming-Yuan and J. W. Hutchinson, "Crack deflection at an interface between dissimilar elastic materials," *International Journal of Solids and Structures*, vol. 25, no. 9, pp. 1053–1067, 1989.

[20] K. Liechti and Y. Chai, "Asymmetric shielding in interfacial fracture under in-plane shear," *Journal of applied mechanics*, vol. 59, no. 2, pp. 295–304, 1992.

[21] Z. Suo and J. W. Hutchinson, "Interface crack between two elastic layers," *International Journal of Fracture*, vol. 43, no. 1, pp. 1–18, 1990.

[22] J. Dundurs, "Edge-bonded dissimilar orthogonal elastic wedge," *J Appl Mech*, vol. 36, pp. 650–652, 1969.

[23] S. Zhigang, "Singularities interacting with interfaces and cracks," *International Journal of Solids and Structures*, vol. 25, no. 10, pp. 1133–1142, 1989.

[24] P. Matos, R. McMeeking, P. Charalambides, and M. Drory, "A method for calculating stress intensities in bimaterial fracture," *International Journal of Fracture*, vol. 40, no. 4, pp. 235–254, 1989.

[25] E. F. Rybicki and M. F. Kanninen, "A finite element calculation of stress intensity factors by a modified crack closure integral," *Engineering Fracture Mechanics*, vol. 9, no. 4, pp. 931–938, 1977.

[26] J. L. Beuth, "Separation of crack extension modes in orthotropic delamination models," *International Journal of Fracture*, vol. 77, no. 4, pp. 305–321, 1996.

[27] R. Smelser, "Evaluation of stress intensity factors for bimaterial bodies using numerical crack flank displacement data," *International Journal of Fracture*, vol. 15, no. 2, pp. 135–143, 1979.

[28] P. G. Charalambides and W. Zhang, "An energy method for calculating the stress intensities in orthotropic bimaterial fracture," *International Journal of Fracture*, vol. 76, no. 2, pp. 97–120, 1996.

[29] M. Williams, "The stresses around a fault or crack in dissimilar media," *Bulletin of the seismological society of America*, vol. 49, no. 2, pp. 199–204, 1959.

[30] F. Erdogan, "Stress distribution in a nonhomogeneous elastic plane with cracks," *Journal of applied mechanics*, vol. 30, no. 2, pp. 232–236, 1963.

[31] A. England, "A crack between dissimilar media," *J. appl. Mech*, vol. 32, no. 2, pp. 400–402, 1965.

[32] C. Berggreen, B. C. Simonsen, and K. K. Borum, "Experimental and numerical study of interface crack propagation in foam-cored sandwich beams," *Journal of composite materials*, vol. 41, no. 4, pp. 493–520, 2007.

[33] ANSYS Inc,, Cannonsburg, PA, USA, *ANSYS Mechanical User's Guide*, 2014.

[34] C. Berggreen, *Damage tolerance of debonded sandwich structures*. PhD thesis, Technical University of Denmark, 2005.

[35] H. Neuber, "Ni muskhelishvili, some basic problems of the mathematical theory of elasticity. 3. verb. und vermehrte auflage.(aus dem russischen übersetzt von jrm radok.) xxxi+ 704 s. m. 66 abb. groonigen (holl.) 1953. verlag p. noordhoff ltd. preis geb. 38.–fl," *ZAMM-Journal of Applied Mathematics and Mechanics/Zeitschrift für Angewandte Mathematik und Mechanik*, vol. 34, no. 12, pp. 479–479, 1954.

[36] R. Moslemian, *Residual Strength and Fatigue Lifetime of Debond Damaged Sandwich Structures*. PhD thesis, Technical University of Denmark, 2011.

[37] S. Prasad and L. A. Carlsson, "Debonding and crack kinking in foam core sandwich beamsi. analysis of fracture specimens," *Engineering Fracture Mechanics*, vol. 47, no. 6, pp. 813–824, 1994.

[38] S. Prasad and L. A. Carlsson, "Debonding and crack kinking in foam core sandwich beamsii. experimental investigation," *Engineering Fracture Mechanics*, vol. 47, no. 6, pp. 825–841, 1994.

[39] F. Aviles and L. Carlsson, "Analysis of the sandwich DCB specimen for debond characterization," *Engineering Fracture Mechanics*, vol. 75, no. 2, pp. 153–168, 2008.

[40] L. Carlsson, L. Sendlein, and S. Merry, "Characterization of face sheet/core shear fracture of composite sandwich beams," *Journal of Composite Materials*, vol. 25, no. 1, pp. 101–116, 1991.

[41] L. Carlsson, "On the design of the cracked sandwich beam (CSB) specimen," *Journal of Reinforced Plastics and Composites*, vol. 10, no. 4, pp. 434–444, 1991.

[42] X. Li and L. A. Carlsson, "The tilted sandwich debond (TSD) specimen for face/core interface fracture characterization," *Journal of Sandwich Structures & Materials*, vol. 1, no. 1, pp. 60–75, 1999.

[43] X. Li and L. A. Carlsson, "Elastic foundation analysis of tilted sandwich debond (TSD) specimen," *Journal of Sandwich Structures & Materials*, vol. 2, no. 1, pp. 3–32, 2000.

[44] X. Li and L. A. Carlsson, "Fracture mechanics analysis of tilted sandwich debond (TSD) specimen," *Journal of composite materials*, vol. 35, no. 23, pp. 2145–2168, 2001.

[45] C. Berggreen and L. A. Carlsson, "A modified TSD specimen for fracture toughness characterization-fracture mechanics analysis and design," *Journal of Composite Materials*, vol. 44, no. 15, pp. 1893–1912, 2010.

[46] C. Berggreen, A. Quispitupa, A. Costache, and L. A. Carlsson, "Face/core mixed mode debond fracture toughness characterization using the modified TSD test method," *Journal of Composite Materials*, vol. 48, no. 16, pp. 1939–1945, 2014.

[47] W. Cantwell and P. Davies, "A test technique for assessing core-skin adhesion in composite sandwich structures," *Journal of materials science letters*, vol. 13, no. 3, pp. 203–205, 1994.

[48] W. Cantwell, G. Broster, and P. Davies, "The influence of water immersion on skin-core debonding in gfrp-balsa sandwich structures," *Journal of reinforced plastics and composites*, vol. 15, no. 11, pp. 1161–1172, 1996.

[49] J. G. Ratcliffe and J. R. Reeder, "Sizing a single cantilever beam specimen for characterizing facesheet–core debonding in sandwich structure," *Journal of Composite Materials*, vol. 45, no. 25, pp. 2669–2684, 2011.

[50] J. R. Reeder and J. H. Crews, "Mixed-mode bending method for delamination testing," *AIAA Journal*, vol. 28, no. 7, pp. 1270–1276, 1990.

[51] A. Quispitupa, C. Berggreen, and L. A. Carlsson, "A debonded sandwich specimen under mixed mode bending (MMB)," in *8th International Conference on Sandwich Structures*, pp. 186–198, Publindústria, Produção de Comunicação, Lda., 2008.

[52] A. Quispitupa, C. Berggreen, and L. A. Carlsson, "On the analysis of a mixed mode bending sandwich specimen for debond fracture characterization," *Engineering Fracture Mechanics*, vol. 76, no. 4, pp. 594–613, 2009.

[53] A. Quispitupa, C. Berggreen, and L. A. Carlsson, "Design analysis of the mixed mode bending sandwich specimen," *Journal of Sandwich Structures & Materials*, vol. 12, no. 2, pp. 253–272, 2010.

[54] A. Quispitupa, C. Berggreen, and L. A. Carlsson, "Face/core interface fracture characterization of mixed mode bending sandwich specimens," *Fatigue & Fracture of Engineering Materials & Structures*, vol. 34, no. 11, pp. 839–853, 2011.

[55] M. Manca, C. Berggreen, and L. A. Carlsson, "G-control fatigue testing for cyclic crack propagation in composite structures," *Engineering Fracture Mechanics*, vol. 149, pp. 375–386, 2015.

[56] M. Manca, C. Berggreen, L. A. Carlsson, and P. Bortolotti, "Fatigue characterization of poly vinyl chloride (pvc) foam core sandwich composite using the g-control method," *Journal of Sandwich Structures & Materials*, vol. 18, no. 3, pp. 374–394, 2016.

[57] B. F. Sørensen, K. Jørgensen, T. K. Jacobsen, and R. C. Østergaard, "DCB-specimen loaded with uneven bending moments," *International Journal of Fracture*, vol. 141, no. 1-2, pp. 163–176, 2006.

[58] C. Lundsgaard-Larsen, B. F. Sørensen, C. Berggreen, and R. C. Østergaard, "A modified DCB sandwich specimen for measuring mixed-mode cohesive laws," *Engineering Fracture Mechanics*, vol. 75, no. 8, pp. 2514–2530, 2008.

[59] J. Ratcliffe and W. Cantwell, "Center notch flexure sandwich geometry for characterizing skin-core adhesion in thin-skinned sandwich structures," *Journal of reinforced plastics and composites*, vol. 20, no. 11, pp. 945–970, 2001.

[60] R. Fields and Z. R.P, "Analysis and Test Methodology for Fracture Mechanics of Unbonded Sandwich Structures," tech. rep., Martin Maerietta Task Report, EDF No MM0 TKR 10722739-001, 1994.

[61] K. Shivakumar, H. Chen, and S. A. Smith, "An evaluation of data reduction methods for opening mode fracture toughness of sandwich panels," *Journal of Sandwich Structures & Materials*, vol. 7, no. 1, pp. 77–90, 2005.

[62] C. Weaver, "Evaluation of Mode I Fracture Mechanics Test Methods For Sandwich Composites," Master's thesis, University of Utah, 2009.

[63] M. Kanninen, "An augmented double cantilever beam model for studying crack propagation and arrest," *International Journal of fracture*, vol. 9, no. 1, pp. 83–92, 1973.

[64] S. Schmauder and M. Meyer, "Correlation between dundurs parameters and elastic constants," *Z. Metallkd*, vol. 83, no. 7, pp. 524–527, 1992.

[65] M. Rinker, J. Ratcliffe, Adams, and R. Krueger, "Characterizing Facesheet/Core Disbonding in Honeycomb Core Sandwich Structure," *NASA Technical Report CR-2013-217959*, 2013.

[66] J. R. Reeder, K. Demarco, and K. S. Whitley, "The use of doubler reinforcement in delamination toughness testing," *Composites Part A: Applied Science and Manufacturing*, vol. 35, no. 11, pp. 1337–1344, 2004.

[67] S. Li, J. Wang, and M. Thouless, "The effects of shear on delamination in layered materials," *Journal of the Mechanics and Physics of Solids*, vol. 52, no. 1, pp. 193–214, 2004.

[68] R. C. Østergaard and B. F. Sørensen, "Interface crack in sandwich specimen," *International Journal of Fracture*, vol. 143, no. 4, pp. 301–316, 2007.

[69] G. A. Kardomateas, C. Berggreen, and L. A. Carlsson, "Energy-release rate and mode mixity of face/core debonds in sandwich beams," *AIAA journal*, 2013.

[70] L. A. Carlsson and J. W. Gillespie Jr, "Mode-ii interlaminar fracture of composites," in *Composite Materials Series*, vol. 6, pp. 113–157, Elsevier, 1989.

[71] S. Timoshenko and J. Goodier, *Theory of elasticity*. McGraw-Hill New York, 1970.

[72] J. R. Barber, *Intermediate mechanics of materials*, vol. 175. Springer Science & Business Media, 2010.

[73] T. Lu, Z. Xia, and J. Hutchinson, "Delamination of beams under transverse shear and bending," *Materials Science and Engineering: A*, vol. 188, no. 1-2, pp. 103–112, 1994.

[74] M. G. Andrews and R. Massabò, "The effects of shear and near tip deformations on energy release rate and mode mixity of edge-cracked orthotropic layers," *Engineering Fracture Mechanics*, vol. 74, no. 17, pp. 2700–2720, 2007.

[75] Y. Frostig, M. Baruch, O. Vilnay, and I. Sheinman, "High-order theory for sandwich-beam behavior with transversely flexible core," *Journal of Engineering Mechanics*, vol. 118, no. 5, pp. 1026–1043, 1992.

[76] C. N. Phan, Y. Frostig, and G. A. Kardomateas, "Analysis of sandwich beams with a compliant core and with in-plane rigidityextended high-order sandwich panel theory versus elasticity," *Journal of Applied Mechanics*, vol. 79, no. 4, p. 041001, 2012.

[77] D. Weissman-Berman, G. L. Petrie, and M. Wang, "Flexural response of foam-cored frp sandwich panels," *Society of Naval Architects and Marine Engineers-Transactions*, vol. 96, 1988.

[78] R. Massabò and A. Cavicchi, "Interaction effects of multiple damage mechanisms in composite sandwich beams subject to time dependent loading," *International Journal of Solids and Structures*, vol. 49, no. 5, pp. 720–738, 2012.

[79] B. F. Sørensen and T. K. Jacobsen, "Characterizing delamination of fibre composites by mixed mode cohesive laws," *Composites science and technology*, vol. 69, no. 3, pp. 445–456, 2009.

[80] B. F. Sørensen, A. Horsewell, O. Jørgensen, A. N. Kumar, and P. Engbæk, "Fracture resistance measurement method for in situ observation of crack mechanisms," *Journal of the American Ceramic Society*, vol. 81, no. 3, pp. 661–669, 1998.

[81] B. F. Sørensen, S. Goutianos, and T. K. Jacobsen, "Strength scaling of adhesive joints in polymer–matrix composites," *International Journal of Solids and Structures*, vol. 46, no. 3, pp. 741–761, 2009.

[82] V. Saseendran, C. Berggreen, and L. A. Carlsson, "Fracture mechanics analysis of reinforced DCB sandwich debond specimen loaded by moments," *AIAA Journal*, vol. 56, no. 1, pp. 413–422, 2018. DOI:10.2514/1.J056039.

[83] S. Freiman, D. Mulville, and P. W. Mast, "Crack propagation studies in brittle materials," *Journal of Materials Science*, vol. 8, no. 11, pp. 1527–1533, 1973.

[84] B. F. Sørensen, P. Brethe, and P. Skov-Hansen, "Controlled crack growth in ceramics: the DCB specimen loaded with pure moments," *Journal of the European Ceramic Society*, vol. 16, no. 9, pp. 1021–1025, 1996.

[85] R. C. Østergaard, B. F. Sørensen, and P. Brøndsted, "Measurement of interface fracture toughness of sandwich structures under mixed mode loadings," *Journal of Sandwich Structures & Materials*, vol. 9, no. 5, pp. 445–466, 2007.

[86] J. Lindhagen and L. A. Berglund, "Bridging law determination in short fibre composites by a DCB-test," *European Structural Integrity Society*, vol. 27, pp. 73–82, 2000.

[87] G. Pappas, *Studies on Traction Separation Relations in Fracture of Layered Composites; Experiments and Modeling*. PhD thesis, École Polytechnique Fédérale de Lausanne, 2017.

[88] D. Plausinis and J. Spelt, "Application of a new constant g load-jig to creep crack growth in adhesive joints," *International journal of adhesion and adhesives*, vol. 15, no. 4, pp. 225–232, 1995.

[89] M. Dessureautt and J. Spelt, "Observations of fatigue crack initiation and propagation in an epoxy adhesive," *International Journal of Adhesion and Adhesives*, vol. 17, no. 3, pp. 183–195, 1997.

[90] V. Saseendran and C. Berggreen, "Honeycomb Sandwich Face/Core Fracture Toughness Measurements using the DCB-UBM Test Method - DoSS Project," tech. rep., Department of Mechanical Engineering, Technical University of Denmark, 2017.

[91] MTS Systems Corporation, Eden Prairie, MN, USA, *FlexTest ® SE Controller*, 2011.

[92] MTS Systems Corporation, Eden Prairie, MN, USA, *MultiPurpose TestWare ® Software*, 2014.

[93] SensorData Technologies Inc., Shelby Township, MI USA, *Fatigue Rated Flange Coupled Reaction Torque SensorT150, T153, T155, T156, T157* , 2012.

[94] TRANSTEK Incorporated, Ellington, CT, USA, *Series 600 High Accuracte ADTs*, 2012.

[95] UDDEHOLM, Hagfors, Sweden, *Uddeholm IMPAX® SUPREME*, 2014.

[96] S. Li, M. Thouless, A. Waas, J. Schroeder, and P. Zavattieri, "Mixed-mode cohesive-zone models for fracture of an adhesively bonded polymer–matrix composite," *Engineering fracture mechanics*, vol. 73, no. 1, pp. 64–78, 2006.

[97] M. Manca, A. Quispitupa, C. Berggreen, and L. A. Carlsson, "Face/core debond fatigue crack growth characterization using the sandwich mixed mode bending specimen," *Composites Part A: Applied Science and Manufacturing*, vol. 43, no. 11, pp. 2120–2127, 2012.

[98] V. Saseendran, C. Berggreen, and L. Carlsson, "Fracture testing of honeycomb core sandwich composites using the DCB-UBM test," 20^{th} *International Conference on Composite Materials (ICCM 20), Copenhagen, Denmark*, 19- 24 July, 2015.

[99] L. A. Carlsson, D. F. Adams, and R. B. Pipes, *Experimental characterization of advanced composite materials*. CRC press, 2014.

[100] Huntsman Advanced Materials, The Woodlands, Texas, USA, *Araldite® LY 1568 / Aradur® 3489*, 2007.

[101] ASTM International, "ASTM D7078/D7078M-12 Standard Test Method for Shear Properties of Composite Materials by V-Notched Rail Shear Method.," 2014.

[102] ASTM International, "ASTM D3039/D3039M-08 Standard Test Method for Tensile Properties of Polymer Matrix Composite Materials.," 2014.

[103] Diab Group, Laholm, Sweden, *Divinycell H Technical Data*, 2016.

[104] Huntsman Advanced Materials, The Woodlands, Texas, USA, *Araldite® 2015 Structural Adhesive*, 2007.

[105] L. Carlsson, R. Matteson, F. Aviles, and D. Loup, "Crack path in foam cored DCB sandwich fracture specimens," *Composites science and technology*, vol. 65, no. 15, pp. 2612–2621, 2005.

[106] J. R. Rice *et al.*, "A path independent integral and the approximate analysis of strain concentration by notches and cracks," ASME, 1968.

[107] M. Thouless, A. Evans, M. Ashby, and J. Hutchinson, "The edge cracking and spalling of brittle plates," *Acta Metallurgica*, vol. 35, no. 6, pp. 1333–1341, 1987.

[108] SCHÜTZ GmbH & Co. KGaA, Selters, Germany, *Cormaster C1 Technical Data*, 2016.

[109] SCHÜTZ GmbH & Co. KGaA, Selters, Germany, *Cormaster N636 Technical Data*, 2016.

[110] Hexcel Corportation, Stamford, CT, USA, *HexPly® 913 125C curing epoxy matrix*, 2016.

[111] V. Saseendran, C. Berggreen, R. Schäuble, R. Hilgers, Y. Albertone, and C. Reichensperger, "Disbond of sandwich structures doss," tech. rep., European Aviation Safety Agency (EASA), EASA.2016.C20, 2017.

[112] R. Schäuble, M. Goldstein, and M. Petersilge, "SCB Fracture Toughness Tests on Honeycomb Sandwich Material - Technical Report," tech. rep., Fraunhofer IMWS Internal report IMWS V793/2017, 2017.

[113] Hexcel Corportation, Dublin, CA, USA, *HexWeb® HRH-10 Aramid Fibre/Phenolic Honeycomb*, 2016.

[114] S. Kelsey, R. Gellatly, and B. Clark, "The shear modulus of foil honeycomb cores: A theoretical and experimental investigation on cores used in sandwich construction," *Aircraft Engineering and Aerospace Technology*, vol. 30, no. 10, pp. 294–302, 1958.

[115] J. Zhang and M. Ashby, "The out-of-plane properties of honeycombs," *International Journal of Mechanical Sciences*, vol. 34, no. 6, pp. 475–489, 1992.

[116] M. Grediac, "A finite element study of the transverse shear in honeycomb cores," *International journal of solids and structures*, vol. 30, no. 13, pp. 1777–1788, 1993.

[117] I. Masters and K. Evans, "Models for the elastic deformation of honeycombs," *Composite structures*, vol. 35, no. 4, pp. 403–422, 1996.

[118] W. Burton and A. Noor, "Assessment of continuum models for sandwich panel honeycomb cores," *Computer methods in applied mechanics and engineering*, vol. 145, no. 3-4, pp. 341–360, 1997.

[119] L. J. Gibson and M. F. Ashby, *Cellular solids: structure and properties*. Cambridge university press, 1999.

[120] J. Hohe and W. Becker, "A refined analysis of the effective elasticity tensor for general cellular sandwich cores," *International Journal of Solids and Structures*, vol. 38, no. 21, pp. 3689–3717, 2001.

[121] C. C. Foo, G. B. Chai, and L. K. Seah, "Mechanical properties of nomex material and nomex honeycomb structure," *Composite structures*, vol. 80, no. 4, pp. 588–594, 2007.

[122] R. A. Staal, *Failure of Sandwich Honeycomb Panels in Bending*. PhD thesis, The University of Auckland, 2006.

[123] A. Karakoç and J. Freund, "Experimental studies on mechanical properties of cellular structures using nomex® honeycomb cores," *Composite Structures*, vol. 94, no. 6, pp. 2017–2024, 2012.

[124] S. Malek and L. Gibson, "Effective elastic properties of periodic hexagonal honeycombs," *Mechanics of Materials*, vol. 91, pp. 226–240, 2015.

[125] F. Hähnel, A. Bugiel, and K. Wolf, "Determination of macroscopic properties of different aramid paper based honeycomb cores," tech. rep., Technische Universität Dresden, Chair of Aircraft Engineering, Internal report ILR/LFT-IR17-19, 2017.

Appendix A

Appended Publications

The following journal articles are appended to this Thesis.

[P1] **V. Saseendran**, C. Berggreen, and R. Krueger, "Mode mixity analysis of face/core debonds in a single cantilever beam sandwich specimen", *Journal of Sandwich Structures & Materials*, 2018. DOI: 10.1177/1099636218788223.

[P2] **V. Saseendran**, L. A. Carlsson, and C. Berggreen, "Shear and foundation effects on crack root rotation and mode-mixity in moment- and force-loaded single cantilever beam sandwich specimen", *Journal of Composite Materials*, vol. 52, no. 18, pp. 2537-2547, 2018. DOI: 10.1177/21998317749714.

[P3] C. Berggreen,**V. Saseendran**, and L. A. Carlsson, "A modified DCB-UBM test Method for interfacial fracture toughness characterization of sandwich composites", *Engineering Fracture Mechanics*, 2018. DOI: 10.1016/j.engfracmech.2018.06.036.

[P4] **V. Saseendran**, L. A. Carlsson, and C. Berggreen, "Fracture mechanics analysis of reinforced DCB sandwich debond specimen loaded by moments", *AIAA Journal*, vol. 56, no. 1, pp. 413-422, 2018. DOI: 10.2514/1.J056039.

[P5] **V. Saseendran**, and C. Berggreen, "Mixed-mode fracture evaluation of aerospace grade honeycomb core sandwich specimens using the Double Cantilever Beam- Uneven Bending Moment test method", *Journal of Sandwich Structures & Materials*, 2018. DOI: 10.1177/1099636218777964.

Publication P1

V. Saseendran, C. Berggreen, and R. Krueger

Mode Mixity Analysis of Face/Core Debonds in a Single Cantilever Beam Sandwich Specimen

Journal of Sandwich Structures & Materials, 2018

Accepted: 19 April 2018
Available online: 31 July 2018
DOI: https://doi.org/10.1177/1099636218788223

Mode Mixity Analysis of Face/Core Debonds in a Single Cantilever Beam Sandwich Specimen

Vishnu Saseendran and Christian Berggreen

Department of Mechanical Engineering, Technical University of Denmark, Nils Koppels Allé, Building 404, 2800 Kgs. Lyngby, Denmark

Ronald Krueger

National Institute of Aerospace, 100 Exploration Way, Hampton, VA 23681-2199, USA

Abstract

The Single Cantilever Beam (SCB) sandwich specimen has been proposed, due to its simplicity, as a fracture test standard for mode I peel loading. Critical parameters, including specimen dimensions, determine whether the crack propagates along the face/core interface in mode I during the fracture test. A parametric study based on a numerical method is performed in this paper to study local mode mixity conditions for a wide array of sandwich systems by varying several geometrical and material parameters. Thickness and modulus of the face sheet are seen to influence the mode mixity for most sandwich systems. Core Poisson's ratio is shown to influence the local mode mixity and has the capability of driving the crack along the interface or into the core. The effect of the intact specimen length is analyzed and presented from a mode mixity perspective based on various elastic foundation modulus expressions. An appropriate foundation model along with a minimum loading rod length is recommended. Reinforcement of the SCB specimen with stiff layers is also investigated numerically and compared with a similar analysis in the literature. The analysis presented in this paper shows that, despite reducing the global shear component, the local mode mixity condition can deviate away from the mode I regime for several sandwich specimens. The recommendations provided from the analyses may supplement the ASTM International standardization efforts.

Keywords: SCB; Sandwich; Debond; Mode mixity; Face/core interface; Phase angle; CSDE

1. Introduction

Typical damage modes in sandwich structures include face/core debonding and core crushing; both pose a threat to the structural integrity of a component. These damage modes are of particular interest to certification authorities since several in-service occurrences, such as a rudder structural failure [1] and other control surface malfunctions, have been attributed to debonding [2]. Extensive studies have shown that debonding can lead to failure caused by internal pressure changes in the core due to ground-air-ground (GAG) cycles [1]–[5]. Future composite structure applications, including for instance, composite sandwich construction of the fuselage of business jets that experience higher altitudes than transport aircraft, are also driving a need to understand the phenomenon of debond growth under generalized load

Corresponding Author:
Vishnu Saseendran, Department of Mechanical Engineering,
Technical University of Denmark, Nils Koppels Allé,
Building 404, 2800 Kgs. Lyngby, Denmark
E-mail: vsas@mek.dtu.dk

scenarios that include maneuvers and gust conditions. Furthermore, in spacecraft applications, large scale face/core debonding were reported in [6], [7].

In order to have reliable damage assessment models, the quality of face/core interface strength must be ascertained with a high degree of accuracy. The most critical debonding phenomenon in sandwich composites is likely to be mode I dominated, in which the face sheet is peeled off from the core. Thus, the critical strain energy release rate (interface fracture toughness) related to the face/core separation must be estimated using reliable test methods. In a recent study, the suitability of five test methods for measuring debond toughness associated with face/core peel loading was evaluated [8]. A single cantilever beam (SCB) type configuration, initially discussed in [9] and [10], was identified as the most appropriate test (see Figure 1a). This determination was based on the following findings: (1) the test involves a simple loading fixture; (2) debond front conditions were found to be uniform over a range of debond lengths; (3) debonding was found to take place along or near the face/core interface, rather than kinking into the core; (4) the data reduction method used for computing debond toughness involves a straightforward compliance calibration procedure.

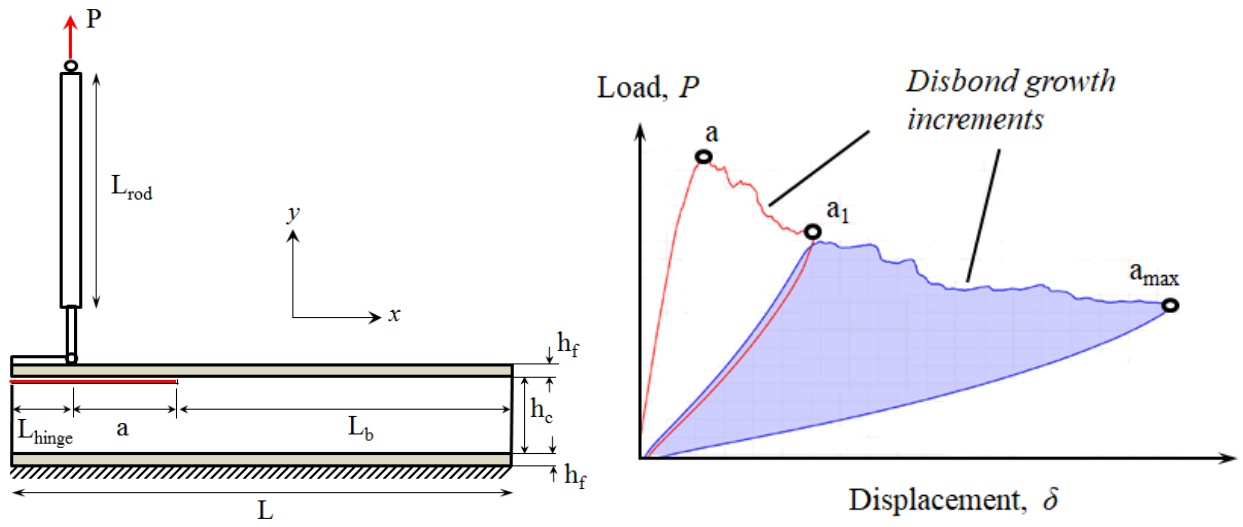

Figure 1. (a) Schematic illustration of the Single Cantilever Beam (SCB) sandwich specimen (b) typical load-unload curve of a sandwich SCB specimen.

The SCB sandwich specimen (see Figure 1a) with a pre-crack (a) lying close to the upper face sheet is fixed on a rigid base and loaded with a loading rod. In general, the pre-crack is a discontinuity in the interface and is usually achieved by inserting a Teflon® film in the production phase. The pre-crack can also be introduced using other measures such as by saw-cut and must have a sharp crack front. In the SCB test method, load is applied to the upper debonded face sheet and the bottom face sheet is rigidly

fixed. The force is applied through a loading rod which is attached to the upper debonded face sheet using a piano hinge. Both loading rod and piano hinge ensure that the load application point remains vertical as the debond grows. The test is conducted in displacement control by pulling the debonded face sheet at a constant rate. The specimen is un-loaded when the crack increases to a_1 (see Figure 1b). A suitable imaging system is used to ascertain crack position during the test and both displacement and force are continuously recorded during the test. Different methods to reduce energy release data have been proposed for the SCB test: area method, modified beam theory, and compliance calibration method [11]. The latter two methods require a linear force-displacement response of the specimen, which specimens with thin face sheets may not yield. To encompass testing of a wide range of specimens, the area method is therefore more generally favorable. In the area method, strain energy release rate is calculated from the load – displacement (P vs. δ) curve obtained during a test. For an infinitesimal increase in debond length, da, the energy release rate is given by:

$$G = \frac{1}{b}\frac{dU}{da} \tag{1}$$

where U is the total elastic strain energy in the specimen (area beneath the P vs. δ curve, see Figure 1b), b is the specimen width and da is the increase in debond length recorded during the test. The test can be repeated for several load/un-load cycles and the energy released for an incremental debond length, da, can be estimated using Equation (1) each time.

Due to the inherent high elastic mismatch present across a sandwich interface, the crack propagation occurs in mixed mode condition. The mode mixity can be roughly described as the measure of shear loading at the crack tip. Therefore, the energy release rate at a bi-material fracture interface is a function of mode mixity as described in [12]. In order for the SCB test to be useful as a “peel” or mode I dominant test, it must be ensured that the debond grows under mode I conditions corresponding to a peel dominated loading on the face sheet. The mode mixity at the crack tip can be expressed in terms of a phase angle, ψ, which is the arc tangent of the ratio of sliding to opening displacement of the crack tip [12]. The reader must note that mode mixity and phase angle can be used interchangeably. The principle of Linear Elastic Fracture Mechanics (LEFM) applied to brittle materials can also be extended to study face/core interface. The failure process zone in terms of crack tip plasticity is very small in brittle materials. This is also valid for sandwich structures, with the exception of specimens with tougher cores or which exhibit fibre bridging resulting in a larger failure process zone.

Efforts are underway to develop an ASTM International testing standard to determine the peel-dominated fracture toughness of sandwich constructions using the SCB sandwich specimen. The SCB fracture test, when developed as an industrial standard, is poised to be used by different industry clientele and in configurations in which the stiffness mismatch across the sandwich interface varies with each user. To establish a reliable test protocol, the specimen must be designed such that a mode I condition prevails at all crack lengths. This implies that the SCB test must be robust enough to account for a wide variety of

face/core combinations. The existing sizing study detailed in [13] is based on the beam on elastic foundation model approach [14]. Several limitations were imposed to ensure that the SCB sandwich specimen response remains linear during testing and the shear component at the crack tip is minimum. In addition, by restricting the specimen geometry, pre-crack length (a), loading rod length (L_{rod}), maximum crack length (a_{max}) and face sheet and core thicknesses (h_f, h_c), to certain values, the specimen yields a linear response. However, in reality not all specimens used across industries yield linear responses, e.g. specimens with thin face sheets ($h_f \leq 0.5$ mm) exhibit a non-linear unloading curve.

The compliance based solution outlined in [13] however, does not ensure that the pre-crack advances along the interface. The measured energy release rate during the test must be associated with interface crack propagation as the fracture toughness of a core material is much lower. Since the crack advances through an interface between highly dissimilar materials, the mode mixity condition will determine whether the crack will dive into the core, propagate along the interface or kink into the face sheet. Thus, limiting the SCB specimen dimensions solely based on kinematic analyses overlooks the local mode mixity condition at the crack tip.

An exhaustive experimental campaign to determine the mode mixity influence in the SCB test, by taking into account a wide variety of core and face sheet material systems, will be very expensive. Moreover, a closed-form expression to ascertain the mode mixity at various crack lengths for the SCB sandwich specimen does not yet exist in the literature. Hence, the objective of the current work is to conduct a parametric analysis to study the influence of various material and geometrical parameters of the SCB sandwich specimen on the mode mixity. The analysis is based on a numerical fracture mechanical tool, the Crack Surface Displacement Extrapolation (CSDE) method [15]. It must be noted that the thermal residual stresses which may affect the crack tip loading conditions are not considered. A crack in a sandwich face/core interface propagates just beneath the interface, and hence is modelled as an interface crack between two dissimilar materials. The bi-material problem is treated in plane strain and LEFM is considered to be valid.

Hypothetical sandwich material systems were studied initially to identify the influence of critical governing parameters that influence the crack tip mode mixity. The phase angle, ψ, evaluated for various face/core interfaces will aid in identifying whether the fracture test remains in a mode I regime at all crack lengths. In terms of the phase angle (in degrees), pure mode I corresponds to 0°, and 90° corresponds to a pure mode II loading at the crack tip. Therefore, in this analysis mode I dominance is considered within the bounds: $-10° \leq \psi \leq 10°$. A case study is presented by taking into account representative sandwich composite systems used in three different industries. Sizing parameters derived in [13] were closely examined and their influence on the phase angle, ψ, was studied. A discussion on the mode mixity phase angle and implementation of the CSDE method are provided in the following section.

2. Finite element modeling of the SCB sandwich specimen

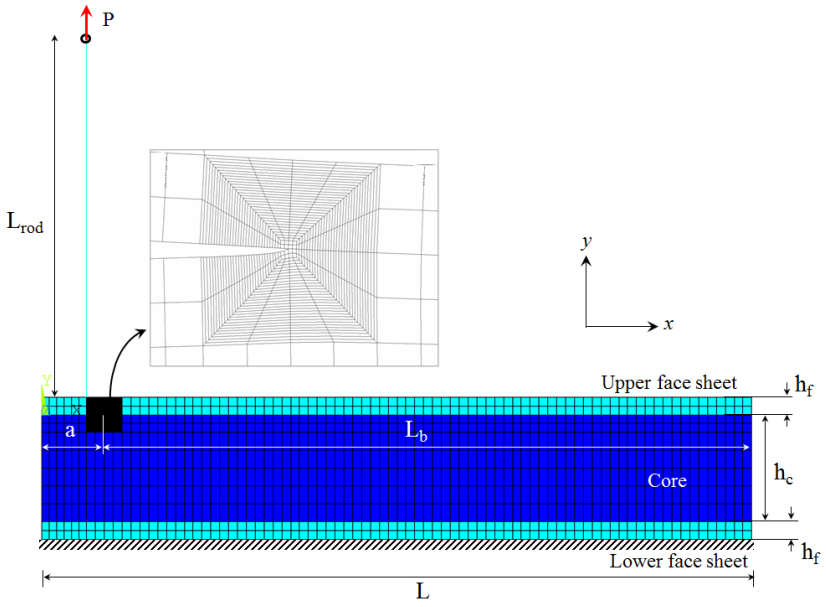

Figure 2. 2-D finite element model of SCB sandwich specimen with highly discretized mesh at the crack tip.

A 2-D plane-strain finite element (FE) model consisting of isoparametric 4-node linear (PLANE182) and 8-node parabolic (PLANE183) elements was built in ANSYS® [16], with the smallest element edge length of 2.5 μm (see Figure 2). PLANE182 elements with 4 corner nodes supporting two degrees of freedom were used at the crack tip to capture large strains. The rest of the model was built using 8-node PLANE183 elements containing two translation degrees of freedom on each node. Highly densified meshing was employed at the crack tip zone for the CSDE mixed-mode partitioning method implementation. The loading rod was modeled using a beam element which takes only tension and was hinged above the top face sheet. The hinge leaf was not considered in the analysis. Unit load per width (P/b = 1 N/mm) was applied on top of the rod. The base was modeled by applying fixed boundary conditions on the lower face sheet. The crack flanks in the debonded region were modeled as frictionless contact surfaces to circumvent interpenetration or overlapping of the surfaces.

Both energy-release rate, G, and mode mixity phase angle, ψ, should be consistent in the crack tip displacement dominated field. A highly dense mesh is required close to the crack tip to accurately model this displacement field. Moreover, the zone is limited by two borders: an inner border in which numerical errors close to the crack tip corrupt the results because the elements close to the crack tip cannot calculate the correct displacement field, and an outer border where the external displacement starts to dominate (see Figure 3). The zone of numerical noise pertains to the small region close to the crack tip where the linear elastic solution shows that the stresses oscillate confined to that small zone. From several numerical investigations, it is observed that the transition from the external displacement field to the

internal crack dominated field is linear with respect to nodal pairs, until the border to numerical error zone is reached [17]. Hence, both G and ψ in the linear transition zone (or K-dominant zone) can be linearly extrapolated to the crack tip. The CSDE method uses only the results from relative crack-flank displacements (δy and δx) to calculate both G and ψ.

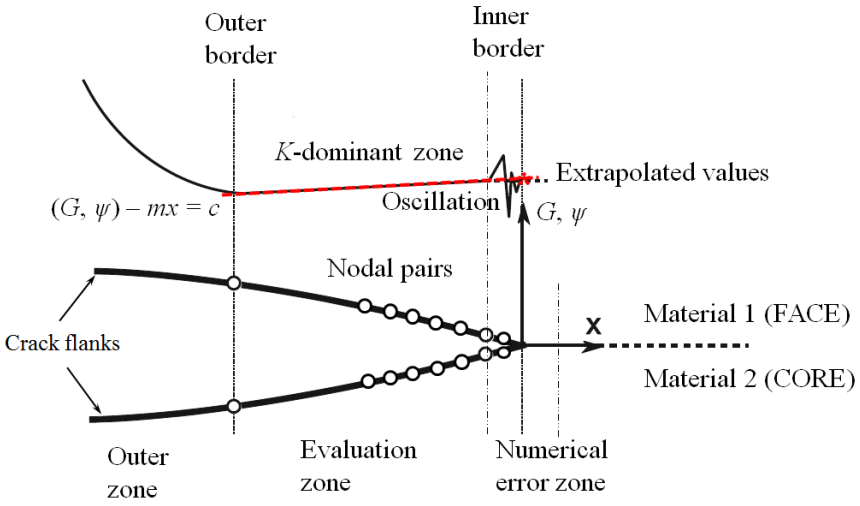

Figure 3. Schematic illustration of CSDE method implementation: face/core interface crack with sliding, δx and opening, δy displacements. G and ψ values are extrapolated from the K-dominant zone.

The phase angle, ψ, defines the ratio between mode II and mode I stress intensity factors of a bi-material interface crack. In terms of relative opening δ_y and sliding δ_x displacements (see Figure 3), the phase angle can be expressed as [12]:

$$\psi_F = \tan^{-1}\left(\frac{\delta_x}{\delta_y}\right) - \varepsilon \ln\left(\frac{x}{h}\right) + \tan^{-1}(2\varepsilon) \tag{2}$$

where x is a short distance within the singular region behind the crack tip, and h is a characteristic length, usually chosen equal to the face sheet thickness, $h = h_f$. It is evident from the linear elastic solution that stresses and displacements oscillate near the crack tip [12]. The oscillatory index ε is given by [12]:

$$\varepsilon = \frac{1}{2\pi} \ln\left(\frac{1-\beta}{1+\beta}\right) \tag{3}$$

where β is a non-dimensional bimaterial interface constant (Dundur's parameter) given by [18]:

$$\beta = \frac{1}{2} \frac{S_1(1-2\nu_2) - S_2(1-2\nu_1)}{S_1(1-\nu_2) + S_2(1-\nu_1)} \tag{4}$$

where S_1 and S_2 represent the shear moduli of face sheet and core located above and below the interface, respectively. The phase angle from Equation (2), calculated using the FE-based CSDE method with values of ε and β from Equations (3) and (4) and with $x = h_f$, is ψ_F, referred to as the "full formulation". Both G and ψ will be affected by oscillations according to the linear elastic solution since stresses oscillate when the crack tip is approached. The influence of crack tip oscillation can be suppressed by assuming $\varepsilon = 0$ in Equation (2), which helps recover the conventional square-root based singular stress intensity factors [19]. Therefore, the phase angle in Equation (2) can be re-expressed in "reduced formulation" ($\varepsilon = 0$), as:

$$\psi_R = \tan^{-1}\left(\frac{\delta_x}{\delta_y}\right) \tag{5}$$

Throughout this paper, the reduced formulation is used and, for brevity, the phase angle will be denoted as ψ, without the subscript. The energy release rate obtained in terms of crack-flank displacements is given by [15]:

$$G = \frac{\pi(\delta_x^2 + \delta_y^2)}{2x(c_1 + c_2)} \tag{6}$$

where x is the distance from the crack tip and c_1 and c_2 are stiffness parameters of the face sheet and core given by:

$$c_m = \frac{k_m + 1}{S_m} \tag{7}$$

The parameter $k_m = (3 - 4\nu_m)$ for plane strain and $k_m = (3 - \nu_m)/(1 + \nu_m)$ for plane stress, where ν_m is Poisson's ratio with $m = 1$ and 2 for the face sheet and core, respectively.

A separate subroutine was implemented in the program ANSYS® [16] in which sliding (δx) and opening (δy) crack-flank displacements were extracted. The CSDE method is very effective in calculating both G and ψ when huge distortions in the near tip elements are present, especially in the case of sandwich in which a huge elastic mismatch across the face/core interface exists. It should be noted that the CSDE method can analyze phase angles in both reduced and full formulation (Equations 2 and 5). If $\psi > 0$, the crack is directed towards the core, whereas if $\psi < 0$, the crack is directed toward the face sheet. A mode I dominant window is assumed to exist in the phase angle regime: $-10° \leq \psi \leq 10°$.

3. SCB parametric fracture analysis

The SCB specimen is intended for mode I fracture testing of a wide array of face/core material systems. Typical through-thickness core moduli can vary from 76 MPa (Nomex Honeycomb used in Aerospace industry) to 6840 MPa (high density balsa widely employed in the marine and wind energy sectors). Face sheet and core thicknesses of sandwich systems invariably differ based on the application. Correct loading rod length in the SCB test is paramount in preventing shear loading at the load application point. Testing frame heights as well as cross head displacement capacities can also vary at different test labs. Therefore, it is necessary to stipulate the loading rod length (L_{rod}) to enable robustness of the SCB fracture test methodology.

A parametric study of the SCB sandwich specimen was conducted using the finite-element model presented in the previous section in conjunction with the CSDE method. A unit load P = 1 N/mm was applied on a pre-cracked specimen for all cases. The list of parameters which were considered to sdetermine whether the fracture testing remains under mode I conditions is provided in Table 1. For the initial study, Poisson's ratio of both face sheet and core were held constant at ν_f = 0.30 and ν_c = 0.35, respectively. A separate section is dedicated to investigating the effect of core Poisson's ratio, ν_c. The length of the hinge was kept constant throughout the analysis, L_{hinge} = 12.7 mm and the total length of the specimen is given by: $L = L_{hinge} + a_{max} + L_b$. The compliance based solution in [13] and [20] recommended a minimum intact length of the specimen (L_b), by stipulating that the compliance coefficients remain at unity; L_b is given by:

$$L_{b,\min} = 2.7\left[\frac{h_c h_f^3 E_f}{3E_c}\right]^{1/4} \tag{8}$$

The maximum debond length was fixed to a_{max} = 150 mm for all cases in the analysis. By selecting a specimen length, L = 300 mm, the intact length (L_b) was found to satisfy the minimum recommended length in Equation (8) for all combinations of materials considered in Table 1. The effect of intact portion length on mode mixity is presented later. To study the effect of different combinations of the parameters (see Table 1) on the mode mixity phase angle (ψ), the parameters are varied in steps in the numerical study. Using the values shown in Table 1, calculated values of $\alpha = \left(\bar{E}_1 - \bar{E}_2\right)/\left(\bar{E}_1 + \bar{E}_2\right)$ vary from 0.65 to 0.99, which are typical values found in a sandwich face/core interface. The Young's modulus for plane stress and plane strain conditions are given by, $\bar{E} = E$ and $\bar{E} = E/\left(1-\upsilon^2\right)$, respectively, with subscripts 1 = face sheet and 2 = core.

Table 1. Parameters altered in the SCB parametric study.

SCB Parameters	
Core modulus, E_c [MPa]	100, 500, 1000
Face sheet Modulus, E_f [GPa]	5, 10, 50, 100, 200, 250
Core thickness, h_c [mm]	10, 40
Face sheet thickness, h_f [mm]	0.5, 3, 7
Loading rod length, L_{rod} [mm]	120, 250, 500

Table 2. Possible $\Sigma = E_f/E_c$ values for E_c = 100, 500 and 1000 MPa.

E_c [MPa] / ***E_f [MPa]***	100	500	1000
$5 \cdot 10^3$	50	10	5
$10 \cdot 10^3$	100	20	10
$50 \cdot 10^3$	500	100	50
$100 \cdot 10^3$	1000	200	100
$200 \cdot 10^3$	2000	400	200
$250 \cdot 10^3$	2500	500	250

Effect of core and face sheet modulus ($\Sigma = E_f / E_c$)

The effect of both core and face sheet moduli on phase angle is presented in this section. Three core moduli were chosen E_c = 100, 500 and 1000 MPa, and face sheet moduli were chosen in the range, E_f = 5 to 250 GPa (see Table 1). The range of $\Sigma = E_f/E_c$ values is provided in Table 2. Three face sheet thicknesses were chosen: h_f = 0.5, 3 and 7 mm, and core thickness was h_c = 40 mm. The length of the loading rod was L_{rod} = 500 mm, and length of the specimen was L = 300 mm. To capture non-linear effects associated with specimens with thin face sheets, a geometrically non-linear Finite Element Analysis (FEA) was performed.

Figure 4 shows the variation of phase angle (ψ) for a 40 mm thick core with three core moduli: E_c = 100, 500 and 1000 MPa. Figures 4(a) – 4(c) show results for E_c = 100 MPa at three face sheet thicknesses. Figures 4(d) – 4(f) and 4(g) – 4(i) show corresponding results for E_c = 500 MPa and E_c = 1000 MPa, respectively. In Figure 4, the region not satisfying the assumed mode I dominant bound ($-10° \leq \psi \leq 10°$) can be identified.

For the case of a low modulus core (E_c = 100 MPa) with a thin face sheet, the phase angle (ψ) increases with Σ for short crack lengths, a ~< 30 mm (see Figure. 4a). A similar trend with a thin face sheet (h_f = 0.5 mm) is observed for stiffer cores (see Figures. 4d and 4g). For all core moduli considered here, ψ increases with Σ. For the case of E_c = 100 MPa, mode I dominant behavior was observed at small values of Σ ($\Sigma \leq 500$).

It is noted that, with increasing core stiffness and at small values of Σ, the phase angle (ψ) shifts toward the negative region. It is also noted that ψ is largely positive (> 10°) for all cases except when Σ <100. For the case of a stiff core (E_c = 1000 MPa), negative values of ψ (< 0°) are observed for small values of Σ (see Figures 4 g-i). Therefore, there is a strong influence on the mode mixity by both face sheet stiffness and core modulus.

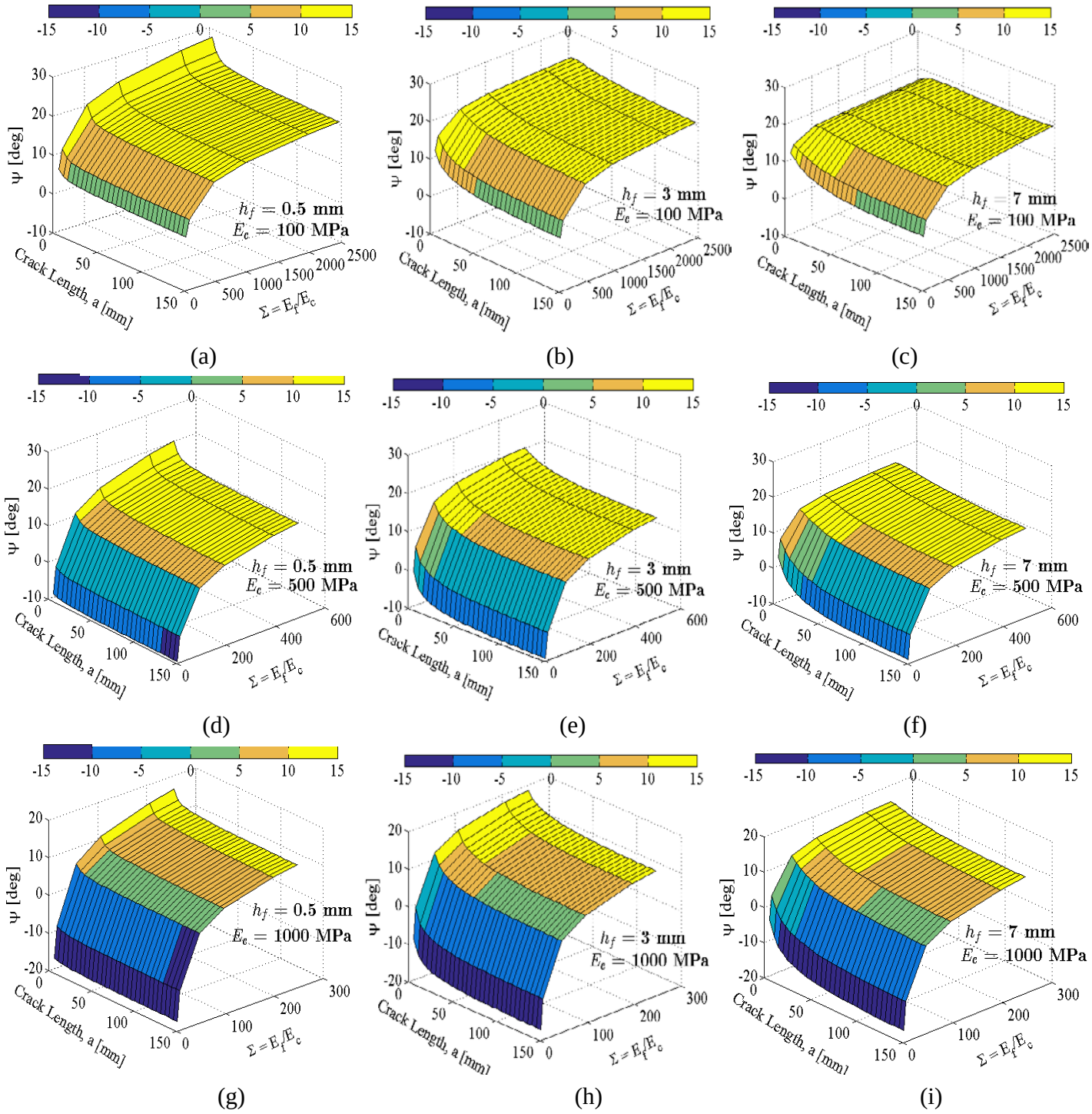

Figure 4. Mode mixity phase angle *(ψ)* vs. crack length with L_{rod} = 500 mm, h_c = 40 mm, L = 300 mm for E_c = 100 MPa*:* (a) h_f = *0.5 mm*, (b) h_f = 3 mm (c) h_f = 7 mm, E_c = 500 MPa*: (d)* h_f = 0.5 mm *(e)* h_f = 3 mm (f) h_f = 7 mm and E_c = 1000 MPa*:* (g) h_f = 0.5 mm (h) h_f = 3 mm (i) h_f = 7 mm.

Effect of core Poisson's ratio (ν_c)

The crack tip mode mixity condition is influenced by crack tip root rotation [21]. In sandwich systems, the core is less stiff compared to the face sheets, which may contribute to the deformation and rotation of the upper face sheet. The effect of core Poisson's ratio (ν_c) on mode mixity phase angle (ψ) was investigated using the SCB FE-model. For the analysis, the core modulus was held constant at E_c = 100 MPa, and the face sheet modulus was chosen in the range E_f = 5 to 250 GPa (see Table 2). Rod length, face sheet thickness, core thickness and length of the SCB specimen were held constant at: L_{rod} = 500 mm, h_f = 2 mm, h_c = 40 mm and L = 300 mm. The core Poisson's ratio was varied from ν_c = 0.15 to 0.45, and the phase angle was computed for each case. Figure 5(a) shows a plot of ψ vs. crack length for three ν_c values for $50 \leq \Sigma \leq 2500$. As shown in the plot, ψ is strongly dependent on the core Poisson's ratio.

The phase angle, ψ, remains higher for a core with lower Poisson's ratio, ν_c, over the entire range of $\Sigma = E_f/E_c$ values. For better inspection, a slice from Figure 5(a) is presented in Figure 5(b) for Σ = 100. It can be noted that for the case, ν_c = 0.45, ψ remains in the mode I regime ($-10° \leq \psi \leq 10°$) for all crack lengths. As ν_c decreases, ψ increases causing the mode mixity to deviate away from mode I condition. At the maximum crack length considered here (a = 150 mm), the mode mixity varies from ψ = 25° for ν_c = 0.15 to ψ = -5° for ν_c = 0.45 (see Figure 5b). However, for a constant core Poisson's ratio (ν_c), the change in ψ across crack lengths remains negligible for a > 20 mm. Therefore, both stiffness and Poisson's ratio of the core influence ψ and can cause the test to deviate away from mode I conditions.

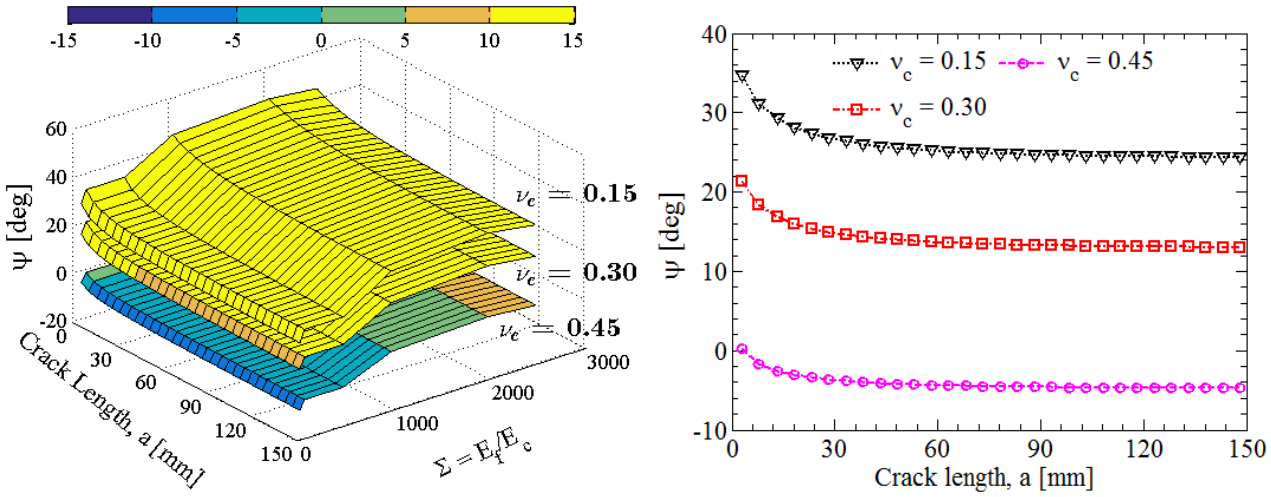

(a) (b)

Figure 5. Mode mixity phase angle *(ψ)* vs. crack length (a) for various Σ values (b) ψ *vs.* crack length at Σ = 100. (h_c = 40 mm, h_f = 2 mm, L = 300 mm, L_{rod} = 500 mm, ν_c = 0.15, 0.30 and 0.45).

Effect of face sheet and core thickness (h_f, h_c)

To investigate the influence of face sheet and core thicknesses on the phase angle (ψ), the face sheet thickness (h_f) was varied from 0.5 mm to 7 mm for two different core thicknesses (h_c = 10 mm and 40 mm). The face sheet and core moduli were considered as: $E_f = 5 \cdot 10^3$ MPa and E_c =100 MPa (Σ = 50). Loading rod length was kept constant at L_{rod} = 500 mm, and total length of the specimen, L = 300 mm. A plot of ψ vs. crack length is shown in Figure 6 for the two core thicknesses, h_c = 10 and 40 mm.

For the thin core case (h_c = 10 mm), ψ levels to a plateau for a > 40 mm for all cases of face sheet thicknesses considered. It is noted that a thicker face sheet has the tendency to drive the crack into the negative mode mixity regime (see Figure 6(a)). For the thick core (h_c = 40 mm) considered here, mode mixity becomes increasingly positive with increasing face sheet thickness (Figure 6b).

The difference in ψ between thin (0.5 mm) and thick (7 mm) face sheets for the case of a thick core is small at larger crack lengths (~ 2°). Furthermore, in the case of thick core (h_c = 40 mm), for face sheet thickness $h_f \geq$ 1.5 mm and at short crack lengths, the mode mixity deviates away from the mode I regime. Thus, the energy release rate computed at short crack lengths will lie outside the mode I regime. When the phase angle is positive (ψ > 0°), the inclination of crack is to dive into the core. For ψ < 0°, the crack will try to kink into the face sheet; but in general, face sheets are too tough and the crack propagates hugging the interface.

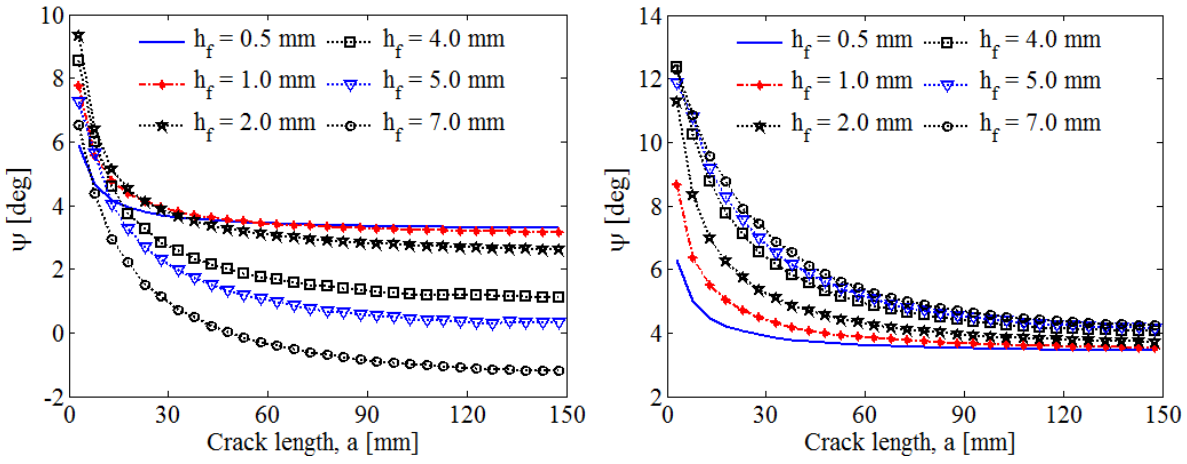

Figure 6. Phase angle *(ψ)* vs. crack length for Σ = 50 *(E_f* = 5 GPa, E_c = 100 MPa) for core thickness; (a) h_c = 10 mm (b) h_c = 40 mm. (L_{rod} = 500 mm and L = 300 mm for both cases).

Effect of intact length (L_b) and elastic foundation modulus (k)

The influence of SCB specimen intact length (L_b) and elastic foundation modulus on the phase angle (ψ) is discussed in this section. The top face sheet can be perceived as a beam resting on a linear elastic foundation [14]. Li et al. [20] derived the deformation of a top face sheet for a Tilted Sandwich Debond (TSD) [22] specimen by using the Winkler foundation model first utilized by Kanninen [14]. The beam on foundation approach of the TSD specimen was extended to the SCB specimen in [13].

The SCB specimen is sized in order to ensure that the global shear deformation introduced on the debonded upper face sheet remains negligible. The intact part of the SCB specimen (L_b) plays a key role in reducing the shear component and must be kept above a minimum length such that $\lambda L_b \geq 2.7$ [13], where parameter λ is the ratio of stiffness of the elastic foundation to the bending stiffness of the upper face sheet:

$$\lambda = \left[\frac{3k}{E_f h_f^3 b} \right]^{1/4} \tag{9}$$

where b is the width of SCB specimen. Several expressions for k exist in the literature, of which three are shown in Table 3. The minimum required intact length ($L_{b,min}$) for a SCB specimen is given by [13]:

$$L_{b,\min} = \frac{2.7}{\lambda} \tag{10}$$

Table 3 shows λ and the minimum required length stipulated by Equation (10) computed for a hypothetical sandwich configuration comprised of an aluminum face sheet (E_f = 68.9 GPa, h_f = 7 mm) and a PVC DIAB H100 (E_c = 130 MPa, h_c = 25.4 mm) core [23].

Table 3. Minimum intact length ($L_{b,min}$) calculated using elastic foundation modulus *(k)* expressions for E_f = 68.9 GPa, h_f = 7 mm and E_c = 130 MPa, h_c = 25.4 mm.

Elastic Foundation Modulus	***k [MPa]***	***λ [mm^{-1}]***	***$L_{b,min}$ [mm]***
Li et al. [20]; $k = \frac{E_c b}{h_c}$	5.31	0.028	94.21
Aviles et al. [24]; $k = \frac{2E_c b}{h_c}$	10.63	0.034	79.22
Quispitupa et al. [25]; $k = \frac{2E_c b}{h_f}$	38.57	0.047	57.40

The recommended minimum length ($L_{b,min}$) ensures that the shear component remains negligible. Therefore, if a fracture test is conducted with a specimen which does not satisfy Equation (10), the mode mixity phase angle (ψ) might deviate from the mode I regime. A numerical study was carried out to check if any variation in ψ occurs when insufficient intact length is used. Two specimen lengths, L = 200 and 300 mm, with a maximum crack length, a_{max} = 150 mm, were considered. This means that when a_{max} = 150 mm, the intact portion length is 50 mm for the former and 150 mm for the latter case. The analysis was performed for face sheet thicknesses in the range: h_f = 0.5 to 7 mm. A plot of ψ vs. crack length is provided in Figure 7 for both specimen lengths (L = 200 and 300 mm).

For a face sheet thickness h_f = 7 mm, Table 3 shows that the foundation modulus expression (k) by Li et al. [20] yields a maximum value $L_{b,min}$ = 94.21 mm, whereas the lowest value $L_{b,min}$ = 57.40 mm, is obtained using the modulus by Quispitupa et al. [25]. The intact length in Figure 7(a) is $L_b = L - a_{max}$ = 50 mm, which is less than the recommended lengths ($L_{b,min}$) listed in Table 3. The phase angle (ψ) for h_f = 0.5 mm remains nearly constant for a > 30 mm, and for h_f = 2 mm a slight deviation in ψ is observed at a = 130 mm. Significant influence on ψ is observed for $h_f \geq 4$ mm. For h_f = 4 mm, the phase angle (ψ) starts to spike at a = 120 mm, and for the thicker h_f = 7 mm, ψ spikes at a = 90 mm. In Figure 7(b), however, no deviation in ψ from the plateau occurs for all face sheet thicknesses which can be attributed to a longer specimen length. Therefore, in line with the observations made here, careful selection of the SCB specimen length and maximum crack length is required to ensure that fracture testing is conducted in the mode I region over all ranges of crack lengths. The intact portion length obtained using Li et al. [20] captures the shift in mode mixity very well compared to other elastic foundation modulus expressions, and is recommended to be used in estimation of L_b for a given a_{max}.

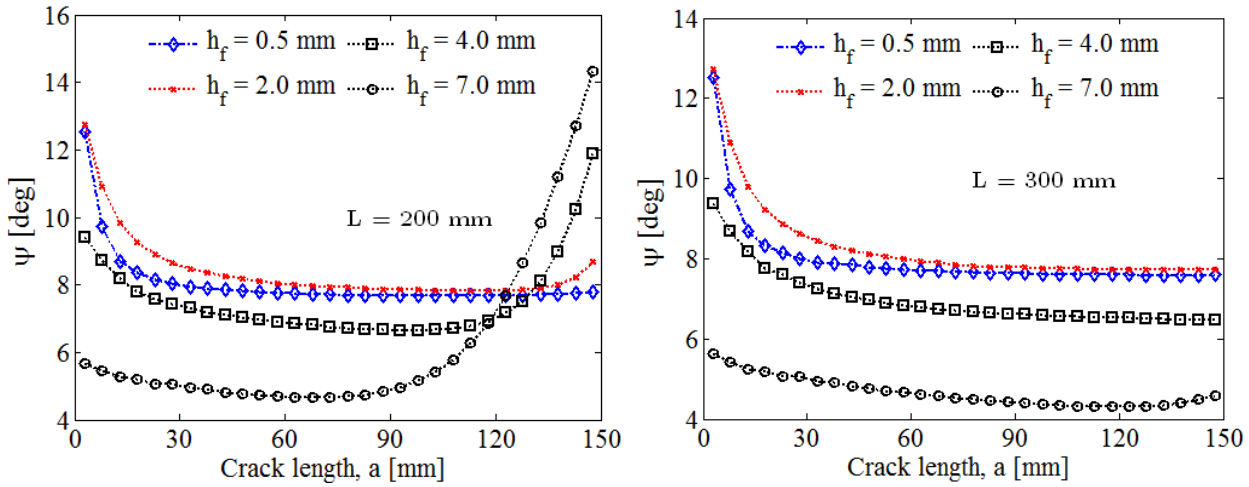

Figure 7. Mode mixity phase angle vs. crack length for an Aluminum/H100 sandwich system; (a) L = 200 mm (b) L = 300 mm with a_{max} = 150 mm.

Effect of loading rod length (L_{rod})

In the SCB fracture test, it is paramount that the load introduction point always remain vertical and avoids any horizontal component, which introduces shear. A conservative estimate of a minimum loading rod length ($L_{rod,min}$) following the kinematic approximation in [20], was provided in [13]:

$$L_{rod,\min} = 1.06\, a_{\max} \tag{11}$$

To prevent shear loading at the face/core interface, a long loading rod length is desired. However, long rod length will require a tall load frame. An analysis using the parametric numerical model from a mode mixity perspective was undertaken to investigate the effect of a reduction of the loading rod length from the recommended value. The maximum crack length in this analysis was a_{max} = 150 mm with a total length of the specimen, L = 300 mm. Hence, according to Equation (11), the minimum required length of the rod should be 159 mm. Three different loading rod length cases (L_{rod} = 50, 120 and 500 mm) were considered, with core thickness kept constant at h_c = 25.4 mm. The bi-material tensile moduli $\Sigma = E_f/E_c$ were 100, 1000 and 2500 for this analysis with a constant core modulus E_c = 100 MPa. Only three values of Σ were considered, since only a trend in the influence of various rod lengths was desired. The results of the analysis for three face sheet thicknesses (h_f = 0.5, 3 and 7 mm) are presented in Figure 8.

It is clearly evident that a short loading rod length introduces a shear component leading to higher mode mixity values (see Figures. 8a-c). The difference in ψ for 50 and 120 mm rod lengths is small, except at very short crack lengths (maximum 5°) and is indistinguishable in the current plot for the cases considered here. Longer rod lengths of 750 and 1000 mm showed no significant influence on ψ compared to a rod length of 500 mm and thus have been omitted in the plot.

The influence of rod length on ψ for a thicker face sheet, h_f = 7 mm is shown in Figure 8(c). For h_f = 7 mm at short crack lengths (a < 10 mm), there is very little difference in ψ between short and long rod lengths. The mode mixity deviates away from mode I regime at short crack lengths, as observed in previous sections. On the other hand, for a thin face sheet, h_f = 0.5 mm, increasing the rod length shifts ψ in to the mode I regime (see Figure 8a). The variation of phase angle at short (a = 30 mm) and long (a = 120 mm) crack lengths are provided for a thick face sheet (h_f = 7 mm) case in Figure 8d and 8e. As observed, the longer rod length yields lower values of ψ at all values of Σ. It should be noted that plots in Figures 8d and 8e are smoothed using an interpolation function to obtain a best trend. A minimum length (L_{rod}) of 500 mm is desired to ensure that ψ remains in the mode I regime for the generality of sandwich systems. Therefore, a new rod length based on the specimen length is proposed here, $L_{rod} \geq 1.70\, L$ to accommodate the generality of sandwich constructions.

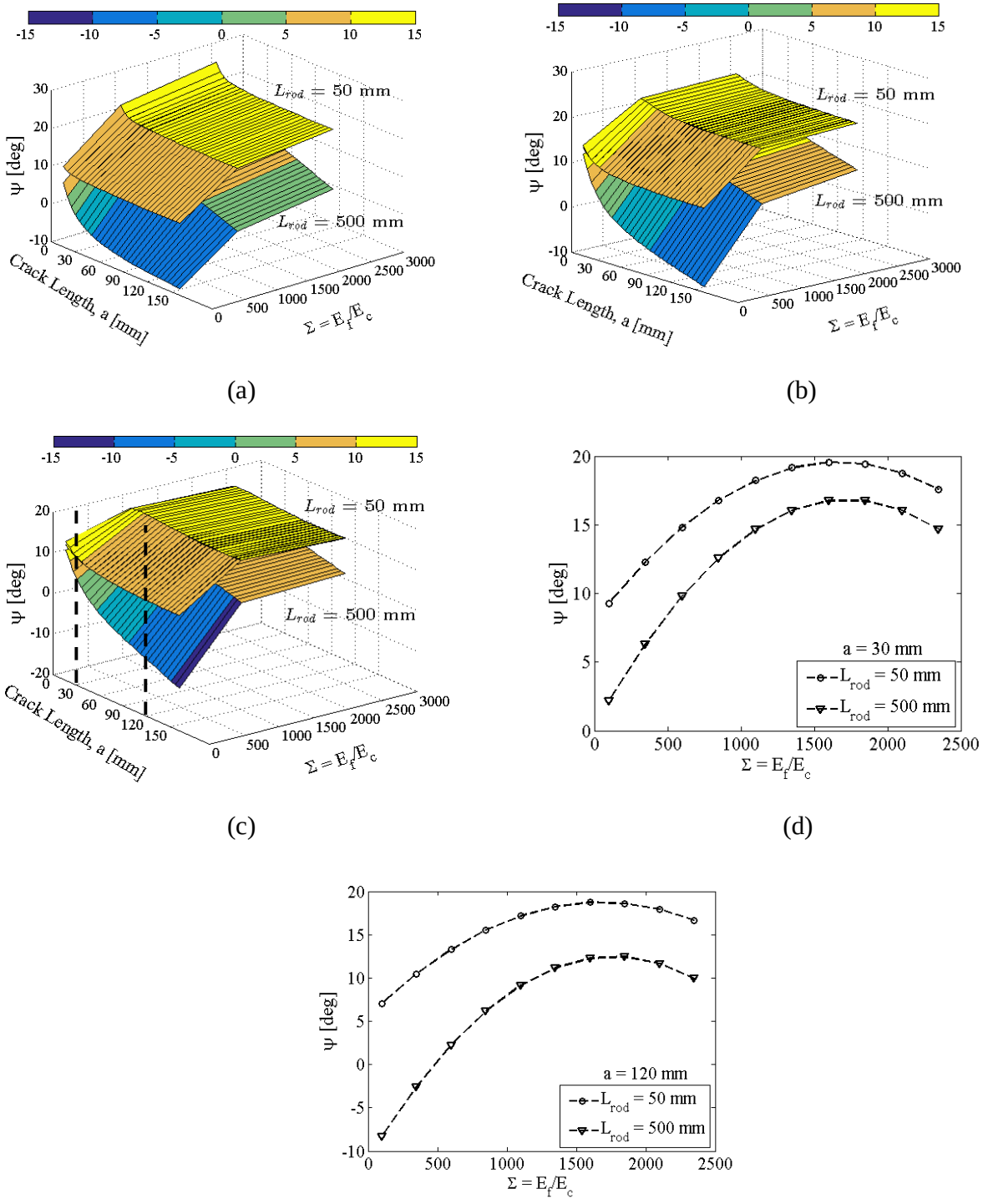

Figure 8. Effect of loading rod length on phase angle (ψ) for three face sheet thicknesses (a) 0.5 mm (b) 3 mm and (c) 7 mm, (ψ) vs. Σ at (d) a = 30 mm and (e) a = 120 mm (L = 300 mm, h_c = 25.4 mm).

4. Case studies

A study was conducted to investigate the mode mixity conditions for typical SCB sandwich specimens used in different industries, namely aerospace, marine and wind. Material properties selected for face sheet and core materials representative of each industry are provided in Table 4. To keep the analysis simple and devoid of any additional failure mechanisms, face sheets comprised of unidirectional (UD) fibers were considered. The geometrical parameters chosen for the analysis are also shown in Table 4. The loading rod length was kept constant at L_{rod} = 500 mm and a maximum crack length of a_{max} = 150 mm was chosen. The minimum required intact length ($L_{b,min}$) was calculated using Equation (10) for each specimen. A unit load of P = 1 N/mm was applied. The core was modeled as orthotropic and the FE-model was solved as geometrically non-linear for all cases.

A plot of the mode mixity phase angle (ψ) vs. crack length is presented in Figure 9 for all three sandwich systems presented in Table 4. Pure mode I conditions in terms of phase angle were defined to exist between $-10° \leq \psi \leq 10°$. A line demarcating $\psi = 10°$ shows the region in which mode I regime exists in Figure 9. For all cases considered here, short crack lengths exhibit increased mode mixity.

The aerospace specimen (Carbon/Nomex honeycomb core), with thin face sheet ($h_f \leq 0.5$ mm) is observed to be in the mode I regime for the entire range of crack lengths. For face sheets with $h_f \geq 1$ mm, a mode I regime exists for crack length a ~> 20 mm (see Figure 9a). It is observed that phase angle for $h_f \geq 1.5$ mm converge and follow the same trend at all crack lengths. The discrepancy in mode mixity for all face sheet thicknesses is very small for crack length, a ≥ 90 mm.

Results for the marine configuration (Glass/epoxy tape/ H100) are shown in Figure 9b for all face sheet thicknesses. The phase angle (ψ) lies in the mode I regime at all crack lengths, but is larger for short crack lengths. The specimen with thin face sheet (h_f = 0.5 mm) exhibits the lowest phase angle at all crack lengths. For specimen with thicker face sheets ($h_f \geq 2$ mm), the phase angle tend to converge with increasing crack lengths, with the exception of face sheet with h_f = 7 mm.

In the case of the sandwich system used in the wind industry (Glass/epoxy – Balsa) for all face sheet thicknesses, a mode I region exists for a > 30 mm (see Figure 9c). For h_f = 0.5 mm, the phase angle is within the mode I bounds at all crack lengths. As observed in the other cases, with increasing crack lengths, the phase angle values tend to converge (~ 8°) for a ≥ 60 mm. Note that for $\psi < 0°$, the propensity of the crack is to kink towards the face sheet. When $\psi > 0°$, the inclination of the crack is to dive into the core especially if the core is soft. The specimen dimensions of the various test cases presented in this study are representative of each industry. In accordance with the analysis presented in this section, it is recommended not to consider the energy-release rate computed for an initial debond increment up to 30 mm. Moreover, an initial cycle with a debond increment close to 30 mm will also aid in creating a natural crack front.

Table 4. Typical material properties of sandwich composites used in aerospace, marine and wind industries.

	Face sheet		Core	
Aerospace	E_{11} [GPa]	162	E_{11} [MPa]	0.082
Carbon/epoxy/Honeycomb	E_{22} [GPa]	14.9	E_{22} [MPa]	0.082
(T300/5208 carbon/epoxy [26]	E_{33} [GPa]	14.9	E_{33} [MPa]	121.6
/Nomex Honeycomb[1] [27] [28])	G_{12} [GPa]	5.7	G_{12} [MPa]	0.092
	G_{13} [GPa]	5.7	G_{13} [MPa]	31.0
h_c = 25.4 mm	G_{23} [GPa]	5.4	G_{23} [MPa]	19.0
$L_{b,min}$ = 120 mm	v_{12}	0.283	v_{12}	1.0
L = 270 mm	v_{13}	0.283	v_{31}	0.40
a_{max} = 150 mm	v_{23}	0.386	v_{32}	0.40
Σ = 1350, α = 0.99, β = 0.323			Density [kg/m^3]	32
			Cell size [mm]	4.8
Marine	E_{11} [GPa]	18.6	E_c [MPa]	135
(Glass/expoy tape/H100)	E_{22} [GPa]	18.0	G_c [MPa]	35
DBLT-850-E10 Quadriaxial	E_{33} [GPa]	9.5	v_c	0.40
glass fiber mats (0/45/90/-45)/ H100	G_{12} [GPa]	6.1	Density [kg/m^3]	100
[29][23]	G_{13} [GPa]	2.7	Cell size [mm]	0.45
	G_{23} [GPa]	2.8		
h_c = 40 mm	v_{12}	0.40		
$L_{b,min}$ = 76 mm	v_{13}	0.37		
L = 226 mm	v_{23}	0.43		
a_{max} = 150 mm				
Σ = 138, α = 0.99 , β = 0.164				
Wind	E_{11} [GPa]	14.79	E_{11} [MPa]	6620
(Glass/epoxy plain weave/Balsa):	E_{22} [GPa]	12.73	E_{22} [MPa]	428.3
S2/8552 Unidirectional Glass-epoxy	E_{33} [GPa]	12.73	E_{33} [MPa]	98.3
Prepreg /	G_{12} [GPa]	9.79	G_{12} [MPa]	355.9
High density Balsa wood [30]	G_{13} [GPa]	4.83	G_{13} [MPa]	243.8
	G_{23} [GPa]	4.48	G_{23} [MPa]	243.8
h_c = 30 mm	v_{12}	0.278	v_{12}	0.3
$L_{b,min}$ = 104.2 mm	v_{13}	0.279	v_{13}	0.5
L = 255 mm	v_{23}	0.403	v_{23}	0.23
a_{max} = 150 mm			Density [kg/m^3]	237
Σ = 7.2, α = 0.75, β = 0.212				

[1] Nomex paper properties: E_{paper} = 3.13 GPa, v_{paper} = 0.4 [31] and cell wall thickness = 0.057 mm.

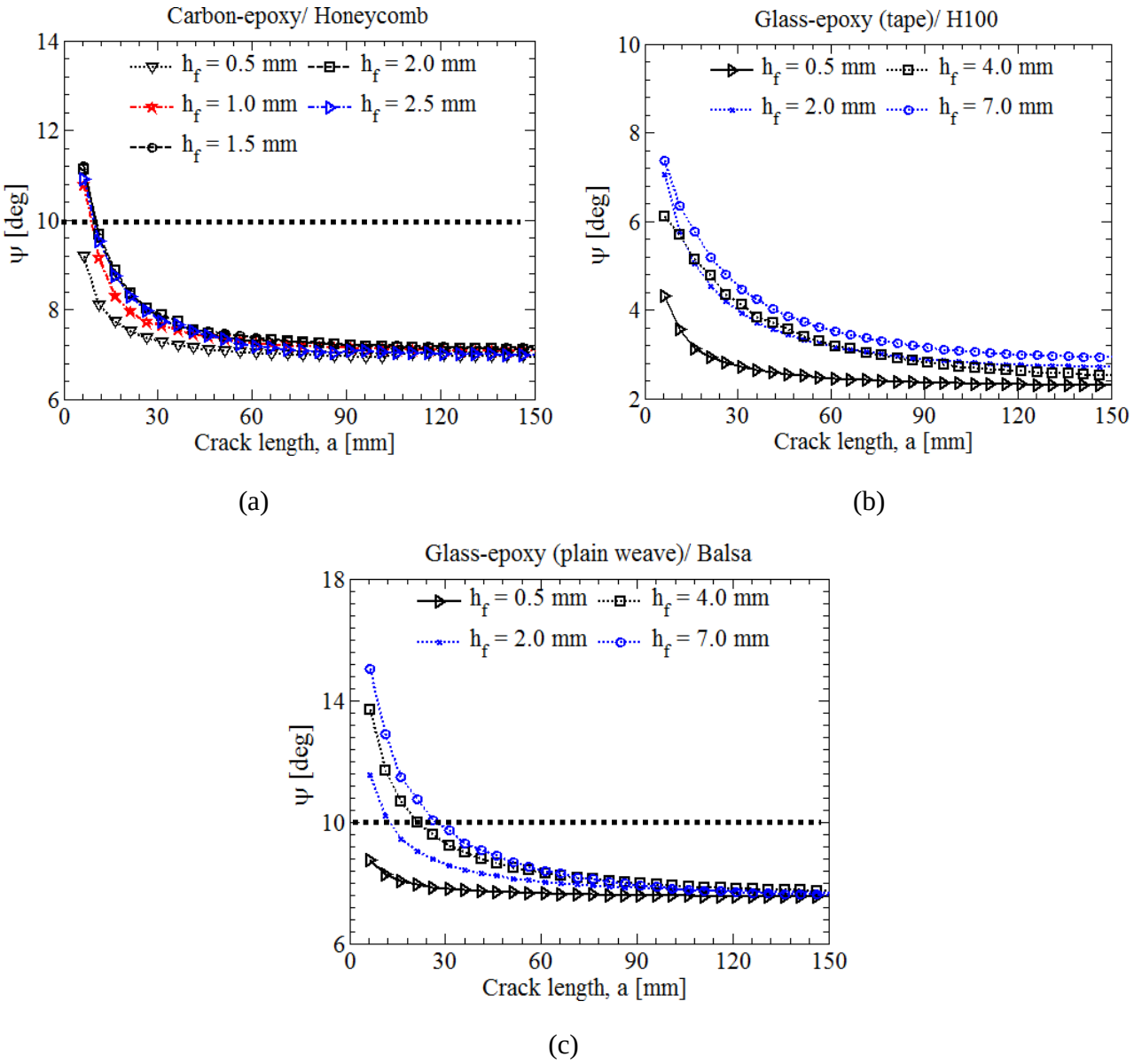

Figure 9. Mode mixity variation of SCB specimens for typical applications in (a) aerospace (Σ = 1350, α = 0.99) (b) marine (Σ = 138, α = 0.99) (c) wind energy (Σ = 7.2, α = 0.75).

5. Energy-release rate of SCB sandwich specimen

In previous sections, the crack tip mode mixity was investigated by applying a unit load (P = 1 N/mm) at all crack lengths in the range a = 0.5 to 150 mm. In a SCB specimen, the energy-release rate, G, invariably depends on magnitude of the applied load (see Equation 12). For a unit load and at a particular crack length, different sandwich systems give rise to various levels of energy release rate values. In order

to study the variation of mode mixity phase angle (ψ) with the applied load magnitude, an analysis was carried out by incrementally varying the load, P, at a given crack length.

A typical marine grade sandwich specimen was used in the analysis: E-glass epoxy tape/H100 (see Table 4 for mechanical properties). The thicknesses of face sheet and core were h_f = 5 mm and h_c = 25.4 mm, respectively. The length of the specimen was L = 300 mm, and the rod length was L_{rod} = 500 mm. Energy-release rate and phase angle were extracted for three different crack lengths (a = 5, 10 and 25 mm) by incrementing the load in steps. The energy-release rate, G, is obtained from the FE-model using the CSDE method (see Equation 6). The energy-release rate expression for the SCB specimen, in terms of the applied load P, can be expressed as [13], [20]:

$$G = \frac{2P^2\lambda^2}{bk}\left[\lambda^2 a^2 + 2\lambda a + 1\right] \tag{12}$$

where λ is defined in Equation (9). The elastic foundation modulus, k, is defined empirically in the literature, and three foundation modulus expressions were employed to compute the energy release rate for comparison [20], [24], [25]. The foundation modulus expressions used in this section are the same ones which were considered before (see Table 3). A comparison of the normalized energy-release rate obtained using the FEA and analytical expression is presented in Figure 10. Both energy-release rate and applied load are normalized with $E_f \cdot h_f$. The various foundation modulus expressions are also provided in the plot (see inset of Figure 10).

For the short crack length (a = 5 mm), the energy-release rate, G, obtained using Quispitupa et al. [25] match closely with results from FEA at lower loads (see Figure 10a) . Significant deviation between FEA and analytical results is observed when the load increases, which can be attributed to the large-scale deformation of the face sheet. For a longer crack length (a = 25 mm), the deviation observed between FEA and analytically obtained G using the k proposed by Quispitupa et al. [25] is also small (see Figure 10b). The other two modulus expressions considered here [20], [24], showed large deviation from FE results for both the crack lengths considered here (see Figure 10).

The mode mixity phase angle (ψ) at various load levels corresponding to each crack length is provided in Figure 11 for the E-glass/H100 sandwich system. For a short crack length (a = 5 mm), the phase angle, ψ, changes from 2.4° to 1.1°, whereas for a = 25 mm, ψ decreases from 2.8° to 0.2°. In addition, ψ tends to decrease linearly with increase in load magnitude. The change in mode mixity with load magnitude is in the range of 2° for the various crack length cases considered here. However, the energy-release rate depends on the applied loading. Therefore, it is recommended to employ the area method to deduce the energy released when the specimen undergoes large-scale deformation during testing.

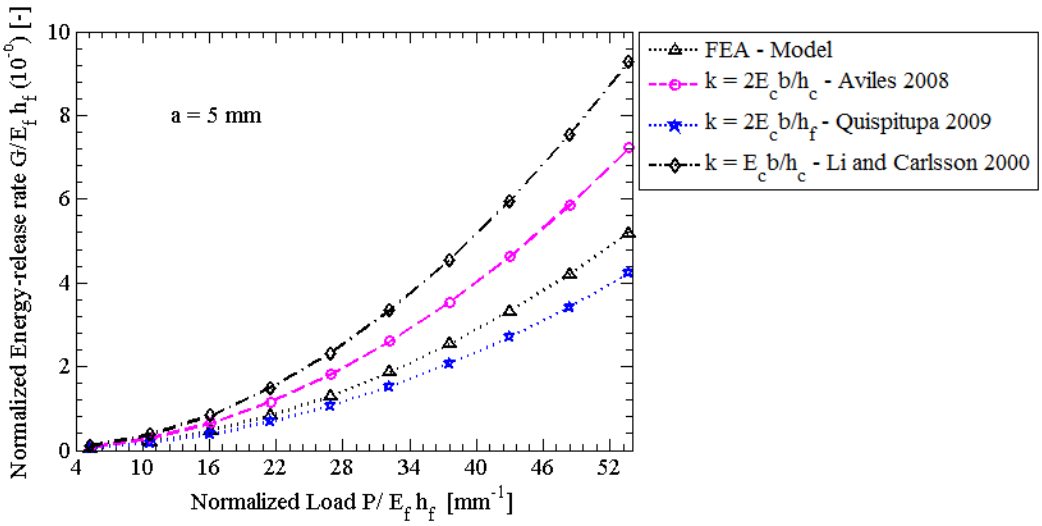

(a)

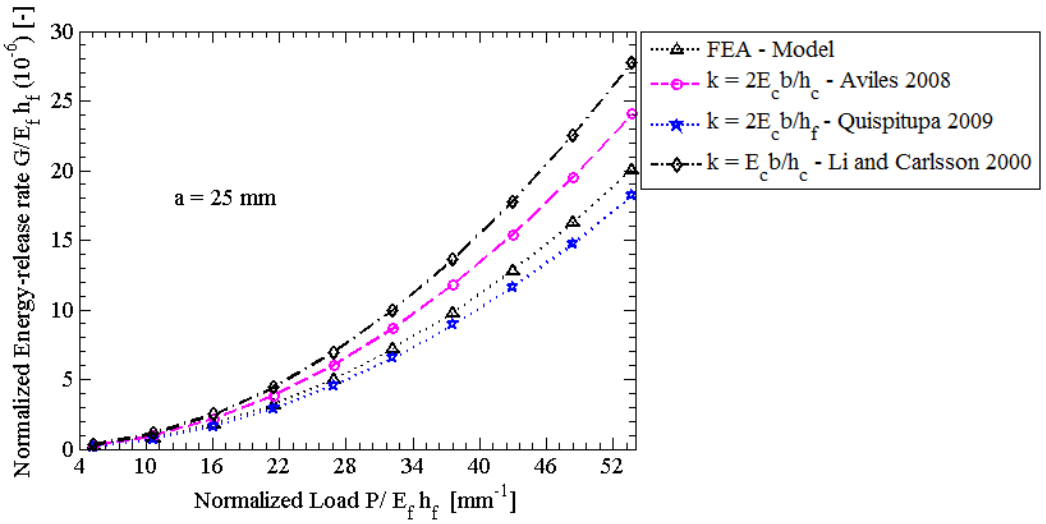

(b)

Figure 10. Comparison of energy-release rate obtained from finite-element results and from analytical approach for E-glass/H100 SCB sandwich specimen (L = 300 mm, L_{rod} = 500 mm), crack length (a) a = 5 mm (b) a = 25 mm.

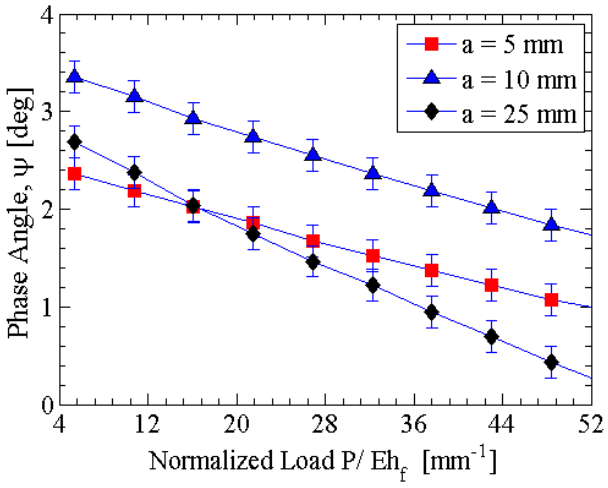

Figure 11. Phase angle vs. applied load for E-glass/H100 SCB specimen at crack lengths, a = 5, 10 and 25 mm.

6. SCB sandwich specimen reinforced with stiff layers (doublers)

Fracture testing of SCB specimens with thin face sheets invariably causes excessive deformation [32]. Such large deformations of the face sheet will make it unviable to employ data reduction methods such as the modified beam theory (MBT) and the compliance calibration method, as the measured compliance ($C = \delta/P$) vs. crack length will yield a non-linear trend. Moreover, a large lift-off of the face sheet will lead to membrane forces, causing matrix cracking/damage. Any additional damage to the specimen is undesirable as the load measured through the machine load cell will contain a component of force that caused the undesired damage. The additional force will affect the fracture toughness data of face/core interface.

One way to circumvent damage in the face sheet, and thereby reduce the excessive lift-off is by attaching a stiff layer atop the upper face sheet. Such stiff reinforcement layers, referred to as “doublers”, can be bonded to specimens with thin, compliant face sheets [33]. However, addition of a doubler layer on the upper face sheet will influence the mode mixity phase angle (ψ). The extent of influence depends on the stiffness and thickness of the doubler layer. A numerical study using the previously presented FE model was undertaken in which the model was expanded by attaching a doubler layer on the top face sheet (see Figure 12). The investigation was carried out for SCB specimens with face sheet thickness less than 1 mm. Note that irrespective of the addition of a doubler layer on the face sheet, the mode mixity phase angle must remain within the earlier assumed bounds ($-10° \leq \psi \leq 10°$) to be in the mode I regime.

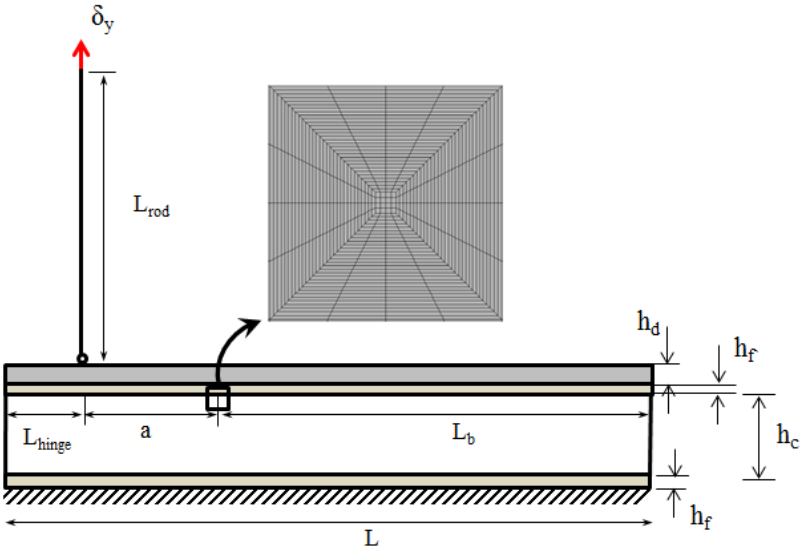

Figure 12. FE-model of a sandwich SCB specimen reinforced with a doubler layer, h_d.

A previous study of a similar nature was conducted on the Tilted Sandwich Debond (TSD) specimen [34] and the influence of a stiffener layer on the phase angle was reported for various tilt angles. To benchmark and extend the analysis performed in [34] to a SCB sandwich specimen, similar face/core sandwich systems were used. The mechanical properties of face sheet, core and doubler layer are provided in Table 5. The minimum length of intact portion was estimated using Equation (10) with $k = E_c b/h_c$ [20] and was kept constant throughout the analysis ($L_{b,min}$ = 32.7 mm). Throughout this section, the total length of the specimen and the loading rod length were fixed at L = 200 mm and L_{rod} = 500 mm, respectively. A unit load was applied at each crack length until a_{max} = 150 mm, and the solution was obtained using the geometrical non-linear solver.

Table 5. Mechanical properties of face sheet, core and doubler layer.

Face sheet			**Core (PVC H100)**		**Doubler Layer (Steel)**	
	GFRP	**CFRP**				
E_{11} [GPa]	20.6	44.0	E_c [MPa]	135	E_d [GPa]	210
E_{22} [GPa]	20.6	44.0	G_c [MPa]	35	ν_d	0.30
E_{33} [GPa]	9.90	9.90	ν_c	0.40		
G_{12} [GPa]	3.10	6.62	Density [kg/m^3]	100		
G_{13} [GPa]	2.90	6.20	Cell size [mm]	0.45		
G_{23} [GPa]	2.90	6.20				
ν_{12}	0.12	0.12				
ν_{13}	0.37	0.37				
ν_{23}	0.37	0.37				

Reinforced SCB: Effect of doubler layer thickness (h_d)

The influence of doubler layer thickness on the mode mixity phase angle (ψ) was investigated by varying the steel doubler layer thickness h_d, from 2 to 12 mm. Core and face sheet thickness of GFRP/H100 sandwich were held constant at h_c = 25 mm and h_f = 2 mm respectively. A plot of ψ vs. crack length for various doubler layer thicknesses is shown in Figure 13. For comparison, the phase angle (ψ) variation of an un-reinforced specimen (h_d = 0 mm) is also provided. It is noted that the phase angle deviates more toward the mixed-mode regime as the doubler thickness (h_d) increases. For the case of an un-reinforced SCB specimen, the mode mixity is observed to remain just above the mode I region (see Figure 13). Hence for the particular case of GFRP/H100 sandwich system considered here, mode I regime cannot be achieved by addition of doubler layers

The phase angle (ψ) for specimens reinforced with doublers is observed to gradually increase at higher crack lengths in Figure 13. The departure occurs at various crack lengths depending on the doubler layer thickness. The shift in ψ indicates the insufficient intact length (L_b) as confirmed in an earlier section. Therefore, Equation (10) must be modified such that the intact portion is calculated taking into account the flexural modulus of the entire upper beam consisting of both doubler and face sheet. An expression for the minimum intact length ($L_{b,min}$) which takes into account a doubler layer attached to top face sheet is provided in Appendix A.

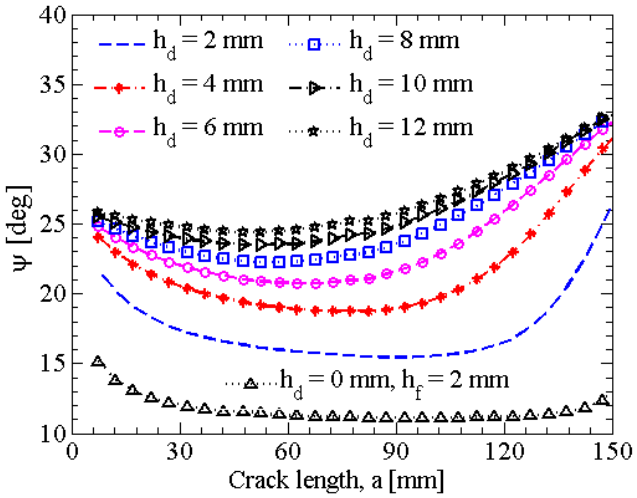

Figure 13. Phase angle *(ψ)* vs. crack length (a) for a GFRP/H100 SCB specimen reinforced with a doubler layer (h_f = 2 mm, h_c = 25 mm).

Reinforced SCB: Effect of face sheet modulus (E_f)

The effect of face sheet modulus (E_f) on the phase angle (ψ) is presented in this section. Two different face sheets (GFRP and CFRP) described in Table 5 were utilized with H100 core. The steel doubler layer thickness was varied from 2 to 12 mm. Face sheet and core thickness were held constant at h_f = 2 mm and h_c = 25 mm, respectively. The specimen was loaded with a unit load as in previous analyses until a_{max} = 150 mm.

A plot of ψ vs. crack length for the two sandwich systems is provided in Figure 14. The phase angle (ψ) increases with increase in doubler thickness for both sandwich systems considered here. It is observed that ψ tends to converge at large values of h_d for both CFRP/H100 and GFRP/H100 cases. The mode I regime characterized within $-10° \leq \psi \leq 10°$ is not observed for any case. A clear indication of insufficient intact portion length is also observed in the plot where an increase in ψ is observed at increasing crack length.

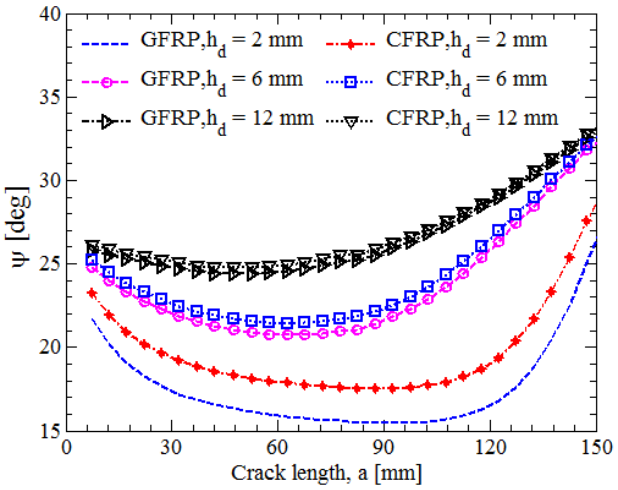

Figure 14. Phase angle *(ψ)* computed for SCB specimens; GFRP/H100 and CFRP/H100 (h_f = 2 mm, h_c = 25 mm) with stiffener layer thickness, h_d = 2-12 mm.

Reinforced SCB: Effect of core thickness (h_c)

The influence of core thickness (h_c) on the phase angle (ψ) in a reinforced SCB sandwich specimen is presented in this section. Three core thicknesses were used for this analysis; h_c = 10, 25 and 40 mm. A GFRP/H100 sandwich specimen with a face sheet thickness h_f = 2 mm was considered. Two steel doubler layer thicknesses, h_d = 2 and 12 mm, were considered for the three core thickness cases. A plot of ψ vs. crack length is provided in Figure 15 for the two doubler layer cases. For comparison, the phase angle obtained for a GFRP/H100 specimen without any doubler layer (h_d = 0 mm) is also presented in Figure 15 for a core thickness, h_c = 25 mm.

It is observed that, for a thick core (h_c = 40 mm), regardless of the doubler layer thickness, ψ remains positive and deviates away from the mode I condition. In the crack length range 30 < a < 120 mm, the phase angle for h_d = 12 mm and h_c = 10 mm is equal to the case with h_d = 0 mm and h_c = 25 mm (see Figure 15b). None of the investigated configurations involving thin and thick cores satisfy the mode I criterion. In addition, insufficient intact length is more evident in the case with a thick doubler layer (Figure 15b), where ψ is observed to deviate away from the plateau for all the three core thicknesses. From the analysis undertaken here, use of a doubler layer is not recommended, as the phase angle is observed to increase toward positive region leading to significant deviation from the mode I condition. For both thin and thick doubler layers, the crack will kink into the core for all cases of $\psi > 0$.

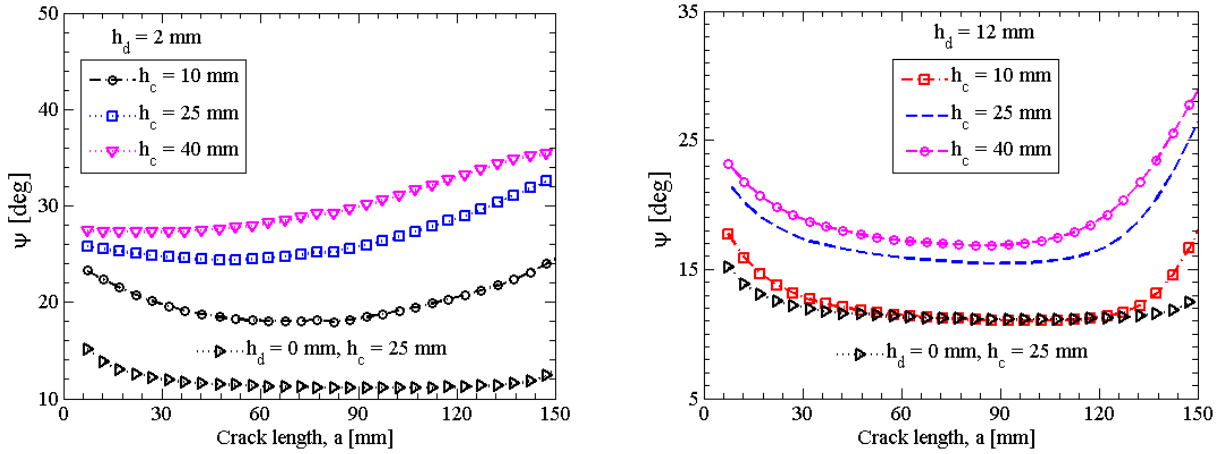

(a) (b)

Figure 15. Phase angle (ψ) vs. crack length (a) various core thicknesses for GFRP/H100 SCB specimen with constant h_f = 2 mm (a) h_d = 2mm (b) h_d = 12 mm.

Reinforced SCB specimen: Effect of doubler modulus (E_d)

To investigate the effect of doubler modulus (E_d) on the mode mixity, a CFRP/H100 sandwich system with three doubler materials was studied. The core, face sheet and doubler layer thickness were held constant: h_c = 25 mm, h_f = 2 mm and h_d = 2 mm. The total length of the specimen and the rod length were kept as previous, L = 200 mm and L_{rod} = 500mm. The three doubler layer materials chosen in this section were: E-glass/epoxy, aluminum and steel with stiffness, E_d = 20, 70 and 210 GPa, respectively.

A plot of ψ vs. crack length is provided in Figure 16. The ψ values for the SCB specimen reinforced with stiffer steel are slightly larger than the ones reinforced with GFRP and aluminum. As previously, ψ deviates from the plateau for crack length, a > 100 mm, indicating an inaccurate intact length estimation. In general, the stiffness of the doubler layer is seen to have less influence on the phase angle. Therefore,

the phase angle is predominantly influenced by a combination of stiffness and thickness of both doubler layer and face sheet.

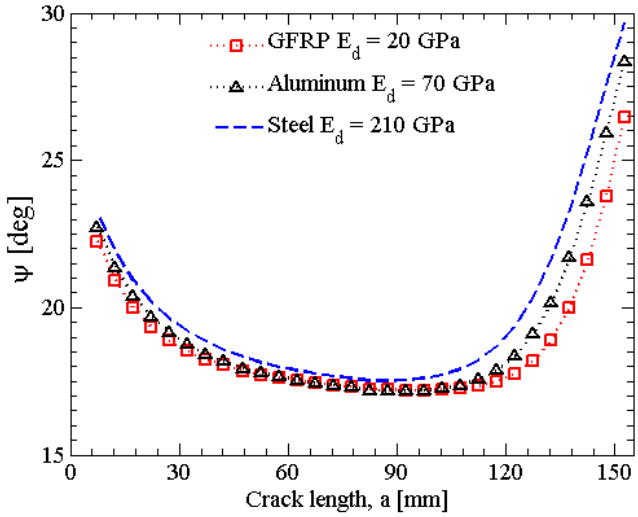

Figure 16. Phase angle *(ψ)* vs. crack length of reinforced CFRP/H100 SCB sandwich specimen with doubler layer stiffnesses; E_d = 20, 70 and 210 GPa (h_d = 2 mm, h_f = 2 mm and h_c = 25 mm).

7. Conclusions

The sandwich SCB specimen was investigated from a local mode mixity perspective using the numerical Crack Surface Displacement Extrapolation (CSDE) method by varying both geometrical and material parameters. The parametric study was carried out using hypothetical SCB sandwich specimens, and the mode I regime was assumed in the range $-10° \leq \psi \leq 10°$.

- For a constant face sheet thickness (h_f), stiffer face sheets led to increasingly positive values of ψ which deviate away from the mode I condition.
- Specimens with thick core and thick face sheets yielded increased phase angle, whereas specimens with thin core and thick face sheets yielded lower phase angles.
- Depending on how stiff the core is, the face sheet thickness (h_f) along with the ratio of face sheet and core moduli ($\Sigma = E_f/E_c$) influence ψ. For constant core properties, the specimens with thinner face sheets exhibited lower values of ψ. In addition, core Poisson's ratio (υ_c) was shown to influence the mode mixity. Crack propagation in a core with higher Poisson's ratio (υ_c) was observed to lie close to mode I regime.
- The intact portion length was seen to influence the phase angle (ψ), especially at large crack lengths. In general, thinner face sheets require shorter intact portions. Various equations for

elastic foundation modulus, *k*, were used to determine the minimum intact portion length and the expression provided by Li et al. [20] was found to provide a valid estimate.

- For the considered sandwich construction, modeled results showed significant deviation from mode I regime with loading rods shorter than 500 mm. Therefore, a loading rod length in terms of the length of the specimen was recommended as: $L_{rod} \geq 1.70\ L$.
- A case study involving typical sandwich systems used in three different industries aerospace, marine and wind energy was presented. The case study demonstrated a mode I window ($-10° \leq \psi \leq 10°$) which exists over various face sheet thickness and crack lengths for the investigated SCB specimen configurations. It was recommended to disregard the initial cycle associated with a debond increment of ~30 mm for the energy-release rate estimation. In addition, an initial cycle will enable creation of a natural crack front.
- For a constant crack length, it was observed that the fluctuation of mode mixity phase angle at various load magnitudes was negligible (~1.5° for a = 5 mm and 3.0° for a = 25 mm). The area method was recommended to deduce the energy released for non-linear specimen response.
- Reinforcing the SCB specimen with a stiff doubler layer was observed to shift the mode condition away from mode I, which qualitatively agrees with the literature. The intact specimen length expression was modified to account for a reinforced SCB specimen.

The parametric analysis was performed in this paper using both hypothetical as well as real sandwich systems. It was found that the existing sizing method yielded specimen configurations which remain in the mode I regime. Furthermore, despite conforming to the sizing requirements, a certain class of specimens was also found to deviate away from the mode I bounds. At the same time specimens which do not adhere to the sizing standard were also observed to satisfy the mode I conditions. Therefore, in the absence of a closed form expression to determine the mode mixity phase angle (ψ) for a SCB sandwich specimen, it is advised to proceed with caution with regard to the selection of specimen configuration. It is highly recommended to perform a limited series of mode mixity analyses prior to fracture testing.

APPENDIX A: Minimum intact length of a reinforced SCB specimen

The expression to calculate intact portion length (L_b) was modified to accommodate a reinforced SCB sandwich specimen and is presented in this section. Equation 10 provides an estimate of L_b based on the parameter λ, which indicates the ratio of stiffness of the elastic foundation to the bending stiffness of the upper beam. Reinforcing the upper face sheet by addition of a stiff layer changes the flexural modulus of the beam. Hence, λ should be modified to account for the reinforced beam. The effective modulus of the face sheet and doubler layer (see Figure 12) can be expressed as [35]:

$$E^*_{x,f} = \frac{12}{d_{11} h^3_{DF}} \tag{A1}$$

where $h_{DF} = h_f + h_d$ and d_{11} is the inverse component of the *D*-matrix given by:

$$D = \frac{1}{3}\sum_{k=1}^{n} \bar{E}_k (y_k^3 - y_{k-1}^3) \tag{A2}$$

where y_k is the *y*-coordinate of the interface between ply *k* and *k* - 1. Now, the parameter λ is modified as:

$$\lambda^* = \left[\frac{3k}{E_{x,f}^* h_f^3 b} \right]^{1/4} \tag{A3}$$

Therefore the new condition for minimum support length for a reinforced SCB specimen can be written as: $\lambda^* L_{b,min} \geq 2.7$.

Acknowledgments

The financial support from the Danish Centre for Composite Structures and Materials (DCCSM) funded by the Danish Council for Strategic Research within Sustainable Energy and Environment (Grant: 09-067212) is gratefully acknowledged. Furthermore, the support from Kaj & Hermilla Ostenfeld's Foundation for the first author's research stay at the NASA Langley Research Center is highly appreciated. The third author's research has been supported by the Federal Aviation Administration (FAA). Funding through the Aviation Research Grants Program, Research Grant Number 16-G-006 is gratefully acknowledged.

References

[1] "Loss of Rudder, Airbus 310-308, Air Transat Flight 961," *Aviation Investigation Report A05F0047*. Transportation Safety Board of Canada, Gatineau, Canada, 2007.

[2] Air Accident Investigation Branch, "AAIB Bulletin 8/92 Ref: EW/A92/5/1," UK, 1992.

[3] Air Accident Investigation Branch, "AAIB Bulletin 2/95 Ref: EW/C94/8/3," UK, 1995.

[4] Air Accident Investigation Branch, "AAIB Bulletin 10/96 Ref: EW/C96/6/6," UK, 1996.

[5] M. Rinker, R. Krueger, and J. Ratcliffe, "Analysis of an Aircraft Honeycomb Sandwich Panel with Circular Face Sheet/Core Disbond Subjected to Ground-Air Pressurization," *NASA Tech. Rep. CR–2013-217974*, 2013.

[6] R. Goetz, R. S. Ryan, and A. F. Whitaker, "Final report of the X-33 liquid hydrogen tank test investigation team," Marshall Sp. Flight Center, Huntsville, AL, 2000.

[7] E. H. Glaessgen, J. R. Reeder, D. W. Sleight, J. T. Wang, I. S. Raju, and C. E. Harris, “Debonding Failure of Sandwich-Composite Cryogenic Fuel Tank with Internal Core Pressure,” *J. Spacecr. Rockets*, vol. 42, no. 4, pp. 613–627, 2005.

[8] C. Weaver, “Evaluation of Mode I Fracture Mechanics Test Methods For Sandwich Composites,” M.Sc Thesis, University of Utah, Salt Lake City, UT, 2009.

[9] R. E. Fields and R. . Zarda, “Analysis and Test Methodology for Fracture Mechanics of Unbonded Sandwich Structures,” *Martin Maerietta Task Report, EDF No. MM0 TKR 10722739-001*, 1994.

[10] W. J. Cantwell and P. Davies, “A test technique for assessing core-skin adhesion in composite sandwich structures,” *J. Mater. Sci. Lett.*, vol. 13, pp. 203–205, 1994.

[11] K. Shivakumar, H. Chen, and S. A. Smith, “An Evaluation of Data Reduction Methods for Opening Mode Fracture Toughness of Sandwich Panels,” *J. Sandw. Struct. Mater.*, vol. 7, no. 1, pp. 77–90, 2005.

[12] J. W. Hutchinson and Z. Suo, “Mixed Mode Cracking in Layered Materials,” *Adv. Appl. Mech.*, vol. 29, pp. 63–191, 1991.

[13] J. G. Ratcliffe and J. R. Reeder, “Sizing a single cantilever beam specimen for characterizing facesheet-core debonding in sandwich structure,” *J. Compos. Mater.*, vol. 45, no. 25, pp. 2669–2684, 2011.

[14] M. F. Kanninen, “An augmented double cantilever beam model for studying crack propagation and arrest,” *Int. J. Fract.*, vol. 9, no. 1, pp. 83–92.

[15] C. Berggreen, B. C. Simonsen, and A. K. K. Borum, “Experimental and Numerical Study of Interface Crack Propagation in Foam-cored Sandwich Beams,” *J. Compos. Mater.*, vol. 41, no. 4, 2007.

[16] “ANSYS Mechanical User’s Guide.” ANSYS, Inc., Southpointe, PA, 2015.

[17] C. Berggreen, “Damage Tolerance of Debonded Sandwich Structures,” Technical University of Denmark, 2004.

[18] J. Dundurs, “Discussion: ‘Edge-Bonded Dissimilar Orthogonal Elastic Wedges Under Normal and Shear Loading’ (Bogy, D. B., 1968, ASME J. Appl. Mech., 35, pp. 460–466),” *J. Appl. Mech.*, vol. 36, no. 3, p. 650, 1969.

[19] M.-Y. He and J. W. Hutchinson, “Kinking of a Crack Out of an Interface,” *J. Appl. Mech.*, vol. 56, no. 2, p. 270, Jun. 1989.

[20] X. Li and L. A. Carlsson, “Elastic Foundation Analysis of Tilted Sandwich Debond (TSD) Specimen,” *J. Sandw. Struct. Mater.*, vol. 2, no. 1, pp. 3–32, 2000.

[21] S. Li, J. Wang, and M. D. Thouless, “The effects of shear on delamination in layered materials,” *J. Mech. Phys. Solids*, vol. 52, no. 1, pp. 193–214, 2004.

[22] X. Li and L. A. Carlsson, “The Tilted Sandwich Debond (TSD) Specimen for Face/Core Interface Fracture Characterization,” *J. Sandw. Struct. Mater.*, vol. 1, no. 1, pp. 60–75, Jan. 1999.

[23] “Divinycell H Technical Data.” DIAB Group, Laholm, Sweden, 2016.

[24] F. Avilés and L. A. Carlsson, “Analysis of the sandwich DCB specimen for debond characterization,” *Eng. Fract. Mech.*, vol. 75, no. 2, pp. 153–168, 2008.

[25] A. Quispitupa, C. Berggreen, and L. A. Carlsson, “On the analysis of a mixed mode bending sandwich specimen for debond fracture characterization,” *Eng. Fract. Mech.*, vol. 76, no. 4, pp. 594–613, 2009.

[26] N. K. Naik, S. I. Tiwari, and R. S. Kumar, “An analytical model for compressive strength of plain weave fabric composites,” *Compos. Sci. Technol.*, vol. 63, no. 5, pp. 609–625, 2003.

[27] Hexcel, “HexWeb Honeycomb Sandwich Design Technology,” Duxford, UK, 2000.

[28] S. Malek and L. Gibson, “Effective elastic properties of periodic hexagonal honeycombs,” *Mech. Mater.*, vol. 91, pp. 226–240, 2015.

[29] M. Manca, C. Berggreen, L. A. Carlsson, and P. Bortolotti, “Fatigue characterization of Poly Vinyl Chloride (PVC) foam core sandwich composite using the G-control method,” *J. Sandw. Struct. Mater.*, vol. 18, no. 3, pp. 374–394, 2016.

[30] A. Da Silva and S. Kyriakides, “Compressive response and failure of balsa wood,” *Int. J. Solids Struct.*, vol. 44, no. 25–26, pp. 8685–8717, 2007.

[31] C. C. Foo, G. B. Chai, and L. K. Seah, “Mechanical properties of Nomex material and Nomex honeycomb structure,” *Compos. Struct.*, vol. 80, no. 4, pp. 588–594, 2007.

[32] M. Rinker, J. G. Ratcliffe, D. O. Adams, and R. Krueger, “Characterizing Facesheet/Core Disbonding in Honeycomb Core Sandwich Structure,” *NASA Tech. Rep. CR-2013-217959*, 2013.

[33] J. R. Reeder, K. Demarco, and K. S. Whitley, “The use of doubler reinforcement in delamination toughness testing,” *Compos. Part A Appl. Sci. Manuf.*, vol. 35, no. 11, pp. 1337–1344, 2004.

[34] C. Berggreen and L. A. Carlsson, “A Modified TSD Specimen for Fracture Toughness Characterization - Fracture Mechanics Analysis and Design,” *J. Compos. Mater.*, vol. 44, no. 15, pp. 1893–1912, 2010.

[35] L. A. Carlsson, D. F. Adams, and R. B. Pipes, *Experimental Characterization of Advanced Composite Materials*, 4th ed. Boca Raton, FL: CRC Press, 2008.

Publication P2

V. Saseendran, L. A. Carlsson, and C. Berggreen

Shear and Foundation Effects on Crack Root Rotation and Mode-Mixity in Moment- and Force-Loaded Single Cantilever Beam Sandwich Specimen

Journal of Composite Materials, vol. 52, no. 18, pp. 2537-2547, 2018

Accepted: 27 November 2017
Available online: 08 January 2018
DOI: https://doi.org/10.1177/0021998317749714

Article

JOURNAL OF COMPOSITE MATERIALS

Journal of Composite Materials
2018, Vol. 52(18) 2537–2547

DOI: 10.1177/0021998317749714
journals.sagepub.com/home/jcm
SAGE

Shear and foundation effects on crack root rotation and mode-mixity in moment- and force-loaded single cantilever beam sandwich specimen

Vishnu Saseendran[1], Leif A Carlsson[2] and Christian Berggreen[1]

Abstract

Foundation effects play a crucial role in sandwich fracture specimens with a soft core. Accurate estimation of deformation characteristics at the crack front is vital in understanding compliance, energy release rate and mode-mixity in fracture test specimens. Beam on elastic foundation analysis of moment- and force-loaded single cantilever beam sandwich fracture specimens is presented here. In addition, finite element analysis of the single cantilever beam specimen is conducted to determine displacements, rotations, energy release rate and mode-mixity. Based on finite element analysis, a foundation modulus is proposed that closely agrees with the numerical compliance and energy release rate results for all cases considered. An analytical expression for crack root rotation of the loaded upper face sheet provides consistent results for both loading configurations. For the force-loaded single cantilever beam specimen (in contrast to the moment-loaded case), it was found that the crack length normalized energy release rate and the mode-mixity phase angle increase strongly as the crack length decreases, a result of increased dominance of shear loading.

Keywords

Elastic foundation, single cantilever beam, root rotation, face/core interface, debond, sandwich, DCB-UBM

Introduction

A serious failure mode of sandwich structures is the separation of face and core. The problem is pertinent to design of such structures not only because this failure mode impairs the strength but also leads to substantial loss of stiffness. A particular characteristic of sandwich structures is that they are 'tri-materials' with very large mismatch in elastic properties of the two faces and core. In general, face/core debonds are loaded in mixed mode (combined opening and shear). Since the fracture resistance depends on the mode-mixity, a reliable way of assessing the mode-mixity is needed. Hence, the mixed-mode face/core sandwich debond problem needs to be addressed in a comprehensive way, both from an analytical and experimental approach. Analysis of face/core crack in sandwich specimens has been presented by Østergaard and Sørensen[1] and Kardomateas et al.[2] Kardomateas et al.[2] developed closed-form expressions for the mode-mixity of a face/core interface crack in a sandwich element under axial force and moment loading. The sandwich element considered, however is free from transverse shear forces.

Transverse shear forces are very common part of the loading of most sandwich structures. Transverse shear forces exist in many fracture test specimens such as double cantilever beam (DCB), End Notched Flexure (ENF), Tilted Sandwich Debond (TSD) and Mixed Mode Bending (MMB).[3–6] Lu et al.[7] considered a homogenous cantilever beam with an embedded delamination under transverse force loading, and generated results for energy release rate using finite element

[1]Department of Mechanical Engineering, Technical University of Denmark, Denmark
[2]Department of Ocean & Mechanical Engineering, Florida Atlantic University, USA

Corresponding author:
Vishnu Saseendran, Department of Mechanical Engineering, Technical University of Denmark, Nils Koppels Allé Building 404, 2800 Kgs. Lyngby, Denmark.
Email: vsas@mek.dtu.dk

analysis (FEA). Li et al.[8] examined the influence of shear in beam-like element under axial and transverse forces and bending moments using FEA. As discussed by Li et al.,[8] a vertical section of the upper face layer indicated in Figure 1 will rotate because of foundation effects. The influence of root rotation significantly affects the fracture parameters. As discussed by Timoshenko and Goodier,[9] Barber[10] and Li et al.,[8] in general the rotation is not uniform across the section. The transverse shear and rotation must be incorporated in the fracture mechanics analysis. Li et al.[8] found large influence of transverse shear on the energy release rate and mode-mixity phase angle at short crack lengths.

More recently, Andrews and Massabò[11] proposed a crack element approach where transverse shear forces are acting and developed a superposition scheme. Their approach utilizes the fact that the root rotation depends linearly on crack tip stress resultants, and provides numerically obtained compliance coefficients. In the case of sandwich face/core interface, understanding the crack tip deformation characteristics is vital especially when the analyzed fracture specimen utilizes a soft core.

The main objective of this paper is to examine foundation effects on crack root rotation, energy release rate and mode-mixity phase angle for two cases of loading of a single cantilever beam (SCB) sandwich fracture test specimen, that is moment and force loadings. The moment-loaded SCB specimen is solved using the Winkler elastic foundation model, to obtain the deformation characteristics of the debonded face sheet. A robust analytical framework which captures the influence of the transverse shear force is developed. In addition, the two SCB configurations are analyzed using FEA. Comparisons are made against commonly used expressions for the foundation modulus.

Sandwich fracture specimens

A sandwich debond specimen, first introduced for testing of monolithic composites by Sørensen et al.[12] and later extended to sandwich debond testing by Lundsgaard-Larsen et al.[13] is the Double Cantilver Beam loaded with Uneven or unequal Bending Moments (DCB-UBM) specimen shown in Figure 2(a). In this test, edge moments M_0 and M_1 are applied until the crack propagates. The right end of the beam is supported to remain horizontal. Moments and rotations of the beams are recorded during the test. The fracture toughness, G_c, is determined from a critical set of moments required to propagate the crack, using a J-integral expression for the energy release rate, G.

The force-loaded SCB specimen, shown schematically in Figure 2(b), was proposed by Cantwell and Davies[14] to determine face/core fracture toughness. This specimen has received much attention recently[15,16] and is currently a candidate for ASTM standardization.[17] The entire lower surface of the bottom face sheet is rigidly supported. A vertical load, P, acts on the top face sheet where a pre-crack of length, a, exists. Load is applied until the crack propagates. Both load and displacement are recorded. Fracture toughness, expressed as the critical energy release rate, G_c, is then computed from experimental test results using several data reduction schemes.[16,17]

In an effort to examine foundation effects in the moment-loaded DCB-UBM specimen (Figure 2(a)), a moment-loaded single cantilever beam specimen is considered here, see Figure 3. The extension of this analysis to the DCB-UBM specimen will be presented in a related paper. It is recognized that the traditional force-loaded SCB specimen, Figure 2(b), is actually both force- and moment-loaded, since the transverse force acts at a distance, a from the crack tip, which corresponds to a moment, $M = Pa$ at the tip. The moment and shear effects in this specimen configuration will be separated in the current paper.

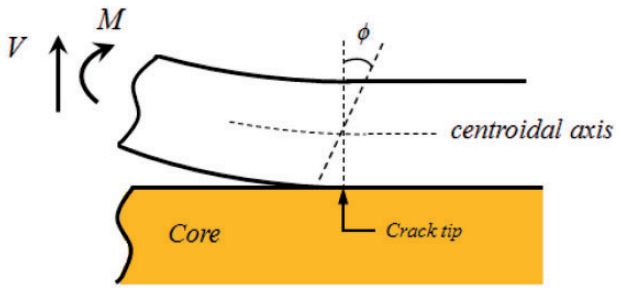

Figure 1. Illustration of crack root rotation.

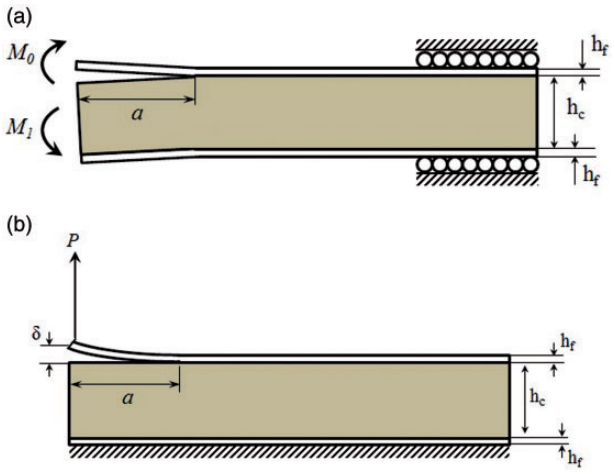

Figure 2. Face/core debond test specimens. (a) Moment-loaded DCB-UBM specimen, (b) Force-loaded single cantilever beam specimen.

Figure 3. Moment-loaded single cantilever beam specimen.

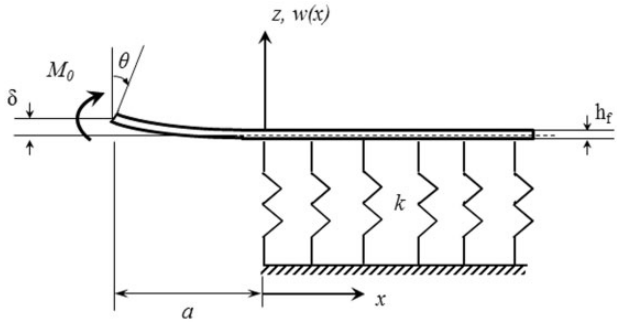

Figure 4. Foundation model of moment-loaded single cantilever beam specimen.

The deformation characteristics of the debonded face sheet in both force- and moment-loaded specimens (see Figures 2(b) and 3) are studied using the beam on elastic foundation approach, first suggested by Kanninen.[18] A Winkler foundation is used to approximate the core. The core has also been modelled using higher-order sandwich theories.[19,20] The Winkler foundation approach, however, is proven to be adequate.[3,8,15,21–23]

Moment-loaded semi-infinite beam resting on an elastic foundation

The sandwich DCB-UBM consists of a moment-loaded upper face sheet resting on the core bonded to the lower face sheet. Figure 4 shows the foundation model representation of this part of the DCB-UBM specimen, that is, a SCB sandwich specimen loaded with an edge couple of magnitude M_0.

In order to derive an analytical framework involving crack root rotation for the moment-loaded SCB specimen, the deformation kinematics must be determined. The un-cracked region of the top face can be perceived as a beam supported on the core acting as an elastic foundation. The governing equation for the deflection, $w(x)$, of a beam supported by an elastic foundation has been presented by Barber,[10]

$$EI\frac{d^4w}{dx^4} + kH(x)w = 0 \tag{1a}$$

where

$$H(x) = \begin{cases} 1, x > 0 \\ 0, x < 0 \end{cases} \tag{1b}$$

where E is the Young's modulus of the face sheet, I is the moment of inertia of the face sheet and k is the foundation modulus. The x-axis is defined in Figure 4. The general solution to the homogenous equation (1a) can be written as:

$$w(x) = B_1e^{\lambda x}\cos(\lambda x) + B_2e^{\lambda x}sin(\lambda x) + B_3e^{-\lambda x}\cos(\lambda x) + B_4e^{-\lambda x}sin(\lambda x) \tag{2}$$

where

$$\lambda = \sqrt[4]{\frac{k}{4E_fI}} \tag{3}$$

In the foundation model representation of the moment-loaded SCB specimen, the debonded face sheet is considered as a beam resting on an elastic foundation (see Figure 4). For the case of a semi-infinite beam, the effects from one end will decay before the other end is reached. In other words, only the exponentially decaying terms in equation (2) may be retained. Therefore, the displacement is of the form[10]

$$w(x) = B_3e^{-\lambda x}\cos(\lambda x) + B_4e^{-\lambda x}\sin(\lambda x) \tag{4a}$$

Progressive derivatives of equation (4a) provide the slope θ, bending moment, M and shear force, V

$$w(x) = B_3f_1(\lambda x) + B_4f_2(\lambda x) \tag{4b}$$

$$\theta(x) = \frac{dw(x)}{dx} = -B_3\lambda f_3(\lambda x) + B_4\lambda f_4(\lambda x) \tag{4c}$$

$$M(x) = -EI\frac{dw^2(x)}{dx^2} = -\frac{B_3k}{2\lambda^2}f_2(\lambda x) + \frac{B_4k}{2\lambda^2}f_1(\lambda x) \tag{4d}$$

$$V(x) = \frac{\mathrm{d}M(x)}{dx} = -\frac{B_3k}{2\lambda}f_4(\lambda x) + \frac{B_4k}{2\lambda}f_3(\lambda x) \tag{4e}$$

where

$$\begin{aligned} f_1(\lambda x) &= e^{-\lambda x}\cos(\lambda x) \\ f_2(\lambda x) &= e^{-\lambda x}\sin(\lambda x) \\ f_3(\lambda x) &= e^{-\lambda x}(\cos(\lambda x) + \sin(\lambda x)) \\ f_4(\lambda x) &= e^{-\lambda x}(\cos(\lambda x) - \sin(\lambda x)) \end{aligned} \tag{5}$$

The parameters B_3 and B_4 in equation (4a) can be determined from any two boundary conditions at $x = 0$.

From Figure 4, the boundary conditions at $x=0$ are: $V=0$ and $M=M_0$. Substitution into equations (4d) and (4e) yields

$$B_3 = M_0\frac{2\lambda^2}{k};\ B_4 = -M_0\frac{2\lambda^2}{k} \tag{6}$$

Substituting equation (6) into equations (4b–4e) gives expressions for displacement, slope, bending moment and shear force for the interval $(0, \infty)$ as

$$w(x) = \frac{M_0 2\lambda^2}{k}(f_1(\lambda x) - f_2(\lambda x)) \tag{7a}$$

$$\theta(x) = \frac{dw(x)}{dx} = -\frac{M_0 2\lambda^3}{k}(f_3(\lambda x) - f_4(\lambda x)) \tag{7b}$$

$$M(x) = EI\frac{dw^2(x)}{dx^2} = -M_0(f_2(\lambda x) - f_1(\lambda x)) \tag{7c}$$

$$V(x) = EI\frac{dw^3(x)}{dx^3} = -M_0\lambda(f_4(\lambda x) + f_3(\lambda x)) \tag{7d}$$

The deflection of the debonded face sheet can be obtained by solving the homogenous equation (1a) for the interval $(-a, 0)$ with $k=0$

$$EI\frac{d^4w}{dx^4} = 0 \tag{8}$$

The general solution is of the form

$$w(x) = C_1\frac{x^3}{6} + C_2\frac{x^2}{2} + C_3x + C_4 \tag{9}$$

The constants C_1 and C_2 are obtained by utilizing the boundary conditions $V(x=0)=0$ and $M(x=0)=M_0$. Furthermore, the deflection, slope and shear force at the top face sheet must be continuous. Such conditions mandate that deflection in the two intervals $(-a, 0)$ and $(0, \infty)$, and the three progressive derivatives must match at $x=0$. Invoking continuity yields

$$C_1 = 0;\ C_2 = \frac{M_0}{EI};\ C_3 = -\frac{4M_0\lambda^3}{k};\ C_4 = \frac{2M_0\lambda^2}{k} \tag{10}$$

Substituting the constants from equation (10) into equation (9) provides the deflection of the top face sheet in the interval $(-a, 0)$ as

$$w(x) = M_0\left[\frac{x^2}{2EI} - \frac{4\lambda^3 x}{k} + \frac{2\lambda^2}{k}\right];\quad -a \le x \le 0 \tag{11}$$

Therefore, the deflection, $w(x)$ and rotation, $\theta(x)$ of the moment-loaded beam are given by

$$w(x) = M_0\begin{cases} \frac{x^2}{2EI} - \frac{4\lambda^3 x}{k} + \frac{2\lambda^2}{k} & (-a \le x \le 0) \\ \frac{2\lambda^2}{k}[f_1(\lambda x) - f_2(\lambda x)] & (0 \le x \le \infty) \end{cases} \tag{12}$$

$$\theta(x) = \frac{dw}{dx} = M_0\begin{cases} \frac{x}{EI} - \frac{4\lambda^3}{k} & (-a \le x \le 0) \\ \frac{2\lambda^2}{k}[-f_3(\lambda x) - f_4(\lambda x)] & (0 \le x \le \infty) \end{cases} \tag{13}$$

where the functions f_1, f_2, f_3 and f_4 are provided in equation (5) and the parameter λ is defined in equation (3). The compliance of the moment-loaded SCB specimen can be defined as the edge rotation divided by the applied moment, that is

$$C = \frac{|\theta(-a)|}{M_0} \tag{14a}$$

Equation (12) gives

$$C = \frac{a}{EI} + \frac{4\lambda^3}{k} \tag{14b}$$

Now, the energy release rate is of the form

$$G = \frac{M^2}{2b}\frac{dC}{da} \tag{15}$$

where C is given in equation (14b). Upon substitution, the energy release rate of the moment-loaded SCB specimen becomes

$$G = \frac{M_o^2}{2bEI} \tag{16}$$

Equation (16) shows that the energy release rate for the moment-loaded SCB specimen is independent of the crack length and foundation modulus, k. It should be noted that the deflection and rotation of beam with a built-in end at $x=0$, can be recovered from equations (12) and (13) by letting $k \to \infty$. For this case

$$\begin{aligned} w(-a) &= M_0a^2/2EI \\ \theta(-a) &= -M_0/2EI \end{aligned} \tag{17}$$

The definition of elastic foundation modulus, k (see equation (1)), is not straight-forward. Kanninen[18] considered a symmetric homogenous isotropic DCB specimen of total thickness, h, and assumed that each half of the specimen will deform and act as a foundation. Li and Carlsson[21] proposed an expression for the

foundation modulus of a SCB sandwich specimen by assuming the full height of the core acts as a foundation. Avilés and Carlsson[3] analysed an un-symmetric DCB sandwich specimen loaded with two forces and assumed that half of the core height acts as a foundation. Quispitupa et al.[24] proposed a foundation modulus for a MMB sandwich specimen where a region of the core equal to ½ of the height of the upper face layer acts as a foundation. The various foundation modulus expressions, k, are listed in Table 1. Note that, in the foundation modulus expression by Kanninen,[18] E is the Young's modulus of the isotropic beam material. For all cases, b is the width of the specimen.

FEA of SCB sandwich specimens

In this section, we will present a detailed numerical FEA of both moment- and force-loaded SCB specimens. The force-loaded SCB specimen, Figure 2(b), has been examined by several researchers.[5,15,16,21] A brief overview of the governing equations for deflection, compliance and energy-release rate is provided in Appendix 1. In addition, the mode-mixity phase angle is determined from FEA. The results from the FEA will be compared with corresponding results from the foundation model. A symmetrical sandwich with aluminium face sheets ($E_f = 68.9$ GPa, $h_f = 6.35$ mm) and a PVC H100 foam core ($E_c = 130$ MPa, $h_c = 25.4$ mm) is considered. Total length of specimen is, $L = 305$ mm and the crack length was varied in the range: $a = 1$–50 mm. This range of crack lengths should not lead to end effects in the 305 mm long specimen.

Table 1. Elastic foundation modulus, k, proposed in various studies.

Elastic foundation modulus	
Kanninen[18]	$k = \frac{Eb}{h/2}$
Li and Carlsson[21]	$k = \frac{E_c b}{h_c}$
Avilés and Carlsson[3]	$k = \frac{E_c b}{h_c/2}$
Quispitupa et al.[24]	$k = \frac{E_c b}{h_f/2}$

The 2D plane stress finite element model of the SCB specimen is constructed in ANSYS®[25] with four-node parabolic elements at the crack tip region with a minimum edge length of 2 μm. Eight-node parabolic elements were also used in rest of the model but with varying sizes. Figure 5 shows the finite-element model with a detailed view of the highly refined mesh near the crack tip. The energy release rate and mode-mixity phase angle are obtained from a method called crack surface displacement extrapolation (CSDE) method[26] implemented in the FEA. A brief description of CSDE method is provided in Appendix 2. Mode-mixity is expressed in terms of phase angle (ψ) which is roughly the ratio between sliding shear and normal opening displacements of the crack flanks. A 'reduced' formulation of phase angle (ψ) is used here so that mode-mixity can be defined similar to that for homogenous materials.[27] This formulation circumvents the oscillation of displacements in the near tip region.

Moment-loaded SCB results

A moment $M_0 = 1$ N·mm/mm is applied to edge of the upper face sheet of the SCB specimen (with $P = 0$, see Figure 5). The moment was applied to a master node at the left edge of the face sheet. Displacement (δ) and rotation (θ) (Figure 4) are recorded for the range of crack lengths considered.

The numerically and analytically obtained end displacement and rotation are shown vs. crack length in Figure 6. Results are shown for the various foundation modulus estimates listed in Table 1. It is noted that the displacement increases with increasing crack length and reduced foundation modulus. The rotation (Figure 6(b)) varies linearly with crack length.

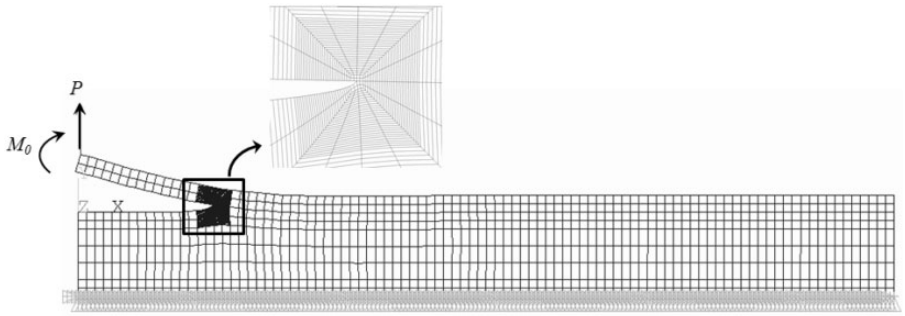

Figure 5. Finite Element (FE) model of a single cantilever beam sandwich specimen end-loaded with force, P or moment, M. Smallest element edge length = 2 μm.

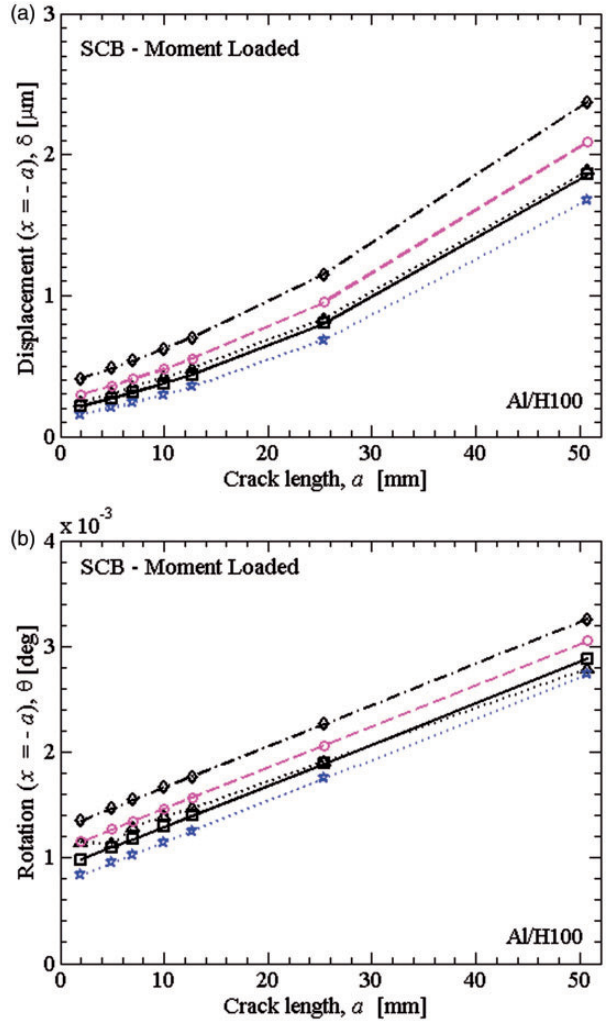

Figure 6. Deflection (a) and rotation (b) at the edge of the upper face layer ($x = -a$) of moment-loaded single cantilever beam specimen (Al/H100) ($M_0 = 1$ N). FEA $k = E_c b/(h_c/2)$ $k = E_c b/(h_f/2)$ $k = E_c b/h_c$ $k = E_c b/(h_c/4)$ (equation (18)).

A foundation modulus expression proposed here, provides a close match with the FEA results.

$$k = \frac{E_c b}{h_c/4} \tag{18}$$

Note that this expression corresponds to ¼ of the core thickness being active as a foundation.

A plot of energy-release rate G, normalized by $E_f h_f^3$ against crack length is provided in Figure 7. G determined from FEA is relatively unaffected by crack length, which is consistent with the analytical foundation model expression for G (equation (16)). The results are in very good agreement. A difference of 3% is observed between the FEA and analytical expression for all the range of crack lengths considered here.

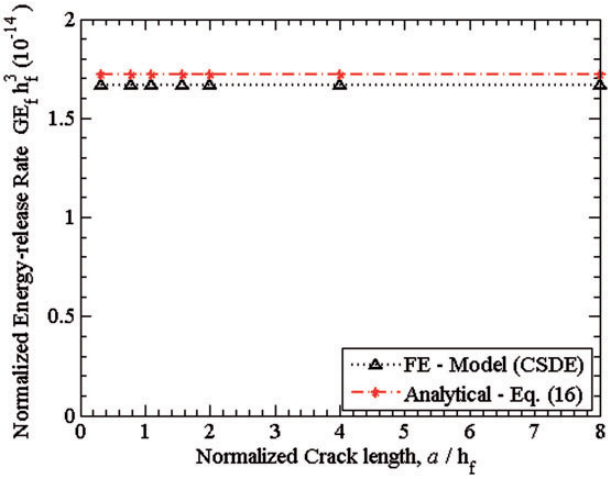

Figure 7. Energy-release rate (normalized) versus crack length for moment-loaded Al/H100 single cantilever beam sandwich specimen calculated from finite element analysis and analytical expression (equation (16)).

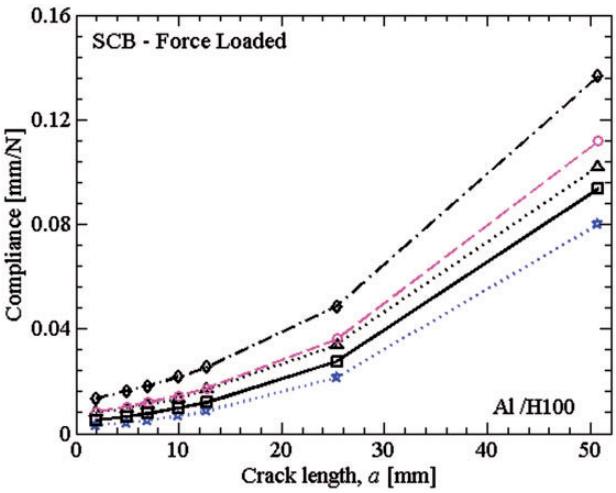

Figure 8. Compliance versus crack length for force-loaded Al/H100 single cantilever beam sandwich specimen ($h_f = 6.35$ mm, $h_c = 25.4$ mm), $P = 1$ N/mm. finite element analysis $k = E_c b/(h_c/2)$ $k = E_c b/(h_f/2)$ $k = E_c b/h_c$ $k = E_c b/(h_c/4)$ (equation (18)).

Force-loaded SCB results

For the force loading, a single unit force ($P = 1$ N) was applied to the edge of the upper face layer in the SCB sandwich specimen, Figure 5 ($M_0 = 0$). The compliance, C, is defined as the displacement, δ, of the load application point divided by the applied force, P. The analytical compliance is obtained from equation (25).

Figure 8 shows a plot of compliance versus crack length for a force-loaded SCB sandwich specimen determined from FEA and the foundation model,

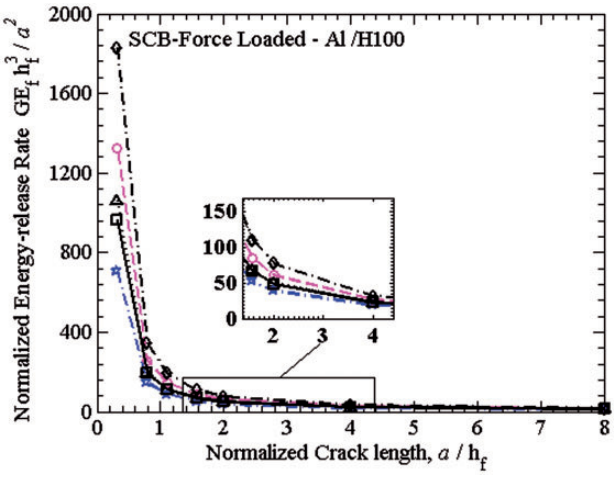

Figure 9. Energy-release rate (normalized) versus crack length for force-loaded Al/H100 single cantilever beam sandwich specimen calculated from finite element analysis (FEA) and foundation model. ··· FEA — $k = E_c b/(h_c/2)$ ··· $k = E_c b/(h_f/2)$ — $k = E_c b/h_c$ $k = E_c b/(h_c/4)$ (equation (18)).

equation (26) with the various foundation modulus expressions listed in Table 1. The compliance increases with increasing crack length and decreasing foundation modulus. The newly proposed foundation modulus expression, equation (18), provides a compliance that closely agrees with the numerically obtained results.

A plot of G normalized by $E_f h_f^3/a^2$ versus crack length is provided in Figure 9. G was also calculated based on equation (27b) for the various foundation modulus expressions provided in Table 1. It is noted that G normalized in this manner increases sharply for short crack lengths. This trend is similar to what was observed by Li et al.[8] for their single shear force case. It can be noted that G computed using the proposed foundation modulus expression (equation (18)) closely agrees with the numerically obtained G.

Crack tip root rotation

There exist several methods in the literature to estimate root rotation in a bi-material interface. Sun and Pandey[28,29] estimated root rotation based on an approximate analytical method. Wang and Qiao[30] determined root rotation from a closed form displacement solution, obtained for two beams by utilizing a modified first-order shear deformable plate theory. Andrews and Massabò[11] obtained root rotation for an orthotropic beam using the finite element method. In the work presented by Andrews and Massabo[11], the analysis of near tip deformation characteristics was extended to orthotropic bi-material interface using a first order shear deformation theory. Li et al.[8] proposed a dimensionless expression for the crack root rotation as a function of axial force, shear force and bending moment as well as elastic constants and geometry of the face sheet which is followed here applied to both force- and moment-loaded SCB sandwich specimens.

As discussed earlier, a section just behind the crack tip initially normal to the centroidal axis of the face sheet will rotate upon loading of the face sheet by application of shear force, V and moment, M, see Figure 1. The root rotation is defined by

$$\phi = \frac{\partial u_x}{\partial z} \tag{19}$$

where u_x is the x-component of the displacement of the initially straight normal to the cross section. Based on the foundation analysis here, the kinematics of the upper face sheet is assumed to follow Euler–Bernoulli beam theory, and the rotation angle is found by differentiating the equation for the deflection to obtain the slope, dw/dx at $x = 0$. For the moment-loaded SCB specimen, the crack root rotation angle is directly obtained from equation (13) as

$$\phi_{Moment} = -\frac{4M_0\lambda^3}{k} \tag{20}$$

For the force-loaded SCB specimen, equation (24) yields

$$\phi_{Force} = \frac{-2\lambda^2}{k} P(1 + 2a\lambda) \tag{21}$$

By considering a crack that is long enough to avoid the boundary effects, Li et al.[8] suggest that the root rotation angle can be expressed as

$$\phi_A = c_M \frac{M}{\bar{E}_f h_f^2} + c_N \frac{N}{\bar{E}_f h_f} + c_V \frac{V}{\bar{E}_f h_f} \tag{22}$$

where the coefficients c_M, c_P and c_V depend on the face and core stiffnesses. M is the moment, N the axial load and V, the shear force in the upper face (all per unit width) at the crack tip, where E_f and ν_f are Young's modulus and Poisson's ratio of face sheet. For plane strain condition, $\bar{E}_f = E_f/(1 - \nu_f^2)$ and for plane stress condition, $\bar{E}_f = E_f$.

Figure 10 shows the root rotation angle (ϕ) versus foundation modulus, k, for the moment-loaded SCB specimen determined from equation (20) at a crack length, $a = 2$ mm, and the angle determined by FEA. The rotation angle is quite sensitive to the foundation modulus, k. The foundation modulus expression (equation (18)), (see vertical dotted line), provides close

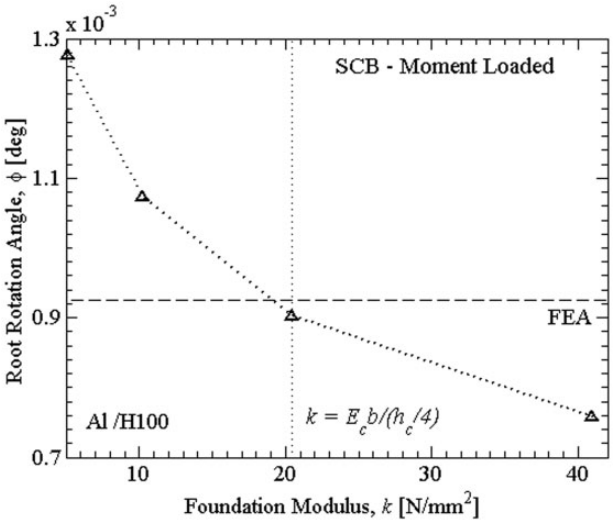

Figure 10. Crack root rotation angle (ϕ) versus foundation modulus, k of a moment-loaded single cantilever beam specimen, $M_0 = 1$ N.

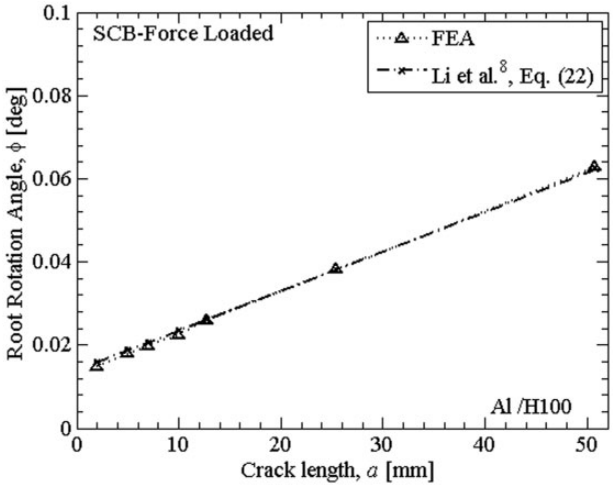

Figure 11. Crack root rotation angle (ϕ) for force-loaded single cantilever beam sandwich specimen ($P = 1$ N/mm).

agreement with ϕ obtained from FEA as marked by the horizontal dotted line the plot.

For force loading, $V = P$, $M = Pa$ and $N = 0$. A load, $P = 1$ N/mm was applied. Root rotation angles calculated for two crack lengths, $a = 12.7$ and 25.4 mm, were used to determine the coefficients c_M and c_V from equation (22): $c_V = 6.093 \times 10^3$ and $c_M = 2.637 \times 10^3$. The coefficients are then used to compute rotation angle for full range of crack lengths using equation (22). Results are presented in Figure 11. The FEA results agree very well with ϕ_A obtained from equation (22) with c_M and c_V values above, lending confidence to the Li et al.[8] formulation. Further examination of the force-loaded SCB specimens reveals that shear dominates the crack root rotation for crack lengths less than about 15 mm. To further examine the generality, equations (18) and (22) would require analysis of SCB specimens with a wide range of face and core materials and face thicknesses.

Now, for the moment-loaded SCB specimen, equation (22) reduces to

$$\phi_A = c_M \frac{M_0}{\bar{E}_f h_f^2} \tag{23}$$

It should be noted that for a moment-loaded SCB specimen, ϕ does not depend on crack length. The coefficient c_M was obtained previously from analysis of the force-loaded Al/H100 SCB specimen as $c_M = 2640$. Substituting the value of c_M into equation (23) gives the root rotation angle for an Al/H100 DCB specimen subject to a moment, $M_0 = 1$ N as: $\phi = 0.000952^\circ$. The root rotation is also obtained from FEA for $M_0 = 1$ N, which gives $\phi = 0.00093^\circ$.

Influence of shear on phase angle (ψ)

The energy-release rate and the complex stress intensity factor for a general bi-material interface was first introduced by Suo and Hutchinson,[31] under the ambit of linear elastic fracture mechanics (LEFM). The expressions for mode-mixity and energy-release rate provided in Suo and Hutchinson[31] assume that shear forces are absent. However, the presence of shear force at the crack tip introduces an additional component to the energy-release rate, which in-turn is affected by the crack tip deformation characteristics.[8,11,30,32,33] Li et al.[8] introduced shear into the energy-release rate and stress intensity factors expressions for isotropic bi-material interfaces, which was later extended by Andrews and Massabò[11] to orthotropic interfaces.

The force-loaded SCB sandwich specimen includes a shear force at the crack tip, in addition to the bending moment. For reliable fracture toughness assessment, the transverse shear component must be incorporated to the energy release rate calculation. However, closed form expressions for both energy release rate and the mode-mixity have not yet been derived for a SCB sandwich specimen. In this section, the influence of transverse shear in a SCB specimen is investigated using the numerical mode-mixity method, CSDE. The crack tip mode-mixity expressed as phase angle, ψ, is estimated using the FEA in conjunction with the CSDE method,[26,27] which is presented briefly in Appendix 2.

The force-loaded Al/H100 SCB specimen ($h_f = 6.35$ mm, $h_c = 25.4$ mm) subject to a load, $P = 1$ N/mm is analyzed using FEA for over a range of crack lengths from 2 to 50 mm. A plot of phase angle (ψ) against normalized crack length (a/h_f) is shown in Figure 12. It is observed that ψ increases

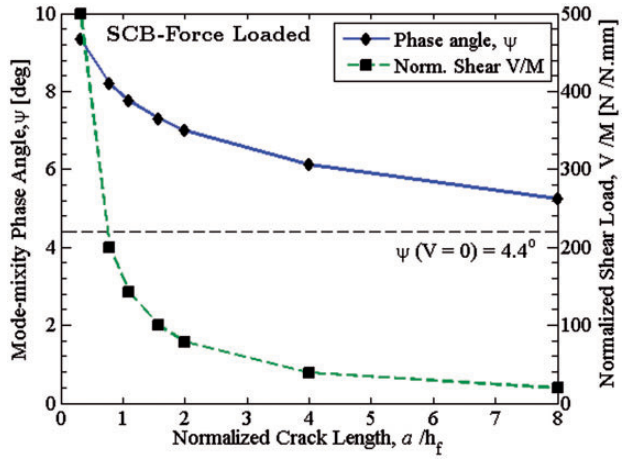

Figure 12. Mode-mixity phase angle (ψ) and normalized shear force versus crack length for force-loaded single cantilever beam (Al/H100) specimen.

when the crack gets shorter, which is attributed to increased dominance of shear loading at short crack length. The results qualitatively agree with the results from Li et al.[8] although they analyzed different material combinations. Note that, the phase angle for a pure moment loading ($V=0$) is $\psi=4.4^{\circ}$. A plot of the normalized shear load, V/M versus crack length is also included in Figure 12. The phase angle versus crack length follows a similar trend as that of the normalized shear load. The phase angle for a moment-loaded SCB specimen seems consistent with the trend of ψ as $V/M \rightarrow 0$.

Conclusions

Analysis of the SCB sandwich specimen under moment and force loading conditions was presented. The analysis of the moment-loaded SCB specimen was conducted using a Winkler beam on elastic foundation approach. The compliance and energy release rate results for both sandwich specimens obtained from foundation model analysis were compared to detailed finite element results. A foundation modulus where ¼ of the core thickness utilized as a foundation was seen to agree well with numerically obtained results for both force- and moment-loaded SCB specimens. A closed form expression for crack root rotation was calibrated using FEA results and produced consistent results for both types of loading of the SCB specimen. For the force-loaded SCB specimen at short crack lengths, the increased dominance of the shear component was reflected on increased energy release rate and mode-mixity phase angle. For the moment-loaded SCB specimen, the energy release rate is independent of both crack length and foundation modulus, in contrast to the force-loaded SCB specimen. Deformation characteristics at the crack front was accurately estimated using beam on elastic foundation model for both the force- and moment-loaded SCB configurations. Therefore, the current analysis aids in understanding compliance, energy-release rate and mode-mixity of moment-loaded fracture test specimens such as the DCB-UBM specimen.

Acknowledgements

The NIA program manager, Dr Ronald Krueger, the EASA program manager, Dr Simon Waite and the ONR program manager, Dr Yapa Rajapakse showed keen interest in this project and are gracefully acknowledged.

Declaration of Conflicting Interests

The author(s) declared no potential conflicts of interest with respect to the research, authorship, and/or publication of this article.

Funding

The author(s) disclosed receipt of the following financial support for the research, authorship, and/or publication of this article: The financial support from the Danish Centre for Composite Structures and Materials (DCCSM) (grant: 09-067212) is gratefully acknowledged. Furthermore, the support from Oticon Foundation (grant: 16-2166) to the first author for visiting Florida Atlantic University is gratefully acknowledged. The second and third author's research has been supported by NIA, EASA, and ONR.

References

1. Østergaard RC and Sørensen BF. Interface crack in sandwich specimen. *Int J Fract* 2007; 143: 301–316.
2. Kardomateas GA, Berggreen C and Carlsson LA. Energy-release rate and mode mixity of face/core debonds in sandwich beams. *AIAA J* 2013; 51: 885–892.
3. Avilés F and Carlsson LA. Analysis of the sandwich DCB specimen for debond characterization. *Eng Fract Mech* 2008; 75: 153–168.
4. Carlsson LA and Gillespie JW Jr. Mode-II interlaminar fracture of composites. *Elsevier Sci Publ Appl Fract Mech Compos Mater* 1989; 6: 113–157.
5. Li X and Carlsson LA. The tilted sandwich debond (TSD) specimen for face/core interface fracture characterization. *J Sandw Struct Mater* 1999; 1: 60–75.
6. Quispitupa A, Berggreen C and Carlsson LA. Design analysis of the mixed mode bending sandwich specimen. *J Sandw Struct Mater* 2010; 12: 253–272.
7. Lu TJ, Xia ZC and Hutchinson JW. Delamination of beams under transverse shear and bending. *Mater Sci Eng A* 1994; 188: 103–112.
8. Li S, Wang J and Thouless MD. The effects of shear on delamination in layered materials. *J Mech Phys Solids* 2004; 52: 193–214.
9. Timoshenko S and Goodier JN. *Theory of elasticity*. New York: McGraw-Hill, 1970.

10. Barber JR. *Intermediate mechanics of materials*. Dordrecht, the Netherlands: Springer, 2011.
11. Andrews MG and Massabò R. The effects of shear and near tip deformations on energy release rate and mode mixity of edge-cracked orthotropic layers. *Eng Fract Mech* 2007; 74: 2700–2720.
12. Sørensen BF, Jørgensen K, Jacobsen TK, et al. DCB-specimen loaded with uneven bending moments. *Int J Fract* 2006; 141: 163–176.
13. Lundsgaard-Larsen C, Sørensen BF, Berggreen C, et al. A modified DCB sandwich specimen for measuring mixed-mode cohesive laws. *Eng Fract Mech* 2008; 75: 2514–2530.
14. Cantwell WJ and Davies P. A test technique for assessing core-skin adhesion in composite sandwich structures. *J Mater Sci Lett* 1994; 13: 203–205.
15. Ratcliffe JG and Reeder JR. Sizing a single cantilever beam specimen for characterizing facesheet-core debonding in sandwich structure. *J Compos Mater* 2011; 45: 2669–2684.
16. Rinker M, Ratcliffe JG, Adams DO, et al. *Characterizing face sheet/core disbonding in honeycomb core sandwich structure*. NASA Technical Publication TP-2013-21. Available at: https://ntrs.nasa.gov/search.jsp?R = 20130010408.
17. Ratcliffe J and Krueger R. Face sheet/core disbonding in sandwich composite components: a road map to standardization: test method development. In: *11th international conference on sandwich structures*, Dania Beach, FL, 20–22 May, 2016.
18. Kanninen MF. An augmented double cantilever beam model for studying crack propagation and arrest. *Int J Fract* 9: 83–92.
19. Frostig Y, Baruch M, Vilnay O, et al. High-order theory for sandwich-beam behavior with transversely flexible core. *J Eng Mech* 1992; 118: 1026–1043.
20. Phan CN, Frostig Y and Kardomateas GA. Analysis of sandwich beams with a compliant core and with in-plane rigidity – extended high-order sandwich panel theory versus elasticity. *J Appl Mech* 2012; 79: 41001.
21. Li X and Carlsson LA. Elastic foundation analysis of tilted sandwich debond (TSD) specimen. *J Sandw Struct Mater* 2000; 2: 3–32.
22. Weissman-Berman D, Petrie GL and Wang M. Flexural response of foam-cored FRP sandwich panels. *Soc Nav Archit Mar Eng* 1988; 96.
23. Massabò R and Cavicchi A. Interaction effects of multiple damage mechanisms in composite sandwich beams subject to time dependent loading. *Int J Solids Struct* 2012; 49: 720–738.
24. Quispitupa A, Berggreen C and Carlsson LA. On the analysis of a mixed mode bending sandwich specimen for debond fracture characterization. *Eng Fract Mech* 2009; 76: 594–613.
25. *ANSYS® Mechanical user's guide*, ANSYS, Inc., Southpointe, PA, 2015.
26. Berggreen C, Simonsen BC and Borum KK. Experimental and numerical study of interface crack propagation in foam-cored sandwich beams. *J Compos Mater* 2006; 41: 493–520.
27. Hutchinson JW and Suo Z. Mixed mode cracking in layered materials. *Adv Appl Mech* 1991; 29: 63–191.
28. Sun CT and Pandey RK. Improved method for calculating strain energy release rate based on beam theory. *AIAA J* 1994; 32: 184–189.
29. Pandey RK and Sun CT. Calculating strain energy release rate in cracked orthotropic beams. *J Thermoplast Compos Mater* 1996; 9: 381–395.
30. Wang J and Qiao P. Interface crack between two shear deformable elastic layers. *J Mech Phys Solids* 2004; 52: 891–905.
31. Suo Z and Hutchinson JW. Interface crack between two elastic layers. *Int J Fract* 1990; 43: 1–18.
32. Nilsson K-F, Asp LE, Alpman JE, et al. Delamination buckling and growth for delaminations at different depths in a slender composite panel. *Int J Solids Struct* 2001; 38: 3039–3071.
33. Bruno D and Greco F. Mixed mode delamination in plates: a refined approach. *Int J Solids Struct* 2001; 38: 9149–9177.
34. Anderson TL. *Fracture mechanics: fundamentals and applications*, 3rd ed. Boca Raton: CRC Press, 2005.
35. He MY and Hutchinson JW. Kinking of a crack out of an interface. *J Appl Mech* 1989; 56: 270–278.

Appendix 1

Foundation analysis of force-loaded SCB sandwich specimen

Foundation analysis of the force-loaded SCB sandwich specimen, Figure 13, has been presented by Li and Carlsson.[21] They extended the Kanninen[18] beam on elastic foundation model for a homogenous DCB specimen to sandwich specimens with a single transverse force applied to the upper face sheet. The elastic foundation analysis[21] of the single force-loaded SCB sandwich specimen will be briefly reviewed here.

Figure 13 shows the foundation model and coordinate system for the force-loaded SCB sandwich

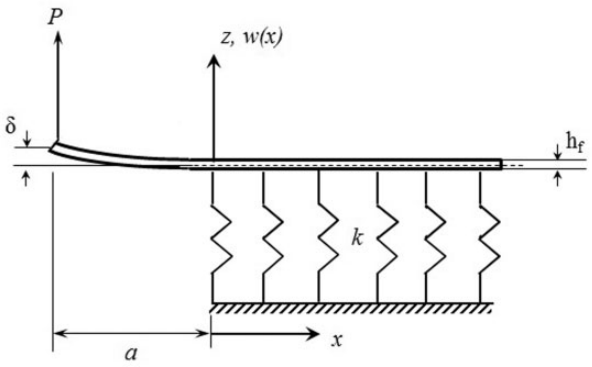

Figure 13. Foundation model of force-loaded single cantilever beam sandwich specimen.

specimen. For simplicity, the analysis will assume that the end effects can be ignored, that is, it applies to specimens where the un-cracked length is sufficiently long.

The displacement solution for the top face sheet is obtained using the governing equation for the beam supported by a Winkler foundation[10] (see Figure 13). Deflection of the face sheet for a force-loaded SCB sandwich specimen is of the form

$$w(x)=\frac{2P\lambda}{k}\begin{cases}\dfrac{\lambda^3x^3}{3}+a\lambda^3x^2-2a\lambda^2x-\lambda(x-a)+1\\ a\lambda\sin(\lambda x)\sinh(\lambda x)\\ \quad -a\lambda\sin(\lambda x)cosh(\lambda x)\\ \quad +(a\lambda+1)cos(\lambda x)cosh(\lambda x)\\ \quad -(a\lambda+1)cos(\lambda x)sinh(\lambda x)\end{cases} \tag{24}$$

where, k is the foundation modulus, see equation (3). Impetus is made here to mention that the analysis is carried out using Euler–Bernoulli beam theory. Hence, deformation of the beam due to transverse shear is neglected. The bending compliance, C of the force-loaded SCB sandwich specimen is given by

$$C=\frac{\delta(x=-a)}{P}=\frac{4\lambda}{k}\left[\frac{\lambda^3a^3}{3}+\lambda^2a^2+\lambda a+\frac{1}{2}\right] \tag{25}$$

The energy release rate is given by Anderson[34]

$$G=\frac{2P^2\lambda^2}{bk}\left[\lambda^2a^2+2\lambda a+1\right] \tag{26}$$

For a sandwich specimen with infinitely stiff core ($k\to\infty$), the compliance and energy-release rate become

$$w(-a)=\frac{Pa^3}{3E_fI} \tag{27a}$$

$$G=\frac{P^2a^2}{2bE_fI} \tag{27b}$$

Appendix 2

Numerical mode-mixity method: CSDE

CSDE method is a numerical mode-mixity method which utilizes a zone near the crack tip. The mode-mixity expressed as phase angle (ψ) is a measure of the relative amount of shear and opening at the crack tip[26]

$$\psi=\tan^{-1}\left(\frac{\delta_x}{\delta_y}\right)-\varepsilon\ln\left(\frac{x}{h}\right)+\tan^{-1}(2\varepsilon) \tag{28}$$

where δ_x and δ_y are sliding and opening displacements, respectively. The parameter, ε is the oscillatory index defined by Hutchinson and Suo[27] as:

$$\varepsilon=\frac{1}{2\pi}\ln\left(\frac{1-\beta}{1+\beta}\right) \tag{29}$$

β is a bimaterial interface parameter given by Hutchinson and Suo[27]:

$$\beta=\frac{G_1(\kappa_2-1)-G_2(\kappa_1-1)}{G_1(\kappa_2+1)+G_2(\kappa_1+1)} \tag{30}$$

where G_m is the shear modulus, $m=1$ for the face and, $m=2$ for the core, $\kappa_m=3-4\nu_m$ for plane strain and $\kappa_m=(3-4\nu_m)/(1+\nu_m)$ for plane stress. ν_m is Poisson's ratio.

Non-zero ε and β imply that stresses and displacements in the near tip region oscillate leading to interpenetration of crack faces which is physically impossible. This phenomenon may be downplayed by assuming $\beta=0$.[35] This approach with $\varepsilon=\beta=0$ is denoted as 'reduced formulation'. The phase angle (ψ) becomes

$$\psi=\tan^{-1}\left(\frac{\delta_x}{\delta_y}\right) \tag{31}$$

The energy release rate can be computed from the crack flank displacement

$$G=\frac{\pi(\delta_x^2+\delta_y^2)}{2x(c_1+c_2)} \tag{32}$$

where x is the distance from the crack tip and the stiffness parameters, c_1 and c_2 are given by

$$c_m=\frac{\kappa_m+1}{G_m} \tag{33}$$

where G_m is the shear modulus ($m=1$ and 2 for face and core). The CSDE method is implemented as a subroutine in ANSYS®.[25]

Publication P3

C. Berggreen, **V. Saseendran**, and L. A. Carlsson

A Modified DCB-UBM Test Method for Interfacial Fracture Toughness Characterization of Sandwich Composites

Engineering Fracture Mechanics, 2018

Accepted: 25 June 2018
Available online: 31 July 2018
DOI: https://doi.org/10.1016/j.engfracmech.2018.06.036

A Modified DCB-UBM Test Method for Interfacial Fracture Toughness Characterization of Sandwich Composites

Christian Berggreen [a,*], Vishnu Saseendran [a], Leif. A. Carlsson [b]

[a] *Department of Mechanical Engineering, Technical University of Denmark, Nils Koppels Allé, Building 404, Kgs. Lyngby, 2800, Denmark*
[b] *Department of Ocean & Mechanical Engineering, Florida Atlantic University, 777 Glades Road, Boca Raton, FL 33431, USA*

Abstract

A novel double cantilever beam test method for interface fracture toughness characterization of debonded sandwich composites is introduced. The method is called DCB-UBM (Double Cantilever Beam loaded with Uneven Bending Moments), where pure moments are applied to the beams at the crack end using torsional actuators, to generate crack propagation along the face/core interface. A data reduction method is proposed to determine the fracture toughness. Fracture testing is performed on a typical marine grade sandwich configuration consisting of PVC H45 foam core and glass fiber face sheets to demonstrate the applicability of the test method. The obtained fracture toughness agrees with interface toughness values in the literature measured using other test methods with the same material system. The effective kinematics of the test rig is measured using Digital Image Correlation (DIC) by studying the rotations and moments of a specially designed calibration specimen and comparing the results against finite element results. The DCB-UBM specimen and test method is a promising candidate for obtaining face/core interface fracture toughnesses in sandwich composites.

Keywords: DCB-UBM; sandwich composite; mode-mixity; CSDE; face/core interface

Nomenclature

a	crack length
b	width of the DCB-UBM specimen
(*EI*)	flexural rigidity of beam
E_{11}	elastic modulus in fiber direction
E_{22}	elastic modulus in transverse direction
E_c	elastic modulus of core
E_s	elastic modulus of steel doubler layer

Corresponding author.
E-mail address: cbe@mek.dtu.dk (C. Berggreen).

G_{12} shear modulus of face sheet

G_c shear modulus of core

G_s shear modulus of steel doubler layer

h_c core thickness

h_f face sheet thickness

h_s doubler layer thickness

L length of the specimen

L_b length of clamped region

M_1 moment applied to beam#1

M_2 moment applied to beam #2

MR moment ratio

G energy release rate

G_{1c} mode I fracture toughness

ψ mode-mixity phase angle

δ crack opening displacement

Λ dimensionless constant

v Poisson's ratio

δ_x relative sliding displacement of crack flanks

δ_y relative sliding displacement of crack flanks

ε oscillatory index

β Dundur's bi-material parameter

κ Muskhelishwili's constant

1. Introduction

Face/core interface adhesion in sandwich structures is important in order to ensure structural integrity. Face and core separation (a disbond/debond) can occur due to inherent manufacturing defects such as "dry regions" formed by inadequate resin impregnation. Disbonding may also occur during in-service conditions due to impact and various other overloading scenarios, where the interface bond is fully or partially lost. The growth of disbonds, which is governed by the face/core interface toughness, invariably reduces and compromises the stiffness and load carrying capacity of the sandwich structure.

A typical sandwich structure consists of highly dissimilar face and core materials. If a face/core interface crack is present in a loaded sandwich structure, normal and shear stresses will develop. The fracture toughness of such an interface crack depends on the mode-mixity which may be expressed as a phase angle, ψ [1], determined by the ratio of relative sliding and normal displacements of the crack flanks just behind the crack tip. Currently several test specimens exist that are capable of static fracture characterization of sandwich face/core interfaces based on linear elastic fracture mechanics (LEFM). Specimens such as the cracked sandwich beam (CSB) [2], single cantilever beam (SCB) [3], three-point sandwich specimen (TPSB) [4], double cantilever sandwich beam (DCB) [5], tilted sandwich debond specimen (TSD) [6] have been used in several experimental studies. The cracked sandwich beam specimen was modified by Smith et al. [7] and the tilted sandwich beam was later modified by Berggreen et al. [8,9].

Fracture characterization for a particular sandwich system requires testing over a range of mode-mixities. Some test methods have the capability to test specimens in a limited range of mode-mixities. However, the mode-mixity often changes when the crack grows. It is therefore desired to perform fracture characterization under a constant mode-mixity, expressed using the phase angle, ψ. The fracture specimen must be designed such that the loads and boundary conditions cause crack growth at a constant mode-mixity. The mixed mode bending (MMB) test [10,11] originally developed for delamination characterization of monolithic composites is an ASTM standard [11], was later modified and extended to sandwich composites [12,13]. However, mixed mode fracture toughness characterization is only possible over a limited range of mode mixity phase angles.

The double cantilever beam specimen loaded with bending moments (DCB-UBM) was first proposed by Sørensen et al. [14], to determine mixed mode delamination toughness of monolithic composites. This test methodology was later applied to sandwich composites by Lundsgaard-Larsen et al.[15] . Pure moments are applied to the end of each delaminated/debonded beam in this specimen (Fig. 1). The original DCB-UBM rig [14] however, is loaded by wires and requires a tall test frame. It has several limitations, such as the inability to perform fracture testing with cyclic loading conditions at a reasonable and practical frequency. Moreover, the original test rig allows only a limited range of phase angles.

The primary goal of this paper is to present a novel test set up which overcomes the shortcomings of previous test methods, including the original DCB-UBM test rig. The new rig applies moments to the cracked ends of the DCB specimen with the aid of two independent torsional actuators. A controller helps to maintain a constant ratio of moments throughout the test. The rig is a stand-alone, compact, high load and fatigue rated. Therefore, this rig is capable of performing fracture characterization over a wide range of mode-mixity phase angles. This paper will present the main principles of the new DCB-UBM rig followed by its construction outline and effective kinematic characterization. Then, the selection of load configuration for mixed-mode fracture testing is discussed and finally, fracture mechanical characterization of the face/core interface of a typical GFRP/H45 foam core sandwich system is performed to illustrate the robustness of the test set-up and methodology for mixed-mode fracture toughness measurement. The interface toughness (G_c) is evaluated experimentally using a proposed data reduction method which is compared against a numerical model.

2. DCB-UBM Test Rig Configuration

The test configuration and assembly of the proposed DCB-UBM specimen and test set up is described in this section. The test principle including load application and specimen support conditions as well as specimen sizing are outlined.

2.1. Test principle and design of test rig

The DCB-UBM specimen is loaded with moments M_1 and M_2 (M_1 and M_2 positive) at the cracked edge (Fig. 1), while the un-cracked end of the specimen is clamped, generating the clamping moment $M_3 = M_1 + M_2$. The objective of the DCB-UBM test principle is to propagate an existing crack and measure the fracture toughness under a certain mode-mixity condition. The mode-mixity phase angle (ψ) governed by the ratio between sliding and opening normal displacements at the crack tip, is controlled by the ratio of moments applied ($MR = M_1/M_2$) to the crack flanks. For example, mode I dominated loading is achieved by opening moments, $M_1 > 0$ and $M_2 < 0$. In order to maintain a constant mode-mixity throughout the fracture test, the two moments applied therefore have to be actively controlled so that the moment ratio (MR) is held constant throughout the test.

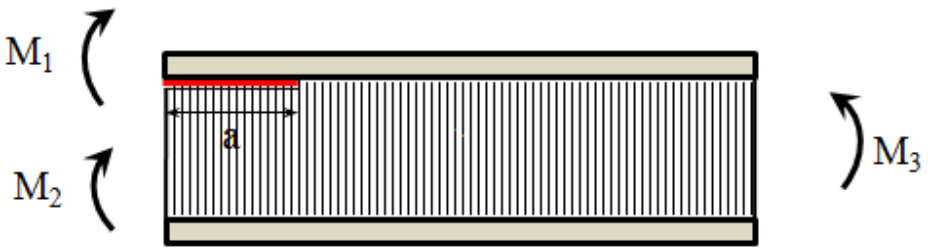

Fig. 1. Schematic illustration of moment loading of a DCB-UBM sandwich specimen.

In the proposed test rig, moments are applied directly on the specimen edges through two independent torsional actuators. The hydraulic actuators are mounted on carriage plates and are able to slide in the specimen plane, *x*-*y* (see Fig. 2). The pre-crack and post-crack propagation scenarios are also illustrated in Fig. 2. As the crack grows, the actuators slide along the *x* and *y* axes accounting for any set of moment ratios (MR) as well as large rotations. Furthermore, to accommodate a range of specimen lengths, the two actuators must be able to slide along the *y*-axis. Moment and rotation of each arm is measured during the test and a dedicated controller is used to configure the channels. A brief description of various parts and the control algorithm follow below.

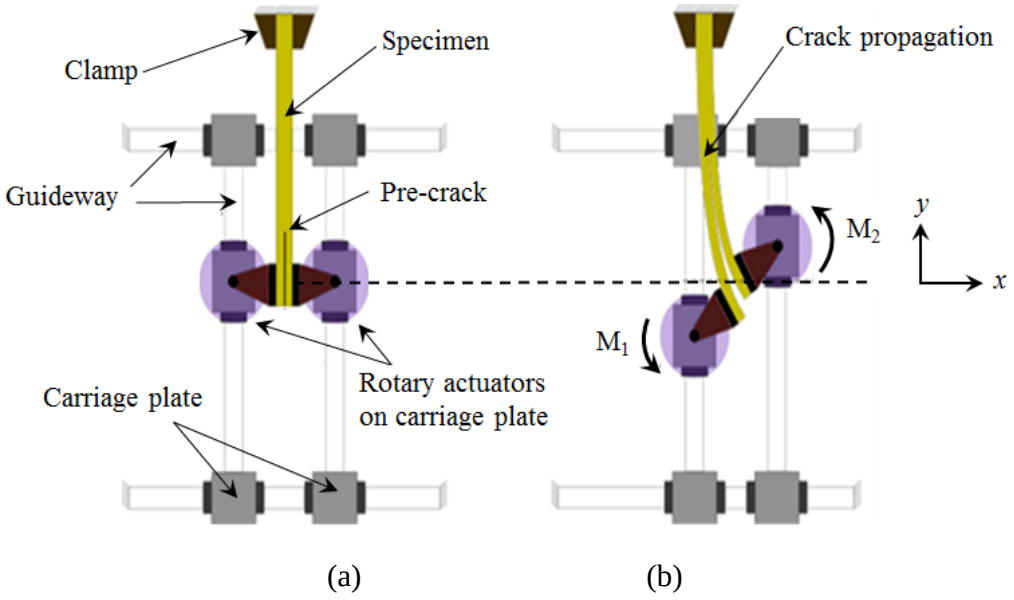

Fig. 2. Principle of the modified DCB-UBM test rig with torsional actuators mounted on rails (a) before start of a test with a pre-crack and (b) application of moments M_1 and M_2 cause crack propagation.

Torsional Actuators: The proposed test rig is capable of applying a wide array of *MR*s by the action and control of two hydraulic torsional actuators mounted on carriage plates (Fig. 2). The double vane hydraulic rotary torsional actuators (from Micromatic) are capable of producing torques up to 773 Nm. The two actuators are clamped to the specimen cracked ends.

Carriage plate and guidance system: As illustrated in Fig. 2, loading of the DCB – UBM specimen typically involves large rotations of the beams. To maintain pure moment loading, all other in-plane and out-of-plane forces must be negligible. The torsional actuators are allowed to move in the *x*-*y* plane, on carriage plates mounted on raceway shafts using track rollers, see detail in Fig. 3. The

carriage is made from anodized aluminum supported by four track rollers. Carriages run clearance-free on the guideways and track rollers are greased with gap seals on both sides to prevent dust accumulation. The inner and outer rings of the track rollers and guideway raceway shafts are made from corrosion-resistant steel. The carriage system can support a static moment of 800 Nm around the *z*-axis.

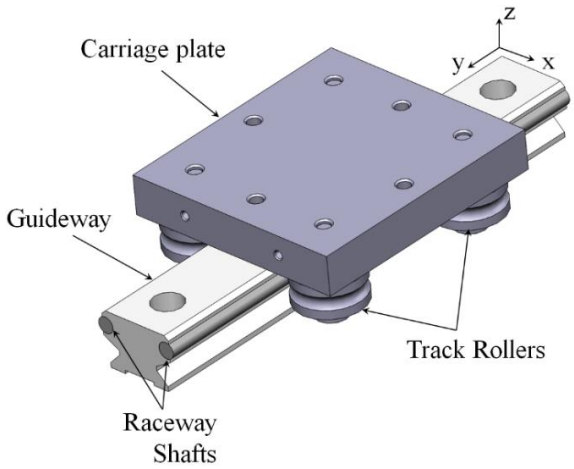

Fig. 3. Carriage plate mounted atop the track roller guidance system.

Clamp: The un-cracked end of the specimen is clamped between a set of cylindrical rollers allowing sliding only along the vertical axis (*y*) (Fig. 2) and thus preventing horizontal (*x*-axis) translation and rotation around the *z*-axis of the uncracked end of the specimen. Any restriction in the *y*-axis sliding of the specimen will lead to axial forces in the specimen which will affect the loading of the specimen and the mode-mixity at the crack tip. The rollers are made of corrosion-resistant high strength steel and facilitates low friction roller bearings. During crack growth these low friction rollers in the clamp enable sliding of the specimen. The width of the clamp can be adjusted to accommodate thicker specimens.

Torsion Load Cell and Angular Displacement Transducer: The magnitudes of the applied moments are measured using torsion load cells (TLC). TLCs are held between the load arm and the torsional actuator using a base plate, see Fig. 4a. The TLCs are capable of measuring moments up to 565 Nm. The moments applied to the two specimen arms by the actuators have a specified ratio, $MR = M_1/M_2$. The specified moment ratio is obtained by the controller through servo-valves mounted on two Hydraulic Servo Manifolds (HSM) (Fig. 4a). The HSMs also provide independent pressure and flow regulation of both actuators and minimize the effect of unexpected actuator movement; thereby

preventing potential damage to the specimens. Furthermore, a Hydraulic Power Unit (HPU) supplies a constant oil pressure of 207 bar to the HSMs.

The rotations of the beam ends are measured with Angular Displacement Transducers (ADT), attached directly below each torsional actuator (Fig. 4a). The moments and rotations of the actuators are controlled using a dual-channel MTS FlexTest® SE controller [16]. The two sets of actuators, TLCs, ADTs, HSMs, and servo valves are connected to the controller to facilitate independent control of each actuator. The carriage plates supporting the actuators are designed to withstand loads up to 250 Nm. However, an extra carriage plate with track rollers can be installed for each actuator to augment the capacity to 500 Nm.

Load arms and Steel tabs: The entire rig assembly with the specimen installed between the load arms is shown in Fig 4a. Steel tabs are glued to the face sheets at the ends of the cracked beam, see Fig. 4b. The load arms which are attached to the top of the torsional load cells, contain T-shaped groove. The specimen is slid in to the load arm clamps (see detailed view in Fig. 4c).

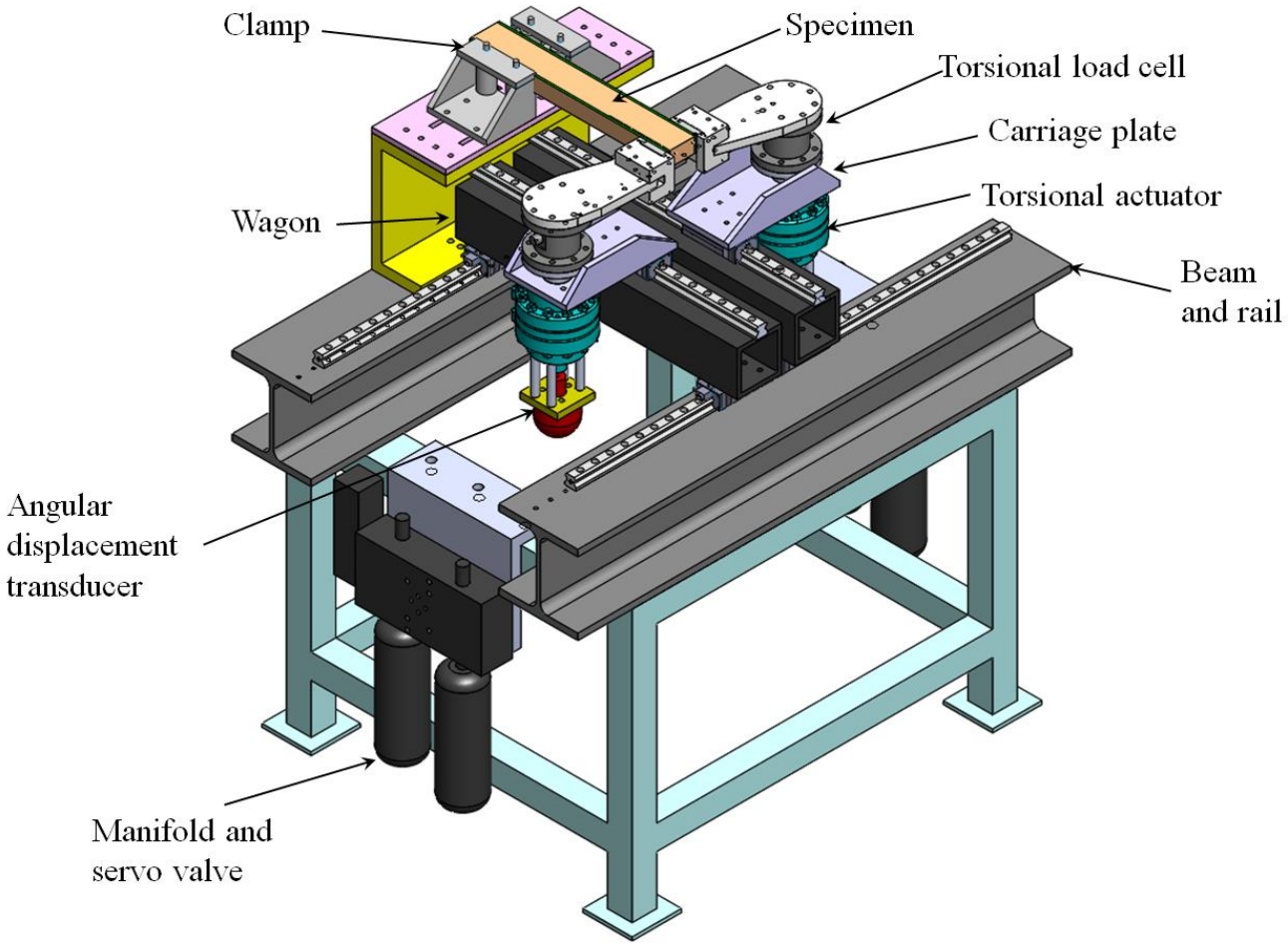

(a)

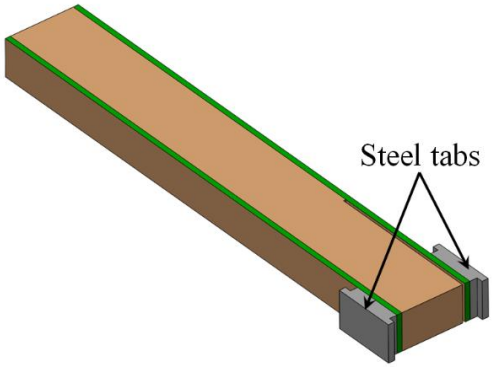

(b)

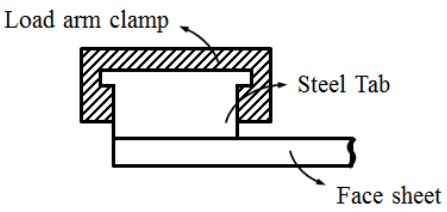

(c)

Fig. 4. a) DCB-UBM test rig, b) steel tabs attached to specimen and (c) detailed view of specimen slid in to the load arm clamp.

2.2. Control Algorithm - CASCADE

As mentioned before, the ratio of moments between the two arms (MR) governs the mode-mixity phase angle (ψ). The two torsional actuators must be controlled such that the moment ratio (MR) is held constant throughout the test by simultaneous control each actuator. Prior to start of an experiment, the moment ratio (MR) is fixed corresponding to the desired phase angle (ψ). The correlation between ψ and MR for the sandwich system under consideration can be determined numerically [17], and a detailed description of how to obtain a MR vs ψ relation for a specific DCB-UBM fracture specimen is provided in Appendix A for a Glass/PVC H45 core sandwich system.

A MTS FlexTest® SE controller along with the PID control software MTS TestSuite™ is used to configure and control the two actuators. The control algorithm is illustrated as a flowchart in Fig. 5. The test is performed in rotation angle control and the rotation angle of one of the load arms is assumed as a primary channel, referred in the flowchart as channel 1 (Arm 1). Channel 2 (Arm 2) is configured as a slave of channel 1 such that it always follows channel 1. As both channels include measurements of both torques and angles, the second channel is continuously updated to satisfy the chosen ratio between the two torque moments (MR). Such a configuration allows continuous control of the second channel throughout the test. This control loop is usually referred as CASCADE control. When the crack grows, the PID augmented control algorithm ensures that the MR is kept constant, ensuring the desired constant mode mixity phase angle (ψ) is maintained throughout the test.

It should be noted that the moment ratio, $MR = M_1/M_2$, determines the direction of rotation of the beams. As shown in Fig. 6, MR > 0 corresponds to two cases: both moments are clockwise (Fig. 6a) and the two moments are counter clock-wise (Fig. 6b). When MR < 0 the crack flanks open relative to each other (see Fig. 6c). These three cases are the possible scenarios of crack propagation and a case where the arms close relative to each other is not considered as it results in crack flank collision. Before the start of a test two inputs are required: 1) the desired value of MR, and 2) the rate of rotation. Usually a rotation rate of 10°/min is used for quasi-static testing conditions.

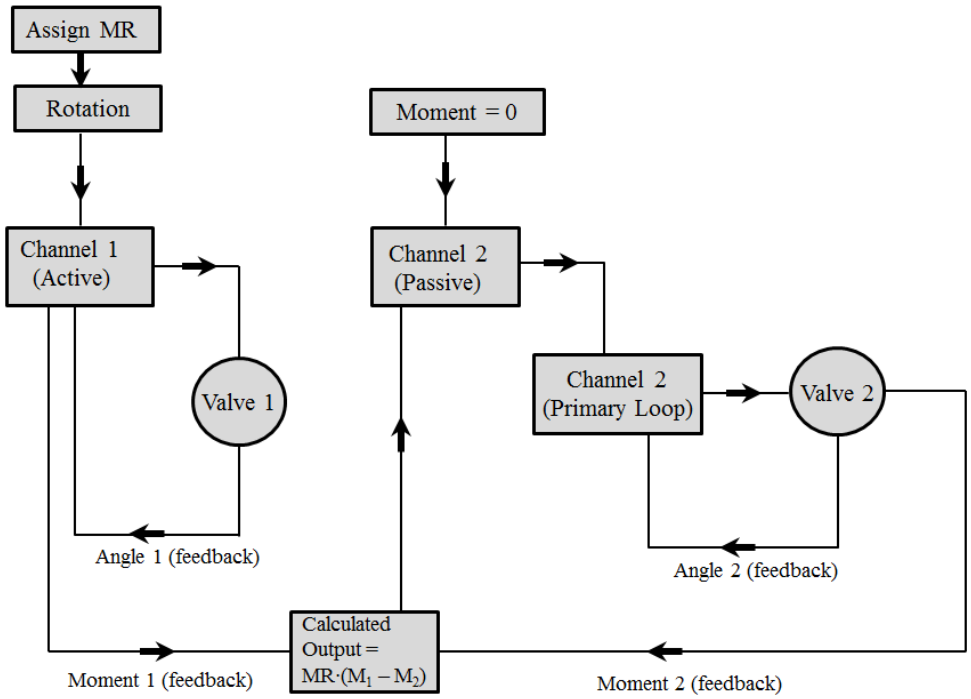

Fig. 5. Flowchart of the CASADE control algorithm.

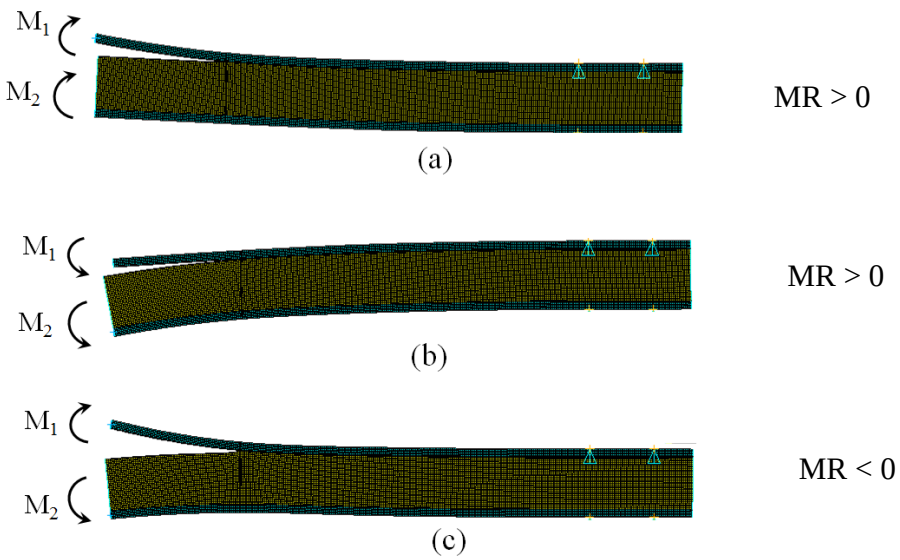

Fig. 6. Moment Ratio (MR) sign convention for a sandwich DCB-UBM specimen, where (a) MR > 0, corresponds to both moments clock-wise (b) MR > 0 when the two moments are counter clock-wise and (c) MR < 0, for both moments acting opposite to each other.

2.3. Sizing of the DCB-UBM specimen – including reinforcement layers

When performing fracture characterization of sandwich composites using the DCB-UBM specimen, competing failure mechanisms such as yielding and other types of energy consuming damages as well as excessive deflections and rotations should be avoided. Hence the fracture analysis carried out here will be in the Linear Elastic Fracture Mechanics (LEFM) regime. A sandwich specimen with very thin facesheets will experience excessive deflections and rotations when subject to moments, which will violate the principle of LEFM. To reduce stresses and deflections of the loaded beams, it is common practice to bond stiff e.g. steel layers onto the face sheets as doubler layers. The effect of such stiff layers on a GFRP/foam core sandwich system was first analyzed in [15][18]. A high strength steel is chosen as stiffener to prevent plastic deformation. Steel reinforcement layers (or "doublers") are easy to bond to the specimen and allow also for easy end tab attachment with screws. The thickness of the reinforcement layers is chosen such that they do not undergo plastic deformation prior to crack propagation.

Specimen length: The distance from the clamp to the extended position of the load arm in the *y*-direction is 670 mm, Fig. 4. With a clamp length of 50 mm, it is possible to test up to 720 mm long specimens in the DCB-UBM test rig.

Specimen Width: Indications of appropriate width are drawn from previously conducted face/core interface studies. Debond tests conducted on foam core based sandwich systems indicate a specimen width in the order of 25-40 mm [9,19,20]. For honeycomb core specimens, it is recommended to include at least six cells across the width [21] [22]. Therefore, a 30-60 mm width is recommended.

2.4. Energy release rate calculation

The energy release rate, G, for the DCB-UBM specimen is calculated from the moments M_1 and M_2 applied during the test. The analysis is restricted to small strains, small displacements and a small fracture process zone. The beams in the DCB-UBM specimen are subject to bending moments, M_1 and M_2 which are recorded during the tests. Furthermore, equilibrating the moments provide: $M_3 = M_1 + M_2$ acting at the opposite end of the specimen (see Fig. 1). The contribution to the energy release rate from each beam must be summed to obtain the total energy release rate. A detailed procedure for obtaining the energy release rate following the J-integral approach derived in [15] is provided in Appendix B. For the DCB-UBM specimen shown in Fig. 7, the total energy release rate can be obtained through summation of energy release rate contributions of each beam: $G = J = J_1 + J_2 + J_3$. The energy release rate, does not depend on crack length for the moment loaded DCB specimen [23].

From an experimental perspective, this simplifies fracture testing as there arises no necessity to continuously monitor the crack length. The critical moment can be identified as the sudden departure in the slope of M *vs.* θ plot, which is discussed in detail in a later section. The fracture toughness can be

computed using Eq. (B1) by substituting experimentally obtained critical moment values. A more detailed discussion on data reduction method is also provided later.

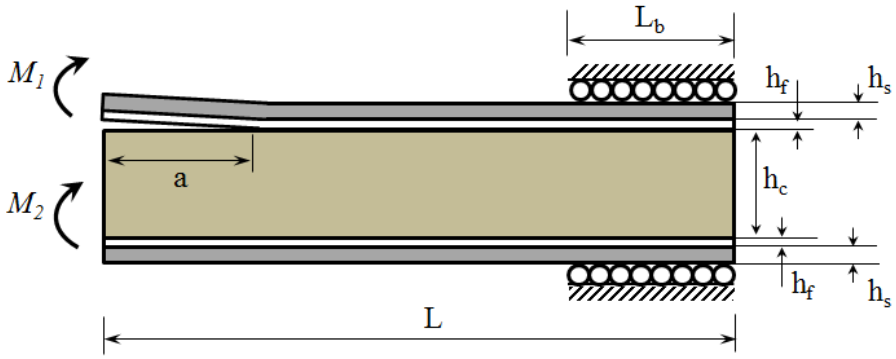

Fig. 7. Reinforced DCB-UBM sandwich specimen loaded with end moments.

2.5. Characterization of effective test rig kinematics

The applied moments cause the DCB-UBM specimen to deflect and move in the *x-y* plane, see Fig. 2. This motion is accommodated by the carriage wagons which slide on the rails. The data reduction method presented in a subsequent section, assumes no friction or slip between the carriage rollers and the rails as well as in the clamped end of the specimen. Similarly, deformations in the load train included in the angular measurements from the ADTs are also assumed to be zero in the data reduction method. Thus, if the effective deviations from the theoretical specimen kinematics assumed in the data reduction scheme are substantial, the deviations have to be accommodated in the data reduction, i.e., the part of the moments associated with the deviation must be subtracted from the measured moment. In order to characterize the effective kinematics of test rig, a calibration specimen with accurately determined geometrical and mechanical properties can be utilized to back out the deviations from the theoretical specimen kinematics.

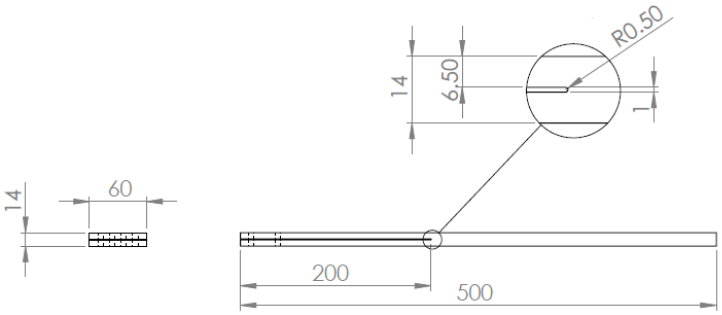

(a)

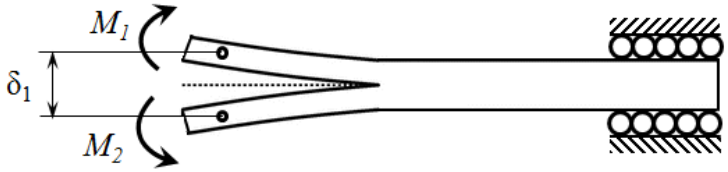

(b)

Fig. 8. (a) Calibration specimen (IMPAX SUPERME® high strength steel). All dimensions are in mm. (b) crack opening displacement (δ_1) measured using DIC.

A calibration DCB-UBM specimen was prepared from Uddeholm IMPAX SUPREME® high strength steel grade (E = 210 GPa, yield strength = 900 MPa). The specimen was sized to provide similar response as a DCB-UBM sandwich specimen reinforced with 6 mm thick steel doubler layers. Each arm of the calibration specimen was 6.5 mm thick and the total specimen length was 500 mm. In addition, the calibration specimen had a 200 mm long crack, see Fig. 8a. The crack was made blunt with a radius of 0.50 mm, to mitigate crack propagation during testing. The crack was introduced using Wire Electric Discharge Machining (WEDM). In order to relieve residual stresses, prior to machining, the specimen was pre-heated to 500 °C (holding time 2 hours) and cooled slowly to room temperature [24]. Tests were carried out by loading and unloading the calibration specimen at a constant rate of 5 °/min at various moment ratios (MR). The crack opening displacement (COD), δ_1, was monitored using the Digital Image Correlation (DIC) technique, see Fig. 8b. A 12 mega-pixel ARAMIS 12M system from the supplier GOM GmbH was utilized for the DIC measurements.

The energy release rate, G, associated with each loading and un-loading cycles are plotted against the COD in order to extract the energy release rate associated with the effective test rig and specimen kinematics, see Fig. 9. The J-integral expression [25] (refer to Appendix B) was used to obtain G from measured moments, which is plotted against the COD (δ_1) measured using DIC. In addition, a finite element (FE) model in conjunction with the CSDE method representing the theoretical specimen kinematics, was also used to numerically compute G values, see Eq. (A5), using the COD (δ_1) values measured using DIC.

The deviation in the energy release rate associated with the effective test rig and specimen kinematics can then be identified from the difference between the measured and theoretical energy release rate curves, see Fig. 9. Kardomateas et al. [26] presented algebraic expressions for energy release rate and mode-mixity of the sandwich DCB-UBM specimen, which was then later extended to a reinforced sandwich DCB-UBM specimen by Saseendran et al. [27]. However, closed-form expressions connecting energy release rate and the kinematics of a moment loaded DCB specimen is currently absent, consequently the measured *G* vs. COD curve is compared here against a similar curve obtained from a numerical FEA model as described above.

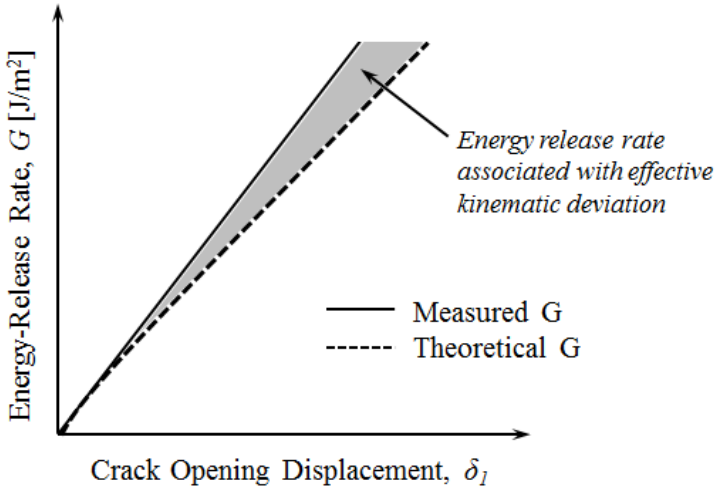

Fig. 9. Schematic illustration of energy loss due to friction.

A plot of measured moments against COD (δ_1) obtained using DIC, as well as moments obtained from the FE-model is provided in Fig. 10a for the case of MR = -1. The measured and theoretical energy release rate values are provided in Fig. 10b. Note that the energy release rate, *G*, is normalized using $E_s \cdot h_s$ and the COD is normalized by thickness of the calibration specimen arm, h_s. The energy release rate associated with deviation in test rig and specimen kinematics was quantified by subtracting the area beneath the theoretical *G* curve obtained using FEA from the area below the curve obtained from the measured *G* values. Subsequently, the area corresponding to the deviation was divided by the area beneath the theoretical *G* curve to express the % deviation of the energy release rate. A MATLAB code was used to extract the area beneath the curves and it should be noted that only the loading curve is considered for the measured *G* values.

The effective kinematic deviation obtained for the moment ratio (MR) in the range -10 to 10 is provided in Fig. 10c. It is noted that the effective deviation at a moment ratio, MR = 1 is the highest obtained at ~ 20%. The lowest value of 5% is obtained for MR = -1. Note that the direction of rotation for MR > 0 is clock-wise, see Fig. 6 for moment ratio sign convention. The study of effective kinematic

deviation indicates a maximum deviation of about 20% in the energy release rate will be incurred for the case of MR = 1 and a minimum of 5 % for MR = -1.

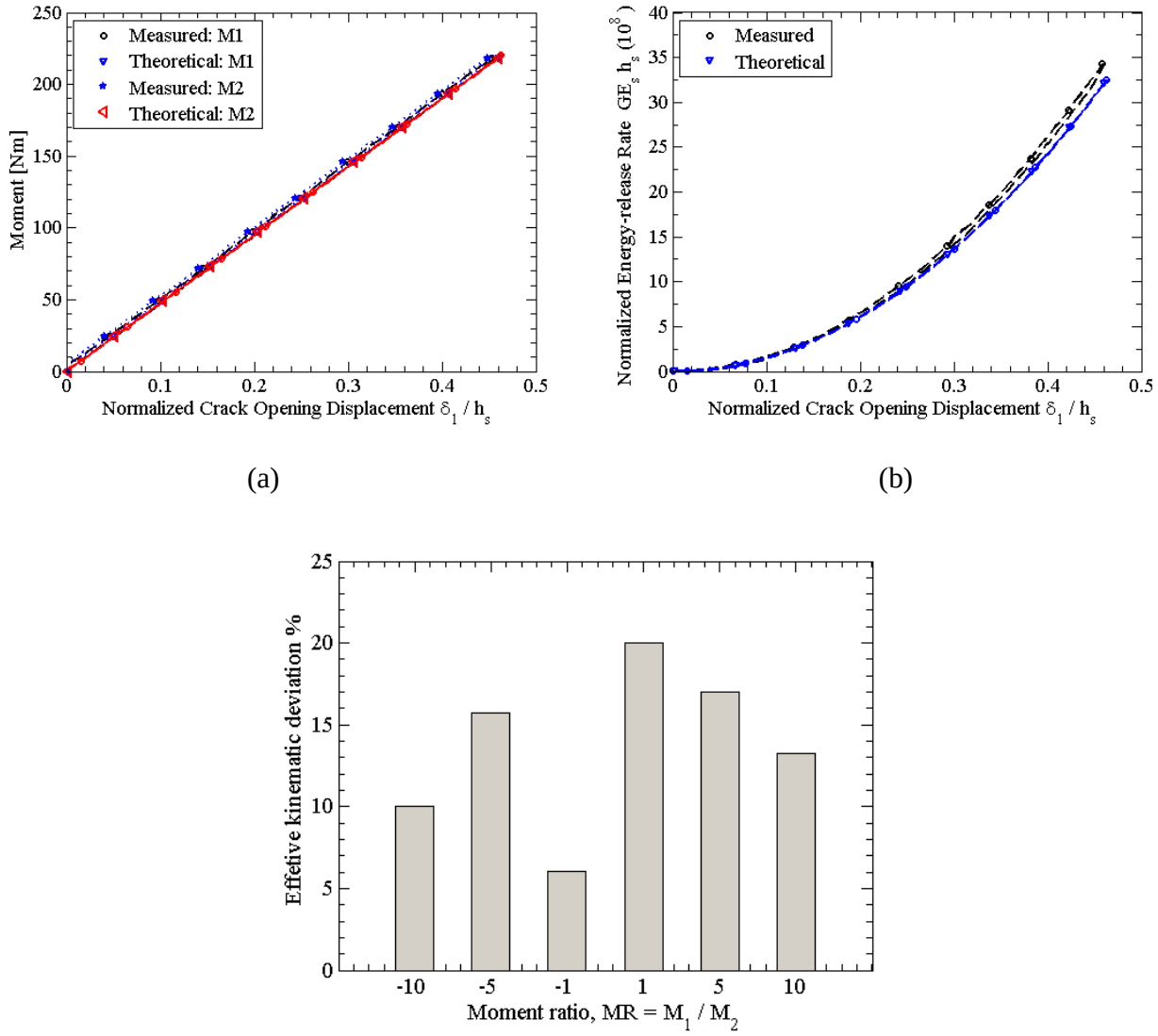

Fig. 10. Calculation of effective kinematic deviation (a) load-unload curve of moments vs. COD (measured and from FE-model) for MR = -1, (b) normalized energy release rate vs. normalized COD for MR = -10, and (c) kinematic deviation expressed in % for $-10 \leq MR \leq 10$.

3. Experimental Illustrations

Fracture characterization of sandwich DCB-UBM specimens was performed on sandwich specimen with E-glass/epoxy faces and H45 PVC foam core. The H45 Divinycell (PVC) foam core with a thickness of 30 mm and density of 45 kg/m^3 was provided by DIAB. A 0.5 x 0.5 (m) sandwich panel was prepared using VARTM processing. The panels were cured at room temperature for at least 24 hours. The face sheets comprise of eight UD E-glass plies [0/90/0/90]s and Araldite® LY 1568 / Aradur® 3489 epoxy system [28] was used with a curing time of 24 hours. After cure of the resin, the face sheet thickness was h_f = 6 mm.

3.1. Specimen preparation and Test Program

DCB-UBM specimens 30 mm wide and 450 mm long were cut from the sandwich panel (in total 10 specimens). A 50 mm long crack was machined at the face/core interface at the edge of the specimen using a hand saw. Steel doublers were adhesively bonded to both faces of the specimen using an epoxy paste adhesive (Araldite® 2015 [29]). Load tabs were attached to the specimen by six steel screws (M5) as shown in Fig. 10. Mechanical properties of face, core and steel doubler materials are provided in Table 1. Material properties for the facesheets were obtained using ASTM standard tests [30,31]. The core and steel properties were obtained from technical data sheets [24,32]. As the ply lay-up is balanced and symmetric, the face sheets are considered as orthotropic.

Table 1. Material properties of face sheet, core and steel doubler layer.

Face sheet		**Core (PVC H45)**		**Doubler layer (Steel)**	
E_{11} [GPa]	19.4	E_c [MPa]	55	E_s [GPa]	210
E_{22} [GPa]	9.90	G_c [MPa]	15	v_s	0.30
G_{12} [GPa]	6.62	v_c	0.40		
v_{12}	0.32	Density [kg/m^3]	38		
v_{21}	0.16	Cell size [mm]	0.70		

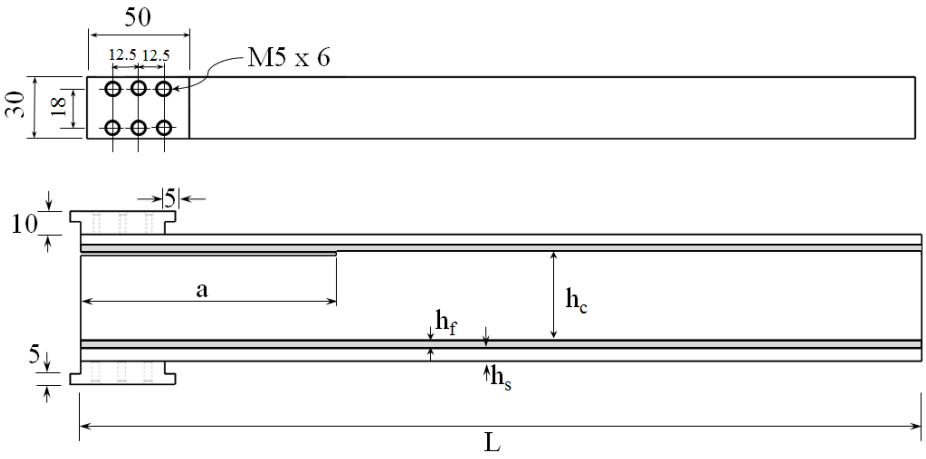

Fig. 11. DCB-UBM specimen geometry with adhesively bonded steel doubler layers. h_c = 30 mm, h_f = 2 mm and h_s = 6 mm, a = 200 mm. All dimensions shown are in mm.

Fracture characterization was carried out in predominant mode I, mode II and mixed-mode conditions. Moment ratio (MR) values corresponding to the desired mode-mixity phase angle is obtained using the numerical CSDE method. A brief discussion on the numerical model employed to estimate mode-mixity phase angle is provided in Appendix A. The fracture testing is performed by selecting moment ratio (MR) values from a plot of ψ vs. MR shown in Fig. A2 for the 30 mm core case. The MR values selected are: MR = -5, -10, 7.5, 5, 3, 1.3, 2 and 1 corresponding to ψ = -8°, -13.3°, -26.4°, -30°, -40°, -50°, -45.4° and -64.1°, respectively. A total of 10 specimens were tested. The test was carried out at an angular velocity of 10 °/min. Moment and angular displacement data from the two actuators were collected at a frequency of 1 Hz.

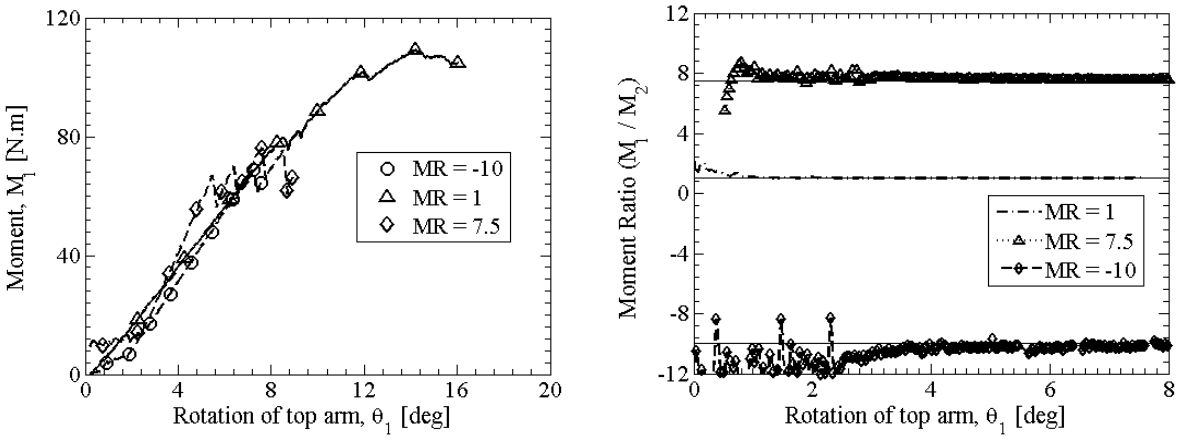

(a) (b)

Fig. 12. (a) Moment vs. rotation of the debonded arm (θ_1) and (b) moment ratio (MR) vs. rotation of the debonded arm (θ_1).

Moment and rotation angle for both crack flank beams were continuously recorded during the fracture test. Beam 1 (top arm: upper face + steel doubler layer) is referred to as “debonded” (or disbonded) arm and beam 2 (lower arm: core + bottom face + steel doubler layer) is referred to as “substrate” arm. The pre-crack lies at the upper face/core interface of the debonded arm (see Fig. 7) and is the arm which is rotation controlled. Beam 2 is the slave arm which follows the master arm, beam 1. Fig. 12a shows moment vs. rotation of the debonded arm (beam 1) for MR of 01, -7.5 and -10. As rotation is applied to the master arm 1, the onset of crack propagation can be identified as a sudden departure from the slope (see Fig. 12a). The moment increases linearly with rotation until the crack is initiated for various MR cases as shown in Fig. 12a. The control algorithm ensures testing at a constant moment ratio. A plot of MR vs. rotation of the debonded arm for MR = 1, 7.5 and -10 is shown in Fig. 12b. It can noticed from Fig. 12b that the MR remains constant throughout the test except for some initial perturbations, illustrating the robustness of the controller. Stable crack growth was observed for all the tested specimens.

Interface crack propagation was observed for all the mode-mixity cases. Fig. 13a shows the DCB-UBM test for ψ = -26°. The fracture surfaces shown in Fig. 13b for ψ = -64° shows very few core residue, indicating face/core interface crack growth. A crack jump of (~ 2-5 cm) along the interface for the case of ψ = -64°, reminiscing a stick slip behavior.

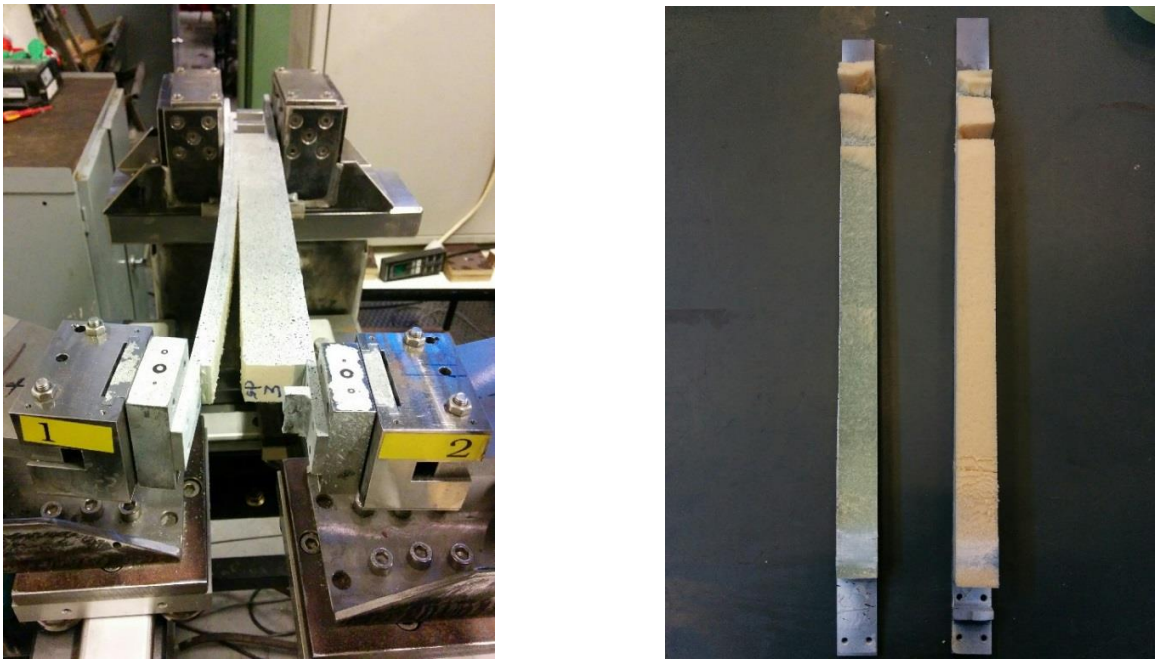

(a) (b)

Fig. 13. Fracture testing of an E-glass/H45 core sandwich DCB-UBM specimen (a) face/core interface crack propagation at MR = 7.5 (ψ = -26.4°) (b) Fracture surfaces for MR = 1 (ψ = -64.1°).

Moment values obtained from both actuators are used to compute the energy release rate by substitution into Eq. (B8). A MATLAB code is used to import and substitute the moment values to obtain the energy release rate. A plot of G vs. rotation angle for MR = 7.5, 1 and -10 of the debonded arm (beam 1) is provided in Fig. 14. The initiation fracture resistance can be identified as the deviation from the slope in G *vs* θ_1 plot, akin to the departure in the slope of M_1 vs. θ_1.

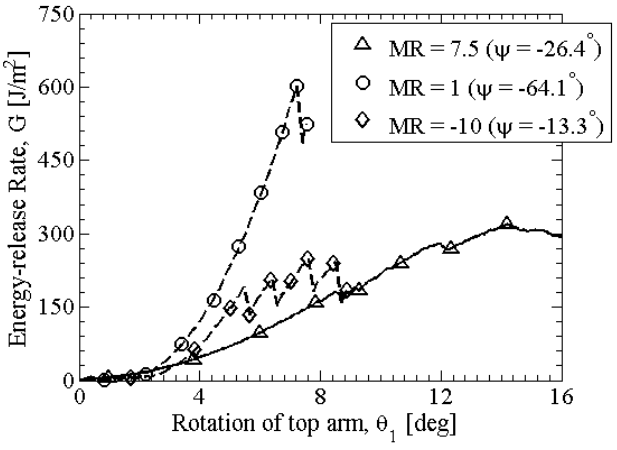

Fig. 14. Energy release rate vs. rotation of debonded beam (θ_1).

Fig. 15 shows the interface fracture toughness values as a function of mode-mixity phase angle (ψ). The toughness increases with decreasing phase angle (ψ), as a result of more shear loading. It can be noted that there appears scatter in the experimental data. The fracture toughness distribution can be fitted using the general expression provided by Hutchinson and Suo [1]:

$$\Gamma(\psi) = G_{1c}\left(1+\tan^2\left[(1-\Lambda)\psi\right]\right) \tag{1}$$

The toughness ranges from about 180 – 600 J/m^2. The fracture toughness values obtained here for the predominant mode I (ψ = -13.3°) and mixed mode (ψ = -26.4°) conditions are comparable to the values obtained using the MMB and TSD test methods for a similar E-glass/H45 sandwich system [19] [33].

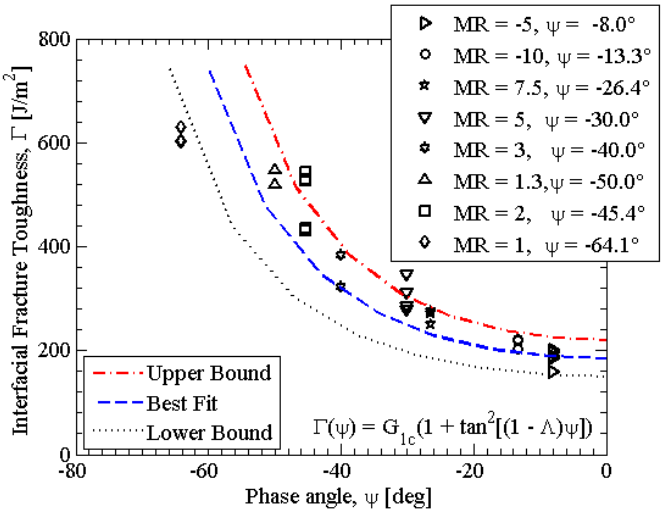

Fig. 15. Interfacial fracture toughness vs. mode-mixity (upper bound: G_{1c} = 220 [J/m^2], Λ = 0.05; best fit: G_{1c} = 185 [J/m^2], Λ = 0.01; lower bound: G_{1c} = 150 [J/m^2], Λ = 0.04).

4. Conclusions

A new DCB-UBM fracture test rig for face/core debonding characterization of sandwich specimens has been presented. The effective deviation from the theoretical kinematic specimen response was characterized using a specially designed calibration specimen. The highest deviation of 20 % was obtained for a moment ratio of 1 and the lowest of 5 % was observed for a ratio of -1. Fracture testing was performed on E-glass/H45 sandwich composite specimens with mixed-mode loading conditions. A data reduction method to calculate the fracture toughness using the moments recorded on each crack flank was presented. The moment loading configuration for the fracture testing was analyzed using finite element analysis. The mode-mixity condition during the entire test was found to remain constant and fracture toughness measurements were performed over a range of mode-mixity phase angles. For all phase angles, the crack propagated along the interface. The fracture toughness values obtained for predominant mode I conditions are comparable to values obtained using other test methods in the literature. Derivation of the kinematic relations for the DCB-UBM specimen is necessary in order to define a calibration procedure, so that the effective kinematic deviation can be corrected in the fracture toughness measurements for all moment ratios.

APPENDIX A: Determination of mode-mixity phase angle (ψ) using numerical CSDE method.

In the DCB-UBM specimen, the moment ratio (MR) is set to achieve a desired mode-mixity phase angle, ψ. In this section, the phase angle is determined using the numerical mode-mixity method, CSDE, for the E-glass/H45 sandwich specimen. The mode mixity phase angle is expressed in terms of opening δ_y and sliding δ_x relative displacements of the crack flanks as:

$$\psi_F = \tan^{-1}\left(\frac{\delta_x}{\delta_y}\right) - \varepsilon \ln\left(\frac{x}{h}\right) + 2\tan^{-1}(2\varepsilon) \tag{A1}$$

where x is a (short) distance within the singular region behind the crack tip. As a consequence of the bi-material character, the linear elastic solution shows that stresses and displacements oscillate near the crack tip [1]. The parameter ε is called the oscillatory index and is defined as:

$$\varepsilon = \frac{1}{2\pi}\ln\left(\frac{1-\beta}{1+\beta}\right) \tag{A2}$$

where

$$\beta = \frac{G_1(\mathrm{k}_2 - 1) - G_2(\mathrm{k}_1 - 1)}{G_1(\mathrm{k}_2 + 1) + G_2(\mathrm{k}_1 + 1)} \tag{A3}$$

G_1 and G_2 are the shear moduli of face and core materials with the face above the interface. The parameter $k_m = 3 - 4\nu_m$ for plane strain and $k_m = (3 - \nu_m)/(1 + \nu_m)$ for plane stress, where ν_m, is Poisson's ratio with $m = 1$ and 2 for the face and core respectively. The phase angle defined in Eq. (A1) is calculated using a FE-coupled numerical procedure called Crack Surface Displacement Extrapolation (CSDE) method [17]. Utilizing relative crack flank displacements from the FE-analysis with actual values of parameters ε and β in Eq. (A1) and $x = h_f$ provides (ψ_F) referred to as the "full formulation". Following He and Hutchinson [34], by assuming $\varepsilon = 0$, the influence of crack tip oscillation can be suppressed. Doing so recovers the conventional square-root based singular stress intensity factors. Hence the phase angle (ψ_R) in Eq. (A1) can re-expressed in "reduced formulation" ($\varepsilon = 0$),

$$\psi_R = \tan^{-1}\left(\frac{\delta_x}{\delta_y}\right) \tag{A4}$$

The reduced formulation is used here and for brevity, the phase angle will be denoted without subscript as ψ.

Finite element analysis is used to calculate phase angle and energy release rate using the commercial FEM code ANSYS® [35]. A 2D finite element model of a sandwich DCB-UBM specimen along with a dense crack tip mesh is shown in Fig. A1. Linear PLANE 42 elements having four nodes with two degrees of freedom were used at the crack tip. Parabolic PLANE 82 elements with eight nodes and two degrees of freedom at each node are used in the rest of the model. Multi point constraint (MPC) elements were used in conjunction with master nodes to apply pure moments on the specimen edges. The MPC elements applied on the steel reinforcement edges of the specimen, emulate the condition of the edges remaining straight while undergoing bending deformation. It should also be noted that the pure rotation introduced is consistent with pure bending. The moments were applied on: beam 1 comprising of top face and steel layer and beam 2 consisting of core, bottom face and steel layer (Fig. A1).

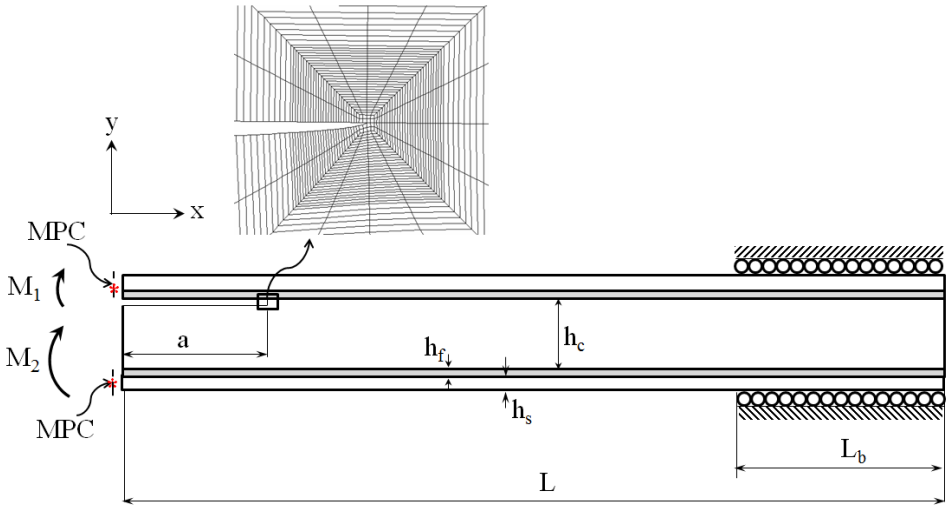

Fig. A1. Illustration of the sandwich DCB-UBM specimen and the near-tip finite mesh for a sandwich DCB-UBM specimen. The near tip element size is 2 μm.

A specimen with total length of L = 450 mm with a clamp length L_b = 50 mm and a pre-crack length, a = 200 mm is considered. Moments were applied such that the ratio, $MR = M_1/M_2$ was varied from -10 to 10 with M_1 held constant at 1 Nmm/mm. It should be noted that a value MR > 0 here corresponds to both crack flanks rotating clock-wise (see Fig. 6). The material properties of the E-glass facesheet, H45 core and high strength steel doubler layer are provided in Table 1. Phase angle (ψ) is mapped against MR values for the E-glass/H45 sandwich system with core thicknesses, h_c = 30 and 45 mm. The mode-mixity phase angle ψ vs. MR, for the two core thicknesses are shown in Fig. A2. For instance at MR = -10, ψ = -13.3° for h_c = 30 mm and ψ = -6.7° for h_c = 40 mm. ψ vs. MR plots such as shown here, allow selection of the phase angle for fracture characterization of a sandwich system.

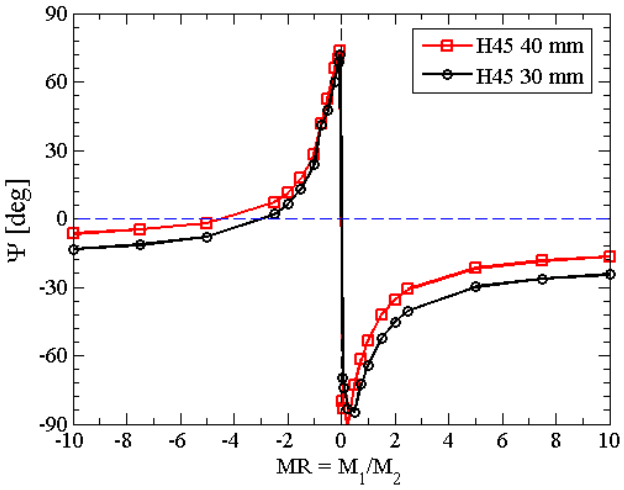

Fig. A2. Phase angle (ψ) vs. Moment ratio (MR) map for an E-glass/H45 sandwich DCB-UBM fracture specimen for h_c = 30 and 40 mm.

The energy release rate obtained in terms of crack flank displacements is given by [17]:

$$G = \frac{\pi(\delta_x^2 + \delta_y^2)}{2x(c_1 + c_2)} \tag{A5}$$

where x is the distance from the crack tip and c_1 and c_2 are stiffness parameters of the face and core given by:

$$c_m = \frac{k_m + 1}{G_m} \tag{A6}$$

where m = 1 for face sheet and m = 2 for core.

APPENDIX B: *J*-integral expression for reinforced DCB-UBM sandwich specimen

The *J*-integral expression for a DCB specimen loaded with pure moments was derived in [15] under plane conditions for multiple layers. In this section, the *J* integral expression is deduced for a reinforced DCB specimen stiffened with doubler layers (penta-layer case), akin to the specimen employed in this study. The principle of DCB-UBM specimen is illustrated in Fig. 1and the non-zero J integral path pieces for a moment loaded sandwich DCB specimen is shown in Fig. B1. Note that the moments act about the respective neutral axis (y_{NA}) in each beam.

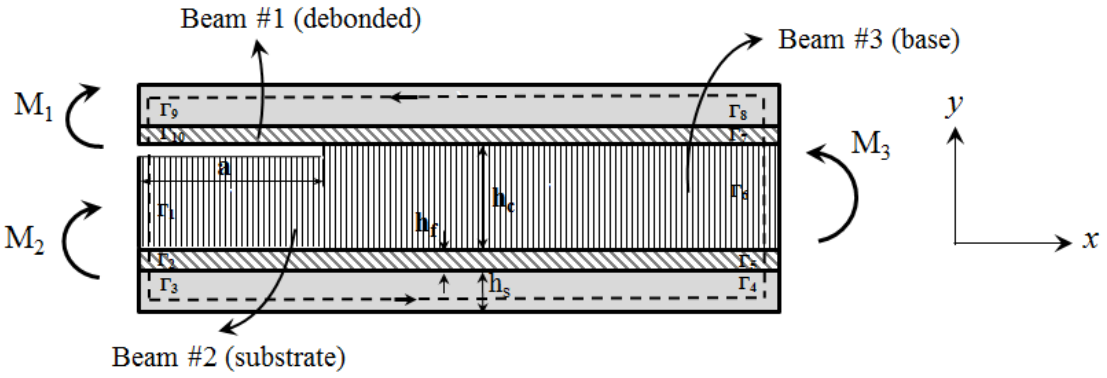

Fig. B1. *J* integral path for sandwich DCB specimen loaded with pure moments.

The *J* for a multilayer beam DCB specimen formulated as function of extension, bending and coupling terms is given by:

$$J=\sum_{p=1}^{10}\frac{\bar{E}_p M_b^2}{6\left(A_b D_b-B_b^2\right)^2}\left[A_b^2\left(y_{p-1}^3-y_p^3\right)-3A_bB_b\left(y_{p-1}^2-y_p^2\right)+3B_b^2\left(y_{p-1}-y_p\right)\right] \tag{B1}$$

The DCB specimen is treated as three beams, each subjected to pure moment. Debonded beam (top doubler layer + face sheet) is subjected to moment, M_1 and the substrate beam (core + bottom face sheet + bottom doubler layer), is acted upon by moment, M_2. The debonded and substrate beams refer to the region behind the crack tip. The intact portion ahead of the pre-crack is referred to as the base part (top doubler and face sheet + core + bottom face sheet and doubler) and is acted upon by moment, M_3. Each beam subjected to moment about the respective neutral axis (y_{NA}) is provided in Fig. B2.

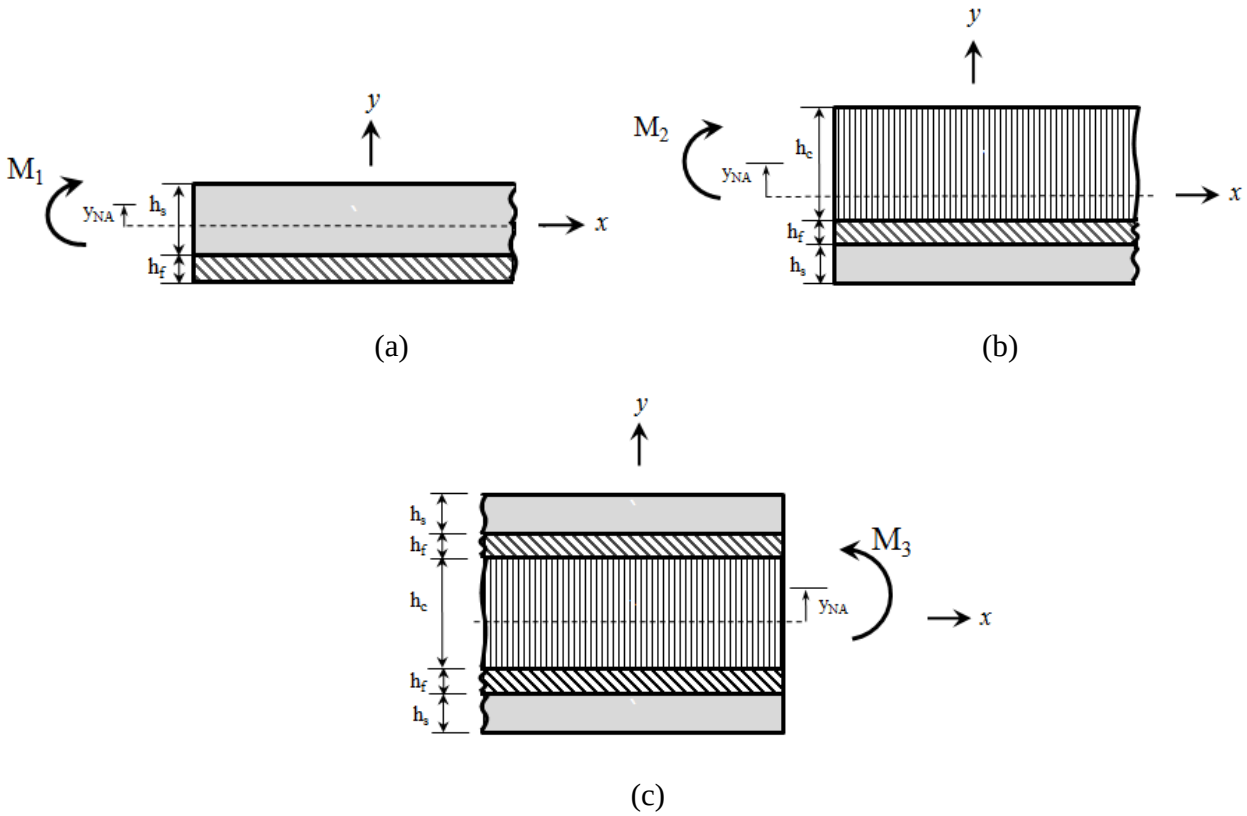

Fig. B2. (a) Debonded, (b) substrate and (c) base parts subjected to moments.

For the debonded beam (see Fig. B2a), the *J*-integral expression is expressed as:

$$J_1 = \frac{M_1^2}{24D_1^2}\left[E_s h_s\left(3h_f^2 + h_s^2\right) + E_f h_f\left(3h_s^2 + h_f^2\right)\right] \tag{B2}$$

where the coupling stiffness of debonded beam, D_1 is given by:

$$D_1 = \frac{1}{12}\left[h_s\left(3h_f^2 + h_s^2\right) + h_f\left(3h_s^2 + h_f^2\right)\right] \tag{B3}$$

The *J*-integral expression for the substrate beam in Fig. B2b is of the form:

$$J_2 = \frac{M_2^2}{6\left(A_2D_2 - D_2^2\right)^2}\left[\begin{array}{l}\frac{A_2^2}{4}\left\{E_s\left[\frac{3}{4}h_f\left(h_c + h_f\right)^2 + \frac{1}{4}h_f^3\right] + E_f\left[\frac{3}{4}h_f\left(h_c - h_s\right)^2 + \frac{1}{4}h_f^3\right] + E_c\left[\frac{1}{4}h_c\left(h_c^2 + 3\left(h_c + h_f\right)^2\right)\right]\right\} + \\ 3A_2B_2\left\{E_s\left(h_s h_c + h_f\right) + E_f h_f\left(h_c - h_s\right) - E_c h_c\left(h_f + h_s\right)\right\} + 3A_2B_2^2\end{array}\right] \tag{B4}$$

25

where the extensional, bending and coupling stiffness terms of the substrate beam are given by:

$$A_2 = E_c h_c + E_f h_f + E_s h_s \tag{B5a}$$

$$B_2 = \frac{1}{2}\left[h_c \left(h_f \left(E_c - E_f \right) + h_s \left(E_c - E_s \right) \right) + h_s h_f \left(E_f - E_s \right) \right] \tag{B5b}$$

$$D_2 = \frac{1}{12}\left[\begin{array}{l} E_c h_c^3 + h_c^2 \left(3E_f h_f + E_s h_s \right) + E_f h_f^3 + 3E_f h_s^2 h_f + 3E_s h_f^2 h_s + \\ E_s h_s^3 + h_c \left(3E_c h_f^2 + 6h_f h_s \left(E_c - E_f + E_s \right) + 3E_c h_s^3 \right) \end{array} \right] \tag{B5c}$$

Similarly, for the base beam (Fig. B2c), the *J*-integral can be expressed as:

$$J_3 = \frac{M_3^2}{24 D_3^2}\left[2E_s \left\{ 3h_s \left(h_c + 2h_f + h_s \right)^2 + h_s^3 \right\} + 2E_f \left\{ 3h_f \left(h_c + h_f \right)^2 + h_f^3 \right\} + E_c h_c^3 \right] \tag{B6}$$

where the D3 is the coupling stiffness term of the base part given by:

$$D_3 = \frac{1}{12}\left[\frac{E_s}{2} \left\{ 3h_s \left(h_c + 2h_f + h_s \right)^2 + h_s^3 \right\} + \frac{E_f}{2} \left\{ 3h_f \left(h_c + h_f \right)^2 + h_f^3 \right\} + E_c \frac{h_f^3}{4} \right] \tag{B7}$$

The total *J* for the entire DCB-UBM specimen is obtained from summation of individual contributions of each beam:

$$J = J_1 + J_2 + J_3 \tag{B8}$$

Acknowledgements

The financial support from the Danish Centre for Composite Structures and Materials (DCCSM) funded by the Danish Innovation Foundation (Grant: 09-067212) is gratefully acknowledged. The support from DIAB, Sweden with supply of core material is highly appreciated. Furthermore, the support of Christopher Augustsson, MTS Systems Norden AB, Sweden during controller installation is greatly appreciated. The third author's research has been supported by grants from FAA, NIA and ONR. The FAA, NIA and ONR program managers, Dr. Zhi Chen, Dr. Ronald Krueger and Dr. Yapa Rajapakse showed keen interest in this project and are gratefully acknowledged.

References

[1] Hutchinson JW, Suo Z. Mixed Mode Cracking in Layered Materials. Adv Appl Mech 1991;29:63–191. doi:10.1016/S0065-2156(08)70164-9.

[2] L.A. Carlsson, L.S. Sendlein, and S.L. Merry. Characterization of Facesheet/Core Shear Fracture of Composite Sandwich Beams. J Compos Mater 1991;25:101–16.

[3] Cantwell W, Broster G, Davies P. The Influence of water immersion on skin-core debonding in GFRP-Balsa sandwich structures. J Reinf Plast 1996;15:1161–72.

[4] Ratcliffe J, Cantwell W. Center notch flexure sandwich geometry for characterizing skin-core adhesion in thin-skinned sandwich structures. J Reinf Plast … 2001;20:945–70.

[5] Aviles F, Carlsson LA. Analysis of the sandwich DCB specimen for debond characterization. Eng Fract Mech 2008;75:153–68.

[6] Li X, Carlsson LA. Fracture mechanics analysis of tilted sandwich debond (TSD) specimen. J Compos Mater 2001;35:2145–68.

[7] Smith S, Shivakumar K. Modified mode-I cracked sandwich beam (CSB) fracture test. AIAA Pap 2001.

[8] Berggreen C, Carlsson LA. A Modified TSD Specimen for Fracture Toughness Characterization - Fracture Mechanics Analysis and Design. J Compos Mater 2010;44:1893–912.

[9] Berggreen C, Quispitupa A, Costache A, Carlsson LA. Face/core mixed mode debond fracture toughness characterization using the modified TSD test method. J Compos Mater 2014;48:1939–45. doi:10.1177/0021998313492358.

[10] Reeder JR, Crews Jr JR. Mixed-mode bending method for delamination testing. AIAA J 1990.

[11] ASTM D6671/D6671M –13. Standard Test Method for Mixed Mode I-Mode II Interlaminar Fracture Toughness of Unidirectional Fiber Reinforced Polymer Matrix Composites 2006.

[12] Quispitupa A, Berggreen C, Carlsson LA. On the analysis of a mixed mode bending sandwich specimen for debond fracture characterization. Eng Fract Mech 2009;76:594–613.

[13] Quispitupa A, Berggreen C, Carlsson LA. Design Analysis of the Mixed Mode Bending Sandwich Specimen. J Sandw Struct Mater 2010;12:253–72. doi:10.1177/1099636209104533.

[14] Sørensen BF, Jørgensen K, Jacobsen TK, Østergaard RC. DCB-specimen loaded with uneven bending moments. Int J Fract 2006;141:163–76. doi:10.1007/s10704-006-0071-x.

[15] Lundsgaard-Larsen C, Sørensen BF, Berggreen C, Østergaard RC. A modified DCB sandwich specimen for measuring mixed-mode cohesive laws. Eng Fract Mech 2008;75:2514–30. doi:10.1016/j.engfracmech.2007.07.020.

[16] MTS Systems Corporation. MTS Models FlexTest® IIm/GT/SE Controller Hardware. Eden

Prairie, MN 55344-2290 USA: 2009.

[17] Berggreen C, Simonsen BC, Borum KK. Experimental and Numerical Study of Interface Crack Propagation in Foam-cored Sandwich Beams. J Compos Mater 2006;41:493–520. doi:10.1177/0021998306065285.

[18] Li S, Thouless MD, Waas AM, Schroeder JA, Zavattieri PD. Mixed-mode cohesive-zone models for fracture of an adhesively bonded polymer–matrix composite. Eng Fract Mech 2006;73:64–78. doi:10.1016/j.engfracmech.2005.07.004.

[19] Manca M, Quispitupa A, Berggreen C, Carlsson LA. Face/core debond fatigue crack growth characterization using the sandwich mixed mode bending specimen. Compos Part A Appl Sci Manuf 2012;43:2120–7. doi:10.1016/j.compositesa.2012.07.001.

[20] Ratcliffe JG, Reeder JR. Sizing a single cantilever beam specimen for characterizing facesheet-core debonding in sandwich structure. J Compos Mater 2011;45:2669–84.

[21] TerMaath S, Ingraffea A, Wawrzynek P. A Computational Fracture Mechanics Approach for the Analysis of Facesheet-from-Core Disbond of Honeycomb Core Sandwich Panels. Fatigue Fract. Mech. 30th Vol., West Conshohocken, PA: ASTM International; n.d., p. 169–82. doi:10.1520/STP13402S.

[22] Saseendran V, Berggreen C, Carlsson LA. Fracture Testing of Honeycomb Core Sandwich Composites Using the DCB-UBM Test. 20th Int. Conf. Compos. Mater., Copenhagen: ICCM20 Secretariat; 2015.

[23] Saseendran V, Carlsson LA, Berggreen C. Shear and Foundation Effects on Crack Root Rotation and Mode Mixity in Moment and Force Loaded SCB Sandwich Specimen. J Compos Mater 2017. doi:10.1177/0021998317749714.

[24] Uddeholm Impax® Supreme 2017.

[25] Rice JR. A Path Independent Integral and the Approximate Analysis of Strain Concentration by Notches and Cracks. J Appl Mech 1968;35:379. doi:10.1115/1.3601206.

[26] Kardomateas GA, Berggreen C, Carlsson LA. Energy-Release Rate and Mode Mixity of Face/Core Debonds in Sandwich Beams. AIAA J 2013;51:885–92. doi:10.2514/1.J051765.

[27] Saseendran V, Berggreen C, Carlsson LA. Fracture Mechanics Analysis of Reinforced DCB Sandwich Debond Specimen Loaded by Moments. AIAA J 2017. doi:10.2514/1.J056039.

[28] Araldite® LY 1568 / Aradur® 3489. Huntsman Corporation, The Woodlands, TX, USA: 2010.

[29] Araldite® 2015 Structural Adhesive. Huntsman Advanced Materials,The Woodlands, Texas: 2007.

[30] ASTM-D3039/D3039M-08. Standard Test Method for Tensile Properties of Polymer Matrix Composite Materials 2014.

[31] ASTM-D7078/7078M-12. Standard Test Method for Shear Properties of Composite Materials by V-Notched Rail Shear Method 2012.

[32] Divinycell H Technical Data 2016.

[33] Moslemian R. Residual Strength and Fatigue Lifetime of Debond Damaged Sandwich Structures. Technical University of Denmark, 2011.

[34] He M-Y, Hutchinson JW. Kinking of a Crack Out of an Interface. J Appl Mech 1989;56:270. doi:10.1115/1.3176078.

[35] ANSYS Inc. ANSYS® Mechanical User's Guide. Southpointe, PA: ANSYS, Inc.; 2015.

Publication P4

V. Saseendran, L. A. Carlsson, and C. Berggreen

Fracture Mechanics Analysis of Reinforced DCB Sandwich Debond Specimen Loaded by Moments

AIAA Journal, vol. 56, no. 1, pp. 413-422, 2018

Accepted: 23 July 2017
Available online: 06 September 2017
DOI: https://doi.org/10.2514/1.J056039

AIAA JOURNAL
Vol. 56, No. 1, January 2018

Fracture Mechanics Analysis of Reinforced DCB Sandwich Debond Specimen Loaded by Moments

Vishnu Saseendran* and Christian Berggreen†
Technical University of Denmark, DK-2800 Kongens Lyngby, Denmark
and
Leif A. Carlsson‡
Florida Atlantic University, Boca Raton, Florida 33431

DOI: 10.2514/1.J056039

Analytical expressions for the energy release rate and mode-mixity phase angle are derived for a sandwich composite double-cantilever beam fracture specimen with the face sheets reinforced by stiff plates. The sandwich beam is considered symmetric, with identical top and bottom facesheets. Only a pure moment loading is considered. The *J*-integral coupled with laminate beam theory is employed to derive closed-form expression for the energy release rate in terms of the applied moments, geometry, and material properties. A scalar quantity ω is obtained to express the mode-mixity phase angle. It is shown that ω is independent of the applied loading conditions. The value of ω is found to be moderately influenced by reinforcement thicknesses.

Nomenclature

a	=	precrack length
E_c	=	Young's modulus of core
E_f	=	Young's modulus of facesheet
E_r	=	Young's modulus of reinforcement layer
e_d	=	neutral axis distance (debonded beam)
e_s	=	neutral axis distance (substrate beam)
G	=	energy release rate
h_c	=	thickness of core
h_f	=	thickness of facesheet
h_r	=	thickness of reinforcement layer
J	=	J-integral
K	=	stress intensity factor
M_d	=	moment applied on debonded beam
β	=	Dundurs bimaterial parameter
Γ	=	integration path for J integral
ε_x^0	=	laminate midplane strain
ε	=	oscillatory index
κ_x	=	laminate midplane curvature
σ_{ij}	=	stress tensor
ψ	=	mode-mixity phase angle

I. Introduction

FACE/CORE interface debonding is a serious failure mode that affects the performance of a sandwich structure. Debonds (face and core separation) can occur during liquid resin processing due to inadequate wetting of the face/core interface region, which reduces the adhesive strength between the face and the core. Face/core debonds may also occur due to service loads such as wave slamming, impact, and fatigue cycling. Debonds may propagate along the interface or kink into the core. The propensity of the crack to propagate is determined by the local stress state at the crack tip for a given loading condition. The stress intensity factors at the crack tip for a given loading condition can be expressed in terms of a mode-mixity phase angle ψ, which quantifies the ratio of shear to normal loading at the crack tip.

Determination of the interface fracture resistance is vital from a design perspective. There are various experimental methods developed to determine the interface fracture toughness, such as the cracked sandwich beam [1], the double-cantilever beam (DCB) [2], the tilted sandwich debond specimen [3], the three-point sandwich beam [4], the mixed-mode bending (MMB) specimen [5], and single-cantilever beam (SCB) sandwich specimen [6]. Most of the devised experimental test methods were inspired by fracture test methods developed for laminate composites. For instance, the MMB test method developed for delamination testing [7,8] was extended to sandwich composites [5,9]. The SCB sandwich specimen is a simple test setup for determining mode I fracture toughness of the face/core interface [10]. However, appropriate sizing of the specimen must be undertaken to ensure that the face/core crack propagates along the interface [11] at mode I loading. Efforts are underway to implement the SCB sandwich specimen as a standard test method for mode I fracture toughness characterization [12].

Due to the high elastic mismatch across the interface in sandwich composites, the face/core crack is inherently mixed mode. A full characterization of the face/core interface inevitably requires testing over a wide array of mode-mixity phase angles. Therefore, it is desirable to control the mode-mixity during the test. A relatively recently developed test method for delamination testing is the double-cantilever beam loaded with uneven bending moments (DCB-UBM) developed by Sørensen et al. [13]. This method was recently extended to sandwich composites by Østergaard et al. [14] and Lundsgaard-Larsen et al. [15], and it is schematically illustrated in Fig. 1. In this method, it is possible to perform a fracture test at a desired mode mixity by controlling the moments M_1 and M_2 applied to the specimen edge.

Reference is made here to the crack element approach by Suo and Hutchinson [16], who developed a fracture mechanics analysis approach for a bilayer element; and Kardomateas et al. [17], who extended this procedure to a cracked sandwich element. These authors considered only in-plane (axial) forces and moment couples acting on the edge of the specimen. An analytical expression for the energy release rate G was obtained through the J integral. The mode decomposition was performed using the stress intensity factors K_I and K_{II}, derived analytically except for a single scalar parameter ω, which was extracted from the numerical solution of one loading combination.

Sandwich panels with thin facesheets (in the range of 0.5 mm) are not uncommon, especially in the aircraft industry. Fracture characterization of such sandwich composites possesses many

Received 31 January 2017; revision received 28 June 2017; accepted for publication 23 July 2017; published online 6 September 2017.

*Ph.D. Fellow, Department of Mechanical Engineering; vsas@mek.dtu.dk.
†Associate Professor, Department of Mechanical Engineering; cbe@mek.dtu.dk.
‡Professor, Department of Ocean and Mechanical Engineering; carlsson@fau.edu.

Fig. 1 DCB-UBM specimen loaded with edge moments.

problems, such as load application to the debonded facesheets that, if thin, will undergo large nonlinear deflections and rotations. A method to reduce displacements is to reinforce one or both faces with stiff layers named doublers. This method was adopted by Lundsgaard-Larsen et al. [15], who bonded stiff steel plates to both facesheets to reduce the rotation. In this paper, expressions for the energy release rate and mode-mixity phase angle are derived for a reinforced DCB-UBM fracture specimen loaded by pure edge moments. The mode-mixity phase angle ψ quantifies the ratio between mode II and mode I stress intensity factors.

II. Analysis of Sandwich Fracture Specimen

The sandwich specimen considered here (see Fig. 2) consists of five layers, two composite facesheet laminates labeled 1 and 2, the core, and two reinforcing plates of thickness h_r, bonded to each of the facesheets. Typically, the facesheets are composed of multidirectional laminates with plies arranged in a symmetric and balanced way. Analysis of such a sandwich element is simplified by homogenizing the laminate into a specially orthotropic composite layer of the same thickness as the laminate, with stiffnesses E_1, E_2, ν_{12}, ν_{21}, and G_{12}. The approach presented here, assumes that all layers are isotropic with Young's modulus E and Poisson's ratio ν. Transformation of the orthotropic elastic constant of the laminate facesheet into the isotropic constant is discussed in Appendix B.

Figure 3 shows the superposition scheme used for the analysis of the DCB-UBM specimen. The original configuration is shown in Fig. 3a. By adding the uncracked configuration subject to pure moments per unit width M_3, as shown in Fig. 3b, the force and moment configuration shown in Fig. 3c is obtained. As indicated in Fig. 3c, beam 1, referred to as the debonded beam, consists of the top facesheet and reinforcement layer (thickness, $H_1 = h_r + h_f$); and beam 2, referred to as the substrate part, consists of the layers beneath the precrack [i.e., core, bottom facesheet, and bottom reinforcement layer (thickness, $H_2 = h_c + h_f + h_r$)]. The intact portion to the right of the crack front (comprising both facesheets, the reinforcement layers, and the core) is referred to as the base part (thickness, $H_3 = 2h_r + 2h_f + h_c$). Hence, the two systems will have same energy release rate and stress intensity factors. This analysis follows the principal approach performed by Suo and Hutchinson for a bimaterial interface [16]. The DCB-UBM specimen is loaded by pure moments per unit width, M_1 and M_2, applied to the left edge as shown in Fig. 1. Hence, there are no axial in-plane forces or transverse shear forces acting on the specimen. Suo and Hutchinson [16] considered axial loads P_1, P_2, and P_3 per unit width. P_1 and P_2 act on the left

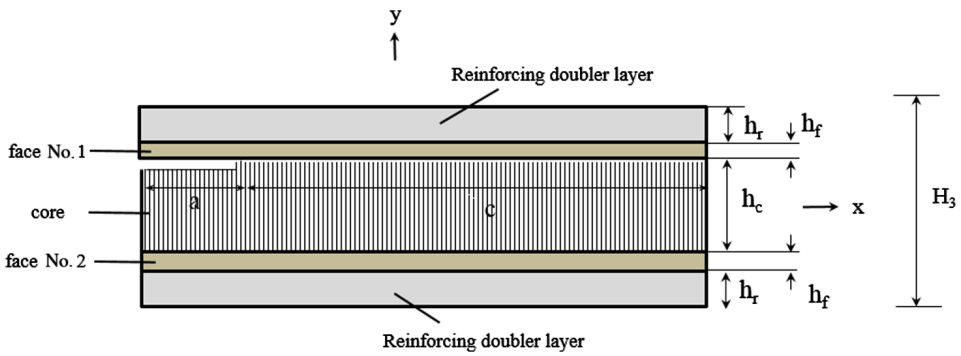

Fig. 2 Sandwich beam element with reinforcing doubler layers of thickness h_r.

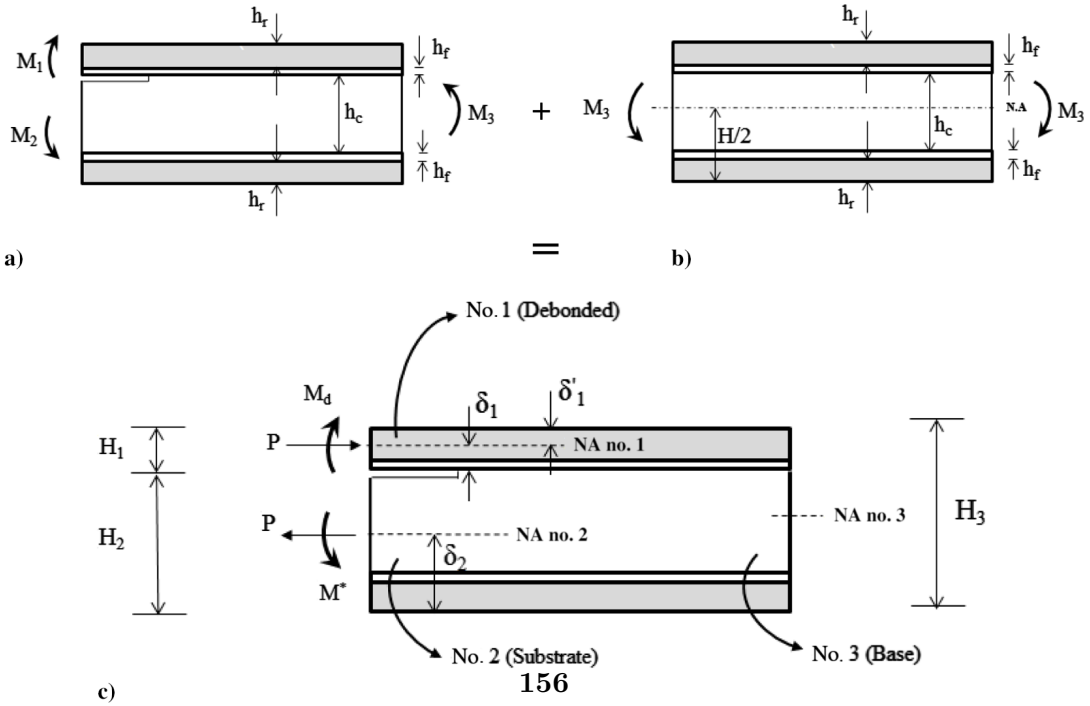

Fig. 3 Superposition scheme of sandwich geometry.

edge, and P_3 acts on the right edge. For the specific test specimen considered here (DCB-UBM), however, there is no axial force present; hence, it is not considered in our analysis.

The moment acting on the debonded arm M_d and axial force P can be expressed in terms of M_3 as follows:

$$P = -c_2 M_3 \tag{1a}$$

$$M_d = M_1 - c_3 M_3 \tag{1b}$$

where expressions for c_2 and c_3 are obtained from a stress analysis of each beam, to be provided later. Notice that the three original loading parameters are reduced to two independent variables, P and M_d. From equilibrium,

$$M^* = M_d + P\Delta_1 \tag{2}$$

where

$$\Delta_1 = H_3 - \delta_1' - \delta_2 \tag{3a}$$

and

$$\delta_1' = H_1 - \delta_1 \tag{3b}$$

The distribution of stress in each sub-beam can be determined from laminate beam theory [18], where each part of the sandwich beam is considered as a multilayered beam (see Fig. 3). The thickness of debonded beam 1 is $H_1 = h_f + h_r$, and that of substrate beam 2 is $H_2 = h_c + h_f + h_r$. The force and moment (per unit width) are given by the following [18]:

$$N_x = A\varepsilon_x^0 + B\kappa_x \tag{4a}$$

$$M_x = B\varepsilon_x^0 + D\kappa_x \tag{4b}$$

where N_x and M_x are the force and moment resultants, and ε_x^0 and κ_x are the midplane strain and curvature. The extension, coupling, and bending stiffnesses (A, B, and D) are defined as follows:

$$A = \sum_{k=1}^{n} \bar{E}_k (y_k - y_{k-1}) \tag{5a}$$

$$B = \frac{1}{2}\sum_{k=1}^{n} \bar{E}_k (y_k^2 - y_{k-1}^2) \tag{5b}$$

$$D = \frac{1}{3}\sum_{k=1}^{n} \bar{E}_k (y_k^3 - y_{k-1}^3) \tag{5c}$$

where the y axis is referenced to the geometric midplane ($y = 0$). Note that k is the layer index $k = 1, 2, \ldots, n$, where n is the number of layers. Also, y_k is the y coordinate of the interface between layers k and $k+1$. Note that $y_0 = -h/2$, where h is the total laminate thickness. $\bar{E}_k$ is the elastic modulus in the x direction for ply k. For plane strain, $\bar{E}_k = E_k/(1-\nu_k^2)$; whereas for plane stress, $\bar{E}_k = E_k$. An example of the layer coordinates y_k for the intact part of the specimen (3 in Fig. 3c) is shown in Fig. 4.

The stress in each layer is as follows:

$$(\sigma_x)_k = \bar{E}_k \varepsilon_x \tag{6}$$

where the strain is given by the following:

$$\varepsilon_x = \varepsilon_x^0 + \kappa_x y \tag{7}$$

Consider first the configuration shown in Fig. 3b. Figure 4 shows the layer coordinates. For the pure bending case, substituting

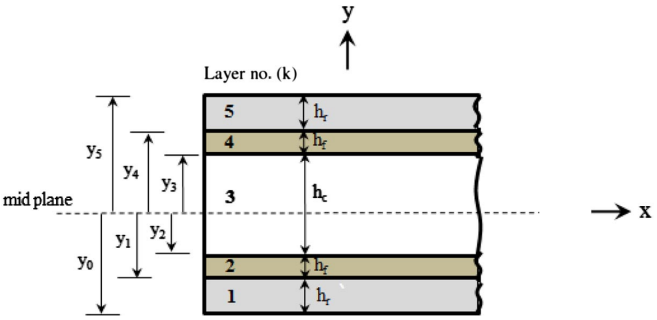

Fig. 4 Layer definition for the intact part (no. 3) of the sandwich specimen.

($N_x = 0$) into Eq. (4) provides the midplane strain and the y coordinate of the neutral axis:

$$\varepsilon_x^0 = -\frac{B\kappa_x}{A} \tag{8a}$$

$$y_{\mathrm{NA}} = \frac{B}{A} \tag{8b}$$

The sandwich beam is assumed to be symmetric ($B = 0$). For this case, Eq. (4b) yields $M_x = D\kappa_x$. Rearranging and substituting for $\varepsilon_x^0 = 0$ in Eq. (7) gives the following:

$$\varepsilon_x = \kappa_x y = \frac{M_3}{D} y \tag{9}$$

Substituting ε_x in Eq. (6): $(\sigma_x)_k = \bar{E}_k (M_3/D) y$. The force P acting on the debonded part (beam 1; Fig. 3) is obtained by integrating the stress $(\sigma_x)_k$ over the cross section as follows:

$$P = -\int_{h_c/2}^{H_3/2} \sigma_x \, \mathrm{d}y = -c_2 M_3 \tag{10}$$

Integration yields

$$c_2 = \frac{\bar{E}_f (y_4^2 - y_3^2) + \bar{E}_r (y_5^2 - y_4^2)}{2D} \tag{11}$$

where the ply coordinates are illustrated in Fig. 4. The moment M_d (Fig. 3) acting on beam 1 (debonded) is given by the following:

$$M_d = M_1 - \int_{h_c/2}^{H_3/2} \sigma_x \left(y - \left(\frac{h_c}{2} + \delta_1 \right) \right) \mathrm{d}y \tag{12a}$$

$$M_d = M_1 - c_3 M_3 \tag{12b}$$

where

$$\begin{aligned} c_3 = {} & \frac{\bar{E}_f}{D}\left[\frac{1}{3}\left(\left(\frac{h_c}{2} + h_f \right)^3 - \frac{h_c^3}{8} \right) \right. \\ & \left. - \frac{(h_c/2 + \delta_1)}{2}\left(\left(\frac{h_c}{2} + h_f \right)^2 - \frac{h_c^2}{4} \right) \right] \\ & + \frac{\bar{E}_r}{D}\left[\frac{1}{3}\left(\frac{H_3^3}{8} - \left(\frac{h_c}{2} + h_f \right)^3 \right) \right. \\ & \left. - \frac{(h_c/2 + \delta_1)}{2}\left(\frac{H_3^2}{4} - \left(\frac{h_c}{2} + h_f \right)^2 \right) \right] \end{aligned} \tag{13}$$

III. J-Integral Calculation

The current analysis is carried out in the ambit of linear elastic fracture mechanics regime. To obtain the energy release rate for a

precracked sandwich element reinforced with stiff doubler layers, the J-integral approach is chosen.

The J integral was calculated for the closed path shown in Fig. 5 using the following general expression [19]:

$$J = \int_{\Gamma} W\,\mathrm{d}y - \sigma_{ij} n_j \cdot \frac{\partial u_i}{\partial x}\,\mathrm{d}S \tag{14}$$

where σ_{ij} is the stress tensor, dS is a length increment along the closed path Γ, n_j is an outward normal vector to the closed contour, and u_i is the displacement vector. W is the strain energy density: $W = (1/2)\sigma_x \varepsilon_x$. The J integral is evaluated for all layers and summed up:

$$J = \sum_{p=1}^{10} \int_{\Gamma} -\frac{1}{2} \bar{E}_p \sigma_x^2\,\mathrm{d}y \tag{15}$$

The J integral is nonzero only along the vertical paths near the left edge marked Γ_1–Γ_3 and Γ_9–Γ_{10}. For the horizontal paths $dy = 0$. Furthermore, the normal vector is directed along the y axis: $\sigma_{ij} n_j = 0$, making no contribution to J. The vertical paths (Γ_4–Γ_8) along the right edge do not contribute to J because no load acts on that edge (see Fig. 5).

The total energy release rate then becomes the following:

$$J = G = J_{\text{Debonded}} + J_{\text{Substrate}} = J_1 + J_2 + J_3 + J_9 + J_{10} \tag{16}$$

J_1 through J_3 and J_9–J_{10} are calculated from the stress in each layer. A detailed derivation of the J integral is provided in Appendix A, which yields the following:

$$G = P^2\left(\frac{L_1}{(\bar{E}h)_d^2} + \frac{V_1}{(\bar{E}h)_s^2} + \frac{V_2\Delta_1^2}{H_s^2} + \frac{V_3\Delta_1}{(\bar{E}h)_s H_s}\right) + M_d^2\left(\frac{L_2}{H_d^2} + \frac{V_2}{H_s^2}\right) + M_d P\left(\frac{2V_2\Delta_1}{H_s^2} + \frac{L_3}{(\bar{E}h)_d H_d} + \frac{V_3}{(\bar{E}h)_s H_s}\right) \tag{17}$$

The preceding expression for G is rearranged to obtain a quadratic form in P and M_d that is similar to [17] as follows:

$$J = G = a_1 P^2 + a_2 M_d^2 - a_3 P M_d \tag{18}$$

where

$$a_1 = \frac{L_1}{(\bar{E}h)_d^2} + \frac{V_1}{(\bar{E}h)_s^2} + \frac{\Delta_1^2 V_2}{H_s^2} + \frac{\Delta_1 V_3}{(\bar{E}h)_s H_s} \tag{19a}$$

$$a_2 = \frac{L_2}{H_d^2} + \frac{V_2}{H_s^2} \tag{19b}$$

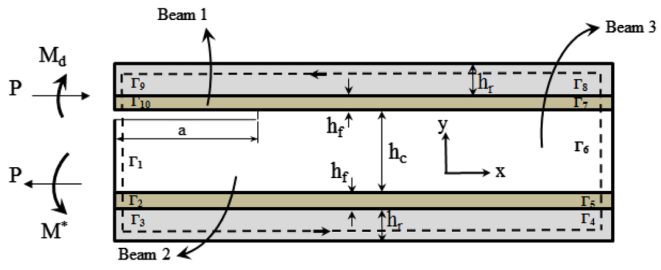

Fig. 5 J-integral path in reinforced sandwich beam.

$$a_3 = \frac{-2\Delta_1 V_2}{H_s^2} - \frac{L_3}{(\bar{E}h)_d H_d} - \frac{V_3}{(\bar{E}h)_s H_s} \tag{19c}$$

IV. Mode-Mixity Expression

The energy release rate may be expressed in terms of a complex stress intensity factor ($K = K_1 + iK_2$) [20,21] as follows:

$$G = B|K|^2 \tag{20}$$

where $i = \sqrt{-1}$ and

$$B = \frac{G_c(\kappa_f + 1) + G_f(\kappa_c + 1)}{16 G_f G_c \cos h^2 \pi\varepsilon} \tag{21}$$

where ε, which is the oscillatory index, is expressed as follows:

$$\varepsilon = \frac{1}{2\pi} \ln\left(\frac{1-\beta}{1+\beta}\right) \tag{22}$$

The Dundurs parameter β is given by

$$\beta = \frac{G_f(\kappa_c - 1) - G_c(\kappa_f - 1)}{G_c(\kappa_c + 1) + G_c(\kappa_f + 1)} \tag{23}$$

G_f and G_c are the shear moduli of the face and core. Note that $\kappa_m = (3 - 4\nu_m)/(1 + \nu_m)$ for plane strain and $\kappa_m = 3 - 4\nu_m$ for plane stress. Also, ν_m is the Poisson's ratio, and $m = 1$ and 2 for the upper facesheet and core, respectively. Substituting the energy release rate G from Eq. (18) into Eq. (20) yields the following:

$$|K|^2 = \frac{1}{B}(a_1 P^2 + a_2 M_d^2 - a_3 P M_d) \tag{24}$$

There are two possible roots for K in Eq. (24). The roots for K include both real and imaginary parts. Kardomateas et al. [17] found the roots of a similar equation following the approach of Thouless et al. [22] and Suo and Hutchinson [16]. Therefore, by exploiting similar arguments, the complex stress intensity factor K can be written as follows:

$$K = \frac{1}{\sqrt{B}}(-aP\sqrt{a_1} + bM_d\sqrt{a_2}) h_f^{-i\varepsilon} \tag{25}$$

It should be noted that Eq. (24) is of same form as in [17]. For the first root, the complex numbers a and b are defined as follows [16]:

$$a = e^{i\varepsilon} \quad b = -ie^{i(\omega+\gamma)} \tag{26}$$

where

$$\sin\gamma = \frac{a_3}{2\sqrt{a_1 a_2}} \tag{27}$$

It is required that a and b are independent of loading for the derivation of the closed-form solution of mode mixity. Thus, by selecting the first root, the parameter ω in Eq. (26) becomes dependent only on the geometry and material properties of the reinforced sandwich specimen but not on loading. Substituting a and b in Eq. (25) leads to the following:

$$K = K_1 + iK_2 = \frac{1}{\sqrt{B}}(-P\sqrt{a_1} - ie^{i\gamma} M_d \sqrt{a_2}) h_f^{-i\varepsilon} e^{i\omega} \tag{28}$$

The definition of the mode-mixity phase angle follows Suo and Hutchinson [16] for a bimaterial interface crack. The mode-mixity phase angle ψ is defined as follows [23]:

$$\psi = \tan^{-1}\left(\frac{\mathrm{Im}[Kh_f^{i\varepsilon}]}{\mathrm{Re}[Kh_f^{i\varepsilon}]}\right) \tag{29}$$

where the real and imaginary parts of the arguments are as follows [21]:

$$\mathrm{Re}[Kh_f^{i\varepsilon}] = \frac{1}{\sqrt{B}}[-P\sqrt{a_1}\cos\omega + M_d\sqrt{a_2}\sin(\omega+\gamma)] \tag{30a}$$

$$\mathrm{Im}[Kh_f^{i\varepsilon}] = \frac{1}{\sqrt{B}}[-P\sqrt{a_1}\sin\omega - M_d\sqrt{a_2}\cos(\omega+\gamma)] \tag{30b}$$

Note that the near-tip oscillation is suppressed by this definition of ψ, and that $\mathrm{Re}[Kh_f^{i\varepsilon}] = |K|\cos\psi$ and $\mathrm{Im}[Kh_f^{i\varepsilon}] = |K|\sin\psi$. An expression for the phase angle ψ can be obtained from Eqs. (29) and (30):

$$\tan\psi = \frac{\lambda\sin\omega - \cos(\omega+\gamma)}{\lambda\cos\omega + \sin(\omega+\gamma)} \tag{31}$$

where

$$\lambda = -\frac{P}{M_d}\sqrt{\frac{a_1}{a_2}} \tag{32}$$

The parameter λ incorporates the influence of the stiffened facesheet through a_1 and a_2. The parameter ω can be expressed in terms of the phase angle as follows:

$$\omega = \tan^{-1}\left[\frac{\cos\gamma + (\lambda+\sin\gamma)\tan\psi}{\lambda + \sin\gamma - \cos\gamma\tan\psi}\right] \tag{33}$$

V. Calculation of ψ and ω

A finite element analysis (FEA) of the DCB-UBM specimen combined with a method to extract the stress intensity factors, called the crack surface displacement extrapolation (CSDE) method [24], is employed here to calculate ω and ψ. Two-dimensional plane strain models of sandwich specimens were made in ANSYS® [25], comprising isoparametric four-node (plane 42) and eight-node (plane 82) elements. A highly discretized mesh was used near the crack tip (see Fig. 6). The facesheets, core, and reinforcement layers were considered linear elastic and isotropic. The plane 42 elements were used at the crack tip with a minimum element size of 0.005 mm. These elements were used to capture the large strain gradients encountered at the crack region. The mode-mixity phase angle ψ was extracted from the near-tip crack flank displacements in the following form:

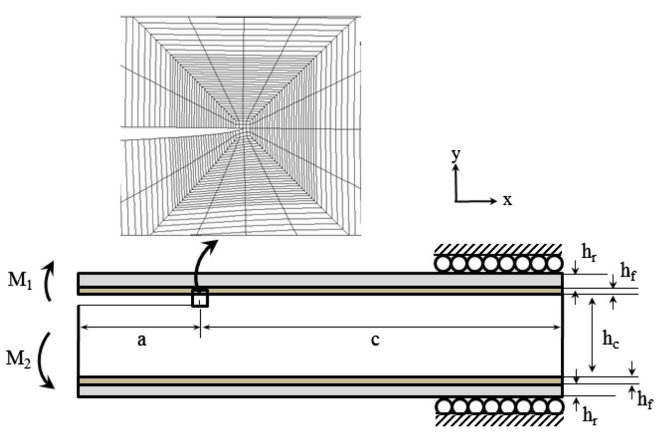

Fig. 6 FE model of reinforced DCB-UBM sandwich specimen.

Table 1 Material properties of core [9]

Core	H45	H100	H250	Aluminum foam core
Young's modulus E_c, MPa	50	130	300	7000
Shear modulus G_c, MPa	15	35	104	2630
Poisson's ratio ν_c	0.32	0.32	0.32	0.32

Table 2 Material properties of facesheet [9]

Facesheet	Aluminum face	E-glass fiber: DBLT-850 (0/45/90/-45)
Young's modulus E_f, GPa	70	16.4
Shear modulus G_f, GPa	26.9	5.8
Poisson's ratio ν_f	0.30	0.306

$$\psi = \tan^{-1}\left(\frac{\delta_x}{\delta_y}\right) - \varepsilon\,\ell_n\left(\frac{x}{h}\right) + \tan^{-1}(2\varepsilon) \tag{34}$$

where x is distance behind the crack tip; ε is the oscillatory index [Eq. (22)]; and h is a characteristic length, which is taken as the facesheet thickness $h = h_f$. The CSDE method is implemented as a subroutine in the commercial finite element (FE) package ANSYS and employs crack flank opening and sliding displacements (δ_y and δ_x) over a region very close to behind the crack tip. The energy release rate is given by the following [24]:

$$G_{\mathrm{CSDE}} = \frac{\pi G_m(1+4\varepsilon^2)}{2x(k_m+1)}(\delta_x^2 + \delta_y^2) \tag{35}$$

where $k_m = (3-4\nu_m)$ for the plane strain, $k_m = (3-4\nu_m)/(1+\nu_m)$ for the plane stress, and ν_m is Poisson's ratio. Note that $m = 1$ and 2 for face and core. G_1 and G_2 are the shear moduli of the face and core materials, respectively.

FEA is performed on both unreinforced and reinforced DCB-UBM sandwich specimens. FEA results for unreinforced specimens are compared to analytical expressions derived here for the energy release rate G_{anal} [Eq. (17)] and expressions available in the literature for unreinforced specimens [17]. The material properties of the face and core employed in the analysis are provided in Tables 1 and 2. In the second part of the analysis, a reinforced sandwich DCB-UBM specimen with a soft polyvinylchloride (PVC) foam core (H45) is considered.

A. Unreinforced DCB-UBM Sandwich Specimen

Two unreinforced sandwich configurations comprising 2-mm-thick aluminum facesheets, a 20-mm-thick soft core (PVC H100), and a stiff core (aluminum foam) were chosen to benchmark the analytical expressions. For both cases, refer to Tables 1 and 2 for material properties. A crack length of $a = 200$ mm was used with a sufficiently long specimen to reduce the edge effects ($c = 300$ mm). The mode mixity of a DCB-UBM specimen was changed by altering the ratio of the moments M_1 and M_2 applied to the edge [moment ratio ($\mathrm{MR} = M_1/M_2$)] (Fig. 1). The MR values, thicknesses, and material properties were taken from [17] in order to compare the energy release rate and mode-mixity results to the results obtained herein [Eqs. (17) and (29)]. Such a direct comparison is made by making the reinforcement layer modulus equal to that of the facesheets and making the sum of each facesheet thickness and reinforcement thickness equal to the face thickness analyzed in [17]. The results are examined over a range of moment ratios.

Tables 3 and 4 list energy release rate results for a large range of moment ratios. Close agreement between the numerical G_{CSDE} and analytical G_{anal} results is noted. The current results for G also agree with [15,17]. Note that results from [17] are compared here with moment loading only. It is further noted that the parameter ω remains relatively constant for each case. For the PVC foam core sandwich, the largest deviation of ω from the average value is 0.5%, whereas the deviation for the stiffer aluminum foam core is below 2.1%. It should

Table 3 G, ψ, and ω results for unreinforced DCB-UBM sandwich specimen with PVC H100 core

	Moment ratio				
	−0.125	−0.25	−1.0	0.25	0.125
M_1, N · mm	75.6	129.6	196.1	118.6	71.1
M_2, N · mm	−604.8	−518.4	−196.1	474.4	568.8
G_{anal}, N/mm	0.4238	0.4349	0.4140	0.3642	0.3749
G_{CSDE}, N/mm	0.4076	0.4214	0.4107	0.3553	0.3626
G, N/mm [17]	0.4239	0.4350	0.4140	0.3613	0.3727
ψ, deg	52.60	35.60	1.11	−62.87	−85.40
ω, deg	74.09	73.66	73.34	73.74	73.54

Table 4 G, ψ, and ω for unreinforced DCB-UBM sandwich specimen with aluminum foam core

	Moment ratio				
	−0.002	−0.02	−0.0625	−1.0	0.0625
M_1, N · mm	8.340	76.80	157.70	199.40	159.50
M_2, N · mm	−4170	−3840	−2523.4	−199.40	2552.0
G_{anal}, N/mm	0.3917	0.3953	0.3944	0.3890	0.4035
G_{CSDE}, N/mm	0.3848	0.3883	0.3895	0.3872	0.3819
G, N/mm [17]	0.3969	0.3997	0.3963	0.3890	0.3862
ψ, deg	54.40	33.90	4.04	−30.90	−72.20
ω, deg	58.22	57.74	57.05	56.36	55.86

be further pointed out that the phase angle results presented in Tables 3 and 4 compare well with those published earlier in [17].

B. Reinforced DCB-UBM Sandwich Specimen

During fracture characterization tests of unreinforced sandwich specimens, excessive deformation of either crack flank will violate the linear elastic fracture mechanics. Reinforcing the fracture specimen with stiff doubler layers prevents excessive crack flank rotations (see Fig. 7). Moreover, such layers will make it easier to attach loading tabs to specimens for experimental testing. The parameter ω is computed for a reinforced DCB-UBM sandwich specimen with a soft PVC foam core (H45). As earlier, aluminum facesheets were chosen ($h_f = 2$ mm). Steel reinforcement layers were chosen ($E_s = 210$ GPa, $\nu_r = 0.3$) with a thickness of $h_r = 6$ mm [15]. The total length of the specimen was $L = 500$ mm with a crack length of $a = 200$ mm.

Results for the reinforced specimen are presented in Table 5. For the range of moment ratios examined, the phase angle ψ varied from 18.7 to 77.3 deg; whereas the scalar parameter ω remained nearly constant with an average of 65.09 deg (±1.5%); see Table 5. An advantage of a ω parameter that is independent of loading is that the mode-mixity phase angle may be computed using a single ω value. To further examine the parameter ω, the phase angle ψ was calculated for a range of MRs using Eq. (31), with the average value of ω as 65.09 deg (Table 5). The results for ψ in Table 5 show that ψ values obtained using a fixed ω value (ψ^*) closely match with the ones from the FEA.

VI. Influence of Reinforcement Layer Thickness

A study was conducted to examine the influence of the reinforcement layer thickness on the ω parameter. A moderately dense H100 core with an aluminum facesheet was considered.

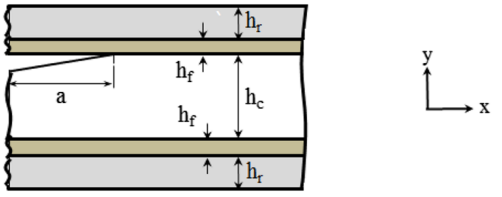

Fig. 7 Sandwich DCB-UBM specimen reinforced with steel plates.

Table 5 G, ψ, and ω results for sandwich DCB-UBM specimen with PVC H45 foam core reinforced with steel layers

	Moment ratio				
	−0.125	−0.25	−1.0	0.25	0.125
M_1, N · mm	210	415	1110	410	210
M_2, N · mm	−1680	−1660	−1110	1640	1680
G_{anal}, N/mm	0.2254	0.1994	0.2005	0.2048	0.2049
G_{CSDE}, N/mm	0.2075	0.2319	0.2078	0.2252	0.2248
ω, deg; Eq. (33)	65.42	66.09	65.77	62.63	65.56
ψ, deg	57.53	50.87	18.74	77.31	72.88
ψ,[a] deg; Eq. (31)	57.24	49.97	18.32	79.61	72.31

[a]calculated using ω(avg.) = 65.09°.

Table 6 ω parameter for a H100 sandwich specimen with varying reinforcement thicknesses

H100 core (130 MPa), $h_c = 30$ mm, $h_f = 6$ mm, $h_r = 1 - 6$ mm					
Moment ratio	−0.250	−0.0625	−1	0.0625	0.250
M_1, N · mm	199	158	199	160	199
M_2, N · mm	−798	−2523	−199	2550	798
		$h_r = 1$ mm			
G_{anal}, N/mm	0.0881	0.7942	0.0140	0.8101	0.0872
ψ, deg	45.2	60.0	9.97	−112	−97.4
ω, deg	64.3	65.3	63.6	63.3	64.4
ω_1 (average)	— —	— —	— —	64.2	
		$h_r = 2$ mm			
G_{anal}, N/mm	0.0672	0.6139	0.0099	0.6261	0.0665
ψ, deg	45.0	58.8	10.6	−114	−100
ω, deg	62.9	63.8	62.3	61.9	62.8
ω_2 (average)	— —	— —	— —	62.7	
		$h_r = 3$ *mm*			
G_{anal}, N/mm	0.0518	0.4769	0.0072	0.4862	0.0512
ψ, deg	44.4	57.5	10.7	−116	−103
ω, deg	61.6	62.4	61.0	60.6	61.4
ω_3 (average)	— —	— —	— —	61.4	
		$h_r = 4$ mm			
G_{anal}, N/mm	0.0404	0.3736	0.0055	0.3809	0.0399
ψ, deg	43.7	56.3	10.6	−117	−104
ω, deg	60.3	61.1	59.9	59.4	60.2
ω_4 (average)	— —	— —	— —	60.2	
		$h_r = 5$ mm			
G_{anal}, N/mm	0.0319	0.2959	0.0042	0.3015	0.0314
ψ, deg	42.9	55.1	10.2	−127.9	−106.0
ω, deg	59.2	59.9	58.8	56.8	59.0
ω_5 (average)	— —	— —	— —	58.8	
		$h_r = 6$ mm			
G_{anal}, N/mm	0.0255	0.2370	0.0033	0.2414	0.0251
ψ, deg	42.0	54.0	9.84	−127	−108
ω, deg	58.1	58.8	57.9	58.8	58.0
ω_6 (average)	— —	— —	— —	58.3	

The facesheet and core thicknesses were held constant at $h_f = 6$ mm and $h_c = 30$ mm (see Tables 1 and 2 for material properties). The thickness of the steel reinforcement doubler layers ($E_r = 210$ GPa, $\nu_r = 0.3$) was varied from 1 to 6 mm. The mode-mixity phase angle ψ, computed using the CSDE method, was used to obtain the ω parameter using Eq. (33). The moment ratio was varied between −0.25 to 0.25.

Results for the phase angle and ω parameter are provided in Table 6. For $h_r = 1$ mm, the maximum deviation in ω is ±1.7%. Similar results are found for the other reinforcement thickness. This confirms that the results of ω for each reinforcement thickness concurred with the load-independent ω hypothesis. The results show, however, that ω depends on the thickness of the reinforcement layer. The difference between ω for thin (64.19 deg) and thick (58.30 deg) steel reinforcement layers is 10.1%.

To further examine the dependence of the ω parameter on the reinforcement layer thickness, the study is extended to other foam-core sandwich configurations: E-glass/H45, E-glass/H100, E-glass/H250, Al/H45, and Al/H250. The E-glass face laminates considered

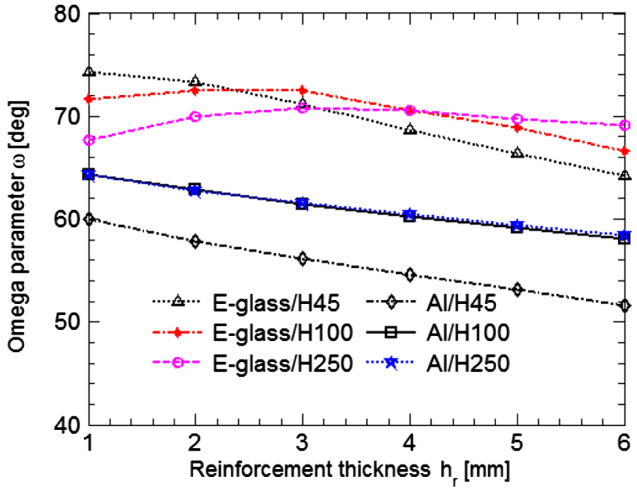

Fig. 8 Omega parameter variations for typical sandwich specimens across reinforcement thicknesses.

Table 7 Curve-fitting parameters for ω vs h_r plot for E-glass/PVC core and aluminum/PVC core sandwich systems

Parameter	Values
Aluminum/PVC core, $\omega = \varsigma_1 h_r + \varsigma_2$	
Al/H45	$\varsigma_1 = -1.649$, $\varsigma_2 = 61.33$
Al/H100	$\varsigma_1 = -1.252$, $\varsigma_2 = 65.40$
Al/H250	$\varsigma_1 = -1.158$, $\varsigma_2 = 65.22$
E-glass/PVC core, $\omega = \eta_1 h_r^2 + \eta_2 h_r + \eta_3$	
E-glass/H45	$\eta_1 = -0.111$, $\eta_2 = 1.34$, $\eta_3 = 76.1$
E-glass/H100	$\eta_1 = -0.401$, $\eta_2 = 1.71$, $\eta_3 = 70.5$
E-glass/H250	$\eta_1 = -0.389$, $\eta_2 = 2.90$, $\eta_3 = 65.4$

are quasi isotropic (see Tables 1 and 2 for material properties). Face thicknesses of 6 and 2 mm were considered for the glass fiber and aluminum faces. As before, the steel reinforcement layer ($E_r = 210$ GPa, $\nu_r = 0.3$) thickness is varied from 1 to 6 mm. The ω parameter is calculated from Eq. (33). An average from two MR values (MR $= -0.250$ and $+0.250$) is used to determine ω.

Figure 8 shows a plot of ω vs the thickness of the steel reinforcement layer. It is noticed that, when stiff aluminum facesheets are combined with a soft core (H45), the omega variation across the range of reinforcement layer thicknesses is 9%. However, for stiffer cores, the variation is below 5%. For sandwich specimens with E-glass facesheets and H45 core, a deviation of 7.2% in ω across h_r is observed. The deviation in ω across h_r for sandwich specimens with E-glass facesheets and a stiffer H250 core is below 2.8%. The trends in ω vs h_r are quantified using a polynomial curve fit to the data. The curve-fitting parameters are provided in Table 7.

VII. Conclusions

Closed-form expressions for the energy release rate and mode-mixity phase angle for a reinforced double-cantilever beam loaded with uneven bending moments sandwich specimen were derived using a superposition scheme, the J-integral and laminate beam theory. The phase angle was expressed in terms of a load-independent scalar parameter ω. A finite element analysis was used to determine the energy release rate and mode-mixity phase angle for the various sandwich systems analyzed. It was found that the ω value remained practically independent of the loading configuration for a fixed reinforcement thickness. The value of ω varied weakly with the reinforcement thickness, and the dependence was expressed by curve fitting for typical sandwich specimens. The closed-form expressions derived in this paper can be used for fracture analysis of various sandwich systems with thin facesheets requiring reinforcement layers.

Appendix A: J-Integral Calculations

Each beam (1 and 2) is analyzed separately; see Figs. A1 and A2. The J integral is calculated from the stress σ_x in each layer along the paths: Γ_1–Γ_3 and Γ_3–Γ_{10}; see Fig. 5. The stress σ_x in each layer due to the moment and force was calculated and substituted in Eq. (15). All equations are expressed in terms of the elastic modulus for ply k in the x direction $\bar{E}_k$. As explained in Sec. II, for the plane strain, $\bar{E}_k = E_k/(1-\nu_k^2)$; whereas for the plane stress, $\bar{E}_k = E_k$.

A.1. Debonded Beam (Beam 1)

Figure A1 shows the beam consisting of the upper facesheet and stiffener layer, acted upon by a force and moment according to the superposition analysis. The force P and moment M_d act on the neutral axis (see Fig. A1). The location of the neutral axis (NA) is given by the ratio between coupling and extensional stiffnesses ($y_{\mathrm{NA}} = B/A$). The stress σ_x in each layer is expressed as follows:

$$\sigma_x = \begin{cases} \frac{-P\bar{E}_r}{(\bar{E}h)_d} + \frac{M_d\bar{E}_r}{(D_d - B_d^2/A_d)}(y - y_{NA}); \; y_1 \le y \le y_2 [\text{Reinforcement}] \\ \frac{-P\bar{E}_f}{(\bar{E}h)_d} + \frac{M_d\bar{E}_f}{(D_d - B_d^2/A_d)}(y - y_{NA}); \; y_0 \le y \le y_1 [\text{Upper Facesheet}] \end{cases} \tag{A1}$$

where $(\bar{E}h)_d = \bar{E}_r h_r + \bar{E}_f h_f$. The J integral is calculated for a debonded beam by substituting Eq. (A1) into Eq. (15) along paths (Γ_9 and Γ_{10}) to obtain the following:

$$\begin{aligned} J_{\Gamma 9} &= \frac{1}{2\bar{E}_r}\int_{y_1}^{y_2}\left(\frac{-P\bar{E}_r}{(\bar{E}h)_d} + \frac{M_d\bar{E}_r}{H_d}(y - e_d)\right)^2 \cdot \mathrm{d}y \\ &= \frac{P^2\bar{E}_r h_r}{2(\bar{E}h)_d^2} + \frac{M_d^2\bar{E}_r}{2H_d^2}\left[\frac{h_r}{3}\left(\frac{3h_f^2}{4} + \frac{h_r^2}{2}\right) - e_d h_f h_r + e_d^2 h_r\right] \\ &\quad - \frac{PM_d\bar{E}_r}{(\bar{E}h)_d H_d}\left[\frac{h_f h_r}{2} - e_d h_r\right] \end{aligned} \tag{A2a}$$

$$\begin{aligned} J_{\Gamma 10} &= \frac{1}{2\bar{E}_f}\int_{y_0}^{y_1}\left(\frac{-P\bar{E}_f}{(\bar{E}h)_d} + \frac{M_d\bar{E}_f}{H_d}(y - e_d)\right)^2 \cdot \mathrm{d}y \\ &= \frac{P^2\bar{E}_f h_f}{2(\bar{E}h)_d^2} + \frac{M_d^2\bar{E}_f}{2H_d^2}\left[\frac{h_f}{12}(h_f^2 + 3h_r^2) + e_d h_f h_r + e_d^2 h_f\right] \\ &\quad + \frac{PM_d\bar{E}_f}{(\bar{E}h)_d H_d}\left[\frac{h_f h_r}{2} + e_d h_f\right] \end{aligned} \tag{A2b}$$

where $H_d = (D_d - (B_d^2/A_d))$, and $e_d = y_{\mathrm{NA}}$ (neutral axis in Fig. A1).

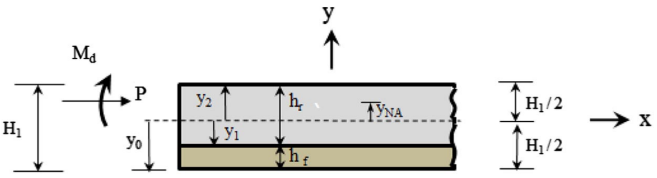

Fig. A1 Force and moment acting on beam 1.

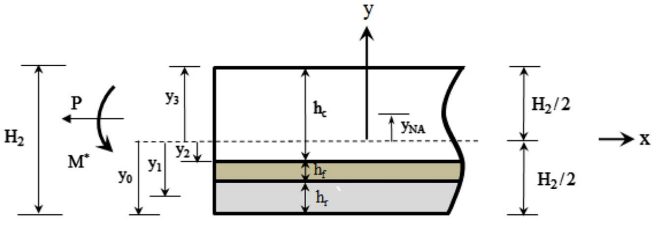

Fig. A2 Loads acting on substrate beam 2.

The J-integral contribution from the debonded beam becomes the following:

$$J_{\text{Debonded}} = J_{\Gamma 9} + J_{\Gamma 10} \tag{A3}$$

$$J_{\text{Debonded}} = \frac{P^2}{(\bar{E}h)_d^2} L_1 + \frac{M_d^2}{H_d^2} L_2 + \frac{PM_d}{(\bar{E}h)_d H_d} L_3 \tag{A4}$$

where

$$L_1 = \frac{1}{2}\left(\bar{E}_r h_r + \bar{E}_f h_f\right) \tag{A5a}$$

$$L_2 = \frac{\bar{E}_r}{2}\left[\frac{h_r}{12}(3h_f^2 + h_r^2) - e_d h_f h_r + e_d^2 h_r\right] + \frac{\bar{E}_f}{2}\left[\frac{h_f}{12}(h_f^2 + 3h_r^2) + e_d h_f h_r + e_d^2 h_f\right] \tag{A5b}$$

$$L_3 = \bar{E}_r\left[\frac{h_f h_r}{2} - e_d h_r\right] - \bar{E}_f\left[\frac{h_f h_r}{2} + e_d h_f\right] \tag{A5c}$$

A.2. Substrate Beam (Beam 2)

An analysis similar to the preceding one for the debonded beam is conducted here. The layers of the substrate beam are the lower reinforcement layer, the bottom facesheet, and the core (see Fig. 3c). J is evaluated along paths (Γ_1–Γ_3) in Fig. 5. The stress σx due to P and $M*$ (Fig. A2) can be expressed as follows:

$$\sigma_x = \begin{cases} \frac{P\bar{E}_c}{(\bar{E}h)_s} - \frac{M^*\bar{E}_c}{(D_s - B_s^2/A_s)}(y - y_{NA}); & y_2 \le y \le y_3 \quad \text{[Core]} \\ \frac{P\bar{E}_f}{(\bar{E}h)_s} - \frac{M^*\bar{E}_f}{(D_s - B_s^2/A_s)}(y - y_{NA}); & y_1 \le y \le y_2 \quad \text{[Lower Facesheet]} \\ \frac{P\bar{E}_r}{(\bar{E}h)_s} - \frac{M^*\bar{E}_r}{(D_s - B_s^2/A_s)}(y - y_{NA}); & y_0 \le y \le y_1 \quad \text{[Reinforcment]} \end{cases} \tag{A6}$$

where $(\bar{E}h)_s = \bar{E}_r h_r + \bar{E}_f h_f + \bar{E}_c h_c$. The location of the neutral axis ($y_{\text{NA}} = B/A$) for the substrate beam (beam 2) is shown in Fig. A2.

Substituting Eq. (A6) into Eq. (15) for each path (Γ_1–Γ_3),

$$\begin{aligned} J_{\Gamma 1} &= \frac{1}{2\bar{E}_c}\int_{y_2}^{y_3}\left(\frac{P\bar{E}_c}{(\bar{E}h)_s} - \frac{M^*\bar{E}_c}{H_s}(y - e_s)\right)^2 \cdot \mathrm{d}y \\ &= \frac{P^2\bar{E}_c h_c}{2(\bar{E}h)_s^2} + \frac{M^{*2}\bar{E}_c}{2H_s^2}\left[\frac{h_c}{12}\left(3h_r^2 + 6h_r h_f + h_c^2 + 3h_f^2\right) - e_s h_c(h_f + h_r) + e_s^2 h_c\right] \\ &\quad - \frac{PM^*\bar{E}_c}{(\bar{E}h)_s H_s}\left[\frac{h_c(h_f + h_r)}{2} - e_s h_r\right] \end{aligned} \tag{A7a}$$

$$\begin{aligned} J_{\Gamma 2} &= \frac{1}{2\bar{E}_f}\int_{y_1}^{y_2}\left(\frac{P\bar{E}_f}{(Eh)_s} - \frac{M^*\bar{E}_f}{H_s}(y - e_s)\right)^2 \cdot \mathrm{d}y \\ &= \frac{P^2\bar{E}_f h_f}{2(\bar{E}h)_s^2} + \frac{M^{*2}\bar{E}_f}{2H_s^2}\left[\frac{h_f}{12}(3h_r^2 - 6h_r h_c + 3h_c^2 + h_f^2) - e_s h_f(h_r - h_c) + e_s^2 h_f\right] \\ &\quad + \frac{PM^*\bar{E}_f}{(\bar{E}h)_s H_s}\left[\frac{h_f(h_c - h_r)}{2} + e_s h_f\right] \end{aligned} \tag{A7b}$$

$$\begin{aligned} J_{\Gamma 3} &= \frac{1}{2\bar{E}_r}\int_{y_0}^{y1}\left(\frac{P\bar{E}_r}{(\bar{E}h)_s} - \frac{M^*\bar{E}_r}{H_s}(y - e_s)\right)^2 \cdot \mathrm{d}y \\ &= \frac{P^2\bar{E}_r h_r}{2(\bar{E}h)_s^2} + \frac{M^{*2}\bar{E}_r}{2H_s^2}\left[\frac{h_r}{12}(h_r^2 + 3h_c^2 + 6h_c h_f + 3h_f^2) + e_s h_r(h_c + h_f) + e_s^2 h_r\right] \\ &\quad + \frac{PM^*\bar{E}_r}{(\bar{E}h)_s H_s}\left[\frac{h_r(h_c + h_f)}{2} + e_s h_r\right] \end{aligned} \tag{A7c}$$

J for the substrate beam is obtained by a summation of contributions from the individual layers:

$$J_{\text{Substrate}} = J_{\Gamma 1} + J_{\Gamma 2} + J_{\Gamma 3} \tag{A8}$$

Substitution yields:

$$J_{\text{Substrate}} = \frac{P^2}{(\bar{E}h)_s^2} V_1 + \frac{M^{*2}}{H_s^2} V_2 + \frac{PM^*}{(\bar{E}h)_s H_s} V_3 \tag{A9}$$

where

$$V_1 = \frac{1}{2}\left(\bar{E}_c h_c + \bar{E}_f h_f + \bar{E}_r h_r\right) \tag{A10a}$$

$$\begin{aligned} V_2 &= \frac{\bar{E}_c}{2}\left[\frac{h_c}{12}(3h_r^2 + 6h_r h_f + 3h_f^2 + h_c^2) - e_s h_c(h_f + h_r) + e_s^2 h_c\right] \\ &\quad + \frac{\bar{E}_f}{2}\left[\frac{h_f}{12}(3h_r^2 - 6h_r h_c + h_f^2 + 3h_c^2) - e_s h_f(h_r - h_c) + e_s^2 h_f\right] \\ &\quad + \frac{\bar{E}_r}{2}\left[\frac{h_r}{12}(h_r^2 + 6h_f h_c \quad + 3h_f^2 + 3h_c^2) + e_s h_r(h_c + h_f) + e_s^2 h_r\right] \end{aligned} \tag{A10b}$$

$$V_3 = \bar{E}_c\left[\frac{h_c(h_f + h_r)}{2} - e_s h_c\right] + \bar{E}_f\left[\frac{h_f(h_r - h_c)}{2} - e_s h_f\right] - \bar{E}_r\left[\frac{h_r(h_c + h_f)}{2} + e_s h_r\right] \tag{A10c}$$

where $H_s = (D_s - B_s^2/A_s)$; and $e_s = y_{\text{NA}}$ (neutral axis in Fig. A2).

Now, M^* can be expressed in terms of M_d as $M^* = M_d + P\Delta_1$ [see Eq. (2)]. Substitution for M^* in Eq. (A9) yields the following:

$$\begin{aligned} J_{\text{Substrate}} &= \frac{P^2}{(\bar{E}h)_s^2} V_1 + \frac{(M_d + P\Delta_1)^2}{H_s^2} V_2 + \frac{P(M_d + P\Delta_1)}{(\bar{E}h)_s H_s} V_3 \\ &= \frac{P^2}{(\bar{E}h)_s^2} V_1 + \frac{M_d^2}{H_s^2} V_2 + \frac{P^2\Delta_1^2}{H_s^2} V_2 + \frac{2M_d P\Delta_1}{H_s^2} V_2 \\ &\quad + \frac{M_d P\Delta_1}{(\bar{E}h)_s H_s} V_3 + \frac{P^2\Delta_1^2}{(\bar{E}h)_s H_s} V_3 \end{aligned} \tag{A11}$$

The J integrals for both substrate and debonded beams are summed to obtain the total J as follows:

$$J = G = J_{\text{Debonded}} + J_{\text{Substrate}} = J_1 + J_2 + J_3 + J_9 + J_{10} \tag{A12}$$

Substituting Eqs. (A4) and (A11) into Eq. (A12),

$$G = P^2\left(\frac{L_1}{(\bar{E}h)_d^2} + \frac{V_1}{(\bar{E}h)_s^2} + \frac{V_2\Delta_1^2}{H_s^2} + \frac{V_3\Delta_1}{(\bar{E}h)_s H_s}\right) + M_d^2\left(\frac{L_2}{H_d^2} + \frac{V_2}{H_s^2}\right) + M_d P\left(\frac{2V_2\Delta_1}{H_s^2} + \frac{L_3}{(\bar{E}h)_d H_d} + \frac{V_3}{(\bar{E}h)_s H_s}\right) \tag{A13}$$

Appendix B: Homogenization of Laminate Facesheet

Several sandwich panels employ multidirectional composite laminates; see Fig. B1. The analysis presented here assumes an isotropic constituent where E_f refers to Young's modulus of an isotropic material. To use the analysis presented here for sandwich specimens with composite laminate facesheets, a homogenized modulus should be appropriate.

The homogenized modulus may be computed using a laminated plate theory [26]. For an element of a laminate, the stress resultants may be expressed as follows:

$$\begin{Bmatrix} N \\ M \end{Bmatrix} = \begin{bmatrix} A & B \\ B & D \end{bmatrix} \begin{Bmatrix} \varepsilon^0 \\ \kappa \end{Bmatrix} \tag{B1}$$

where ε° are the midsurface strains, and κ are the midsurface curvatures. A, B, and D represent the extensional, coupling, and bending stiffness matrices of the laminate. It should be noted that symmetrical laminates are considered for this evaluation; hence, $B = 0$. The 6×6 matrix in Eq. (B1) may be inverted to obtain the following compliance matrix:

$$\begin{bmatrix} \varepsilon_x^0 \\ \varepsilon_y^0 \\ \gamma_{xy}^0 \\ \kappa_x \\ \kappa_y \\ \kappa_{xy} \end{bmatrix} = \begin{bmatrix} a_{11} & a_{12} & a_{16} & 0 & 0 & 0 \\ a_{12} & a_{22} & a_{26} & 0 & 0 & 0 \\ a_{16} & a_{26} & a_{66} & 0 & 0 & 0 \\ 0 & 0 & 0 & d_{11} & d_{12} & d_{16} \\ 0 & 0 & 0 & d_{12} & d_{22} & d_{26} \\ 0 & 0 & 0 & d_{16} & d_{26} & d_{66} \end{bmatrix} \begin{bmatrix} N_x \\ N_y \\ N_{xy} \\ M_x \\ M_y \\ M_{xy} \end{bmatrix} \tag{B2}$$

By subjecting the laminate strip to an axial load N_x only, the extension strain becomes the following:

$$\varepsilon_x^0 = a_{11} N_x \tag{B3}$$

The effective extensional stiffness can be written as follows:

$$E_x^e = \frac{\sigma_x}{\varepsilon_x^0} = \frac{N_x}{h a_{11} N_x} = \frac{1}{h a_{11}} \tag{B4}$$

Similarly, by applying only the moment about the x axis, the curvature can be expressed in terms of moment M as follows:

$$\kappa_x = \frac{M}{E_x^f} = M_x d_{11} \tag{B5}$$

With $I = wh^3/12$ and $M_x = M/w$, this analysis provides the effective flexural modulus:

$$E_x^f = \frac{12}{d_{11} h^3} \tag{B6}$$

The average values of E_x^e and E_x^f may be used to replace E in the analysis.

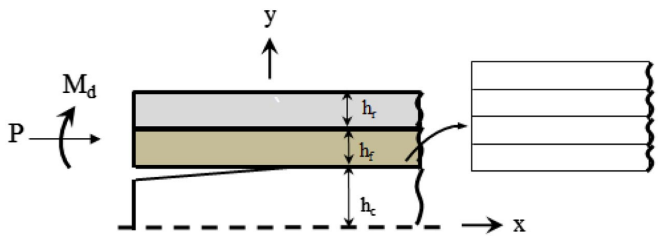

Fig. B1 Schematic of typical face laminate.

Acknowledgments

The financial support from the Danish Centre for Composite Structures and Materials, funded by the Danish Innovation Foundation (grant 09-067212), is gratefully acknowledged. Furthermore, the financial support of the Otto Mønsted Foundation (grant 16-70-0970) to the first author for his visit to Florida Atlantic University is gratefully acknowledged. The third author received support from the National Institute of Aerospace (NIA) and the Office of Naval Research (ONR), U.S. Navy. The NIA and ONR Program Managers, Ronald Krueger and Yapa Rajapakse, showed keen interest in this project and are gratefully acknowledged.

References

[1] Carlsson, L. A., Sendlein, L. S., and Merry, S. L., "Characterization of Face Sheet/Core Shear Fracture of Composite Sandwich Beams," *Journal of Composite Materials*, Vol. 25, No. 1, 1991, pp. 101–116.

[2] Prasad, S., and Carlsson, L. A., "Debonding and Crack Kinking in Foam Core Sandwich Beams—II. Experimental Investigation," *Engineering Fracture Mechanics*, Vol. 47, No. 6, 1994, pp. 825–841.

[3] Li, X., and Carlsson, L. A., "The Tilted Sandwich Debond (TSD) Specimen for Face/Core Interface Fracture Characterization," *Journal of Sandwich Structures and Materials*, Vol. 1, No. 1, 1999, pp. 60–75.

[4] Ratcliffe, J., and Cantwell, W. J., "Center Notch Flexure Sandwich Geometry for Characterizing Skin-Core Adhesion in Thin-Skinned Sandwich Structures," *Journal of Reinforced Plastics and Composites*, Vol. 20, No. 11, 2001, pp. 945–970.

[5] Quispitupa, A., Berggreen, C., and Carlsson, L. A., "On the Analysis of a Mixed Mode Bending Sandwich Specimen for Debond Fracture Characterization," *Engineering Fracture Mechanics*, Vol. 76, No. 4, 2009, pp. 594–613.

[6] Cantwell, W. J., Broster, G., and Davies, P., "The Influence of Water Immersion on Skin-Core Debonding in GFRP-Balsa Sandwich Structures," *Journal of Reinforced Plastics and Composites*, Vol. 15, No. 11, 1996, pp. 1161–1172.

[7] Reeder, J. R., and Crews, J. R., "Mixed-Mode Bending Method for Delamination Testing," *AIAA Journal*, Vol. 28, No. 7, 1990, pp. 1270–1276.

[8] "Standard Test Method for Mixed Mode I-Mode II Interlaminar Fracture Toughness of Unidirectional Fiber Reinforced Polymer Matrix Composites," ASTM International STD "ASTM D6671/D6671M-13e1," West Conshohocken, PA, 2013.

[9] Quispitupa, A., Berggreen, C., and Carlsson, L. A., "Design Analysis of the Mixed Mode Bending Sandwich Specimen," *Journal of Sandwich Structures and Materials*, Vol. 12, No. 2, 2010, pp. 253–272.

[10] Rinker, M., Ratcliffe, J. G., Adams, D. O., and Krueger, R., "Characterizing Facesheet/Core Disbonding in Honeycomb Core Sandwich Structure," NASA Technical Publication TP-2013-21, 2013.

[11] Ratcliffe, J. G., and Reeder, J. R., "Sizing a Single Cantilever Beam Specimen for Characterizing Facesheet-Core Debonding in Sandwich Structure," *Journal of Composite Materials*, Vol. 45, No. 25, 2011, pp. 2669–2684.

[12] Ratcliffe, J., and Krueger, R., "Face Sheet/Core Disbonding in Sandwich Composite Components: A Road Map to Standardization: Test Method Development," *11th International Conference on Sandwich Structures*, Dania Beach, FL, May 2016.

[13] Sørensen, B. F., Jørgensen, K., Jacobsen, T. K., and Østergaard, R. C., "DCB-Specimen Loaded with Uneven Bending Moments," *International Journal of Fracture*, Vol. 141, Nos. 1–2, 2006, pp. 163–176.

[14] Østergaard, R. C., Sørensen, B. F., and Brøndsted, P., "Measurement of Interface Fracture Toughness of Sandwich Structures Under Mixed Mode Loadings," *Journal of Sandwich Structures and Materials*, Vol. 9, No. 5, 2007, pp. 445–466.

[15] Lundsgaard-Larsen, C., Sørensen, B. F., Berggreen, C., and Østergaard, R. C., "A Modified DCB Sandwich Specimen for Measuring Mixed-Mode Cohesive Laws," *Engineering Fracture Mechanics*, Vol. 75, No. 8, 2008, pp. 2514–2530.

[16] Suo, Z., and Hutchinson, J. W., "Interface Crack Between Two Elastic Layers," *International Journal of Fracture*, Vol. 43, No. 1, 1990, pp. 1–18.

[17] Kardomateas, G. A., Berggreen, C., and Carlsson, L. A., "Energy-Release Rate and Mode Mixity of Face/Core Debonds in Sandwich Beams," *AIAA Journal*, Vol. 51, No. 4, 2013, pp. 885–892.

[18] Carlsson, L. A., Matteson, R. C., Aviles, F., and Loup, D. C., "Crack Path in Foam Cored DCB Sandwich Fracture Specimens," *Composites Science and Technology*, Vol. 65, No. 15, 2005, pp. 2612–2621.

[19] Rice, J. R., "A Path Independent Integral and the Approximate Analysis of Strain Concentration by Notches and Cracks," *Journal of Applied Mechanics*, Vol. 35, No. 2, 1968, p. 379.

[20] Rice, J. R., "Elastic Fracture Mechanics Concepts for Interfacial Cracks," *Journal of Applied Mechanics*, Vol. 55, No. 1, 1988, pp. 98–103.

[21] Hutchinson, J. W., Mear, M. E., and Rice, J. R., "Crack Paralleling an Interface Between Dissimilar Materials," *Journal of Applied Mechanics*, Vol. 54, No. 4, 1987, pp. 828–832,

[22] Thouless, M. D., Evans, A. G., Ashby, M. F., and Hutchinson, J. W., "The Edge Cracking and Spalling of Brittle Plates," *Acta Metallurgica*, Vol. 35, No. 6, 1987, pp. 1333–1341.

[23] Hutchinson, J. W., and Suo, Z., "Mixed Mode Cracking in Layered Materials," *Advances in Applied Mechanics*, Vol. 29, Dec. 1991, pp. 63–191.

[24] Berggreen, C., Simonsen, B. C., and Borum, K. K., "Experimental and Numerical Study of Interface Crack Propagation in Foam-Cored Sandwich Beams," *Journal of Composite Materials*, Vol. 41, No. 4, 2006, pp. 493–520.

[25] *ANSYS Mechanical User's Guide*, ANSYS, Inc., Southpointe, PA, 2015.

[26] Carlsson, L. A., Adams, D. F., and Pipes, R. B., *Experimental Characterization of Advanced Composite Materials*, CRC Press, Boca Raton, FL, 2014, pp. 20–23.

C. Bisagni
Associate Editor

Publication P5

V. Saseendran, and C. Berggreen

Mixed-Mode Fracture Evaluation of Aerospace Grade Honeycomb Core Sandwich Specimens using the Double Cantilever Beam–Uneven Bending Moment Test Method

Journal of Sandwich Structures & Materials

Accepted: 23 April 2018
Available online: 03 June 2018
DOI: https://doi.org/10.1177/1099636218777964

Mixed Mode Fracture Evaluation of Aerospace Grade Honeycomb Core Sandwich Specimens using the DCB-UBM Test Method

Vishnu Saseendran[1] and Christian Berggreen[1]

Abstract

Fracture testing of aerospace grade honeycomb core sandwich composites is carried out using the Double Cantilever Beam specimen loaded with Uneven Bending Moments (DCB-UBM) and a DCB-UBM test rig capable of applying pure moments is utilized. Specimens with carbon fiber reinforced plastic (CFRP) face sheets are employed with a range of honeycomb core grades Nomex® and Kevlar paper. The sandwich specimens are reinforced with steel doublers to reduce excessive rotation of the face sheets. The mode-mixity phase angle pertaining to a particular ratio of moments between the two arms of the DCB specimen is determined using the numerical mode-mixity method – Crack Surface Displacement Extrapolation (CSDE) method. For Nomex® honeycomb core sandwich specimens, it is observed that the mode I interface fracture toughness increases with increase in core density. The interface fracture toughnesses for Nomex® based honeycomb cores is also compared against specimens with Kevlar paper based honeycomb cores. Crack propagation is observed at the interface just beneath the meniscus layer for the majority of the tested specimen configurations. The DCB-UBM test methodology with the concept of direct application of moments on both crack flanks has proven to have significant potential for mixed mode face/core fracture characterization of aerospace grade sandwich composites.

Keywords

DCB-UBM; Sandwich; Honeycomb; Nomex®; Face/core interface; Debond; CSDE

Introduction

Honeycomb core sandwich composites are widely used in aerospace industry and are employed in flight control surfaces as well as in several interior components. A crucial factor determining the integrity of a sandwich structure is the adhesive bonding between the face sheet and the core. The face/core debonding (or “disbonding”) can be instigated through a bird strike, hail strike, blunt body impact or tool drop, as well as during the manufacturing phase due to insufficient wetting of face and core surfaces.

[1] Department of Mechanical Engineering, Technical University of Denmark, Nils Koppels Allé, Building 404, 2800 Kgs. Lyngby, Denmark

Corresponding Author:

Vishnu Saseendran, Technical University of Denmark, 2800 Kgs. Lyngby, Denmark

E-mail: vsas@mek.dtu.dk

The presence of debonds have led to several in-service failures [1,2]. In a debonded sandwich structure, the propensity of the crack to propagate through the interface or kink into the core is driven by the loading conditions. Therefore, the critical strain energy release rate required to separate the face from the core referred to as the fracture toughness, must be ascertained accurately in order to aid in design of sandwich structural components.

The interface fracture toughness must be determined for a range of phase angles to serve as input into analysis models, as the load conditions may induce mode conditions varying from mode I to mode II and even mode III in some cases. The mode-mixity, expressed using the phase angle, ψ, can be attributed to the ratio of mode II to mode I loading at the crack tip.

Many fracture mechanical methodologies exist to characterize face/core debonding. Prasad and Carlsson [3,4] used the Double Cantilever Beam (DCB) test method to measure interface fracture properties in sandwich composites, but the inclination of the crack in a force loaded DCB test inherently depends on the face/core material system, and therefore kinking out of the interface is often in violation of the DCB sandwich test. The Tilted Sandwich Debond (TSD) test [5] evolved from the DCB test for mode I fracture testing allows the sandwich specimen to be tilted, thereby ensuring crack propagation along the interface. However, within reasonable tilt angles only a limited range of mode-mixity phase angles are possible for mixed mode face/core fracture characterization, even by reinforcing the face sheets with doubler layers [6,7]. The Single Cantilever Beam (SCB) specimen first discussed in [8,9] is also gaining popularity for mode I fracture characterization owing to its simplicity. For mode II conditions, the Cracked Sandwich Beam (CSB) test, developed by Carlsson [10] and End Notched Flexure (ENF) test introduced by Zenkert [11] have been proposed. The Mixed Mode Bending (MMB) test is capable of face/core interface characterization under mixed mode conditions [12,13]. The sandwich SCB specimen is being considered to be developed as an ASTM International test standard for mode I fracture toughness assessment [14]. Initial sizing of the sandwich SCB specimen is detailed in [15], in which the shear component at the crack tip is kept to a minimum based on kinematics of the SCB specimen. However, the mode-mixity varies with crack length in a SCB specimen. In a sandwich MMB test, depending on the geometrical and material properties of the specimen, the lever arm distance may be adjusted to perform fracture testing at several mode-mixity conditions [16]. It should be noted that, as is the case with the TSD specimen, the possible range of mode-mixity phase angle (ψ) in a MMB test is limited.

A mixed-mode fracture specimen, known as the Double Cantilever Beam loaded with Uneven or unequal Bending Moments (DCB-UBM), capable of achieving a wide array of mode-mixity conditions was first introduced by Sørensen et al. [17] for laminates, and was later to extended to sandwich composites by Lundsgaard-Larsen et al. in [18]. A schematic illustration of the sandwich DCB-UBM specimen is shown in Figure 1, in which pure moments are applied to both crack flanks. For a fixed moment ratio ($MR = M_1/M_2$), the mode-mixity phase angle (ψ)

remains constant. Therefore, by holding the moment ratio (*MR*) constant throughout the crack propagation during the fracture testing, toughness characterization can be performed at a fixed phase angle (ψ). Closed form expressions for both energy release rate and mode-mixity phase angle for an un-reinforced (see Figure 1a) [19] and reinforced (Figure 1b) [20] sandwich DCB-UBM specimens exist in the literature. Attachment of reinforcement layers, referred to as "doublers", on both sides of the specimen reduces excessive rotations and displacements, especially for specimens with thin face sheets [21].

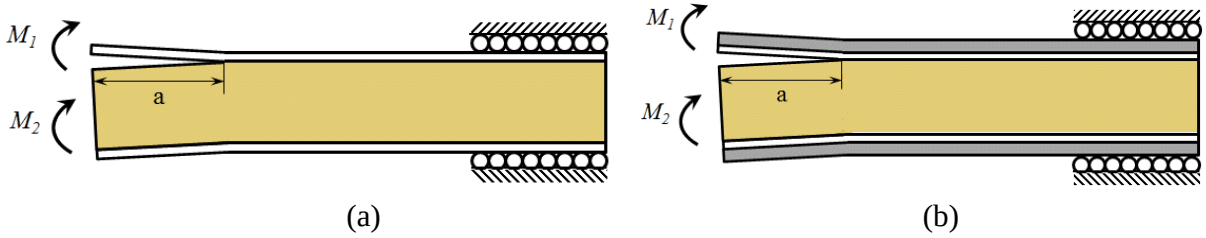

(a) (b)

Figure 1. Schematic illustration of the sandwich DCB-UBM specimen (a) un-reinforced (b) reinforced with doubler layers.

Face/core fracture toughness measurements under predominant mode I conditions of honeycomb cored sandwich specimens were previously conducted using the DCB and SCB test methods [22,23]. The objective of this paper is to perform mixed mode fracture characterization of honeycomb cored sandwich specimens using the DCB-UBM test method. The fracture testing was carried out in a novel test rig in which the moments were applied using independent torsional actuators. In order to understand the influence of core density, cell-size and core paper properties on the fracture toughness, four different classes of sandwich systems were analyzed. A detailed discussion of materials and specimen preparations are also provided.

Materials, Specimen Preparation and Test Method

Specimen preparation and material characterization

The sandwich specimens studied in this work consisted of aerospace grade honeycomb cores manufactured by Schütz GmbH. Two core types – Cormaster C1 [24] comprising of Nomex® T412 paper and Cormaster N636 [25] made of para-aramid Kevlar N636 paper were considered. Three density classes of the Cormaster C1 type (32, 64 and 96 kg/m^3) and one density class (32 kg/m^3) of the Cormaster N636 were investigated. A plain weave Carbon Fiber Reinforced Plastic (CFRP) prepreg (Hexcel fabric with HexPly®913 epoxy resin) manufactured by Hexcel corporation [26] was chosen as face sheets with two stacking sequences - [0/90] and [45/0/0/45]. The nominal cured thickness of the CFRP prepreg was 0.35 mm.

The DCB-UBM specimens (450 x 60 mm) were cut from sandwich panels which were manufactured at the Airbus Stade facility. An AF163 film adhesive [27] was used to adhere the face sheets onto the core. The sandwich panels were vacuum bagged and cured with a one shot curing (co-curing) cycle under 2 Bar pressure in an autoclave. The panel used a 125°C curing system. The adhesive film had no contribution the thickness of the face sheet and formed only the meniscus layer. DCB-UBM specimens (450 x 60 mm) were cut from each cured sandwich panel using a diamond cutter and doubler layers were glued, see Figure 2.

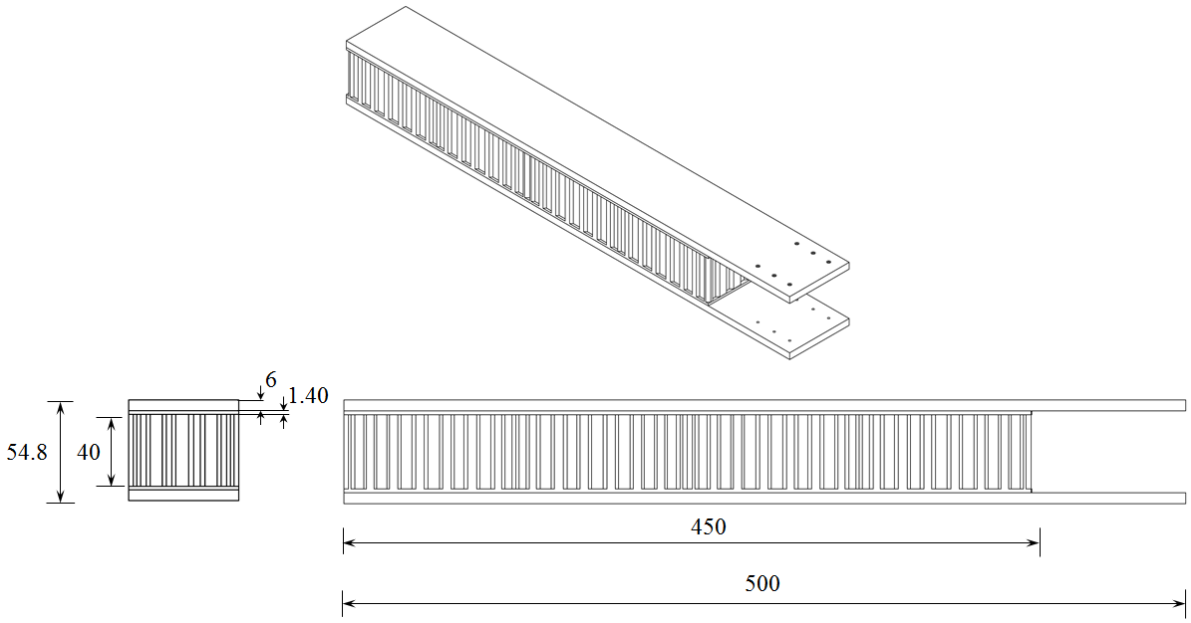

Figure 2. DCB-UBM specimen dimensions (in mm).

The DCB-UBM specimens were bonded to reinforcement layers to prevent excessive rotation of thin face sheets. Adhesion of such "doubler" material restrict the fracture analysis to be in the Linear Elastic Fracture Mechanics (LEFM) regime by preventing excessive crack tip distortions [21]. The doublers were chosen in this study such that they do not undergo yielding during fracture testing. A high strength Uddeholm IMPAX SUPREME® steel [28] (E = 210 GPa, yield strength = 900 MPa) with a thickness of 6 mm was used throughout. The steel doublers were bonded to the specimens using 3M DP460 epoxy glue [29], and was cured at room temperature for a duration of 24 hours. Clamps were employed to achieve even glue thickness and to prevent misalignment, see Figure 3(a). The prepared specimens are shown in Figure 3(b).

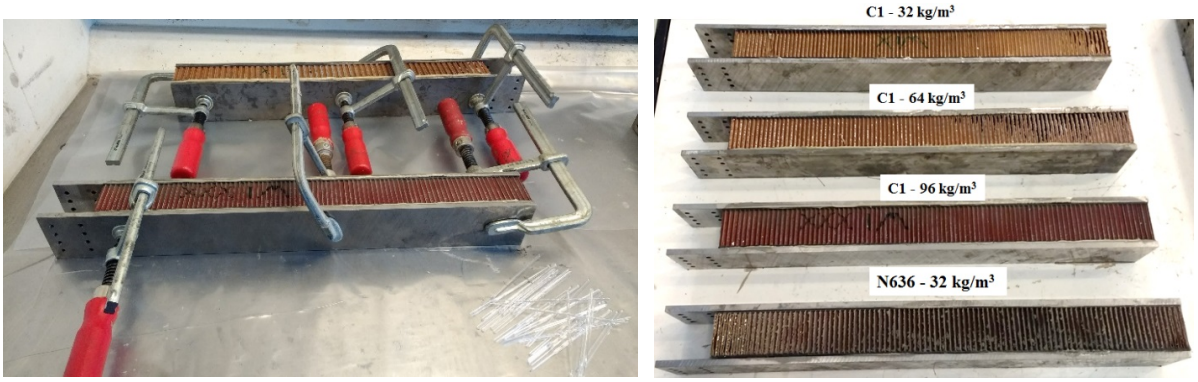

(a) (b)

Figure 3. Preparation of reinforced DCB-UBM specimens: (a) Adhesion of doubler layers to specimens with the aid of clamps, (b) prepared DCB-UBM specimens with doublers.

In this study, the influence of core density, crack propagation direction, face sheet thickness and paper material properties on the fracture toughness were investigated. Thus, a total of twenty specimens were tested including specimens with two face sheet thicknesses (h_f = 0.35 mm and 1.4 mm), three core densities (32, 64 and 96 kg/m^3) and two core paper materials (Nomex® T412 and Kevlar N636). The core thickness was constant throughout out the analysis, h_c = 40 mm. The material properties of the face sheets were determined using ASTM standard tests [30,31] at Fraunhofer IMWS, Halle [32]. The steel properties were obtained from technical data sheet [28]. The face sheet and doubler material properties are provided in Table 1, where index 1 refers to 0° direction and index 2 refers to the transverse direction.

Table 1. Material properties for face sheet and steel doubler [28,32,33].

Face sheet [0/90] h_f **= 0.35 mm**		**Face sheet [45/0/0/45]** h_f **= 1.40 mm**		**Doubler layer (Steel)** h_r **= 6.0 mm**	
E_{11} [GPa]	63.20	E_{11} [GPa]	49.30	E_r [GPa]	210
E_{22} [GPa]	48.10	E_{22} [GPa]	47.00	v_r	0.30
G_{12} [GPa]	5.27	G_{12} [GPa]	1.84		
v_{12}	0.0539	v_{12}	0.3159		

The honeycomb core material properties were estimated using the analytical expressions derived by Gibson and Ashby [34] for cellular materials. The original expressions in [34] were expanded to a wide range of honeycombs in [35] by proposing more accurate expressions based on both analytical and numerical approaches. These expressions can be applied to typical

honeycomb cores with double cell walls, such as the ones used in this study and require elastic constants of the honeycomb paper material as input. The paper properties of the various core types investigated here were measured at TU Dresden [36]. A detailed description of measurement of the core paper properties can be found in [36]. The honeycomb core properties are provided in Table 2. It should be noted that for all the core types considered in this paper, the cell size and core thickness were 4.8 mm and 40 mm respectively. Figure 4 provides a schematic illustration of cell size and cell wall thicknesses, where T refers to the cell thickness direction, L – ribbon direction and W – transverse direction. For brevity, the honeycomb core is designated as core type – cell size – density throughout this paper, e.g. C1-4.8-32 refers to Cormaster C1 type core with a 4.8 mm cell size and a density of 32 kg/m^3. The N636 core type is referred to as CN1.

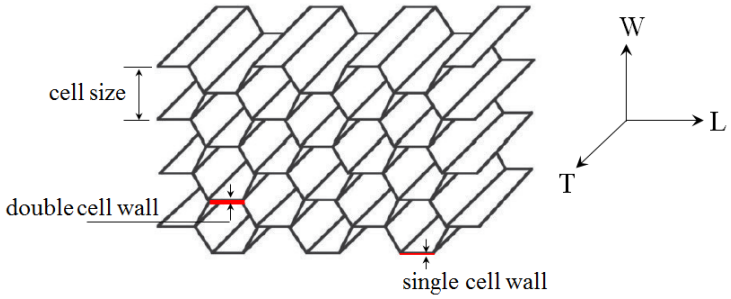

Figure 4. Schematic illustration of a typical hexagonal honeycomb core cell.

Table 2. Material properties for honeycomb cores [35,36].

	C1-4.8-32	**C1-4.8-64**	**C1-4.8-96**	**CN1-4.8-32**
E_L [MPa]	0.075	0.226	0.492	0.104
E_W [MPa]	0.075	0.226	0.492	0.104
E_T [MPa]	121.9	176.3	228.5	298.1
G_{LW} [MPa]	0.033	0.010	0.022	0.092
G_{TL} [MPa]	20.7	29.9	38.7	59.6
G_{TW} [MPa]	13.1	18.9	24.5	35.9
ν_{LW}	1.0	1.0	1.0	1.0
ν_{TL}	0.354	0.36	0.354	0.354
ν_{TW}	0.350	0.35	0.350	0.354
Density [kg/m^3]	32	64	96	32
Paper thickness, μm (single cell wall)	56	81	105	62

DCB-UBM Test Procedure

In the DCB-UBM test method pure moments are applied to the specimen edges or crack flanks, see Figure 1. Thus, the mode mixity can be altered by changing the ratio of the applied moments, $MR = M_1/M_2$. As the moment ratio, *MR*, is held constant throughout the test, the DCB-UBM test methodology is characteristically a steady-state fracture specimen. Hence, both energy release rate, *G*, and mode mixity expressed as phase angle, ψ, remain constant throughout the crack propagation. The original test rig introduced by Sørensen et al. [17] applied moments to the crack flanks using long wires. A new test rig capable of applying moments directly on the crack flanks through independent torsional actuators [37] was used in the current study. A honeycomb cored sandwich specimen mounted in the new test set up prior to testing is shown in Figure 5. Loading tabs are screwed to the doubler ends which is then slid between load arm clamps, see Figure 5. Here, the doublers also help in application of moments through loading arms. The width of clamp support was adjusted to account for the specimen thickness. The clamp support contains rollers which enable sliding of the specimen in its longitudinal direction. The new test rig is capable of achieving a wide range of moment ratios (*MR*). Moreover, the current rig is capable of applying moments up to 250 Nm, with a provision to hike the capacity to 500 Nm [37].

A MTS FlexTest ™ SE [38] controller was used to maintain the moment ratio, *MR*, throughout the test to ensure that the test is conducted at a constant mode-mixity condition. The control algorithm was programmed such that, when rotation is applied to arm-1, arm-2 follows arm-1 to satisfy a pre-defined moment ratio such that, $M_2 = M_1/MR$ (see Figure 5). The direction of rotation of each arm can be altered such that: a) both arms open relative to each other b) rotate in clock-wise direction with respect to plane of paper or c) rotate in counter clock-wise direction. The selection of *MR* pertaining to a particular mode-mixity condition for a particular sandwich configuration was obtained numerically. The mode-mixity expressed as phase angle (ψ), was obtained using the numerical mode separation method – Crack Surface Displacement Extrapolation Method (CSDE) [39]. A detailed description of the selection of a *MR* to obtain a specific phase angle (ψ), is provided in Appendix A. A pre-crack length of 50 mm was introduced at the face/core interface of each specimen using a band-saw. This procedure enabled introduction of the crack along the face/core interface just above the meniscus layer. To produce a clean crack front, the crack front was further sharpened by using a very thin razor blade.

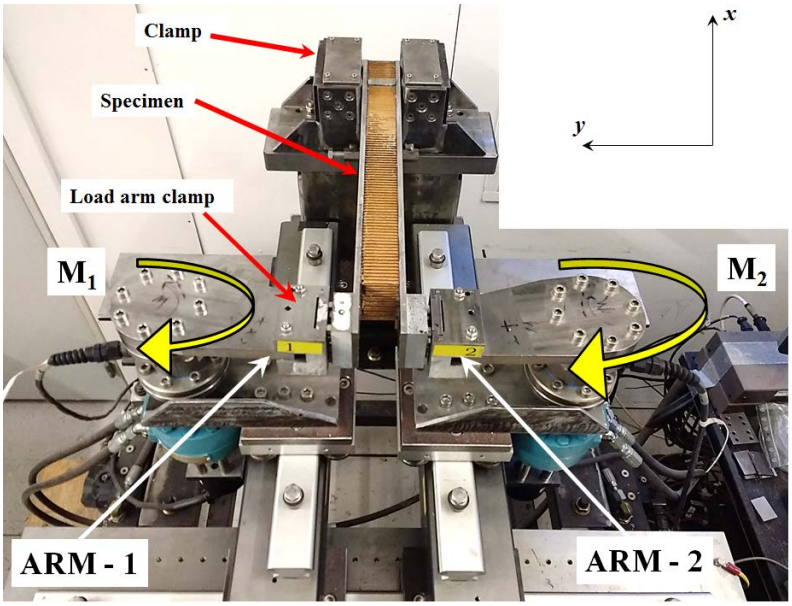

Figure 5. DCB-UBM test rig with a honeycomb core sandwich specimen held between both arms prior to testing.

All specimens were loaded in rotation control at a quasi-static rate of 10° /min. The loading was continued until the disbond grew by ~10 mm (approximately two cells), following which the specimens were un-loaded manually. The crack propagation in a DCB-UBM specimen occurs at constant mode-mixity. Therefore, a single specimen may be employed to perform fracture characterization at multiple mode mixity conditions.

Rotation (θ) and moment (M) of both arms were continuously logged during each load cycle at a fixed rate of 5 Hz. The crack increment of each loading cycle was marked on the doubler edges. It should be noted that the energy release rate in a DCB-UBM specimen is independent of crack length. Therefore, accurate monitoring of the crack front using high resolution cameras is not required as opposed to other test methods such as the DCB, SCB or MMB. Moreover, the crack initiation can be noted from the deviation in slope in the M vs. θ plot. The detailed data reduction procedure is outlined in the next section.

Data Reduction Method

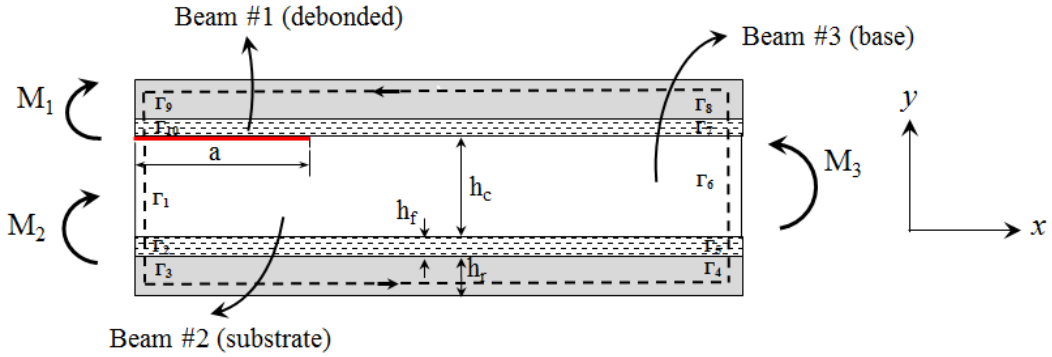

Figure 6. *J*-integral path in the DCB-UBM sandwich specimen reinforced with steel doubler layers.

The recorded moments were used to compute the energy-release rate and the fracture analysis was carried out under the ambit of the LEFM regime. For a DCB-UBM sandwich specimen reinforced with doubler layers, the energy-release rate can be expressed using the path independent *J*-integral [40], derived by Lundsgaard et al. [18] as:

$$J = \sum_{p=1}^{10} \frac{\bar{E}_p M_b^2}{6\left(A_b D_b - B_b^2\right)^2}\left[A_b^2\left(y_{p-1}^3 - y_p^3\right) - 3A_b B_b\left(y_{p-1}^2 - y_p^2\right) + 3B_b^2\left(y_{p-1} - y_p\right)\right] \quad (1)$$

where *A*, *B* and *D* are extensional, bending and coupling terms, y_k is the distance between the neutral axis between ply *k* and *k -1*. The subscript "*b*" refers to each beam, whilst "*p*" refers to the path evaluated using the *J*-integral (Equation 1), as shown in Figure 6. It can be noted in Equation (1) that the energy-release rate is independent of the crack length, a. The energy release rate contribution for each beam can be obtained using Equation (1) and summed to calculate the total energy release rate as: $J = G = J_1 + J_2 + J_3$. A detailed derivation is provided in Appendix B.

A typical loading curve (M_1 vs. θ_1) of the debonded beam is shown in Figure 7 for a CFRP/C1-4.8-32 core specimen with 1.4 mm thick face sheet. The energy-release rate, *G*, was obtained using Equation (1) was plotted against rotation, θ_1, of the debonded beam. When the crack starts to propagate, the slope drops sharply and nearly approaches zero. Thus, the initiation fracture toughness, Γ, can be identified from the deviation of the slope in the *G* vs. θ_1 plot (see Figure 7b). This approach is qualitatively akin to finding the delamination initiation toughness in the standard DCB test (ASTM D5528) [41]. A MATLAB code was employed to substitute moments in Equation (1) and to identify the departure of the slope in *G* vs. θ_1 plot. The deduced initiation fracture toughness was recorded for a range of mode mixity conditions to create a map of the interface fracture toughness as a function of phase angle, $\Gamma(\psi)$.

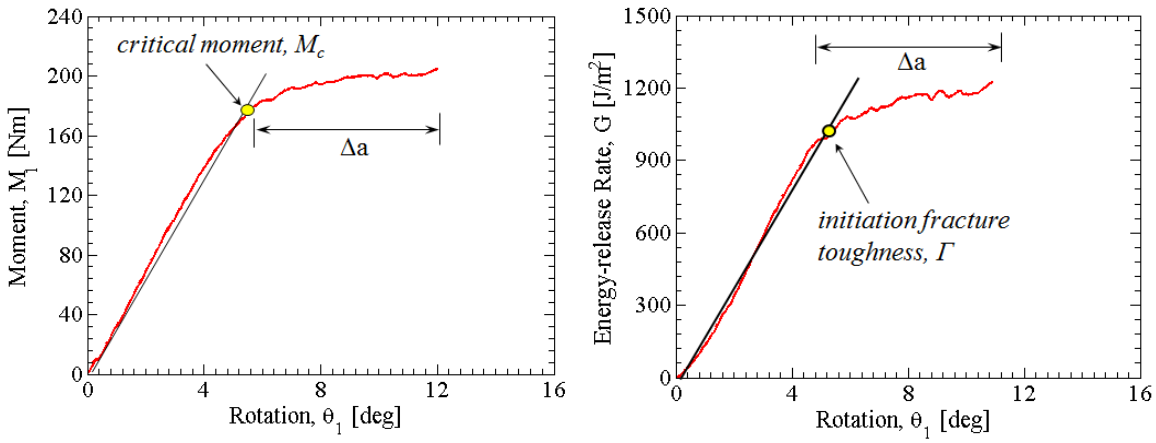

(a) (b)

Figure 7. Typical moment and energy-release rate plots for a CFRP/C1-4.8-32 honeycomb cored specimen with h_f = 1.4 mm, h_c = 40 mm: (a) Moment, M_1 vs. Rotation, θ_1, and (b) Energy release rate, G vs. Rotation, θ_1 of the debonded beam.

Experimental Results and Discussion

Testing was carried out on the prepared DCB-UBM sandwich specimens and fracture toughness was calculated using the proposed data reduction scheme. The influence of various parameters on the fracture toughness such as core density, face sheet thickness, core paper material properties and crack propagation direction were studied. Prior to start of each test, the moment ratio (*MR*) pertaining to a specific mode-mixity phase angle (ψ) has to be provided as input. The phase angle (ψ) for each specimen type was obtained numerically (refer to Appendix A). Table 3 provides a list of *MR* values and the corresponding phase angles for each specimen type tested. Each specimen was loaded at a constant rate of 10 °/min until crack propagation occurred and was un-loaded manually. DCB-UBM fracture testing for a CFRP/C1-4.8-64 honeycomb core specimen at *MR* = 2 (ψ = -35°) is shown in Figure 8.

To collect ample amount of datasets, the test was repeated several times at a specific *MR* on a single specimen which resulted in a crack increment of 10 mm for each cycle. In Table 3, *MR* < 0 corresponds to arms opening relative to each other and *MR* > 0 refers to arms rotating in the clock-wise direction (see Figures 5 and 6). In terms of the phase angle values (in degrees) a pure mode I scenario corresponds to 0°, whilst a pure mode II loading exist at 90°. Mode I dominance can be assumed within the bounds: $-10° \leq \psi \leq 10°$.

Table 3. Moment ratio (*MR*) chosen for the tested DCB-UBM honeycomb cored specimens with various core types. Phase angle (ψ) is provided in parenthesis.

Core Type	Moment Ratio (ψ [deg])
W - direction	
C1-4.8-32 (h_f = 0.35 mm)	1 (-49°), 1.5(-40°), 2 (-32°), 3 (-24°), 5 (-19°), -20 (-6°), -10 (-4°)
C1-4.8-32 (h_f = 1.40 mm)	1 (-52°), 2 (-35°), 3 (-29°), 10 (-20°), -20 (-14°), -10 (-12°), -3 (-2°)
C1-4.8-64 (h_f = 1.40 mm)	1 (-52°), 2 (-35°), 3 (-29°), 10 (-20°), -20 (-14°), -3 (-2°)
C1-4.8-96 (h_f = 1.40 mm)	2 (-36°), 3 (-29°), -3 (-8°), -3 (-2°)
CN1-4.8-32 (h_f = 1.40 mm)	1 (-54°), 2 (-36°), 7.5 (-21°), 10 (-18°), -6 (-6°)
L - direction	
C1-4.8-32 (h_f = 0.35 mm)	1 (-49°), 2 (-32°), 5 (-19°), 15 (-12°), -20 (-6°), -10 (-4°)
C1-4.8-32 (h_f = 1.40 mm)	1 (-49°), 2 (-32°), 3 (-24°), 5 (-19°), -20 (-6°), -10 (-4°), -7.5 (-2°)
C1-4.8-64 (h_f = 1.40 mm)	1 (-52°), 2 (-35°), 3 (-29°), 10 (-20°), -20 (-14°), -3 (-2°)
C1-4.8-96 (h_f = 1.40 mm)	2 (-36°), 5 (-25°), -20 (-17°), -5 (-12°), -3 (-2°)
CN1-4.8-32 (h_f = 1.40 mm)	1 (-54°), 2 (-36°), 7.5 (-21°), 10 (-18°), -20 (-12°), -6 (-6°)

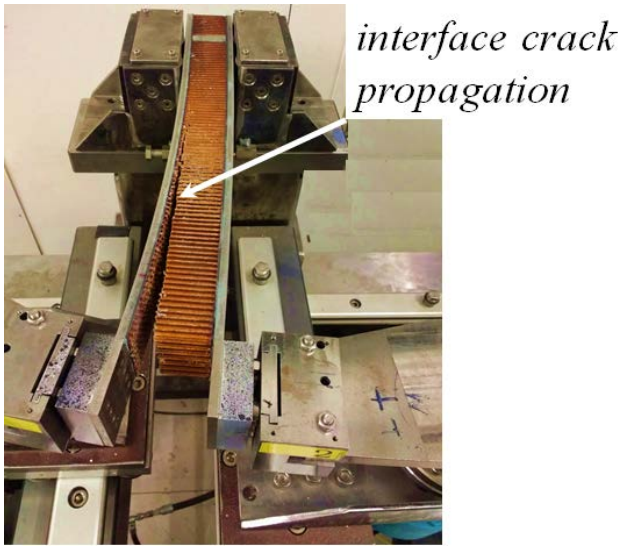

Figure 8. Face/core interface crack propagation at *MR* = 2 (ψ = -35°) for CFRP/C1-4.8-64 honeycomb core specimen (L-direction) with h_f = 1.4 mm, h_c = 40 mm.

Effect of honeycomb core density on fracture toughness, Γ

To study the influence of the honeycomb core density on the interface fracture toughness, three core densities (32, 64 and 96 kg/m^3) of the Cormaster C1 type core were examined. The cores were composed of Nomex® T412 paper material with face sheet and core thickness, h_f = 1.4 mm and h_c = 40 mm, respectively. Fracture toughness measurements were carried out at several mode-mixity conditions (refer to Table 3) and is shown as a function of phase angle (ψ) in Figure 9. The experimental interface toughness data was fitted with the general expression provided by Hutchinson and Suo [42]:

$$\Gamma(\psi) = G_{1c}\left(1+\tan^2\left[(1-\Lambda)\psi\right]\right) \tag{2}$$

where G_{1c} is the mode I interface toughness, Γ (ψ = 0°) and Λ is a dimensionless constant. The interface fracture toughness in Figure 9 was fitted (by eye) using Equation (2) and the measured mode I fracture toughness, G_{1c}. The curve fitting dimensionless constant, Λ are provided in each plot. Testing were performed in both L and W directions, commonly referred to as the ribbon and transverse directions, respectively. It is observed that the fracture toughness (Γ) in W-direction was consistently higher than the L-direction for all the density classes studied here (see Figure 9). This is due to cell wall alignment (see Figure 4) with respect to crack propagation. When the crack advances in the W-direction, there are more cell wall material compared to the ribbon direction. In addition, at a constant mode mixity phase angle (ψ) and a given crack propagation direction, the fracture toughness, Γ, was seen to increase with rise in core density. Furthermore and as expected, the fracture toughness increases with increase in phase angle (ψ). Thus, at higher values of ψ higher moment values are required to initiate crack propagation.

For a given mode mixity phase angle (ψ) and crack propagation direction, specimens with the 96 kg/m^3 dense core exhibited the highest interface fracture toughness while the lowest toughness was obtained for the specimen with 32 kg/m^3 dense core. At increased mode-mixity scenarios into the negative phase angle regime, higher moment magnitudes are required for crack propagation. For specimens with 96 kg/m^3 dense honeycomb core, fracture testing was carried out only until a mixed-mode regime of ψ = -32°. The magnitude of moments needed to propagate a crack in predominant mode II conditions are higher. The carriage plates supporting the actuators were designed to carry a load up to 275 Nm. Hence, for the denser core cases testing were limited until the mixed-mode regime. Whereas, for other core types testing was carried out at predominant mode I, mixed-mode I/II and predominant mode II conditions.

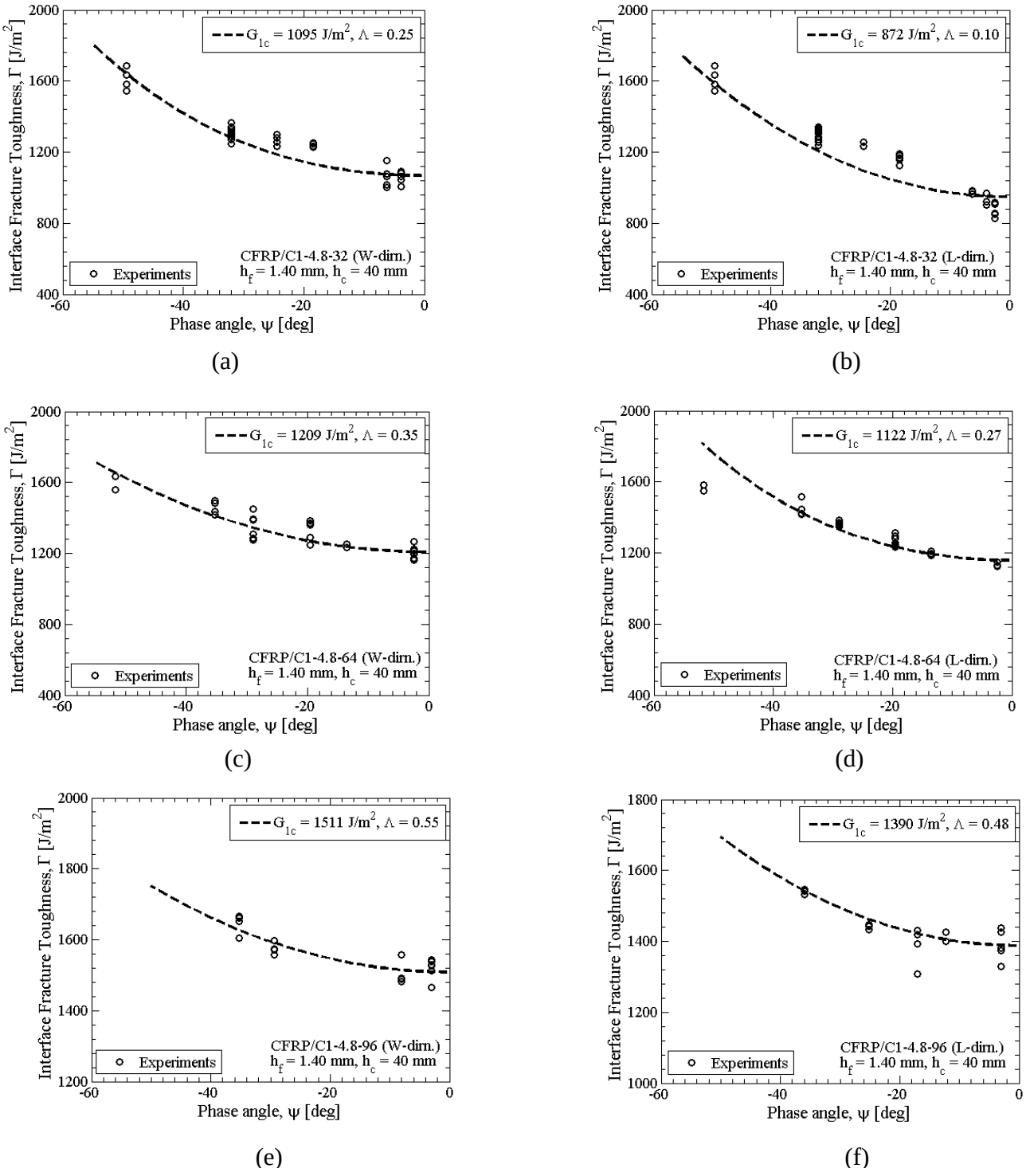

Figure 9. Interface fracture toughness as a function of mode mixity phase angle (ψ) for CFRP/C1 type honeycomb core sandwich specimens with densities: (a) 32 kg/m^3 (W-direction), (b) 32 kg/m^3 (L-direction), (c) 64 kg/m^3 (W-direction), (d) 64 kg/m^3 (L-direction), (e) 96 kg/m^3 (W-direction), and (f) 96 kg/m^3 (L-direction).

The crack path in a honeycomb sandwich face/core interface is highly non-uniform. For most of the tested cases, crack propagation was observed to occur at the face/core interface just beneath the meniscus layer. The toughness data shown in Figure 9 shows scatter which may be attributed to the crack propagation through resin rich cells. A schematic illustration of this typical behavior is provided in Figure 10b. During the sandwich panel manufacturing process, the epoxy adhesive layer is amassed at the face/core interface creating a local resin profile in the cells [43], which affects the crack advancement path. It was observed that when the crack propagates through the core and encounter the meniscus layer, it dives back again to the interface to continue further advancement. Figure 10(a) shows such a behavior of crack switching between interface-core-interface to avoid resin rich cells in a C1-4.8-32 honeycomb core specimen. This was further confirmed upon inspection of fracture surfaces after testing, see Figure 10(c).

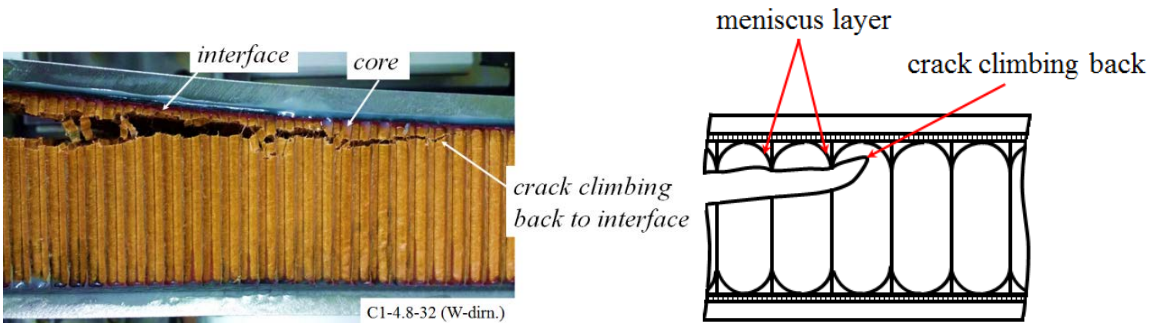

(a) (b)

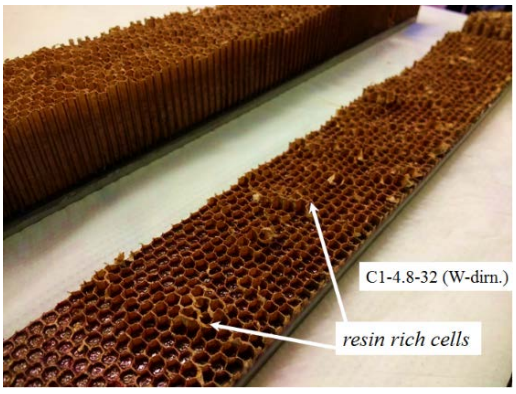

(c)

Figure 10. CFRP/C1-4.8-32 honeycomb core specimen, h_f = 1.4 mm, h_c = 40 mm: (a) crack propagation through interface-core-interface regions at MR = 5 (ψ = -19°), (b) schematic illustration of crack advancement just beneath the meniscus layer, and (c) fracture surface with resin rich pockets.

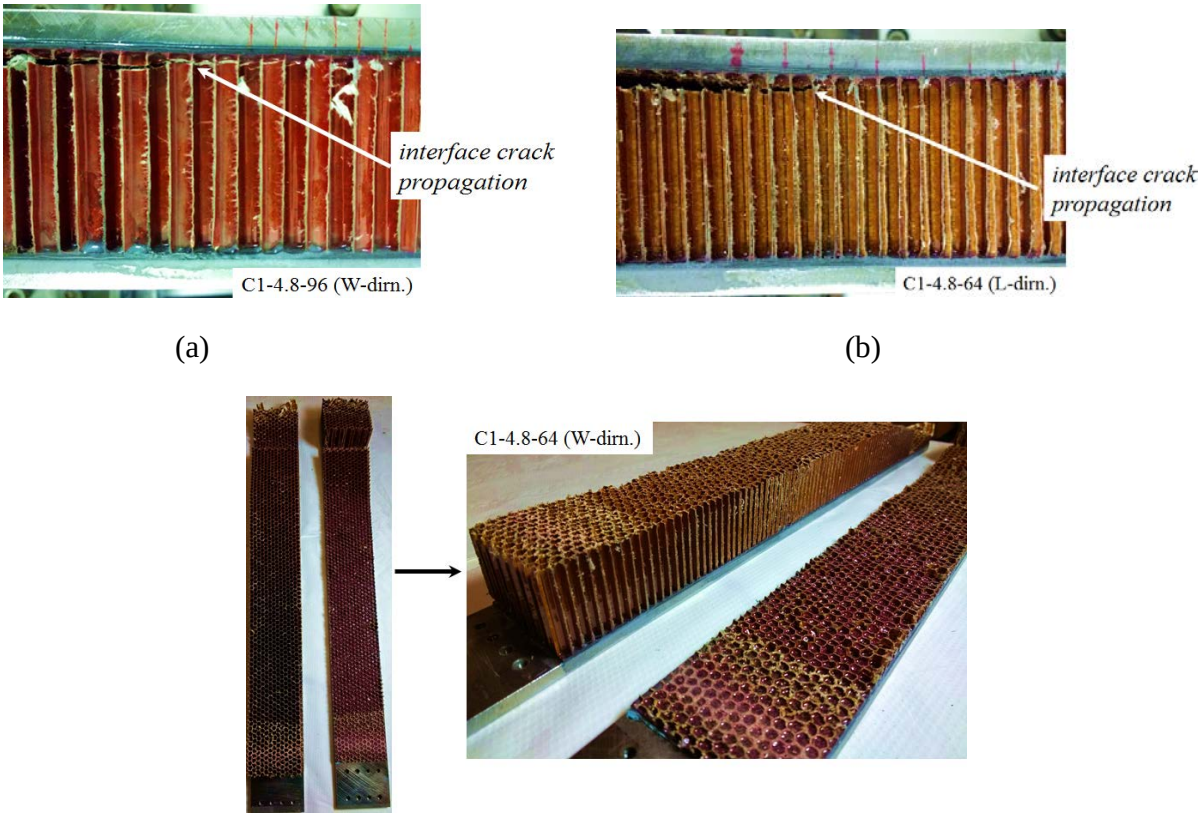

Figure 11. Face/core interface crack propagation for: (a) CFRP/C1-4.8-96 (W-direction) core specimen at *MR* = -5 (ψ = -12°), (b) CFRP/C1-4.8-64 (L-direction) core specimen at *MR* = 10 (ψ = -20°), and (c) fracture surface of C1-4.8-64 (W-direction).

Figures 11 (a) and (b) show the crack propagation paths in DCB-UBM specimens with 64 and 96 kg/m^3 dense honeycomb cores. Figure 11(c) shows fracture surfaces for a specimen with C1-4.8-64 type core. The fracture surfaces showed similar characteristics as that of the 32 kg/m^3 cored specimens. As with previous case, the crack propagated just beneath the meniscus layers (see Figures 11(a) and (b)).

A comparison of the mode I fracture toughness of specimens with three core densities, namely 32, 64 and 96 kg/m^3 of the Cormaster C1 core type was undertaken. In terms of the phase angle, ψ, pure mode I conditions can be assumed to exist in the range, $-10° \leq \psi \leq 10°$. Fracture toughness obtained from mode I dominant tests for both L- and W- directions were compared across core densities, and are provided in Figure 12. It must be noted that the face sheet and core thickness were constant across all core densities at, h_f = 1.4 mm and h_c = 40 mm respectively. Moreover, all the core types considered in this section were made from Nomex® T412 paper sheets. A highest mode I fracture toughness of 1511 J/m^2 was measured for the 96 kg/m^3 dense core in the W direction, and a lowest value of 872 J/m^2 was obtained for the 32 kg/m^3 core type

in the L direction. The 96 kg/m^3 dense core specimens exhibited highest coefficient of variation, CV, in both L and W directions (see Figure 12).

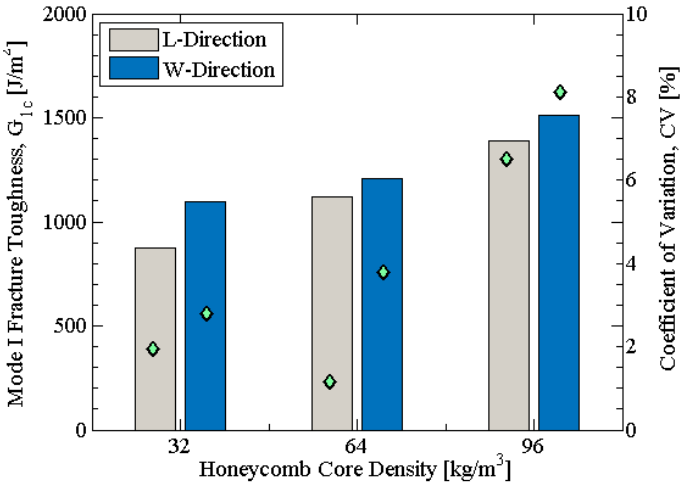

Figure 12. Mode I fracture toughness and coefficient of variation, CV, in L and W crack propagation directions for CFRP/C1 type core with various densities; h_f = 1.4 mm, h_c = 40 mm.

Effect of face sheet thickness on fracture toughness, Γ

Fracture characterization of CFRP/C1-4.8-32 honeycomb core specimens with a thinner face sheet, h_f = 0.35 mm was performed and compared with interface toughness values obtained for specimens with the thicker face sheet, h_f = 1.4 mm. Testing was carried out in both W and L directions for the thin face sheet CFRP/C1-4.8-32 cored specimens at several mode mixity phase angle (ψ) values. Equation (2) was employed to plot the fracture toughness as a function of phase angle, and is provided in Figure 13. The curve fitting was performed by eye and the dimensionless constant, Λ, along with mode I interface toughness, G_{1c}, are provided in the plot. Refer to Table 3 for the tested moment ratio (*MR*) and the corresponding phase angle (ψ) for specimens in both crack propagation directions (L and W). Similar to previous tests scatter in the data was observed.

Similar to specimens with thicker face sheets, the interface fracture toughness in the W direction is higher compared to the L direction. The toughness ranged from 1500 to 2400 J/m^2 for the W direction and from 1200 to 2300 J/m^2 for the L direction case. The fracture toughness values are higher compared to the specimens with thicker face sheets. A comparison was also made against mode I fracture toughness, G_{1c}, of specimens with thicker face sheet and same core density, see Figure 14. A toughness value of 1510 J/m^2 in the W direction and 1240 J/m^2 in the L direction were recorded. Coefficient of variation, CV was observed to be higher for specimens with the

thinner face sheets in both crack propagation directions. A highest CV of 4% was obtained for the thinner face sheet specimens in the L crack propagation direction.

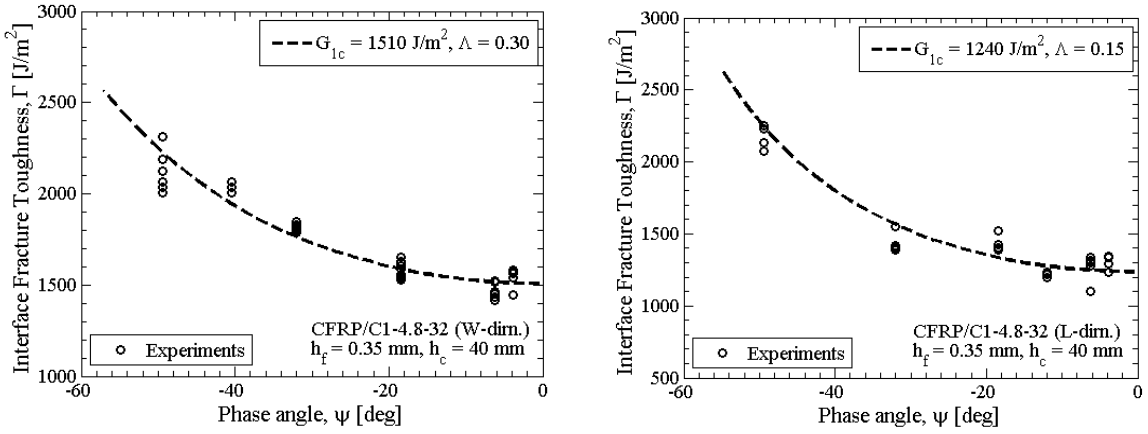

Figure 13. Fracture toughness (Γ) vs. phase angle (ψ) for a CFRP/C1-4.8-32 honeycomb core sandwich specimen with h_f = 0.35 mm and h_c = 40 mm: (a) W direction, (b) L direction.

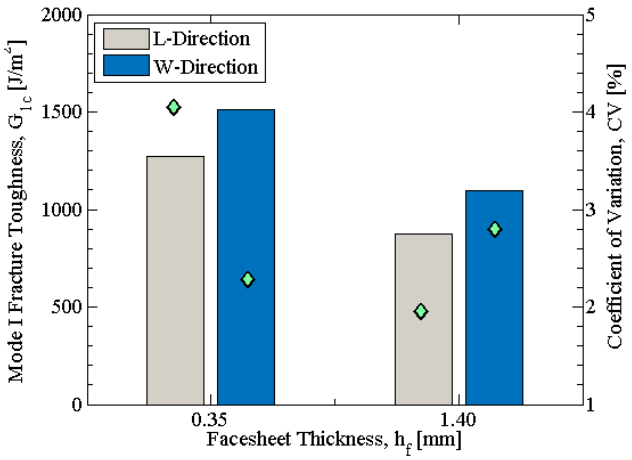

Figure 14. Mode I fracture toughness and coefficient of variation, CV, in L and W crack propagation directions for CFRP/C1-4.8-32 honeycomb core specimens; h_c = 40 mm and h_f = 0.35 and 1.4 mm.

Figure 15(a) shows a typical crack propagation path for CFRP/C1-4.8-32 honeycomb cored specimens with face sheets of h_f = 0.35 mm. Interface crack propagation was observed at all phase angles and the crack surface region is shown in Figure 15(b). It was also observed that the epoxy adhesive had trickled down into the cells during sandwich panel fabrication creating a

localized resin rich pocket as shown in Figure 15(c). The crack path shifted into the core, away from the face/core interface to circumvent this localized zone and climbed back to the surface again to resume propagation along the interface. This behavior was similar to what was observed in specimens with thicker face sheets (h_f = 1.4 mm). The higher fracture toughness for specimens with thinner face sheets may be attributed to the crack propagation occurring very close to the face sheet through the meniscus layer (see Figure 16(a)). In the case of specimens with thicker face sheets, the crack propagates well beneath the meniscus layer with more core residue, see Figure 16(b).

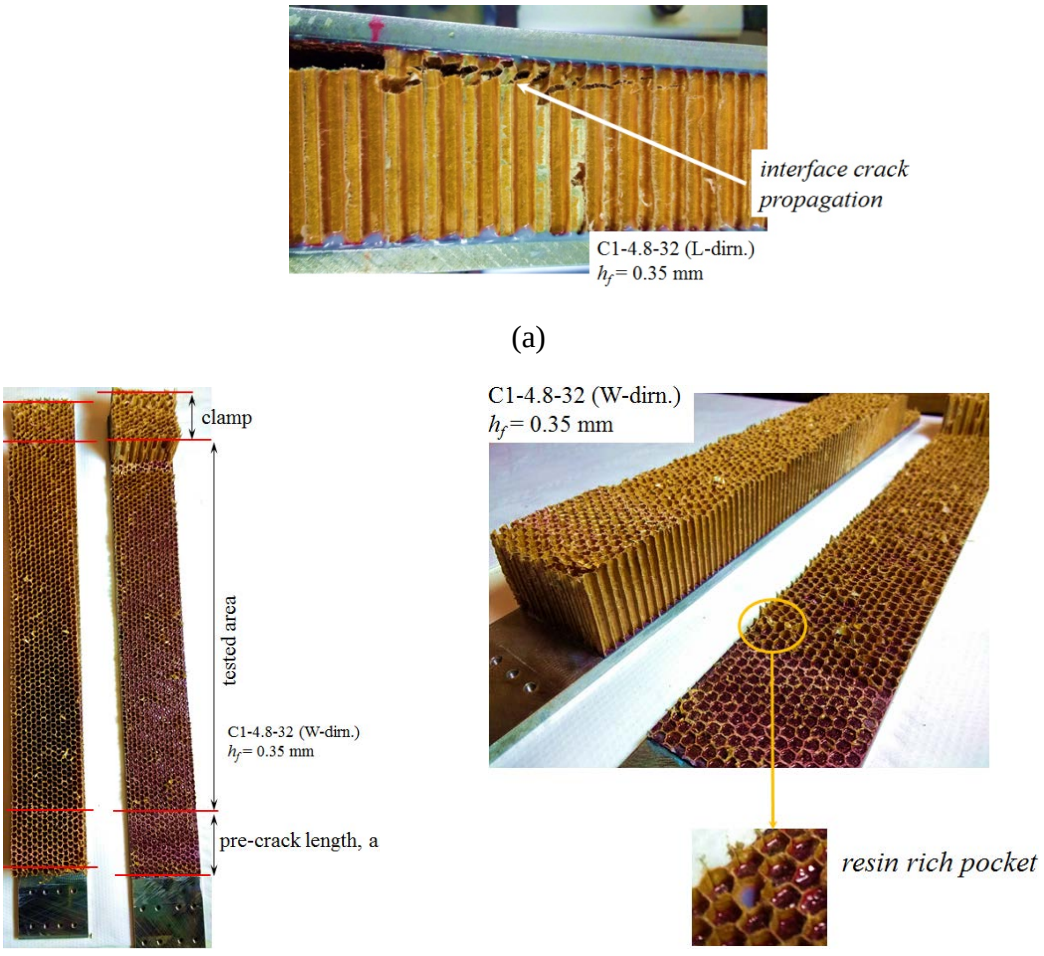

Figure 15. (a) Face/core interface crack propagation path in a CFRP/C1-4.8-32 core specimen, h_f = 0.35 mm, h_c = 40 mm, (b) fracture surface showing interface crack propagation throughout (W-direction), and (c) resin rich pocket observed in cells.

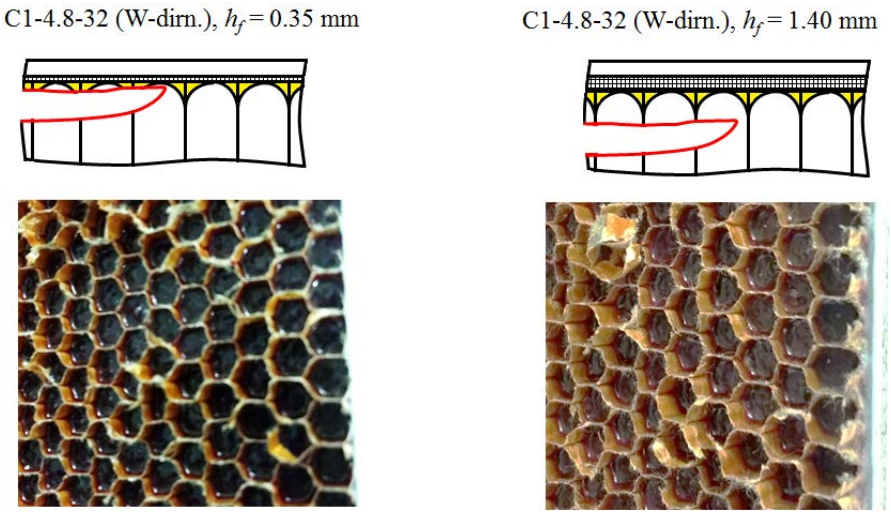

Figure 16. Crack propagation paths in specimens with thin and thick face sheets (a) schematic illustration of crack propagation close to face sheet (above) and fracture surface revealing short meniscus layer residue (below), and (b) schematic illustration of crack propagation beneath the meniscus layer in specimen with thick face sheet (above) and fracture surface with more core residue (below).

Effect of honeycomb paper material on fracture toughness, Γ

In the previous sections, the investigated specimens consisted of Cormaster C1 type cores which were composed of Nomex® T412 paper. The effect of core paper material on the interface fracture toughness is presented in this section and a 32 kg/m^3 dense core with a Cormaster N636 core type comprising of Kevlar N636 paper material was utilized. The study was conducted in both W and L crack propagation directions with, h_f = 1.40 mm and h_c = 40 mm. As previous, the interface fracture toughness was expressed as a function of phase angle (ψ) using Equation (2) and are shown in Figure 17. The interface fracture toughness measured in the W direction was found to be higher than L direction, akin to previous measurements involving Cormaster C1 type core.

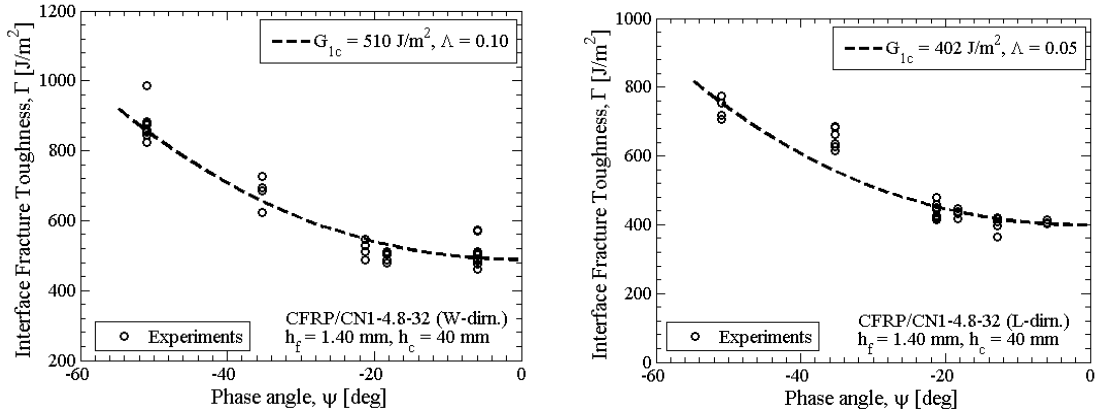

Figure 17. Interface fracture toughness (Γ) vs. phase angle (ψ) for a CFRP/CN1-4.8-32 honeycomb core sandwich specimen with h_f = 0.35 mm and h_c = 40 mm, for crack propagation in: (a) W direction, and (b) L direction.

Comparison of the mode I fracture toughness, G_{1c}, for specimens with C1-4.8-32 and CN1-4.8-32 core types is presented in Figure 18. The Cormaster C1 core type exhibited higher toughness values when compared with core with Kevlar N636 paper. For the CN1-4.8-32 core type, a mode I fracture toughness of 510 J/m^2 and 402 J/m^2 were obtained in W and L directions, respectively. The coefficient of variation, CV, is also provided in Figure 18 for both crack propagation directions. A highest CV of 5.8 % was found for the N636 core type in W direction.

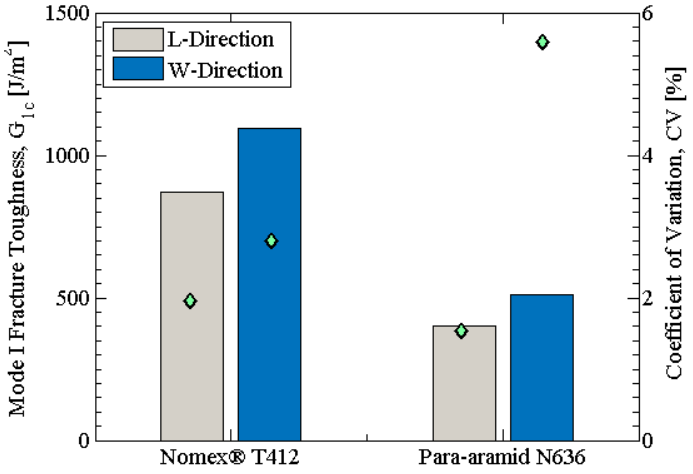

Figure 18. Comparison of mode I fracture toughness and coefficient of variation, CV, in L and W crack propagation directions for CFRP/C1-4.8-32 and CFRP/CN1-4.8-32 honeycomb core specimens; h_c = 40 mm and h_f = 1.4 mm.

Similar to specimens tested with Cormaster C1 cores, interface crack propagation just beneath the meniscus layer was observed at all tested mode mixity conditions. The moment ratios (*MR*) and the corresponding phase angles at which tests were carried out for both L and W directions are provided in Table 3. Figure 19(a) shows interface crack propagation for the CFRP/N636 honeycomb core specimen. A higher amount of core residue was observed on fracture surfaces, see Figure 19(b). This may be attributed to the inherent difference in nature of the core paper material.

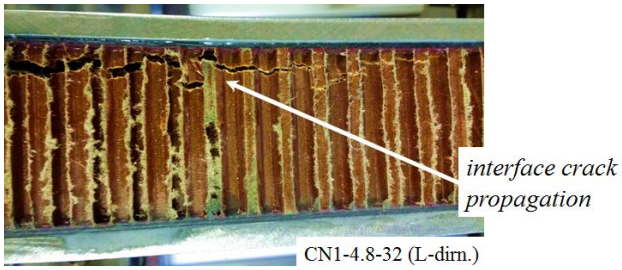

(a)

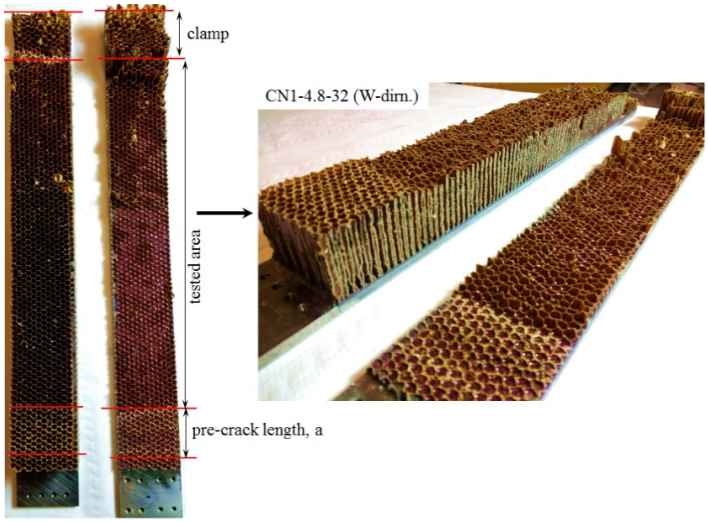

(b)

Figure 19. (a) Crack propagation path, and (b) fracture surface for CFRP/CN1-4.8-32 cored specimen; h_f = 1.40 mm, h_c = 40 mm.

Conclusions

Fracture testing on honeycomb cored sandwich specimens were performed using the DCB-UBM test method. Two core types Cormaster C1 and Cormaster N636 were employed. The Cormaster C1 type specimens consisting of Nomex® T412 paper showed higher fracture toughness compared to specimens with N636 core comprising of Kevlar N636 paper. The measured fracture toughness increased with rise in core density. Furthermore, it was observed that for a given core material, specimens with thinner face sheets exhibited higher fracture toughness due to a shift in crack propagation in the meniscus layer. For all the specimens, the interface fracture toughness measured in the W direction was higher than the L direction (ribbon direction). For sane face sheet properties, specimens with 96 kg/m^3 dense Cormaster C1 honeycomb core yielded the highest interface fracture toughness. The DCB-UBM test methodology with the unique way of applying pure moments directly on the crack flanks was shown to be a very robust and efficient test method for mixed mode fracture characterization of typical honeycomb core sandwich systems.

Appendix A: Mapping of Moment Ratio (*MR*) vs. Mode-mixity Phase Angle (ψ)

The moment ratio, *MR*, corresponding to the desired mode-mixity at which the test is carried out, must be provided as input prior to each test. The mode mixity expressed using the phase angle, ψ, was estimated using a 2D plane strain finite element (FE) model built in ANSYS® [44], in conjunction with the Crack Surface Displacement Extrapolation (CSDE) method [39]. The FE-model consisted of 4-noded linear (PLANE182) and 8-noded parabolic (PLANE183) elements with a smallest element edge length of 2.5 μm, see Figure 20. The 4-noded linear elements were used near the crack tip zone to utilize CSDE mode-mixity method. Moments were applied on master nodes located at the neutral axis of the debonded and substrate beams (refer to Figure 6). The CSDE mixed-mode partitioning method utilizes relative crack flank displacements (δ_x and δ_y) to compute the phase angle, ψ. The mode mixity phase angle can be expressed in terms of relative crack tip displacements in the following form:

$$\psi = \tan^{-1}\left(\frac{\delta_x}{\delta_y}\right) \tag{3}$$

The phase angle provided in Equation (3) is referred to as the reduced formulation, where the near-tip oscillations have been discounted [39,42]. The CSDE method is very effective in calculating mode-mixity phase angles (ψ) and especially when large crack tip distortions are present, which is typically the case for sandwich composites due to the high elastic mismatch across the interface [45]. The CSDE was implemented as a separate subroutine in ANSYS®, which was used to extract relative crack flank displacements.

FE-analysis was performed to create a map of moment ratio, *MR* vs. phase angle, ψ, for the various CFRP/honeycomb cored sandwich configurations studied in this paper. A large range of

moment ratios were explored to vary the mode mixity. It should be noted that in addition to the numerical method, the phase angle, ψ, can also be obtained using closed form expressions for a moment loaded DCB sandwich specimen [19,20]. The mechanical properties of face sheet and core materials are provided in Tables 1 and 2 respectively. The total length of the DCB-UBM specimen was 500 mm and the pre-crack length was chosen to be 200 mm for all analyses. In all simulations, the magnitude of moments, M_1 and M_2 were selected such that, an energy release rate $G \approx 100$ J/m^2 was achieved.

The sign of MR is dependent on the sign of the applied moments, M_1 and M_2. There are three possible ways of rotating the crack flanks: a) M_1 and M_2 rotate clock-wise (CW), b) M_1 and M_2 open relative to each other (Open) or c) M_1 and M_2 rotate counter-clock wise (CCW) with respect to the plane of paper. The rotation of the beam in counter clock-wise direction was taken as positive which yielded $MR > 0$ for the cases when both beams rotate in CW and CCW directions. The case in which crack flanks open relative to each other will yield a negative moment ratio, $MR < 0$.

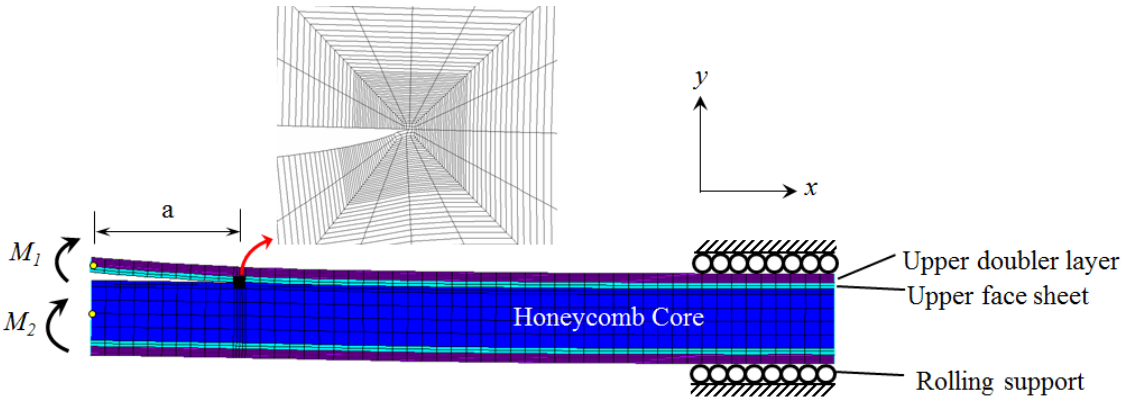

Figure 20. 2D FE-model of the reinforced DCB-UBM sandwich specimen with moments applied on the crack flanks containing high dense mesh in the near tip zone.

Plot of moment ratio, MR, vs. mode-mixity phase angle, ψ, for the CFRP/Cormaster C1 honeycomb core configurations with the three core density classes 32, 64 and 96 kg/m^3 are provided in Figure 21. For $MR > 1$ in the CCW direction, it was observed in the FE-model that the crack flanks collided with each other. Hence, the phase angle values for the CCW case are provided only in the range for $0 \leq MR \leq 1$ for all three core types in Figure 21.

The influence of core thickness, on phase angle is clearly evident from the Figures 21 (a) - (c). For a constant MR, a thinner core results in a higher phase angle values in the negative scale for MR in the ranges $-20 < MR < -1$ and $1 < MR < 20$. However, the difference in phase angle is small in the range $-1 < MR < 1$ for the two core thicknesses considered here. For testing, the MR values were picked to target three mode-mixity regions: 1) mode I ($-10° \leq \psi \leq 10°$), mixed-mode ($-45° \leq \psi \leq -10°$) and mode II dominant ($\psi \leq -45°$). The MR values and the corresponding

phase angle (ψ) for each specimen are enlisted in Table 3. It should be noted that a negative phase angle (ψ) indicates that the crack has propensity to kink into the face sheet. In general, face sheets are tougher and hence the crack will continue to grow hugging the interface. A positive ψ will tend to drive the crack into the core. Therefore it is desired that the fracture testing is carried out at *MR* corresponding to a negative ψ. All the *MR* values selected in this paper for various sandwich configurations pertained to a negative ψ. Similarly, *MR* vs. ψ maps for the CFRP/C1-4.8-32 core configuration with h_f = 0.35 mm and for the CFRP/CN1-4.8-32 configuration are provided in Figures 22 and 23.

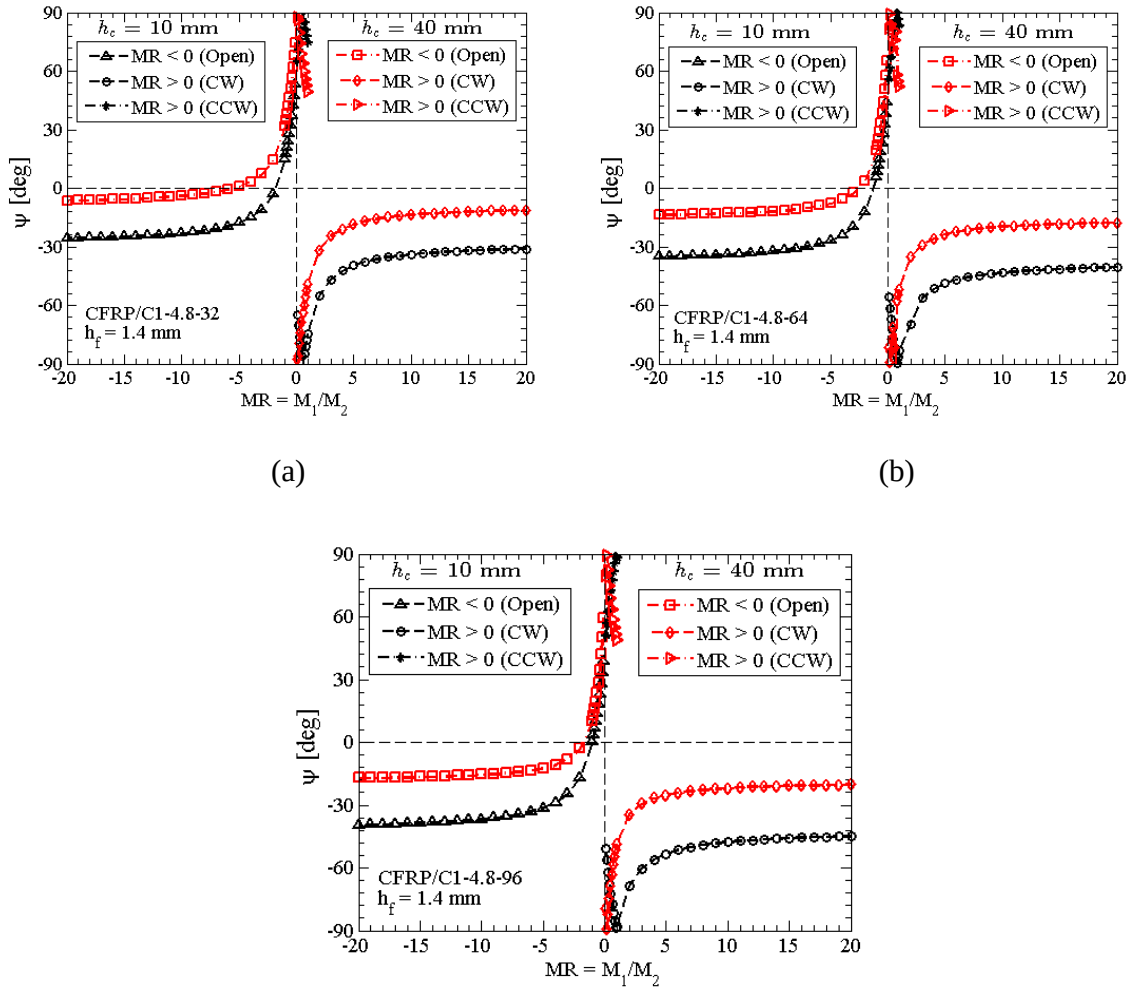

Figure 21. Plot of moment ratio, *MR*, vs. phase angle, ψ, for the CFRP/Cormaster C1 honeycomb core specimen configurations with: (a) 32, (b) 64, and (c) 96 kg/m^3 density class and with a face sheet thickness, h_f = 1.4 mm.

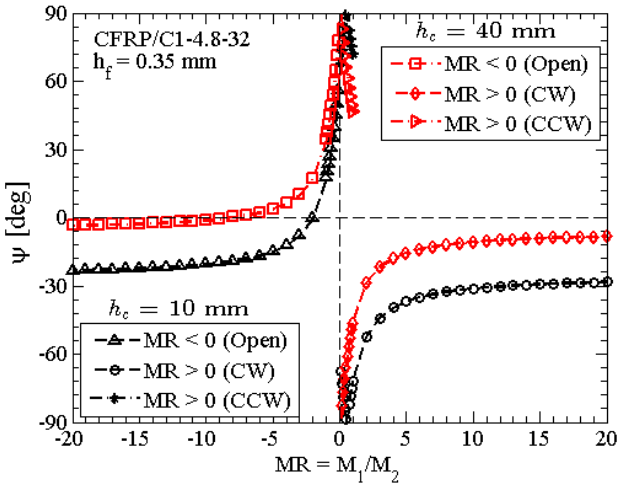

Figure 22. Moment ratio (*MR*), vs. phase angle (ψ), for 32 kg/m^3 dense honeycomb core specimen configuration with h_f = 0.35 mm.

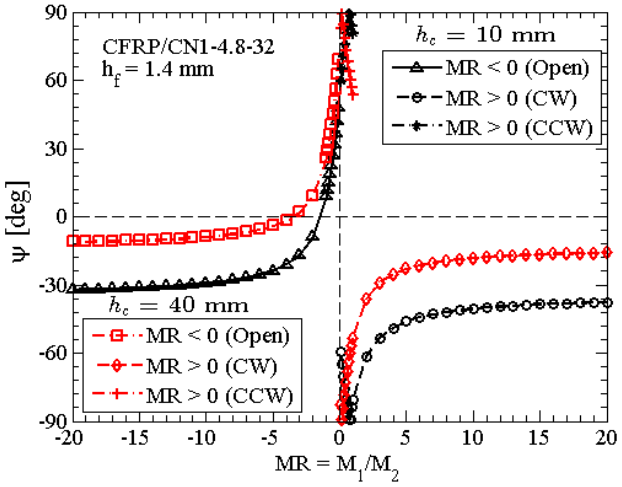

Figure 23. Moment ratio (*MR*), vs. phase angle (ψ), for CFRP/N636 core specimen configuration (CN1-4.8-32) with h_f = 1.40 mm.

Appendix B: Energy release rate of reinforced DCB-UBM specimen

The energy release rate of a multi-layer DCB sandwich specimen subjected to moments can be computed using the *J*-integral expression provided in Equation (1) [18]. The *J*-integral expression is simplified and re-expressed for the reinforced DCB-UBM specimen. Beam #1 comprises of

the upper face sheet (h_f) and doubler layer (h_r) until the pre-crack length, a. The J integral evaluated for beam #1, J_1 is given as:

$$J_1 = \frac{\bar{E}_r M_1^2}{6\left(A_1 D_1 - B_1^2\right)^2}\left[-A_1^2\frac{h_r}{4}\left(h_f^2 + 3h_r^2\right) + 3A_1B_1\left(h_f h_r\right) - 3B_1^2\left(h_f\right)\right] + \frac{\bar{E}_f M_1^2}{6\left(A_1 D_1 - B_1^2\right)^2}\left[-A_1^2\frac{h_f}{4}\left(h_f^2 + 3h_r^2\right) + 3A_1B_1\left(h_f h_r\right) - 3B_1^2\left(h_f\right)\right] \quad (4)$$

where $A_1 = E_f h_f + E_r h_r$, $B_1 = \frac{h_f h_r}{2}\left(E_f - E_r\right)$ and $D_1 = \frac{E_r h_r}{4}\left(h_f^2 + \frac{h_r^2}{3}\right) + \frac{E_f h_f}{4}\left(h_r^2 + \frac{h_f^2}{3}\right)$.

Similarly, for beam #2, the *J*-integral is in the form:

$$J_2 = \frac{\bar{E}_c M_2^2}{6\left(A_2 D_2 - B_2^2\right)^2}\left[-A_2^2\frac{h_c}{4}\left(h_c^2 + 3\left(h_f + h_r\right)^2\right) - 3A_2B_2h_c\left(h_f + h_r\right) - 3B_2^2\left(h_c\right)\right] + \frac{\bar{E}_f M_2^2}{6\left(A_2 D_2 - B_2^2\right)^2}\left[-A_2^2\frac{3h_f}{4}\left(h_c^2 - 2h_r h_c + \frac{1}{3}h_f^2 + h_r^2\right) - 3A_2B_2h_f\left(h_r - h_c\right) - 3B_2^2\left(h_f\right)\right] + \frac{\bar{E}_r M_2^2}{6\left(A_2 D_2 - B_2^2\right)^2}\left[-A_2^2\frac{3h_r}{4}\left(h_c^2 + 2h_f h_c + \frac{1}{3}h_r^2 + h_f^2\right) + 3A_2B_2h_r\left(h_f + h_c\right) - 3B_2^2\left(h_r\right)\right] \quad (5)$$

where $A_2 = E_c h_c + E_f h_f + E_r h_r$, $B_2 = \frac{E_f h_f}{2}\left(h_c - h_r\right) + \frac{E_r h_r}{2}\left(h_c + h_f\right) - \frac{E_c h_c}{2}\left(h_f + h_r\right)$ and

$$D_2 = E_c h_c\left(\frac{h_c^2}{12} + \frac{h_f^2}{4} + \frac{h_f h_r}{2} + \frac{h_r^2}{4}\right) + E_f h_f\left(\frac{h_c^2}{4} + \frac{h_f^2}{12} - \frac{h_c h_r}{2} + \frac{h_r^2}{4}\right) + E_r h_r\left(\frac{h_c^2}{4} + \frac{h_f^2}{4} + \frac{h_c h_f}{2} + \frac{h_r^2}{12}\right).$$

The *J*-integral for beam #3 can be expressed as:

$$J_3 = \frac{\bar{E}_c M_3^2}{6D_3^2}\left[\frac{h_c^3}{4}\right] - \frac{\bar{E}_f M_3^2}{3D_3^2}\left[\frac{h_f}{4}\left(3h_c^2 + 6h_c h_f + 4h_f^2\right)\right] - \frac{\bar{E}_r M_3^2}{3D_3^2}\left[\frac{3h_r}{4}\left(\left(2h_c + 4h_f\right)h_r + \frac{4}{3}h_r^2 + \left(h_c + 2h_f\right)^2\right)\right] \quad (6)$$

where $D_3 = 2E_r h_f h_r\left(h_f + h_r + h_c\right) + E_r h_r\left(\frac{2}{4}h_r^2 + h_c h_r + \frac{h_c^2}{2}\right)$.

Acknowledgements

The financial support from the European Aviation Safety Agency (EASA) and the Danish Centre for Composite Structures and Materials (DCCSM) funded by the Danish Council for Strategic Research within Sustainable Energy and Environment (Grant: 09-067212) are gratefully acknowledged. Furthermore, the support from AIRBUS with supply of honeycomb core specimens is highly appreciated. EASA program manager, Dr. Simon Waite and Mr. Ralf Hilgers, AIRBUS Operations GmbH, showed keen interest in this project and are gratefully acknowledged.

References

1. Transportation Safety Board of Canada. *Loss of Rudder in Flight*. Minister of Public Works and Government Services, Canada, 2007.

2. Glaessgen EH, Reeder JR, Sleight DW, et al. Debonding Failure of Sandwich-Composite Cryogenic Fuel Tank with Internal Core Pressure. *J Spacecr Rockets* 2005; 42: 613–627.

3. Prasad S, Carlsson LA. Debonding and crack kinking in foam core sandwich beams—I. Analysis of fracture specimens. *Eng Fract Mech* 1994; 47: 813–824.

4. Prasad S, Carlsson LA. Debonding and crack kinking in foam core sandwich beams—II. Experimental investigation. *Eng Fract Mech* 1994; 47: 825–841.

5. Li X, Carlsson LA. The Tilted Sandwich Debond (TSD) Specimen for Face/Core Interface Fracture Characterization. *J Sandw Struct Mater* 1999; 1: 60–75.

6. Berggreen C, Carlsson LA. A Modified TSD Specimen for Fracture Toughness Characterization - Fracture Mechanics Analysis and Design. *J Compos Mater* 2010; 44: 1893–1912.

7. Berggreen C, Quispitupa A, Costache A, et al. Face/core mixed mode debond fracture toughness characterization using the modified TSD test method. *J Compos Mater* 2014; 48: 1939–1945.

8. Fields RE, Zarda R. Analysis and Test Methodology for Fracture Mechanics of Unbonded Sandwich Structures. *Martin Maerietta Stud Report, EDF No MM0 TKR 10722739-001* 1994.

9. Cantwell WJ, Davies P. A test technique for assessing core-skin adhesion in composite sandwich structures. *J Mater Sci Lett* 1994; 13: 203–205.

10. Carlsson LA. On the Design of the Cracked Sandwich Beam (CSB) Specimen. *J Reinf Plast Compos* 1991; 10: 434–444.

11. Zenkert D. Poly(vinyl chloride) sandwich core materials: Fracture behaviour under mode

II loading and mixed-mode conditions. *Mater Sci Eng A* 1989; 108: 233–240.

12. Quispitupa A, Berggreen C, Carlsson LA. On the analysis of a mixed mode bending sandwich specimen for debond fracture characterization. *Eng Fract Mech* 2009; 76: 594–613.

13. Quispitupa A, Berggreen C, Carlsson LA. Design Analysis of the Mixed Mode Bending Sandwich Specimen. *J Sandw Struct Mater* 2010; 12: 253–272.

14. Ratcliffe J, Krueger R. Face Sheet/Core Disbonding in Sandwich Composite Components: A Road Map to Standardization: Test Method Development. In: *11th International Conference on Sandwich Structures*. Dania Beach, Florida, 2016.

15. Ratcliffe JG, Reeder JR. Sizing a single cantilever beam specimen for characterizing facesheet-core debonding in sandwich structure. *J Compos Mater* 2011; 45: 2669–2684.

16. Quispitupa A, Berggreen C, Carlsson LA. Face/core interface fracture characterization of mixed mode bending sandwich specimens. *Fatigue Fract Eng Mater Struct* 2011; 34: 839–853.

17. Sørensen BF, Jørgensen K, Jacobsen TK, et al. DCB-specimen loaded with uneven bending moments. *Int J Fract* 2006; 141: 163–176.

18. Lundsgaard-Larsen C, Sørensen BF, Berggreen C, et al. A modified DCB sandwich specimen for measuring mixed-mode cohesive laws. *Eng Fract Mech* 2008; 75: 2514–2530.

19. Kardomateas GA, Berggreen C, Carlsson L a. Energy-Release Rate and Mode Mixity of Face/Core Debonds in Sandwich Beams. *AIAA J* 2013; 51: 885–892.

20. Saseendran V, Berggreen C, Carlsson LA. Fracture Mechanics Analysis of Reinforced DCB Sandwich Debond Specimen Loaded by Moments. *AIAA J* 2017; 56: 413–422.

21. Reeder JR, Demarco K, Whitley KS. The use of doubler reinforcement in delamination toughness testing. *Compos Part A Appl Sci Manuf* 2004; 35: 1337–1344.

22. Grau DL, Qiu XS, Sankar B V. Relation between Interfacial Fracture Toughness and Mode-mixity in Honeycomb Core Sandwich Composites. *J Sandw Struct Mater* 2006; 8: 187–203.

23. Rinker M, Ratcliffe JG, Adams DO, et al. Characterizing Facesheet/Core Disbonding in Honeycomb Core Sandwich Structure. *NASA/CR-2013-217959 NIA Rep No 2013-0115* 2013.

24. Schütz GmbH & Co. *Cormaster C1 Technical Data*. Selters, Germany, 2016.

25. Schütz GmbH & Co. *Cormaster N636 Preliminary technical data*. Selters, Germany, 2016.

26. Hexcel Corporation. *HexPly ® 913 125°C curing epoxy matrix*. Stamford, CT, 2016.

27. 3M Aerospace and Aircraft Maintenance Department. *Scotch-Weld ™ Structural Adhesive Film AF 163-2 Technical Datasheet*. 2009.

28. UDDEHOLM. *Uddeholm Impax ® Supreme*. Udeeholm, 2014.

29. 3M. *Scotch-Weld ™ Epoxy Adhesives DP460 Off-White and DP460NS*. St. Paul, MN, 2017.

30. ASTM-D3039/D3039M-08. Standard Test Method for Tensile Properties of Polymer Matrix Composite Materials. 2014.

31. ASTM-D7078/7078M-12. Standard Test Method for Shear Properties of Composite Materials by V-Notched Rail Shear Method. 2012.

32. Schäuble R, Goldstein M, Petersilge M. *Elastic properties of the CFRP Facesheets in Honeycomb core Sandwich Panels (DoSS/TFSanDis)*. Internal report IMWS V554/2017, Halle, 2017.

33. Schäuble R, Goldstein M, Petersilge M. *SCB Fracture Toughness Tests on Honeycomb Sandwich Material - Technical Report*. Internal report IMWS V793/2017, Halle, 2017.

34. Gibson LJ, Ashby MF. *Cellular Solids: Structure and Properties*. Cambridge University Press, 1999.

35. Malek S, Gibson L. Effective elastic properties of periodic hexagonal honeycombs. *Mech Mater* 2015; 91: 226–240.

36. Hähnel F, Bugiel A, Wolf K. *Determination of macroscopic properties of different aramid paper based honeycomb cores*. Technische Universität Dresden, Chair of Aircraft Engineering, Internal report ILR/LFT-IR17-19, Dresden, 2017.

37. Berggreen C, Saseendran V, Carlsson LA. A Modified DCB-UBM Test Method for Interfacial Fracture Toughness Characterization of Sandwich Composites. *(Manuscript in preperation)* 2017.

38. MTS Systems Corporation. *FlexTest ™ SE Digital Servo Test Controller*. Eden Prairie, 2010.

39. Berggreen C, Simonsen BC, Borum KK. Experimental and Numerical Study of Interface Crack Propagation in Foam-cored Sandwich Beams. *J Compos Mater* 2007; 41: 493–520.

40. Rice JR. A Path Independent Integral and the Approximate Analysis of Strain Concentration by Notches and Cracks. *J Appl Mech* 1968; 35: 379.

41. ASTM International. ASTM D5528-13 Standard Test Method for Mode I Interlaminar Fracture Toughness of Unidirectional Fiber-Reinforced Polymer Matrix Composites. 2013.

42. Hutchinson JW, Suo Z. Mixed Mode Cracking in Layered Materials. *Adv Appl Mech* 1991; 29: 63–191.

43. Giglio M, Manes A, Gilioli A. Investigations on sandwich core properties through an experimental–numerical approach. *Compos Part B Eng* 2012; 42: 361–374.

44. ANSYS Inc. *ANSYS® Mechanical User's Guide*. Canonsburg, PA, 2015.

45. Berggreen C. *Damage Tolerance of Debonded Sandwich Structures*. Ph.D. Thesis, Technical University of Denmark, 2004.

DTU Mechanical Engineering
Section of Solid Mechanics
Technical University of Denmark

Nils Koppels Allé, Bld. 404
DK-2800 Kgs. Lyngby
Denmark
Phone (+45) 4525 4250
Fax (+45) 4593 1475
www.mek.dtu.dk
ISBN: 978-87-7475-524-1

DCAMM
Danish Center for Applied Mathematics and Mechanics

Nils Koppels Allé, Bld. 404
DK-2800 Kgs. Lyngby
Denmark
Phone (+45) 4525 4250
Fax (+45) 4593 1475
www.dcamm.dk
ISSN: 0903-1685